ESTABLISHMENT OF AN ENVIRONMENTAL CONTROL TECHNOLOGY LABORATORY WITH A CIRCULATING FLUIDIZED-BED COMBUSTION SYSTEM

FINAL REPORT

COOPERATIVE AGREEMENT NO. DE-FC26-03NT41840

PROJECT PERFORMANCE PERIOD: September 15, 2003 – August 31, 2008

SUBMITTED BY

WEI-PING PAN

YAN CAO

JOHN SMITH

INSTITUTE FOR COMBUSTION SCIENCE AND ENIRONMENTAL TECHNOLOGY
WESTERN KENTUCKY UNIVERSITY (WKU)
2413 Nashville RD. BOWLING GREEN, KY 42101

PREPARED FOR

U.S. DEPARTMENT OF ENERGY
NATIONAL ENERGY TECHNOLOGY LABORATORY
PITTSBURGH, PENNSYLVANIA 15236

REPORT SUBMITTAL DATE: August 31, 2008

DISCLAIMER

TABLE OF CONTENTS

LIST OF FIGURES

LIST OF TABLES

1. Background

On February 14, 2002, President Bush announced the Clear Skies Initiative, a legislative proposal to control the emissions of nitrogen oxides (NO_x), sulfur dioxide (SO_2), and mercury from power plants. In response to this initiative, the National Energy Technology Laboratory organized a Combustion Technology University Alliance and hosted a Solid Fuel Combustion Technology Alliance Workshop. The workshop identified multi-pollutant control; improved sorbents and catalysts; mercury monitoring and capture; and improved understanding of the underlying reaction chemistry occurring during combustion as the most pressing research needs related to controlling environmental emissions from fossil-fueled power plants. The Environmental Control Technology Laboratory will help meet these challenges and offer solutions for problems associated with emissions from fossil-fueled power plants.

The **goal** of this project was to develop the capability and technology database needed to support municipal, regional, and national electric power generating facilities to improve the efficiency of operation and solve operational and environmental problems. In order to effectively provide the scientific data and the methodologies required to address these issues, the project included the following aspects:

• Establishing an Environmental Control Technology Laboratory using a laboratory-scale, simulated fluidized-bed combustion (FBC) system;

• Designing, constructing, and operating a bench-scale (0.6 MW_{th}), circulating fluidized-bed combustion (CFBC) system as the main component of the Environmental Control Technology Laboratory;

• Developing a combustion technology for co-firing municipal solid waste (MSW), agricultural waste, and refuse-derived fuel (RDF) with high sulfur coals;

• Developing a control strategy for gaseous emissions, including NO_x, SO_2, organic compounds, and heavy metals; and

• Developing new mercury capturing sorbents and new particulate filtration technologies.

Major tasks during this period of the funded project's timeframe included:

• Conducting pretests on a laboratory-scale simulated FBC system;

• Completing detailed design of the bench-scale CFBC system;

• Contracting potential bidders to fabricate of the component parts of CFBC system;

• Assembling CFBC parts and integrating system;
• Resolving problems identified during pretests;
• Testing with available Powder River Basin (PRB) coal and co-firing of PRB coal with first wood pallet and then chicken wastes.
• Tuning of CFBC load

Following construction system and start-up of this 0.6 MW CFBC system, a variety of combustion tests using a wide range of fuels (high-sulfur coals, low-rank coals, MSW, agricultural waste, and RDF) under varying conditions were performed to analyze and monitor air pollutant emissions. Data for atmospheric pollutants and the methodologies required to reduce pollutant emissions were provided. Integration with a selective catalytic reduction (SCR) slipstream unit did mimic the effect of flue gas composition, including trace metals, on the performance of the SCR catalyst to be investigated. In addition, the following activities were also conducted:

- Developed advanced mercury oxidant and adsorption additives; and
- Performed laboratory-scale tests on oxygen-fuel combustion and chemical looping combustion;
- Conducted statistical analysis of mercury emissions in a full-scale CFBC system.

Future work on this CFBC system will include modification of the bench-scale CFBC system to allow advanced combustion technologies such as “chemical looping” and “oxygen-enhanced” combustion to be investigated.

- Chemical looping is a process by which the combustion of a hydrocarbon occurs in two stages. In the first stage, air is used to oxidize a “metal carrier” to a “metal oxide carrier.” In the second stage, the “metal oxide carrier” is used to oxidize a fuel as it is reduced to its original “metal carrier” form.
- “Oxygen-enhanced” combustion occurs in a gas mixture of oxygen and recycled carbon dioxide. The carbon dioxide functions as a heat sink for combustion, much like the nitrogen in air, but produces a flue gas that is composed of carbon dioxide and water vapor. Removal of the water vapor results in a sequestration-ready, concentrated carbon dioxide stream.

2. Executive Summary

All documents for managing this project, including Quarterly Technical Progress Reports, Project Milestones, a Hazardous Substance Plan and Hazardous Waste Report, have been prepared and submitted to the U. S. Department of Energy's (DOE's) National Energy Technology Laboratory (NETL).

The renovation of a new space for a 0.6 MW_{th} Circulating Fluidized-Bed Combustion (CFBC) system and new Combustion Laboratory was completed. The final specifications for the renovation of the new Combustion Laboratory and the construction of the Circulating Fluidized Bed (CFB) Combustor Building are compatible with the design of the CFBC system. Half of the space located under the new Combustion Laboratory has also been allocated to the setup of the laboratory-scale reactor, which has provided relevant data to help with running the CFBC system.

Prior to the construction of the 0.6 MW_{th} CFBC facility, the design calculations, including the mass balances, energy balances, heat transfer, facility strength, and construction dimensions were intensively discussed. Considerable modifications have been made on the draft design of the CFBC system based on discussions conducted during the project kick-off meeting held on January 13, 2004 at the NETL. Comments received from various experts were also used to improve the design. Finally, the drawings of all assembly parts were completed in order to develop specifications for the fabrication of individual parts. A detailed design of supporting and hanging structures for the CFBC was completed in early 2005. The fabrication and manufacturing contract for the CFBC system was awarded to Sterling Boiler & Mechanical, Inc. of Evansville, Indiana. Sterling manufactured and assembled all component parts of the CFBC system. Discussions with a potential contactor regarding the availability of materials and current machining capabilities was resulted in the first modification of the original designs. At this same time, the CFBC coolant production and feed-water supply system have been strengthened with the addition of a boost pump to assure that coolant can be admitted to the cooling system under all operating conditions. Except for the main body of the CFBC facility, the induced draft fan, along with its machine base and power supply, was received and installed. The flue gas duct from the secondary cyclone outlet to the induced draft fan inlet was received and installed, as well as the induced fan flue gas discharge duct. Additionally, a dust control system has been installed, which could help maintain a cleaner and safer work environment around the fuel and

limestone bunkers during filling operations. Further, all materials for the high temperature insulation of the riser, both cyclones and the downcomer were installed.

Substantial effort was made on the development and application of software for the effective operation and safe control of the CFB system, as well as for the display and logging of acquired data and operating parameters. Electric power distribution for pumps, blowers, variable speed drives, valves and the bed preheater was completed. Installation of CFBC system temperature, pressure, coolant and air flow sensors, as well as load cells, were completed, along with actuator installation and wiring. Calibration, display and logging of pressure and air flow sensor data were also performed.

Powder River Basin (PRB) coal was used for performance evaluation of the CFBC system. Slag from an operating Integrated Gasification Combined Cycle (IGCC) facility and fly ash from a full-scale CFBC utility boilers were used as recirculation fly ash during initiation of CFBC "hot-modeling" tests. For co-firing tests, biomass (wood pallet and chicken waste) was prepared.

Additional thermal expansion joints were installed, first between the ash supply duct to the lower loop seal; and second between the lower loop seal to the riser. The purpose of adding up additional thermal expansion joints is to provide stable support for the riser and downcomer, as well as safely accommodating the dramatic change that occurs under high temperature operation. The third modification of the CFBC system began after the initial firing CFBC system in early 2008. Major modifications included an additional heat exchanger and additional sensor ports as well as sampling ports. During an earlier CFBC system test, high temperatures were detected in the vicinity of the riser flange joint when the system load was increased. Some riser insulation components were damaged. The initial design review also indicated that this area of the riser would likely benefit from additional heat exchange surface below this area.

Three full evaluation tests were conducted on July 23, July 30 and August 7, 2008 under different loads and different fuel mixtures. A day prior to the initial firing of CFBC system, an overnight firing was conducted to gradually increase the temperature of the whole system to normal operational conditions. On July 23, the first full evaluation of the 0.6 MW_{th} CFBC system was conducted by firing PRB coal in the morning and co-firing of PRB coal and wood pallets (WP) in the afternoon. On July 30, the second full evaluation of the 0.6 MW_{th} CFBC system was conducted starting with firing PRB coal at feed rates higher than the test conducted on July 23. In the afternoon, the system was switched to co-fire PRB coal with chicken waste

(CW). An evaluation of the system at its **full-load** and its tuning were conducted on August 7. The purpose of this test was to investigate whether different parts of the whole CFBC system could properly function under full-load or over full-load, during the tuning period. Special focus was on evaluations of the optimal particle size of feeding fuels, the compatibility of feeding materials including fuels and air, the maximum Heat Exchanger (HX) capability and ash recirculation capability by the loop seal. During this period of testing, the co-firing of PRB coal and wood pallet (WP) was co-fired.

Evaluation of tests on CFBC system performance indicated load tuning, fuel switching and heat transfer by available heat exchangers were successful. When feeding coal and the delivering different air streams, the CFBC system performed constant and smooth. The heat expansion joint worked perfectly to absorb system expansion under high temperatures of the CFBC system. Better setup of the control system, signal collection and transfer system made CFBC operation more automated. The current CFBC system could work properly under a low ash re-circulation rate with the assistance of two cyclones and two loop seals. Loss-of-ignition (LOI) in fly ash at the flue gas exit of the facility, which were about 18 %, seemed acceptable under the current initial full-load operation. However, a future modification of the air delivery system into a low loop seal has been planned, because the loss of ash re-circulation was found during full-load operation on the last day. Final troubleshooting of the loop seal showed that there was not enough pressure on the loop seal. Air caused the failure of ash re-circulation. Additional tests outside the scope of this project will be performed.

Major air pollutants were measured during three full evaluation tests. These included sulfur dioxide (SO_2), nitrogen oxide (NOx), carbon monoxide (CO), mercury (Hg), condensable particulate matter (CPM), sulfuric mist (SO_3), halogens, and trace metals. Test results indicated limestone could effectively control SO_2 emissions, but its effectiveness depended on temperature profile of the CFBC system and its particle size distribution. Oxygen concentration, available reducing agents and system temperature profiles had major impacts on both NO and N_2O emissions. Co-firing of coal and biomass could increase emissions of CO and volatile of organic compounds (VOCs) and semi-VOCs emissions. Better combustion of the CFBC system could largely abate emissions of CO and VOCs and Semi-VOCs. The emissions of trace metals were a minor issue during test firing. However, mercury emissions were not efficiently controlled. Several major halogens, which impacted mercury oxidation, was probably effectively controlled

by limestone and also alkali earth metal oxides in the solid feedstocks. A higher portion of elemental mercury inside the flue gas correlated to less adsorption on the fly ash. On the other hand, the lack of availability of common air pollutant control devices (APCD) caused unexpected mercury removal efficiency.

Based on tasks defined in this project, several extensive tests have been done, either in laboratory-scale evaluation reactors, or in a slipstream facility setup at a full-scale utility, or direct tests at a full-scale utility by firing different coals (listed in Appendix 1). **Major achievements during the period of the project execution included the following:**

1. A novel concept and an additive on to promote simultaneous mercury oxidation and adsorption were developed. Hydrogen bromide (HBr) was found to be very effective for mercury oxidation in a coal-derived flue gas atmosphere. Compared to other typical mercury oxidants, such as hydrogen chloride (HCl), the effectiveness of HBr on mercury oxidization can be 100 times greater. This effectiveness works under both higher (350^{o}C) and lower (150^{o}C) temperatures. The additional benefits of injected HBr include the subsequent adsorption of oxidized mercury on the fly ash surface. This additive has been tested in several full-scale utility power plants using a slipstream reactor to evaluate its function and efficiencies. Tested coals include typical eastern bituminous coal and sub-bituminous coal, such as Powder River Basin coal (PBR). Considering 90 % of coal-burning utility power plants are equipped with particle collection facilities, this novel additive is likely to soon be widely used in utilities for mercury emission control. A patent application on using HBr injection to control mercury emission is pending (U.S.P. 11875583).

2. A laboratory-scale investigation of chemical looping combustion using solid fuels, such as coal, biomass and plastics, has been conducted. Conceptual designs of the chemical looping process, based on the results of testing conducted in the fluidized bed combustor (FBC) system, have been completed. A promising oxygen carrier, which is a copper-based oxygen carrier, has been identified. A theoretical analysis of the looping cycle, oxygen carrier reaction, enthalpy variation and compatibility of the properties of oxygen carrier with different solid fuels has been thoroughly investigated. The first industrial contract from a major oil shale company in Canada has been signed with Western Kentucky University for a period of two-year to pursue the development of the chemical looping combustion process using oil shale residue, such as bitumen. The final stage of this project will be the pilot-scale operation of chemical looping

combustion to generate steam in a modified 0.6 MW_{th} CFBC system.

3. Oxygen-fuel combustion tests have been pursued in a laboratory-scale FBC system to investigate the impact of the switch of air firing to oxygen firing with CO_2 recirculation on combustion performance and emission characterization, especially mercury emissions. Tests demonstrated that the combustion performance control was stable when switching between air firing and oxygen firing. It was also found that mercury speciation and emission rates did not change with operational modes.

4. Because of a delay in setting up the 0.6 MW_{th} CFBC system, a ready-to-go selective catalytic reduction (SCR) slipstream facility was extensively used in several utility power plants during this project to evaluate several typical commercial SCR catalysts, ammonia cracking catalysts, additive injections on mercury oxidation (ICSET of WKU) and mercury adsorbent injection. Several other groups have contracted with ICSET of WKU to develop a mercury adsorbent using this slipstream reactor. The final slipstream reactor will be located downstream of the 0.6 MW_{th} CFBC system to permit additional evaluations to be conducted.

5. Co-firing of coal and multiple biomass and solid wastes has been intensively investigated using a laboratory-scale FBC system. Coal and chicken waste were co-fired on a laboratory-scale fluidized bed combustor to investigate the effect of CW combustion on pollutant emissions. The experimental results show that CW introduction, at mixing ratio by 30 wt%, increases CO emissions, but reduces the levels of SO_2. The ratio of hydrogen sulfide (H_2S)/SO_2 increases with increasing percentages of CW. The temperature in the freeboard region increases with increasing fractions of CW while the reverse is true for the bed temperature. Other tests on mercury emissions with co-firing PRB coal and multiple biomass wastes, including CW, wood pallet (WP), tobacco stalks (TS) and coffee residue (CR), indicated mercury emissions were strongly correlative to the chlorine levels in the gas phase, but not necessarily correlative to the chlorine levels in co-firing fuels. Mercury emissions could be reduced by 35% during firing of sub-bituminous coal using only a quartz filter. Co-firing high-chlorine fuel, such as CW, could largely reduce mercury emissions by over 80%. When co-firing low-chlorine biomass, such as WP and CR, mercury emissions could only be reduced by about 50%. Co-firing TS with more chlorine did not significantly reduce mercury emissions. This was also true when adding limestone while co-firing coal and CW with high chlorine content, because the chlorine in the flue gas was reduced in the freeboard of the FBC, where the temperature was generally below

650^{o}C without adding the secondary air. Both higher content of alkali metal oxides or alkali earth metal oxides in the biomass sample tests, and the occurrence of temperatures lower than 650^{o}C in the upper part of the FBC seemed to be responsible for the reduction of gaseous chlorine, and consequently limited mercury emissions reduction during co-firing. This study identified the important impacts of the temperature profile and oxides of alkali metal (alkali earth metal) on mercury emissions during co-firing in the FBC.

6. A statistical analysis was conducted to investigate the dependence of mercury emissions on coal rank and electric utility boilers, including full-scale CFBC equipped with fabric filter baghouses (FF). The data were collected from the Environmental Protection Agency Information Collection Request (EPA ICR) and WKU ICSET's mercury testing program. A statistical stepwise regression procedure was used to determine significant factors such as coal rank and types of boilers equipped with FF on mercury emissions during coal combustion. The higher mercury emission rates were generally found in both CFB and pulverized coal (PC) units when lignite was burned. The lower mercury emission rates were generally found in both CFB equipped with FF and PC units equipped with FF when bituminous coal was burned. There was a statistically significant lower mercury emission in the CFBC systems equipped with FF than that in the PC units when sub-bituminous coal was burned. Lower mercury emission rates in electric utility boilers equipped with FF are due to the active fly ash generated with a larger specific surface area and pore volume. Higher mercury emission rates observed during lignite-fired boilers may be due to their lower specific area of the fly ash.

3. Design and Manufacture

3.1 Design of 0.6 MW_{th} CFBC System

Based on requirement of load capacity (0.6MW_{th} with selection of bituminous coal), design parameters of CFBC system were determined by setup calculations of mass balance (Table 1), heat balance (Table 2) and hydrodynamics (Table 3). A summary of design parameters is listed in Table 4, and system dimensions are listed in Table 5.

Table 1. System Mass Balance Calculation

Calculation for CFBC Design - 4. Mass Balance							
4.1. Mass Balance in Dense Zone							
No.	Name	Symbol	Unit (E)	Value (E)	Calculation	Value (SI)	Unit (SI)
1	**In**						
2	Coal Feed Rate	R	lb/hr	175.74		79.72	kg/h
3	Coal Ash Content	A	%	7.82		7.82	%
4	Limestone Feed Rate	W_{lime}	lb/h	64.61		29.31	kg/h
5	Solid Recirculation Rate	R_s	lb/h	5272.26		2391.50	kg/h
6	Air Feed Rate into Dense Z.	V_1	ft^3/h	15670.48		443.80	m3/h
7	Combus. Fraction in Dense-Z	d_1		0.65		0.65	
8	Combustion Efficiency	h	%	100	Assuming value	100	%
9	Coal burnt in dense zone	R_{cdz}	lb/h	114.23		51.82	kg/h
10	Real Air Excess Factor in DZ	a_{dz}		1.2		1.2	
11	Fraction of Solid Discharged	q_{cd}		0.7		0.7	
12	Ash Generated in Dense Z.	R_{adz}	lb/h	8.93		4.05	kg/h
13	Solid Waste Generated by L.	R_{ldz}	lb/h	36.57		16.59	kg/h
14	Limestome Comsumed in DZ	R_{lcd}	lb/h	42.00		19.05	kg/h
15	Solid Recirculation Ratio	g		30	In the range of 2~40 (RS/CA)	30	
18	**Out**						
19	Solid Discharged from DZ	R_{sdi}	lb/h	31.85		14.45	kg/h
20	Solid leaving DZ for Dilute Z.	Rsdf	lb/h	5285.91		2397.69	kg/h
21	Coal leaving DZ for Dilute Z.	R_{cdf}	lb/h	61.51		27.90	kg/h
22	Flue gas leaving DZ for Di. Z.	V_{gdf}	ft^3/h	16964.05		480.37	m^3/h
23	Limestone leaving DZ for Di.Z	R_{ldf}	lb/h	22.61		10.26	kg/h
4.2. Mass Balance in Dilute Zone (1st Section)							
No.	Name	Symbol	Unit (E)	Value (E)	Calculation	Value (SI)	Unit (SI)
1	**In**						
2	Coal Coming from DZ	R_{cdf}	lb/hr	61.51		27.90	kg/h
3	Solid Coming from DZ	R_{sdf}	lb/h	5285.91		2397.69	kg/h
4	Flue gas coming from DZ	V_{gdf}	ft^3/h	16964.05		480.37	m^3/h
5	Combus. Fraction in This Zone	d_{21}		0.25		0.25	
6	Secondary Air Frac.	a_{21}		0.25		0.25	
7	Limestone coming from DZ	R_{ldf}	lb/h	22.61		10.26	kg/h
8	Combustion Efficiency	h	%	100	Assuming value	100	%
9	Coal burnt in this zone	R_{cf1}	lb/h	43.94		19.93	kg/h
10	Real Air Excess Factor	a_{df1}		1.2		1.2	
11	Limestone consumed	R_{lcf1}	lb/h	16.15		7.33	kg/h
12	Ash Generated in This Zone	R_{af1}	lb/h	3.44		1.56	kg/h
13	Solid Waste Generated by L.	R_{lf1}	lb/h	14.07		6.38	kg/h
14	Air Feed Rate into This Z.	V_{21}	ft^3/h	6027.11		170.67	m^3/h
15	Flue gas generated in This Z.	V_{g21}	ft^3/h	6524.63		184.76	m^3/h
19	**Out**						
20	Limestone leaving this zone	R_{lf2}	lb/h	6.46		2.93	kg/h
21	Solid leaving this zone	R_{sf2}	lb/h	5303.41		2405.63	kg/h
22	Coal leaving this zone	R_{cf2}	lb/h	17.57		7.97	kg/h
23	Flue gas leaving this zone	V_{gf2}	ft3/h	23488.68		665.12	m^3/h

Continued

4.3. Mass Balance in Dilute Zone (2nd Section)							
No.	Name	Symbol	Unit (E)	Value (E)	Calculation	Value (SI)	Unit (SI)
1	**In**						
2	Coal Coming from 1st Dilu. Z.	R_{cf2}	lb/hr	17.57		7.97	kg/h
3	Solid Coming from 1st Dilu. Z.	R_{sf2}	lb/h	5303.41		2405.63	kg/h
4	Flue gas entering this zone	V_{gf2}	ft^3/h	23488.68		665.12	m^3/h
5	Combus. Fraction in This Zone	d_{22}		0.1		0.1	
6	Secondary Air Frac.	a_{22}		0.1		0.1	
7	Limestone entering this zone	R_{lf2}	lb/h	6.46		2.93	kg/h
8	Combustion Efficiency	h	%	100	Assuming value	100	%
9	Coal burnt in this zone	R_{cf2}	lb/h	17.57		7.97	kg/h
10	Real Air Excess Factor	a_{df2}		1.2		1.2	
11	Limestone consumed	R_{lcf2}	lb/h	6.46		2.93	kg/h
12	Ash Generated in This Zone	R_{af2}	lb/h	1.37		0.62	kg/h
13	Solid Waste Generated by L.	R_{lf2}	lb/h	5.63		2.55	kg/h
14	Air Feed Rate intoThis Z.	V_{22}	ft^3/h	2410.84		68.27	m^3/h
15	Flue gas generated in This Z.	V_{g22}	ft^3/h	2609.85		73.90	m^3/h
19	**Out**						
20	Limestone leaving this zone	R_{lfe}	lb/h	0.00		0.00	kg/h
21	Solid leaving this zone	R_{sfe}	lb/h	5310.41		2408.80	kg/h
22	Coal leaving this zone	R_{cf2}	lb/h	0		0	kg/h
23	Flue gas leaving this zone	V_{gf2}	ft^3/h	26098.54		739.03	m^3/h
4.4. Mass Balance in Cyclones and Standpipe							
No.	Name	Symbol	Unit (E)	Value (E)	Calculation	Value (SI)	Unit (SI)
1	Primary Cyclone						
2	Solid Recirculation Rate	R_s	lb/hr	5272.26		2391.50	kg/h
3	Solid entering P. Cyclone	R_{sc1}	lb/h	5310.41		2408.80	kg/h
4	Flue gas entering P. Cyclone	V_{gc1}	ft^3/h	26098.54		739.03	m^3/h
5	Sepatation Efficiency	h_1	%	90	Assuming value	90	%
6	Separated Solid Rate	R_{ss1}	lb/hr	4779.37		2167.92	kg/h
7	Secondary Cyclone						
8	Flue gas enetring S. Cyclone	V_{gc1}	ft^3/h	5272.26		739.03	m^3/h
9	Solid Entering S.Cyclone	R_{sc2}	lb/h	531.04		240.88	kg/h
10	Sepatation Efficiency	h_2	%	93	Assuming value	93	%
11	Separted Solid Rate	R_{ss1}	lb/hr	493.87		224.02	kg/h
12	Solid leaving seconday cyc.	R_{sf}	lb/hr	37.17		16.86	kg/h
13	Solid Concent. In Flue Gas	m_s	lb/ft^3	0.01		22.82	g/m^3
14	Standpipe Section						
15	Solid Enetering Standpipe	R_{sp}	lb/hr	5273.24		2391.94	kg/h
16	Ratio to Solid Recir. Rate	y		1.00		1.00	
17	Inventory						
18	In Dense Zone						
19	Solid Density	rs	lb/ft^3	1498.32		2400	kg/m^3
20	Static Bed Height	H_{sb}	ft	3.94	Assuming value	1.2	m
21	Voidage of Static Bed	e_{sb}		0.42	Assuming value	0.42	
22	Inventory in Static Bed	W_{insb}	lb	268.56		121.82	kg
23	Solid Height in Standpipe	H_{sp}	ft	8.20	Assuming value	2.5	m
24	Invetory in Standpipe	W_{insp}	lb	99.60		45.18	kg
25	Total inventory	W_{in}	lb	368.16		167.00	kg
26	Time Needed per cycle	t_{sc}	min	4.19		4.19	min

Table 2. Calculation on System Heat Balance

Calculation for CFBC Design							
5. Overall Heat Balance of CFBC's Furnace (Dense and Dilute Zones, 1st and 2nd Cyclones, and Standpipe)							
No.	Name	Symbol	Unit (E)	Value (E)	Calculation	Value (SI)	Unit (SI)
1	Coal Consumed Rate	R	lb/h	175.74		79.72	kg/h
2	CFBCThermal Input	Q	Btu/s	569.04	Set by proposal (input)	600	kWth
3	Coal Heat	H	Btu/lb	11650	KY bituminous coal (S=3.69%)	27096.01	kJ/kg
4	Heat Loss from Dense Zone	Q_{hldz}	Btu/hr	6135.64	592.59	1806.22	W
5	Heat Loss Ratio	y_{hldz}	%	0.30		0.30	%
6	Heat Loss from 1st Dilute Z.	Q_{hlf1}	Btu/hr	20858.96	760.22	6140.48	W
7	Heat Loss Ratio	y_{hlf1}	%	1.02		1.02	%
8	Heat Loss from 2nd Dilute Z.	Q_{hlf2}	Btu/hr	22036.86	760.13	6487.23	W
9	Heat Loss Ratio	y_{hlf2}	%	1.08		1.08	%
10	Heat Loss from 1st Cyclone	Q_{hlpc}	Btu/hr	8147.54	894.21	2398.48	W
11	Heat Loss Ratio	yhlpc	%	0.40		0.40	%
12	Heat Loss from Standpipe	QhlD	Btu/hr	21043.49	348.61	6194.80	W
13	Heat Loss Ratio	ydhl	%	1.03		1.03	%
14	Heat Loss from 2nd Cyclone	Q_{hlsc}	Btu/hr	5278.64	695.21	1553.93	W
15	Heat Loss Ratio	y_{hlsc}	%	0.26		0.26	%
16	Heat Loss from Standpipe	Q_{hlD}	Btu/hr	21043.49		6194.80	W
17	Enthaply of Flue Gas	I_g	Btu/lb.coal	4160.59		9670.56	kJ/kg.coal
18	Enthalpy of Inlet Flue Gas	I_g	Btu/lb.coal	4160.59		9670.56	kJ/kg.coal
19	2nd Cyc.Out. Temp. of F. G.	T_{sc}	oF	1292		700	°C
20	Heat carried by soilds	Hsl	Btu/h	10594.42		11169.66	kJ/h
21	Heat carried by Coal + Lime.	H_{ins}	Btu/h	2052379.55		2163816.08	kJ/h
22	Heat carried by disch. Solid	H_{ods}	Btu/h	9792.55		10324.25	kJ/h
23	Heat carried by Total Air	H_{ait}	Btu/h	21365.97		22526.06	kJ/h
24	Total Heat Absorbed	H_{abt}	Btu/s	335.45		353.66	kW
25	Ratio of Absorbed heat	j_{cfb}	%	58.94		58.94	%
26	Ash Temp. at ESP	T_{aes}	oF	392	Assuming value	200	°C
27	Weight of Ash Entering Zone	W_{at}	lb	37.17		16.86	kg
28	Heat Loss Ratio in This Zone	j_{hlt}	%	3	Assuming value	3	%
29	Total Heat Lost in This Zone	H_{hlt}	Btu/s	4796.10		5057.57	W
30	Heat Loss by exhaust flue gas	Q_{2hl}	Btu/s	43212.59		45.55	kW
31	Ratio of Flue Gas Heat loss	j_{2hl}	%	7.59		7.59	%
32	Ratio of Dis. Ash. Heat Loss	jhld	%	0.48		0.48	%
33	Ratio of Heat Loss in Furnace.	j_{dhl}	%	4.10		4.10	%
34	Heat carried by soilds	H_{sl}	Btu/h	2711.07		2858.28	kJ/h
35	Total Heat Absorbed	H_{abt}	Btu/s	154.35		162.73	kW
36	Ratio of Absorbed heat	H_{cfb}	%	27.12		27.12	%
37	Ratio of Solids Heat Loss	j_{51d}	%	0.13		0.13	%
38	Total Ratio	j	%	99.21		99.21	%
39	Total H. L. Ratio of Dis. Solid	j_5	%	0.61		0.61	%

Table 3. Design Parameter – Overall Hydrodynamics Calculation

Calculation for CFBC Design - 3. Overall Hydrodynamics							
No.	Name	Symbol	Unit (E)	Value (E)	Calculation	Value (SI)	Unit (SI)
3	Combustion Efficiency	h	%	100	Assuming value	100	%
4	Coal Consuming Rate	R	lb/h	175.74	79.72	79.72	kg/h
5	Bed Temperature	Tbed	°F	1562	Assuming value	850	°C
6	Excess Air Factor	a		1.2	Assuming value	1.2	
7	Air Required by 1lb Coal	Vo	ft^3/lb	137.18		8.56	m^3/kg
8	Total Needed Air	Vt	ft^3/h	24108.43	682.674105	682.67	m^3/h
9	Primary Air Ratio	a1		0.65	Assuming value	0.65	
10	Primary Air Flowrate	V1	ft^3/h	15670.48	15670.48	443.80	m^3/h
11	Secondary Air Flowrate	V2	ft^3/h	8437.95	8437.95	238.97	m^3/h
15	Gas Superfical Velocity	$U_0(850)$	ft/s	22.81	6.95	6.95	m/s
16	Total Flue Gas Flowrate	Q_f	ft^3/h	26098.51		739.03	m^3/h
17	Avg. Particle Diameter	d_p	in	0.03		0.8	mm
18	Bubble Cap Hole Air Velocity	U_h	ft/s	154.30		47.03	m/s
19	Pressure Drop of Distributor	DP_d	bar	2.67		267.06	Pa
20	Superfical Velocity in D.Z.	U(850)	ft/s	22.81		6.95	m/s
21	Superfical Velocity in F1	$U_{f1}(825)$	ft/s	20.70		6.31	m/s
22	Superfical Velocity in F2	$U_{f2}(825)$	ft/s	23.00		7.01	m/s
23	Gas Residence Time in De-Z	t_1	s	0.44		0.44	s
24	Gas Residence Time in F1	t_{f1}	s	1.28		1.28	s
25	Gas Residence Time in F2	t_{f2}	s	1.22		1.22	s
26	Total Residence Time	t	s	2.94		2.94	s
27	Bed Temperature in Dilute Z.	Tfz	oF	1517		825	oC
28	Velocity of 2nd Air in Duct	V_{2a}	ft/s	25.67	7.82	7.82	m/s
29	Velocity of 2nd Air in Nozzle	V_{2an}	ft/t	47.40	14.45	14.45	m/s
30	Theoretical Air Volume	Vo	ft3/lb	114.32		7.14	m^3/kg
31	Theoretical Flue Gas Volume	V_{0g}	ft3/lb	125.27		7.82	m^3/kg
32	Real Flue Gas Volume	V_g	ft3/lb	148.50	9.27	9.27	m^3/kg
33	Min. Fluidization Velocity	$U_{mf}(850)$	ft/s	0.80	Eqn. 2.3 (Basu)	0.24	m/s
34	Initial Turbulent Velocity	$U_{it}(850)$	ft/s	19.26	Eqn. 2.10 (Basu)	5.87	m/s
35	Terminal Velocity	$U_t(850)$	ft/s	23.18	39.07	7.07	m/s
36	Transport Velocity	$U_{tr}(850)$	ft/s	32.65	Eqn. 2.14 (Basu)	9.95	m/s

The designed CFBC system is designed to operate at the ambient pressure and temperature at the dense bed of 850°C with a full-load thermal capacity at $0.6MW_{th}$. Over-fire combustion operation makes the primary air ratio at 65%, and the secondary air ratio at 0.35 (Staged 1 secondary air of 25% and the Stage 2 secondary air of 10%). The excessive air will be controlled at a ratio of 1.2. Based on this assumption, the total air inventory is 682.8 M^3/hr. Based on hydrodynamics calculations and a selected particle size of coal (0.8 mm), the total pressure drop is calculated to be 22905 Pa. Therefore, an air compressor was selected to supply the primary air and secondary air. Approximate heat losses from the surface, flue gas stream and discharging ash are 10%, thus, the duties of all heat exchangers are about 90%. The majority of heat transfer surface is in the riser. The design temperatures of the cyclones are approximately 700°C. The flue gas exit temperature is approximately 160°C. This CFBC system will be operated at an ash

recirculation rate with variation between 2 (low recirculation rate) to 40 (high recirculation rate).

The final dimensions of CFBC system are summarized in Table 5. Two sections in the riser have two diameters, 0.3048 m at the dense bed (3.048 m in height) and 0.3874 m at the dilute bed (16.6116 m in height). There are two sections left for the transition (0.4572 m in height) between dense bed and dilute bed, and the thermal expansion joints (0.9144 in total height, 3 pieces). The diameter for the stand pipe is 0.1286 m. Therefore, the total height of CFBC system is 20.4216m. The critical parameters of the cyclones are 0.5969 m in diameter of the primary cyclone and 0.4953 m for the secondary cyclone. There are 30 bubble caps setup for the primary air with each cap diameter having 4.5 mm (totally 6 holes on each cap). There are three layers of secondary air setup, nozzles each having diameter is about 0.0266 m. The detailed schematic of 0.6 MW_{th} CFBC system is shown in Figure 1 and Figure 2.

Table 4. Summary of Design Parameters

Calculation for CFBC Design - 1. Calculation Summary of CFB Combustor							
No.	Name	Symbol	Unit (E)	Value (E)	Calculation	Value (SI)	Unit (SI)
1	Total Solid Inventory in Bed	W	lb	375.39		170.28	kg
2	Avg. Solid Con. Inside Bed	C_s	lb/ft^3	13.73		78.15	kg/m3
3	Total Heat Loss	Q_{loss}	Btu/min	47853.56		29638.71	W
4	Percentage of Heat Loss	y_{loss}	%	4.94		4.94	%
5	Total Heat Sucked by H.E.S.	Qeh	Btu/min	8332.12		547.34	W
6	Percentage of absorbed Heat	yeh	%	91.22		91.22	%
7	Bed Temperature in Dense Z.	Tdz	oF	1562		850	°C
8	Total Needed Air	Vt	ft^3/h	24108.43		682.76	m^3/h
9	Total Flue Gas	Q_{2f}	ft^3/h	26098.51		739.03	m^3/h
10	Flue Gas Temp. at Exit	T_{exit}	°F	320		160	°C
11	Total Bed Pressure Drop	DPb	Bar	229.05		22904.64	Pa
12	Total Pressure Drop	DP_T	Bar	231.72		23171.71	Pa
13	Solid Recirculation Flowrate	R_S	lb/h	5272.26		2391.50	kg/h
14	Each element height	h_0	ft	5		1.524	m
15	Bed I. D. in Dense Zone	d_{id}	in	12		0.3048	m
16	Bed I. D. in Dilute Zone	d_{if}	in	15.25		0.38735	m
17	Heat Loss of Exhaust Gas	Q_{2hl}	Btu/s	43212.59		45.55	kW
18	Ratio of Flue Gas Heat loss	j_{2hl}	%	7.59		7.59	%
19	Heat Loss of discharged Ash	H_{ds}	Btu/s	3.47		3.66	kW
20	Total H. L. Ratio of Dis. Solid	j_6	%	0.61		0.61	%
21	Sum of Heat Ratio	j	%	99.21		99.21	%
22	Temp. in 1st Sect of Dilute Z.	T_{f1}	°F	1517		825	°C
23	Temp. in 2nd Sect of Dilute Z.	T_{f2}	°F	1517		825	°C
24	Temperature in 1st Cyclone	T_{pc}	°F	1382		750	°C
25	Temperature in 2nd Cyclone	T_{sc}	°F	1292		700	$_o$C
26	Temperature in Standpipe	T_{sp}	°F	1292		700	°C
27	CFBC Thermal Input	Q_{in}	Btu/s	569.04	Set by proposal (input)	0.6	MWth
28	CFBC Thermal Output	Q_{out}	Btu/s	519.10		0.55	MWth
29	Combus. Fraction in Dense-Z	d_1		0.65	Assuming value	0.65	
30	Combus. Fraction in F1	d_{21}		0.25	Assuming value	0.25	
31	Combus. Fraction in This Zone	d_{22}		0.1		0.1	
32	Primary Air Ratio	a1		0.65	Assuming value	0.65	
33	Secondary Air Frac. In F1	a21		0.25	Assuming value	0.25	
34	Secondary Air Frac. In F2	a_{22}		0.1		0.1	
35	Excess Air Factor	a		1.2	Assuming value	1.2	
36	Avg. Particle Diameter	dp	in	0.03	Assuming value	0.8	mm
37	Fraction of Solid Discharged	qcd		0.7	Assuming value	0.7	
38	Solid Recirculation Ratio	g		30	In the range of 2~40 (RS/CA)	30	

Table 5. Dimension of CFBC System

Calculation for CFBC Design - 2. Dimension of CFBC Facility							
No.	Name	Symbol		Value (E)	Calculation	Value (SI)	Unit (SI)
1	I.D. in Dense Zone	d_{idz}	in	12		0.3048	m
2	O.D in Dense Zone	d_{odz}	in	12.75		0.3239	m
3	Height of Dense Zone	h_{dz}	ft	10		3.0480	m
4	I.D. in Dilute Zone	d_{if}	in	15.25		0.3874	m
5	O.D in Dilute Zone	d_{of}	in	16		0.4064	m
6	Total Height of Dilute Zone	h_f	ft	54.5	including the transition section	16.6116	m
7	Heigh of Transition Section	h_{tr}	ft	1.5		0.4572	m
8	Height of Windbox	h_{iw}	ft	2.5		0.7620	m
9	I.D. of Windbox	d_{iw}	in	12		0.3048	m
10	O.D. of Windbox	d_{ow}	ft	12.75		0.3239	m
11	Height of 1st Sec. in Dilute Z.	h_{f1}	ft	26.5	Dilute Z. is divided into 2 sections	8.0772	m
12	Height of 2nd Sec. in Dilute Z.	h_{f2}	ft	28	for heat balance and transfer cal.	8.5344	m
13	Height of Thermal Expansion Joint	h_{te}	ft	3		0.9144	m
14	I.D. of Standpipe	d_{isp}	in	5.063		0.1286	m
15	O.D. of Standpipe	d_{osp}	in	5.563		0.1413	m
16	I.D. of Coal Feed Pipe	d_{ic}	in	2.5		0.0635	m
17	O.D.of Coal Feed Pipe	d_{oc}	in	3		0.0762	m
18	I.D. of Ash Discharge Pipe	d_{ia}	in	1.278		0.0325	m
19	O.D. of Ash Discharge Pipe	d_{oa}	in	1.66		0.0422	m
20	I.D. of Air Inlet Pipe	d_{iai}	in	3.5		0.0889	m
21	O.D. of Air Inlet Pipe	d_{oai}	in	4.5		0.1143	m
22	Total Height of CFBC	h	ft	67		20.4216	m
23	I.D. in Primary Cyclone	d_{ipc}	in	23.5		0.5969	m
24	O.D in Primary Cyclone	d_{opc}	in	24		0.6096	m
25	Height of Straigtht Section	h_{spc}	ft	4		1.2192	m
26	Height of Cone Section	h_{cpc}	ft	4		1.2192	m
27	I.D. of Outlet Pipe	d_{iopc}	in	12		0.3048	m
28	O.D. of Outlet Pipe	d_{oopc}	in	12.75		0.3239	m
29	Cone Angle of Primary Cycl.	a_{pc}	o	11		11.0000	o
30	Leg pipe Inside diameter	d_{inspp}	in	5.047		0.1282	m
31	I.D. in Seconday Cyclone	d_{isc}	in	19.5		0.4953	m
32	O.D in Secondary Cyclone	d_{osc}	in	20		0.5080	m
33	Height of Straigtht Section	h_{ssc}	in	40		1.0160	m
34	Height of Cone Section	hcsc	ft	40		1.0160	m^2
35	I.D. of Outlet Pipe	d_{iosc}	in	10.25		0.2604	m
36	O.D. of Outlet Pipe	d_{oosc}	in	10.75		0.2731	m
37	Cone Angle of Secondary Cycl.	asc	o	11		11.0000	o
38	Leg pipe Inside diameter	d_{insps}	in	3.548		0.0901	m
39	Height of Standpipe	h_{sp}	ft	53		16.1544	m
40	I.D. of Seconday Air Pipe	d_{sai}	in	2.469		0.0627	m
41	O.D. of Secondary Air Pipe	d_{sao}	in	2.875		0.0730	m
42	I.D. of S. Air Nozzle	dani	in	1.049		0.0266	m
43	O.D. of S. Air Nozzle	d_{ano}	in	1.315		0.0334	m
44	Number of S. Air Duct	N		3	Total 3 layers	3	
45	Number of S. Air Nozzle	n		9	Each layer has 3 nozzles	9	
46	Number of Bubble Caps	N		30	Structure data	30	
47	Hole diameter on Cap	d_H	in	0.1772	Structure data	4.5	mm
48	Hole Number on Cap	n		6	Structure data	6	

Figure 1. Schematic of 0.6 MW_{th} CFBC System

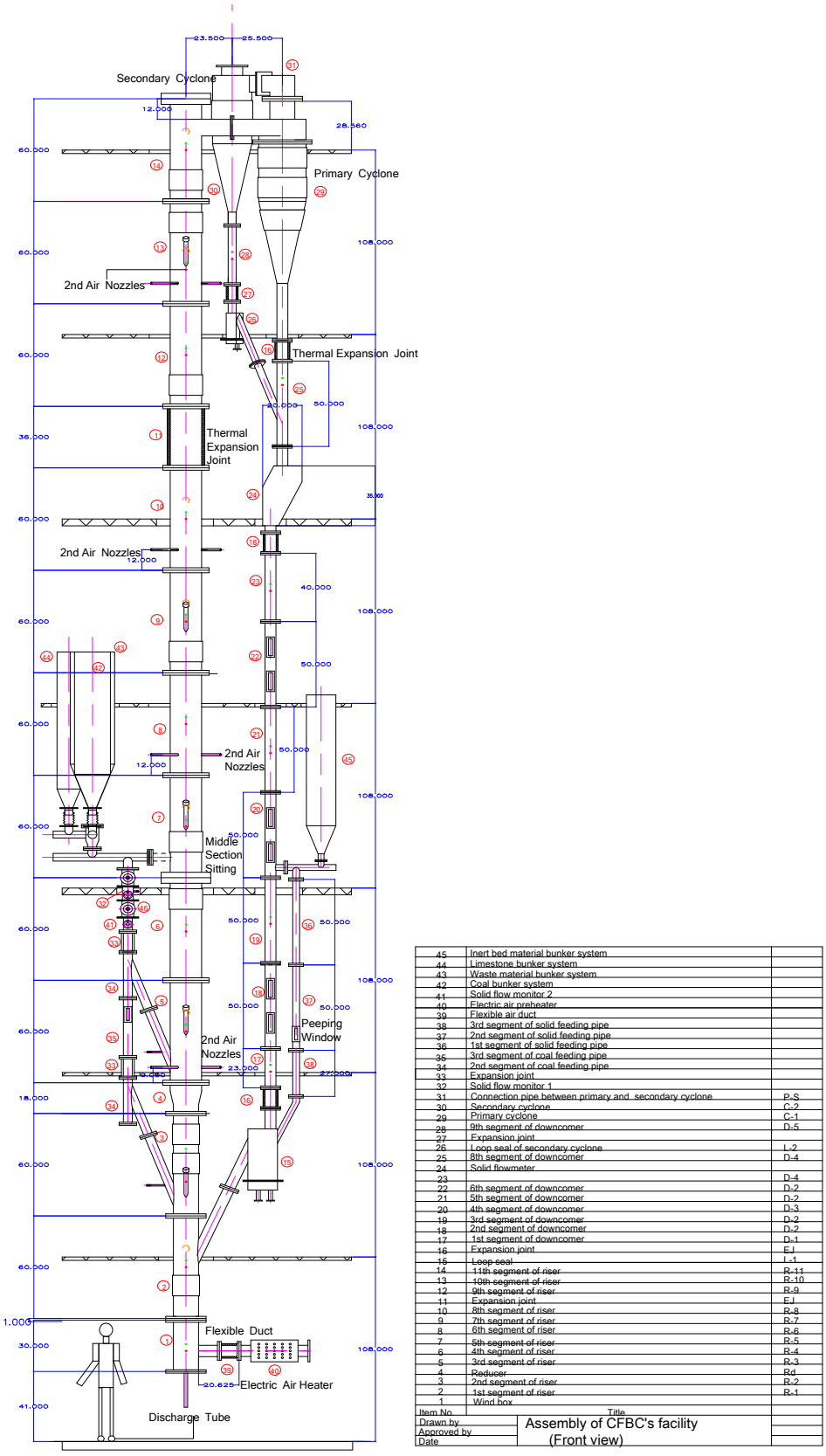

45	Inert bed material bunker system	
44	Limestone bunker system	
43	Waste material bunker system	
42	Coal bunker system	
41	Solid flow monitor 2	
40	Electric air preheater	
39	Flexible air duct	
38	3rd segment of solid feeding pipe	
37	2nd segment of solid feeding pipe	
36	1st segment of solid feeding pipe	
35	3rd segment of coal feeding pipe	
34	2nd segment of coal feeding pipe	
33	Expansion joint	
32	Solid flow monitor 1	
31	Connection pipe between primary and secondary cyclone	P-S
30	Secondary cyclone	C-2
29	Primary cyclone	C-1
28	9th segment of downcomer	D-5
27	Expansion joint	
26	Loop seal of secondary cyclone	L-2
25	8th segment of downcomer	D-4
24	Solid flowmeter	
23		D-4
22	6th segment of downcomer	D-2
21	5th segment of downcomer	D-2
20	4th segment of downcomer	D-3
19	3rd segment of downcomer	D-2
18	2nd segment of downcomer	D-2
17	1st segment of downcomer	D-1
16	Expansion joint	E-J
15	Loop seal	L-1
14	11th segment of riser	R-11
13	10th segment of riser	R-10
12	9th segment of riser	R-9
11	Expansion joint	E-J
10	8th segment of riser	R-8
9	7th segment of riser	R-7
8	6th segment of riser	R-6
7	5th segment of riser	R-5
6	4th segment of riser	R-4
5	3rd segment of riser	R-3
4	Reducer	R-t
3	2nd segment of riser	R-2
2	1st segment of riser	R-1
1	Wind box	
Item No.	Title	
Drawn by	Assembly of CFBC's facility (Front view)	
Approved by		
Date		

Figure 2. Schematic of CFBC System with Critical Parts Labeled

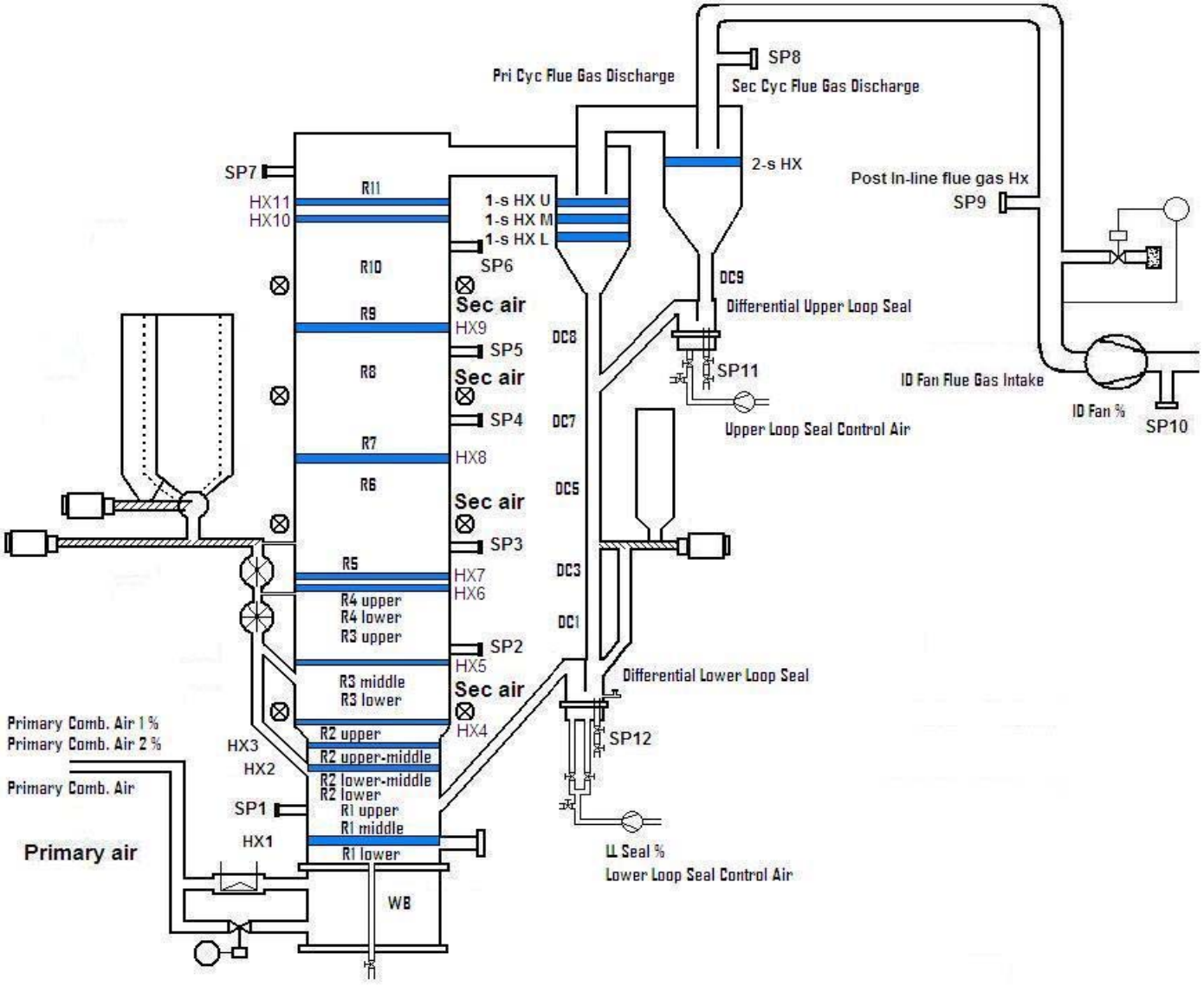

3.2 CFBC System Tower

A. Structure's General Description. The CFBC system is primarily housed in an 87-foot tall insulated, steel framed, steel-sided building comprised of seven steel grate floors, a concrete ground floor and a small mezzanine. The Tower is equipped with a fire suppression sprinkler system and with emergency lighting. An internal stairway is provided at the south side of the tower from ground level to the eighth floor with ladder access to the mezzanine. Two double-wide personnel doors lead outside from the tower and one personnel door leads to the remainder of the Combustion Laboratory and to the CFBC System Control Room.

B. Utilities. The Tower is provided with extensive electric power distribution equipment, including 120/240 volt single phase and 208 volt and 480 volt three phase services. Many of the circuits are backed-up, in case of a utility power interruption, with an 80 KW natural gas powered generator set. Each level of the Tower is well lighted with a minimum of eight 90 watt HID lighting fixtures. The Tower has municipal water supply, as well as waste water drains, furnished through the sixth floor. Natural gas service is available on the ground floor. Dehydrated and well-filtered compressed air, produced in an adjacent mechanical room of the Combustion Laboratory, is distributed to a minimum of four outlets on each level of the tower. Wireless internet is also provided throughout the tower, as well as, throughout the entire Combustion Laboratory.

C. Heating and Ventilation. No air conditioning is provided in the Tower. To prevent winter freezing of water-containing systems, adequate heat is provided by fan coil unit ventilators at the ground floor level. Ventilation is accomplished with four thermostatically controlled exhaust fans, each rated at 30,000 cubic feet per minute, located near the apex of the building and six motorized louvers to the outside at the second floor level.

D. Materials Movement Crane. Presently, a guard rail enclosed lift-way opening of about six feet by eight feet is located on each floor for transporting bulk quantities of fuel, bed material and ash, as well as, components required for additional CFBC construction and maintenance. A 1½ ton bridge crane, used extensively for initial combustor assembly when a 20-foot square central opening was available, is now used to transport a cargo basket or individual components from one level to another in the Tower.

E. Dust Control. A 7½-HP dust collector system is located on the fifth floor of the tower adjacent to the fuel and bed material bunker tops. This arrangement greatly reduces the escape

of dust when replenishing these supply bunkers, making for a safer and cleaner work environment.

3.3 Air Supply

3.3.1 Primary Air

A. Regenerative Blowers. Two 21-HP regenerative turbine blowers provide primary combustion air to the combustor through a six-inch supply duct from an adjacent mechanical room. Each of these blowers can furnish up to 154 inches of water column pressure and together will, as presently configured, provide up to 48 pounds per minute of primary combustion air to the CFBC system.

B. Bed Preheater. Prior to the primary combustion air being admitted to the windbox, a six inch pneumatically-operated butterfly valve is used to route the combustion air exclusively through a 36-KW electric air heater capable of increasing the temperature of the flowing air up to 1,500 ºF. The air heater is locally controlled as to temperature and incorporates redundant safety controls to reduce the risk of equipment damage or fire in case of insufficient air flow. The high temperature air flow is able to heat the lower riser segments and an initial charge of bed material (typically 175 pounds of crushed limestone) to the kindling point for coal in about four hours or less.

C. Windbox. The windbox, as shown in Figure 3, serves as an air plenum at the bottom-most segment of the CFBC system. It receives primary combustion air either directly from the forced draft fan and supply duct during normal operation or by way of the bed preheater during start-up. The windbox is insulated to the same extent as the riser in order to maintain the temperature during preheating operations.

E. Bubble Plate. The one-inch thick bubble plate serves to separate the primary combustion air supply from the bed area where the initial fuel combustion occurs. Also known as a distributor plate, the bubble plate provides the mounting for 30 bubble caps, arranged in three concentric circles. The design of these bubble caps, along with their placement and the ‘bowl’ shaped area below them, help distribute the combustion and fluidizing air in such a manner as to uniformly fluidize the bed material.

3.3.2 Secondary Air

A. Regenerative Blower. A 15-HP regenerative turbine blower located on the fifth floor of the tower provides all secondary combustion air supplies for the combustor. This blower is capable of furnishing up to 195 inches of water-column pressure to the secondary air distribution system with a total flow capacity of 15 pounds of air per minute. Operation of this blower is controlled by the process control computer.

B. Secondary Combustion Air Distribution. Secondary combustion air produced by the regenerative blower is supplied to a manifold that distributes pressurized air to as many as four levels of the combustor for controlled injection at these levels, as shown in Figure 3.

C. Proportional Air Control Valves. Secondary Combustion Air may be delivered to a set of three ports and nozzles arranged to establish a control clockwise rotation of the ascending flue gases at up to four levels of the riser, namely R3, R6, R8 and R10, as indicated in Figure 2. Provided that a minimum pressure is maintained by the secondary air blower, solenoid valves are opened at one, two, three or four levels and the proportional valve for that level opens as required to allow the selected quantity of air flow and to be injected. Secondary air flow quantities are selected at the user interface and the proportional valves are closed-loop controlled to maintain the selected rate.

D. Ash Back-flow Prevention. Unwanted ash back-flow into valves, supply ducts and blowers are of significant concern in that ash back-flow can cause these components to malfunction. Therefore, if secondary air is supplied to any level(s) of the riser, protective solenoid valves will only open when the secondary air blower provides sufficient pressure to insure ash cannot back-flow into unwanted areas. This serves to protect both the solenoid valves and proportional valves in the secondary air supply system.

E. Solenoid Valves Excess Temperature Protection. Brought about by the need to protect components of the secondary air supply system from ash back-flow, solenoid valves have been installed at each of the three ports at each of the four levels used for secondary air injection. As these valves are close to the riser and subject to excess temperatures, they are periodically pulsed with a small amount of cooling air to insure their continued function and reliability.

3.3.3 Induced Draft Fan and Flue Gas Path

A. Flue Gas Duct. Ten-inch schedule 10 stainless steel pipe and fittings are used to connect the secondary cyclone discharge on the eighth floor to the induced draft fan on the seventh floor of the Tower, as shown in Figure 3.

B. Induced Draft Fan. Located on the seventh floor of the Tower is induced draft fan. This fan is equipped with a 20-HP motor and variable speed drive that operates under programmed control. This fan is capable of producing more than 20 inches of water column differential pressure at operating temperatures and inlet pressure conditions. Components of the fan in contact with the flue gas stream are constructed of 304 stainless steel and rated for operation at temperature up to 700ºF. A tempering stream of ambient air may be admitted by operating a motorized valve near the fan intake if flue gas temperature should become excessive. Control of this valve is accomplished at the user interface. Ordinarily, the induced draft fan is operated to maintain minus 0.5 inches water column static pressure in the top-most riser segment.

C. Discharge Flue Gas Camera. Aimed at the flue gas discharge duct as it exits the Tower wall on the seventh floor is a video camera that displays on a monitor in the CFBC system control room an image of flue gas and any particulate emissions. The images of these emissions provides additional information about CFBC system operation, particularly during start-up periods until on-line flue gas analysis is available.

Figure 3. Pictures of Air Delivery and Flue Gas Pass

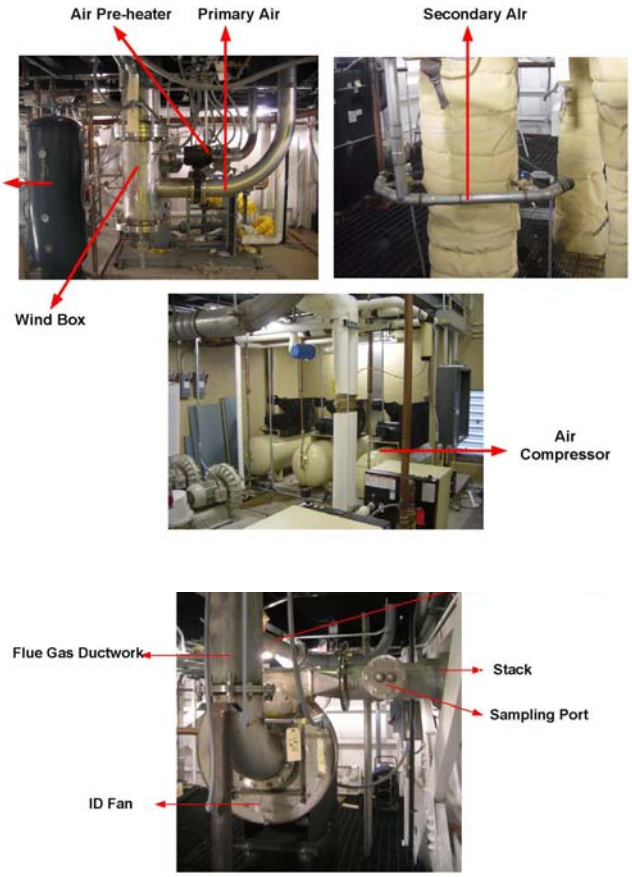

3.4 Riser, Ash Recovery Cyclones, Downcomer and Loop Seals

The design parameters on cyclones and loop seal were listed in Tables 6-1, 6-2, and Table 7. Figure 4 are pictures of their on-site setup.

A. Construction Materials. All structural portions of the CFBC system that come into contact with heated bed material, ash and flue gases are fabricated from welded seam, 310 stainless steel, schedule 40 pipe. Class 150 weld flanges are used to join most segments of the riser, downcomer and cyclones. Class 300 weld flanges are used at points of support for the riser. High temperature Grafoil® gaskets are used at each of these flanges to insure gas tight connections.

B. Support Point. As 310 stainless steel alloy has a large thermal expansion coefficient, special design considerations were employed to avoid structural support problems. The Tower building structural framing supports the riser at only two points. Riser segments R1, R2, R3 and R4 (as indicated in Figure 2), as well as, the transition segment (12" to 16") and the windbox segment are suspended from the forth floor. As these segments are heated to the operating temperature, the bottom-most windbox approaches the ground floor level by approximately four inches. Additionally, the fourth floor frame also supports riser segments R5, R6, R7 and R8 (as indicated in Figure 2), which expand upward as they approach the operating temperature. Riser segments R9, R10 and R11 (as indicated in Figure 2), supported at the eighth floor of the tower, expand downward with increased temperature.

C. Thermal Expansion Joints. This latter thermal expansion of riser segments supported between the fourth and eighth floor is accommodated by a thermal expansion joint located between riser segment R8 and R9 (as indicated in Figure 2). This joint is constructed with an interior telescoping construction designed to maintain alignment of the column of risers. This joint is fitted with programmed purge air to reduce ash accumulation, which otherwise would interfere with its required freedom of movement. Additionally, there are a total of nine conventional expansion joints located throughout the downcomer segments, fuel supply ducts and the primary combustion air duct, in order to accommodate the temperature induced displacements of these components.

D. Loop Seals. The CFBC system employs two loop seals. The upper loop seal is located below the secondary cyclone and is provided to reduce the possibility of unwanted circulation of ash between the primary and secondary cyclone discharges. Only a smaller quantity of ash

accumulates below the secondary cyclone. The lower loop seal receives ash from both primary and secondary cyclones through the downcomer and controls overall recirculation of this ash back to the R1 riser segment (as indicated in Figure 2). Each loop seal has control air provided by individually regenerative blowers by computer.

E. Viewing Ports. There are five inclined viewing ports on the riser segments. These ports are equipped with round quartz windows and preheated purge air supplies. The lowest most riser port has proven effective for observing the action on the bed surface and of the combustion process. A video recording can be made from this view. Distributed along the downcomer is a total of six rectangular quartz windows beginning approximately 24-feet above and extending to within 5 feet of the lower loop seal. Purge air is applied to these windows as well. These windows have provided important information on ash flow and ash height in the downcomer segments. Additionally, there is a rectangular quartz window in the ash supply duct to monitor the ash level used to precharge the lower loop seal. Finally, there is a rectangular quartz window in the fuel supply duct and two pairs of round quartz windows below each rotary air-lock valve for a fuel flow subsystem.

F. Insulation. The complete riser segments, both cyclones, both loop seals and the entire downcomer segments are encased with a combination of high temperature, high performance insulation components. Except in areas where heat exchanger jackets are present, the exterior surfaces listed above may reach temperatures in excess of 1,800ºF. Therefore, careful inspections and material selection of insulation components were needed. An important goal of the insulation system installation was to not only limit the unwanted loss of heat from all areas of the process operation, but also to limit the potential exposure of personnel to nuisance or hazardous materials and to dangerously high temperatures during normal combustor operations.

G. Ash/Combustion Gas Sampling Ports. There are ten, 3-inch ports along the riser and flue gas duct on the path to the induced draft fan intake that can accommodate sample probes. These sample probe are capable of collecting ash and gas samples from the combustion process. Each of these sample ports has a nearby temperature and pressure sensor for data acquisition. Also, cooling water supply and returns are provided near each sampling port location for those occasions when probe cooling is required. Additionally, a port on the upper most riser segment, R11 (as indicated in Figure 2), has been installed to provide a filtered and dehydrated gas sample to an IMR 5000 flue gas analyzer. This analyzer has been interfaced with the data acquisition and

process control computer, providing an on-line display of carbon monoxide and oxygen concentration at the user interface. Ash samples may also be taken from each loop seal and from the bottom of the bed area during regular operation.

Figure 4. Pictures of Loop Seals, Ash Supply, Downcomer and Cyclones

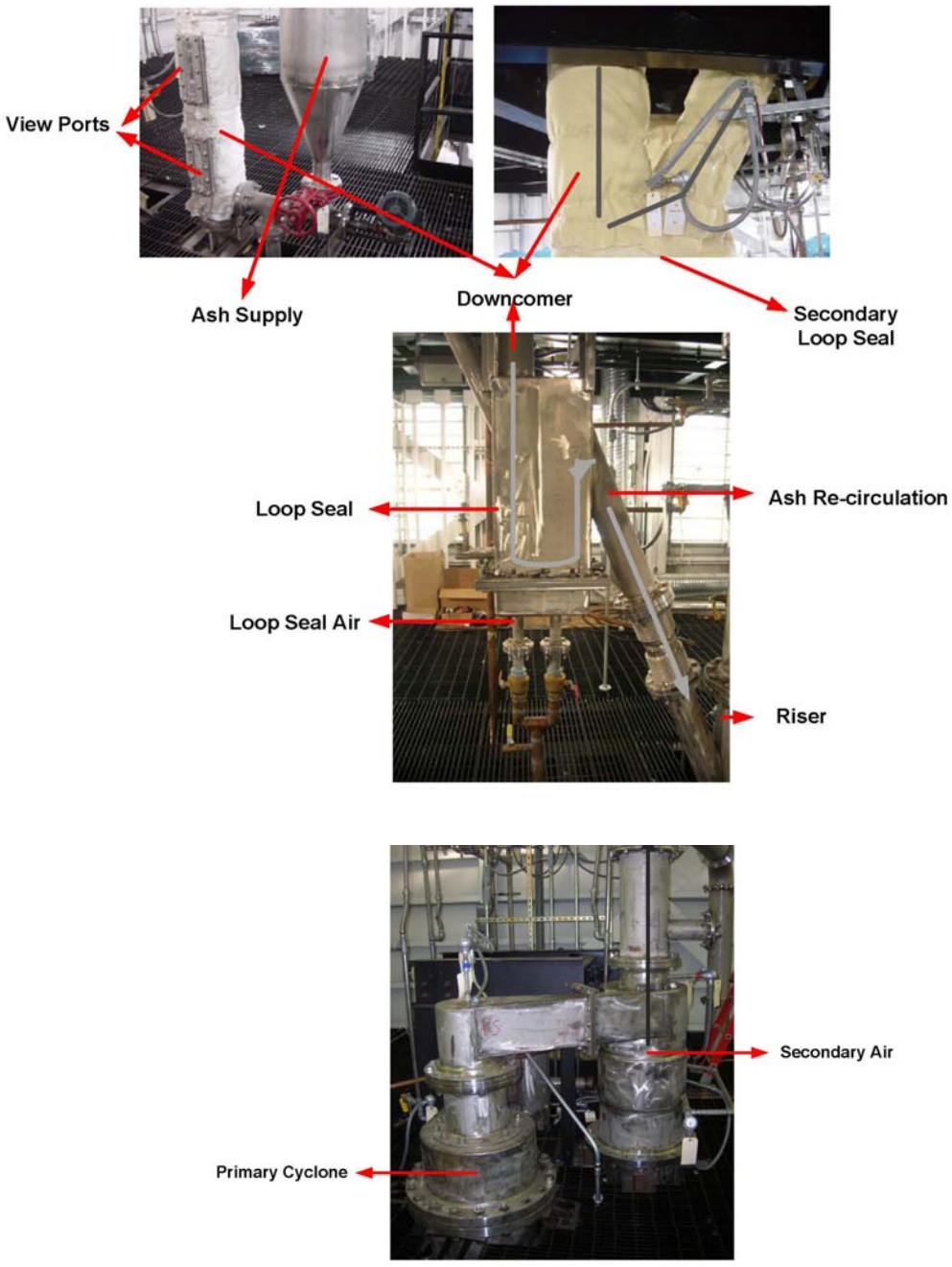

Table 6-1. Design Calculation on the Primary Cyclone

Calculation for Cyclone Design - 7. Calculation of Primary Cyclone							
No.	Name	Symbol	Unit (E)	Value (E)	Calculation	Value (SI)	Unit (SI)
1	Cyclone inside diameter	d_c	inch	23.5	O.D.24", I.D. 23.5"	0.5969	m
2	Cyclone height (straight sect.)	h_s	inch	48	47	1.2192	m
3	Outlet tube inside diameter	d_{io}	inch	12	I.D. 12.0", O.D. 12.75"	0.3048	m
4	Depth of outlet tube	h_o	inch	15	1.62	0.381	m
5	Inside Width of Inlet	w	inch	4.75	5.875	0.12	m
6	Inside Height of Inlet	h_i	inch	9.25	11.75	0.23	m
7	Dipleg tube diameter	d_d	inch	5.047	I.D. 5.047", O.D. 5.563"	0.13	m
8	Height of cone sectiion	h_c	inch	48		1.2192	m
9	Flue gas velocity at inlet	V_{i0}	ft/s	98.43	Choose based on experience	30	m/s
10	Real Flue gas velocity at inlet	V_i	ft/s	95.56	29.13	29.13	m/s
11	Total flue gas flowrate	Q_f	ft^3/h	26098.51		739.03	m^3/h
12	Inlet flue gas temperature	T_{inlet}	°F	1517		825	°C
13	Half angle of cone section	a	o	10.88		10.88	o
14	Total height of cyclone	h	inch	96	94	2.4384	m
15	Solid efflux rate of dipleg	W_s	lb/s	157.07	71.25	71.25	kg/s
16	Solid recirculation fowrate	R_s	lb/s	1.464516		0.66	kg/s
17	Effective No. of spiral turns	N_s		4.98	Check Fig. 7.4 (Basu) by Vi	4.98	
18	Flue gas density	r_g	lb/ft^3	0.02006958	0.32	0.32148361	kg/m^3
19	Flue gas viscocity	m_g	lb/ft.s	3.0161E-05		4.4883E-05	Pa.s
20	Cut diameter of particle	d_{th}	inch	0.00018581	separation efficiency=50%	4.71956309	mm
21	Calculated cyclone diameter	d	inch	18.18		0.46	m
22	Reynolds number in inlet	Re		33261.79		33261.79	
23	Required Cyclone Diameter	D_{CRE}	inch	18.47		0.47	m
24	Inlet Cross-Section Area	$A_{in'}$	ft^2	0.30		0.03	m^2
25	Real Inlet Cross Area	A_{in}	ft^2	0.31		0.03	m^2
26	Inlet Solid Concentration	C_{si}	lb/ft^3	2.03		3.26	kg/m^3
27	Outlet Solid Concentration	C_{so}	lb/ft^3	0.20		0.33	kg/m^3
28	Flue gas velocity at outlet	V_o	ft/s	37.14	11.32	11.32	m/s
29	Pressure Drop	DP_{pc}	lb/in^2	0.02	C=7.5~18.4	171.52	Pa
30	Parameter C	C	ft/s	7.84		2.39	m/s
31	Falling Velocity	U_f	ft/s	200.29	Vi<Uf, no entrainment	61.05	m/s
32	dp for 10% Separation Effic.	dp_{10}	in	5.7601E-05		1.46	mm
33	dp for 20% Separation Effic.	dp_{20}	in	8.3614E-05		2.12	mm
34	dp for 30% Separation Effic.	dp_{30}	in	0.00010777		2.74	mm
35	dp for 40% Separation Effic.	dp_{40}	in	0.00014679		3.73	mm
36	dp for 60% Separation Effic.	dp_{50}	in	0.00025084		6.37	mm
37	dp for 70% Separation Effic.	dp_{60}	in	0.00033446		8.50	mm
38	dp for 80% Separation Effic.	dp_{70}	in	0.00052027		13.21	mm
39	dp for 90% Separation Effic.	dp_{80}	in	0.00092905		23.60	mm
40	dp for 95% Separation Effic.	dp_{90}	in	0.00120776		30.68	mm
41	dp for 99% Separation Effic.	dp_{100}	in	0.00165371		42.00	mm

Table 6-2 . Design Calculation on the Secondary Cyclone

Calculation for Cyclone Design - 8. Calculation of Secondary Cyclone							
No.	Name	Symbol	Unit (E)	Value (E)	Calculation	Value (SI)	Unit (SI)
1	Cyclone inside diameter	d_c	inch	19.5	O.D.20", I.D. 19.5"	0.4953	m
2	Cyclone height (straight sect.)	h_s	inch	40	39	1.016	m
3	Outlet tube inside diameter	d_{io}	inch	10.25	I.D. 10.25", O.D. 10.75"	0.26035	m
4	Depth of outlet tube	h_o	inch	12	1.30	0.3048	m
5	Inside Width of Inlet	w	inch	4.75	4.875	0.12065	m
6	Inside Height of Inlet	h_i	inch	9.25	9.75	0.23495	m
7	Dipleg tube diameter	d_d	inch	3.548	I.D. 3.548", O.D. 4.000"	0.09	m
8	Height of cone sectiion	h_c	inch	40		1.016	m
9	Flue gas velocity at inlet	V_{i0}	ft/s	98.43	Choose based on experience	30	m/s
10	Real Flue gas velocity at inlet	V_i	ft/s	89.03	27.14	27.14	m/s
11	Total flue gas flowrate	Q_f	ft^3/h	26098.51		739.03	m^3/h
12	Inlet flue gas temperature	T_{inlet}	°F	1382		750	°C
13	Half angle of cone section	a	o	11.28		11.28	o
14	Total height of cyclone	h	inch	80	78	2.032	m
15	Solid efflux rate of dipleg	W_s	lb/s	1.07	0.49	0.49	kg/s
16	Solid fowrate	R_s	lb/s	0.14		0.06	kg/s
17	Effective No. of spital turns	N_s		4.84	Check Fig. 7.4 (Basu) by Vi	4.84	
18	Flue gas density	r_g	lb/ft^3	0.02	0.35	0.35	kg/m^3
19	Flue gas viscocity	m_g	lb/ft.s	0.00		0.00	Pa.s
20	Cut diameter of particle	d_{th}	inch	0.00019121	separation efficiency=50%	4.86	mm
21	Calculated cyclone diameter	d	inch	16.19		0.41	m
22	Reynolds number in inlet	Re		34683.97		34683.97	
23	Required Cyclone Diameter	D_{CRE}	inch	17.83		0.45	m
24	Inlet Cross-Section Area	$A_{in'}$	ft^2	0.28		0.03	m^2
25	Real Inlet Cross Area	A_{in}	ft^2	0.31		0.03	m^2
26	Inlet Solid Concentration	C_{si}	lb/ft^3	0.20		0.33	kg/m^3
27	Outlet Solid Concentration	C_{so}	lb/ft^3	0.01		0.02	kg/m^3
28	Flue gas velocity at outlet	V_o	ft/s	47.43	14.46	14.46	m/s
29	Pressure Drop	DP_{pc}	lb/in^2	0.03	C=7.5~18.4	204.07	Pa
30	Parameter C	C	ft/s	7.37		2.25	m/s
31	Falling Velocity	U_f	ft/s	194.69	Vi<Uf, no entrainment	59.34	m/s
32	dp for 10% Separation Effic.	dp_{10}	in	0.00		1.51	mm
33	dp for 20% Separation Effic.	dp_{20}	in	8.6045E-05		2.19	mm
34	dp for 30% Separation Effic.	dp_{30}	in	0.0001109		2.82	mm
35	dp for 40% Separation Effic.	dp_{40}	in	0.00015106		3.84	mm
36	dp for 60% Separation Effic.	dp_{50}	in	0.00025814		6.56	mm
37	dp for 70% Separation Effic.	dp_{60}	in	0.00034418		8.74	mm
38	dp for 80% Separation Effic.	dp_{70}	in	0.00053539		13.60	mm
39	dp for 90% Separation Effic.	dp_{80}	in	0.00095606		24.28	mm
40	dp for 95% Separation Effic.	dp_{90}	in	0.00124288		31.57	mm
41	dp for 99% Separation Effic.	dp_{100}	in	0.00170178		43.23	mm

Table 7. Design Calculation on the Loop Seal

Calculation for Loop Seal Design - 6. Calculation of Loop Seal							
No.	Name	Symbol	Unit (E)	Value (E)	Calculation	Value (SI)	Unit (SI)
1	Solid Recirculation Flowrate	G_s	lb/s	1.46		0.6643	kg/s
2	Cross Area of Standpipe	A_{sp}	ft^2	0.140		0.0130	m^2
3	Voidage in Standpipe	e_{sp}		0.50	Assuming value	0.5000	
4	Solid Density	r_s	lb/ft^3	1498.32		2400.00	kg/m^3
5	Required Standpipe Diameter	d_s	inch	3.22		0.1	m
6	Real Standpipe I.D.	d_{isp}	inch	5.06		0.13	m
7	Solid Velocity in Standpipe	$\varsigma\sigma$	ft/s	1.50	Vs <0.5m/s, Satisfication.	0.46	m/s
8	Calculated Standpipe I.D.	$\delta_{\sigma\chi}$	inch	1.48		0.04	m
9	Length of Loop Seal	L_{ls}	inch	12.66		0.322	m
10	Width of Loop Seal	W_{ls}	inch	6.33		0.16	m
11	Solid Velocity in H. Direction	V_h	ft/s	0.41	Choose from 0.25 to 0.05m/s	0.125	m/s
12	Temperature in Loop Seal	T_{ls}	oF	1292.00		700.00	°C
13	Height of Opening	$\eta_{o\varkappa}$	inch	1.0847	hop>10dpm, OK	0.0276	m
14	Maximum Particle Size	$\delta_{\varkappa\mu}$	inch	0.08		2.00	mm
15	Height of Loop Seal	H_{ls}	inch	15.00	Design data	0.38	μ
16	P. Drop through L.S. Bed	DP_{lsb}	lb/in^2	0.65		4485.13	Pa
17	Height of S. Recirculate Port	H_{srp}	ft	40.000	Design data	1.02	m
18	Bed Voidage in Dense Zone	e_{bed}		0.85		0.85	
19	Bed P. Drop under S. R. Port	DP_{srp}	lb/in2	2.15		14806.92	Pa
20	Pressure Difference	DP_{m-l}	lb/in2	1.50	Assuming same distributor P.Drop	10321.78	Pa
21	Minimum Fluidization Velocity	$\Upsilon_{\mu\phi}$	ft/s	0.86		0.26	m/s
22	Superficial Velocity in L.S.	U_0	ft/s	2.15	U_0=2.5Umf	0.65	m/s
23	Air Supply for Loop Seal	Q_{aTls}	ft^3/h	4299.50		121.75	m^3/h
24	Air Volume at T=273K	Q_a	ft^3/h	1206.33		34.16	m^3/h

3.5 Process Cooling, Heat Rejection and Water Treatment

System cooling is shown in Figure 5-1 and Figure 5-2.

A. Cooling Jacket Heat Exchangers. The riser segments of the CFBC system and both cyclones are constructed with a total of 15 heat exchangers of a cooling jacket or band type design. Riser segments R1, R4, R5, R7, R9, R10 and R11 (as indicated in Figure 2) are provided with a single heat exchanger. Riser segment R3 and the 12-inch by 16-inch transition joint segments were not initially equipped with heat exchanger, a new heat exchanger was installed after preliminary tests demonstrated a need for these additions. R2 is equipped with two heat exchangers; the primary cyclone has three heat exchangers and the secondary cyclone has one heat exchanger. All heat exchangers are 12 inches in height and vary in circumference according to the segment to which they are welded. Each heat exchanger is supplied with coolant through a solenoid valve and discharges through either a proportional valve for control of regular coolant recirculation or through a steam-rated solenoid valve used when a heat exchanger is taken off-line. At maximum design flow, each of these heat exchangers can capture up to

360,000 Btu per hour. Each coolant solenoid and proportional valve is controlled at the user interface.

B. Internal Loop Coolant Pumps. Coolant is pumped through the CFBC system heat exchangers described above by a 10-HP pump. This pump is capable of circulating more than 100 gallons per minute through the internal coolant loop. Upon discharge from each heat exchanger, coolant passes through a 240-gallon separator tank located on the mezzanine above the eighth floor of the Tower to insure that steam and dissolved gases are separated from the return flow. The internal loop pump is located on the ground floor of the Tower and is preceded by a 120-gallon still well tank. An identical back-up pump is arranged in parallel with the primary pump and a 2-HP single phase circulator pump, is also arranged in parallel with the other pumps, The back-up pump is to reduce the likelihood of serious damage to the combustor in case of pump failure. The status of all the pumps is available and is controlled at the user interface.

C. Coolant-to-Coolant Heat Exchanger. Part of the internal coolant loop is a liquid-to-liquid heat exchanger, which couples heat recovered from the combustor to an external cooling system.

D. External Loop Heat Rejection System. A heat rejection system consisting of a liquid-to-liquid heat exchanger, outdoor fan coils, expansion tank, circulator pump and controls is used to reject the heat load from the CFBC system operation. The coolant employed by this external heat rejection system is a propylene-glycol and water mixture. This heat rejection system is capable of rejecting more than 2 million Btu per hour.

E. Water Treatment System. Due to the design of the CFBC system band type heat exchangers, when a heat exchanger is taken off-line, for example to minimize heat removal from the on-going combustion or start-up process, the residual coolant must be vaporized for removal. To prevent accumulation of mineral deposits in these heat exchangers, a water-treatment system is provided. Municipal water supply is piped to the sixth floor of the tower where the water treatment system has been installed. The water transfer system consists of a municipal water pressure boost pump, pressurized storage tank, filtration and water softening equipment and controls.

F. Make-up Coolant System. De-mineralized water produced by the water treatment system is stored under pressure and is automatically added to the return coolant loop to maintain a

specified level in the coolant separator tank. The majority of make-up coolant is required to replace that which is lost when CFBC system heat exchangers are put on-line or taken off-line. The make-up coolant system is capable of furnishing a sustained 12 gallons per minute.

Figure 5-1. Pictures of Cooling System

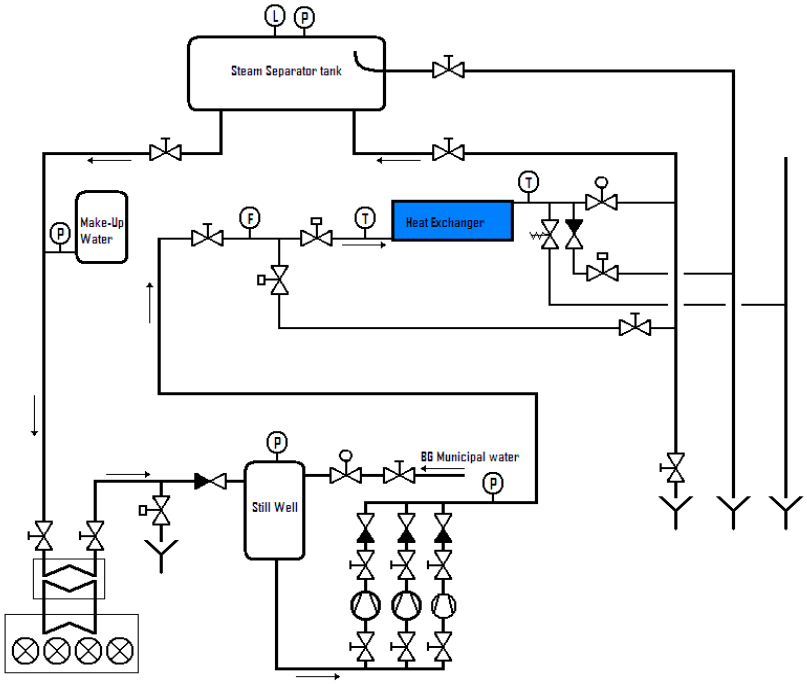

Figure 5-2. Schematic of Cooling System Setup

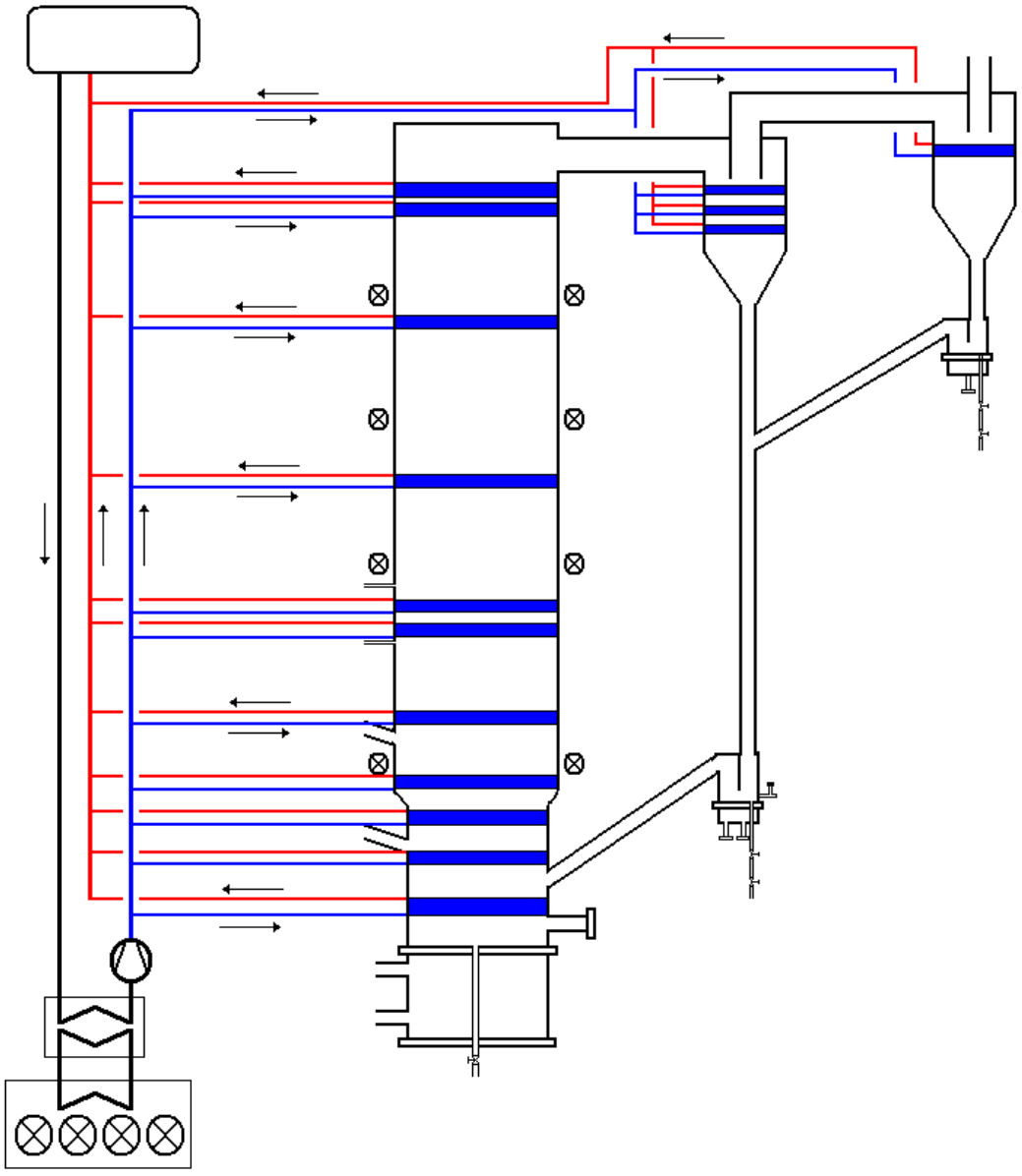

3.6 Solid Materials Delivery

3.6.1 Fuel Blending and Delivery

Delivery systems of solid materials are shown in Figure 6-1. Delivery materials are shown in Figure 6-2.

A. Gravimetric Fuel Bunkers. There are two fuel bunkers, made of 304 stainless steel, that are equipped with load cells. The larger bunker can hold approximately 600-pound of RDF (wood pellets) and the smaller bunker can hold approximately 550-pound of coal. Both bunkers are replenished at the fifth-floor level from 55-gallon drums and both are equipped with a slide gate at the bottom outlet to facilitate servicing and change-overs.

B. Fuel Blending Augers. Each fuel bunker discharges through a bellows connection to the respective variable speed auger. Each auger is driven by a stepper gear motor that allows on-line fuel blend ratios change as experimental design and combustion results require. The coal feed auger can transport more than 150-pound of coal per hour. The RDF feed auger can transport more than 100-pound of RDF per hour as wood pellets. The speed of each stepper motor is controlled at the user interface and is used to set the firing rate for the CFBC system. The individual fuel bunker augers discharge into a blend receiver.

C. Transport Auger. The blend receiver discharges fuel into the transport auger which serves to further mix and transport supply materials where they will drop into a rotary air-lock valve in the supply duct. The transport auger rotational speed is controlled at the user interface and is set to not impede the flow of combined supply material.

D. Rotary Air-Lock Valves. Two rotary air-lock valves are used in series to provide better pressure isolation and back-flow reduction that insure high-temperature gases are unable to escape upstream into the fuel supply area. The rotational speed of the rotary air-lock valves' is controlled at the user interface and is likewise, set to not impede the flow of supply materials.

3.6.2 Bed Material/Sorbent Delivery

A. Gravimetric Bunker. Similar to the fuel supply bunkers, the bed material bunker is constructed from 304 stainless steel and is fitted with load cells. This bunker can hold as much as 700 pounds of finely crushed limestone and is also replenished at the fifth floor level from 55-gallon drums. This bunker is also provided with a bottom mounted slide gate to facilitate servicing and discharging the contents of the bunker

B. Supply Auger. The bed material bunker discharges through a bellows connection to its own variable speed supply auger. This auger is also driven by a stepper gear motor, controlled from the user interface to allow for on-line proportioning of limestone or other sorbent materials as the experimental design and combustion results require. The bed material auger can transport more than 20 pounds of bed material per hour as limestone. This auger discharges, along with the fuel supply auger(s), into the blend receiver.

3.6.3 Pre-Operation Ash Delivery

A. Storage Bunker. This bunker is provided for pre-operation ash delivery. Approximately 450 pounds of ash can be held in this bunker which is used for pre-charging the lower loop seal prior to a CFBC system tests. This bunker is not provided with load cells as the ash flow rate is generally unimportant and accomplished in advance of a combustion run. A slide valve is located at the bottom of this bunker to facilitate auger servicing.

B. Supply Auger. This auger is used for transporting ash from the ash storage bunker into a separate ash duct and into the lower loop seal. The auger is capable of moving up to 150 pounds of ash per hour.

C. Ash Duct to Lower Loop Seal. A dedicated three-inch supply duct receives ash from the ash supply auger and delivers it to the downcomer side of the lower loop seal.

Figure 6-1. Feeding Systems of Solid Materials

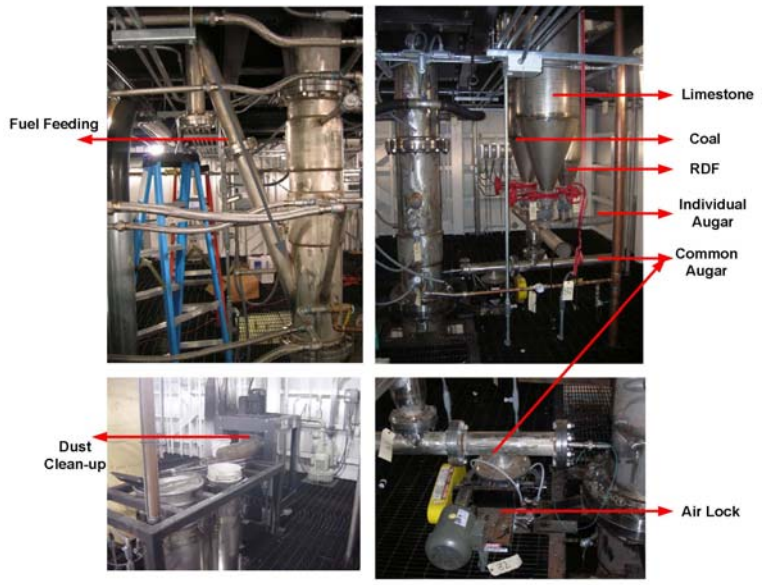

Figure 6-2. Pictures of Fuels and Limestone

3.7 System Central Control (Sensors and Actuators, User Interface, Sensor/Actuator Interfaces and Data Handling)

3.7.1 Sensors and Actuators

A. Temperature Sensors. Temperature sensors consist exclusively of thermocouples. All thermocouples are Type K and nearly all have industrial protection head construction. Thermocouples are used to measure coolant temperature at each heat exchanger inlet and outlet, as well as, that of ash, bed and flue gas temperatures throughout the riser, cyclones, downcomer and flue ducts, including the induced draft fan inlet. Applications have been designed so all thermocouples with protection head construction are interchangeable. There are 63 thermocouples in the configuration.

B. Pressure Sensors. All pressure transducers have 4 to 20 mA signal outputs. There are two basic types of pressure transducers used in the CFBC system. Sensors with a range of 0 to 200 psi range are used to measure coolant pressure at various important locations throughout the cooling system, including the municipal water supply pressure. All other pressure transducers are differential types with ranges from as little as 10-inch to as much as 200-inch water. These water column range sensors are used to measure differential pressures throughout the riser, cyclones, downcomer and flue gas ducts, as well as, the pressures of primary and secondary combustion air supplies. There are 38 pressure transducers in the configuration.

C. Load Cells. Load cells are used to measure the mass of fuel and bed material in the three Gravimetric Bunkers. An array of four 500-pound load cells is used to suspend each of the supply bunkers. The stain gauge signal from the array of each bunker is averaged, scaled and presented to a local digital display showing the net mass of the contents of the respective bunker. This information is for the guidance of those replenishing the bunker. The same information for each supply bunker is displayed at the user interface.

D. Flow Sensors. Two types of flow sensors are used in the CFBC system. Air mass flow sensors are used to measure primary and each of four levels of secondary air flow, lower and upper loop seal control airflow and the flow of tempering air at the induced draft fan inlet. Another type of flow sensor is a turbine water meter used to measure the flow of coolant into each of thirteen CFBC system heat exchangers and two more used in the make-up coolant supply. The air mass flow sensors develop a 4 to 20 mA signal proportional to air flow in the respective ducts. The turbine meters provide a contact closure (1 pulse per gallon) as coolant flows

through them. There are eight air mass flow sensors and 15 turbine water meters in the configuration. All flow data in displayed at the user interface.

E. Video Camera. As described in the previous section, a video display of the flue gas and particulate exiting the induced draft fan discharge is located in the CFBC system control room. This display provides useful information about the combustion performance. When combustion efficiency is high, there is very little particulate that is visible. Only diffraction patterns are visible.

F. Variable Speed Drives. Variable speed drives have found extensive use in the CFBC system design. Variable frequency inverter drives are used for many three-phase motors to effectively control their speed, allowing fan and blower capacity to be easily adjusted to match operating requirements. The same properties make these drives useful for controlling the rate of material transport by augers and rotary air-lock valves, with the notable exception of the fuel and bed material bunker augers. These bunker augers were instead operated with stepper gear motors because of the highly repeatable and reliable correlation between the control signal applied to the stepper motor drives and the actual rate of auger rotation. As the bunker augers are the feed rate determiners for fuel and bed material, the stepper motor solution was selected for this application.

G. Solenoid Valves. Many solenoid valves are employed in the heat exchanger coolant management system with a supply solenoid and a steam-rated coolant drain solenoid used for each CFBC system heat exchanger. Additionally, each heat exchanger supply circuit has a by-pass solenoid valve that opens a path by-passing coolant directly to the coolant return manifold whenever the supply solenoid valve is closed. This by-pass helps maintain the overall coolant loop flow volume, thereby reducing excess pressures when some circuits are closed and helps insulate water meters and supply solenoid valves from high temperature steam damage. When a heat exchanger is brought on-line or taken off-line, the steam-rated drain valve is opened for a short-term deluge to reduce prolonged steam development in the heat exchanger. Further, this valve remains open to drain when the respective heat exchanger is off-line, thus preventing high pressure steam from developing internally. Other solenoid valves are used in protecting secondary air and loop seal control air components from ash backflow. Also, solenoid valves are employed to control compressed air used to operate the primary air bed-preheater bypass

valve and the riser thermal expansion joint ash purge. There are 57 solenoid valves in the configuration.

H. Proportional Valves. Each of the CFBC system heat exchangers is provided with a coolant flow control proportional valve after their respective heat exchanger discharge. These valves are used to adjust flow of coolant over a range of about 0.8 to 18 gallons per minute. This arrangement provides a significant control of the heat uptake from the nearby combustion process and/or flue gas stream, while maintaining the maximum pressure in the heat exchanger for reduction of any tendency to boil the coolant. Proportional valves are also used in controlling the amount of secondary combustion air delivered to each level of the riser. By using proportional valves at each level, one supply blower can furnish all secondary air requirements with individual levels receiving a regulated flow as required. All proportional valves are controlled at the user interface. There are 19 proportional valves in the configuration.

I. Motorized Valves. There are two electric, motorized valves used in the CFBC system. One valve controls the amount of tempering air admitted at the induced draft fan intake. This valve actuator either opens, or by selecting the reverse direction, closes a four-inch butterfly valve, admitting ambient air to the induced draft fan as needed to keep combined inlet temperatures below 700 ºF. A second motorized valve is a part of an emergency cooling method that uses municipal water directly in the case when all circulation pumps fail or when a back-up generator fails during a combustion test. This valve and a solenoid valve directs municipal water through all CFBC system heat exchangers and to the drain, helping to reduce equipment damage that might otherwise occur.

3.7.2 User Interface, Sensor/Actuator Interfaces and Data Handling

A. *Process Control Computer*. The entire CFBC system process control, support of user interface, and all data logging is accomplished by a Dell Optiplex GX620 duel core work station computer. instruNET ® software installed on this computer manages digital data communication to and from peripheral interfaces and devices and a custom user interface program developed by Visual Basic® which serves as an operating environment. Many computer screens have been developed, including graphical representations of parameters such as hourly temperature trends, current data tables organized by types (e.g., pressures or flows) and screens that show crucial operating parameters, along with virtual control buttons or slider controls. If a parameter reaches a pre-programmed limit, the data field flashes to alert the operator of the limit condition. If a

parameter on a screen not currently displayed reaches a limit condition, the selection tab for that screen flashes, as well.

B. *Sensor/Actuator Interfaces*. As shown in Figure 7-2, sensor/actuator interfaces are housed in equipment cabinets located in the Tower on floors two through seven. These interfaces provide digital input/output (I/O) channels that can control a solid-state relay for power switching (e.g., solenoid valves) or can monitor switch contact closures (e.g., coolant level switch in separator tank). These interfaces provide analog voltage inputs for such devices as thermocouples or the voltage developed across a viewing resistor (e.g., the output of a 4 to 20 mA transducer developing 1 to 5 volts across a 250 ohm resistor). Finally, these interfaces provide an analog voltage output used to control devices (e.g., a proportional valve opening or, through a drive, the speed of a stepper motor). Through the use of these interfaces on most floors of the Tower, sensor and actuator wiring lengths are greatly reduced with only a data cable connecting these interfaces to the process control computer.

C. *Data Logging and Data Log Exportation to Excel® Spread Sheet*. Data logging is continuous whenever the control program is running with updates logged to file once every minute. Both sensor data and actuator status are logged. A program is resident on the process control computer, as presented in Figure 7-2, that supports the exportation of logged data in an Excel® file format.

Figure 7-1. Signal Transfer System

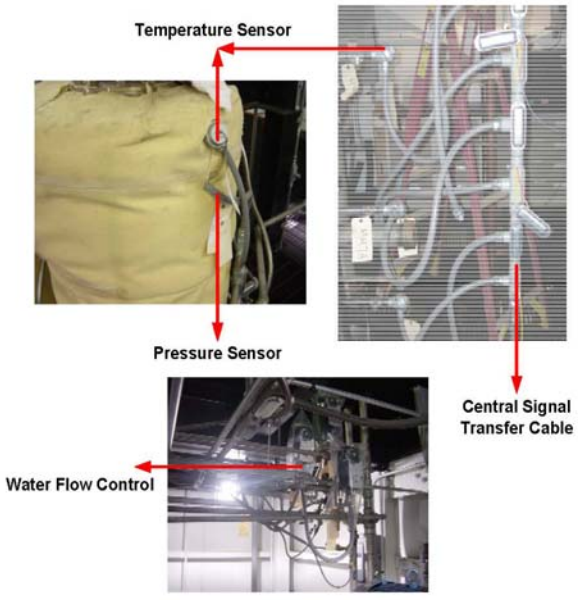

Figure 7-2 Data Collection

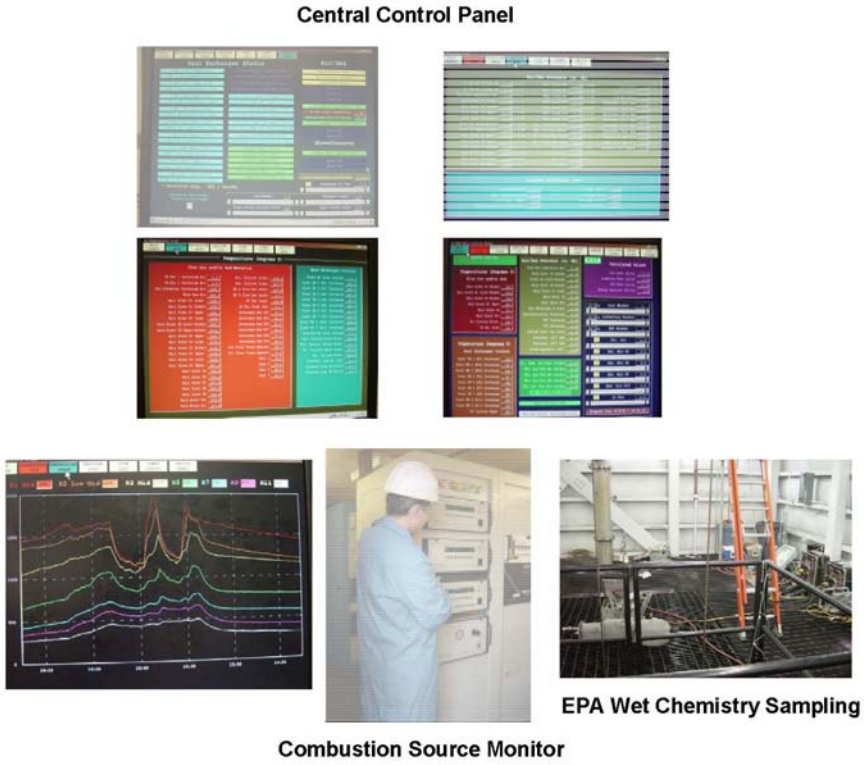

4. System Modification

4.1 Additional Thermal Expansion Joints

A. Ash Supply Duct to Lower Loop Seal. Although not described in the final version of the mechanical drawings for the CFBC system, points of support for each assembly of riser and downcomer segments had to be chosen in consideration of the Tower structural framing locations and the need to provide stable support for the riser and downcomer components, while at the same time, safely accommodating the dramatic change in combustor lengths resulting from temperature change. Accordingly, the riser segments were designed to be supported between R4 and R5 segments (as indicated in Figure 2) by the fourth floor framing of the Tower and at the top of R11 by the eighth floor framing.

It was decided to support the downcomer at the fourth floor. This simplified the task of providing proper support for the ash bunker and contents, its auger and gear motor drive. Further, it was decided that in consideration of its weight, the lower loop seal and its associated

components should be firmly supported from under the third floor framing so that the expansion joint (16A) located just above the lower loop seal in the downcomer could work properly. As the downcomer segments DC1, DC2, DC3 (as indicated in Figure 2), and the ash duct AD1, AD2 and AD3 (as indicated in Figure 2) form a loop that will experience different temperatures at different times, it was decided to add an expansion joint in the ash duct to prevent stress on these components. For this reason, AD3 was shortened to accommodate this expansion joint installation.

B. Lower Loop Seal to Riser R1 Segment. Again, referring to the rigid mounting of the lower loop seal under the third floor framing, a loop is formed between the third floor framing, the lower loop seal, the riser segments R1, R2, R3 and R4 (as indicated in Figure 2) and the fourth floor framing. Clearly, as the riser below the fourth floor lengthened with increasing temperature, stress would develop in the lower loop seal connecting the duct and the lower-loop seal supports. Therefore, it was decided to add an expansion joint in this connecting duct to prevent stress in these components. The portion of the connecting duct from R1 (as indicated in Figure 2) was shortened to accommodate this expansion joint installation.

4.2 Additional Sensor Ports

Although not provided in the final mechanical drawings, a design review concluded that additional temperature and pressure measurement points would be useful in such an important area of the CFBC system riser. These additional measurement points were expected to play a major roll in bed height management strategies and in actual tests. The value of these additional measurement point have proven.

A. Riser R1 Segment. The existing set of pressure and temperature sensor ports were located in the approximate middle of the riser R1 (as indicated in Figure 2) vertical dimension. Two additional sensor ports were installed, one above and one below the existing ports, dividing this distance in half again, and yielding a pressure and temperature port at about every 15-inch. Riser R1 now has a total of three pressure and temperature sensing ports. Also, a different utilization of all temperature and pressure ports has been adopted throughout the riser and downcomer segments.

As originally designed, a sensor port, whether temperature or pressure, was constructed by wielding a ½ inch pipe nipple equipped with pipe threads on the outer end to the riser wall and. These ports were set up in pairs about three inches apart at every sensor position. Industrial

protection head thermocouples have ½ inch male pipe threads to connect to the process. Instead of using a pipe coupling to connect the thermocouple to the riser pipe nipple, which would immerse the thermocouple junction in the process, a pipe tee was used. This provided another port to be used to obtain pressure measurements. This arrangement works well to hold a plug of quartz wool in the side-leg of the tee that acts as an ash filter for protection of the pressure sensor. As a result, all added pressure and temperature sensor ports require only one pipe nipple installation.

B. Riser R2 Segment. Similarly, three pressure and temperature sensor ports have been added to the riser R2 segment (as indicated in Figure 2). The choice of location for these additional ports was somewhat restricted due to the presence of two band- or jacket-type heat exchangers. However, a reasonable distribution of these ports has been achieved to provide representative temperature and pressure measurements from this riser segment. Riser R2 (as indicated in Figure 2) now has four pressure and temperature sensing ports.

C. Riser R3 Segment. In the same way, two pressure and temperature sensor ports have been added to the riser R3 segment (as indicated in Figure 2). These additional ports were able to achieve a more uniform distribution as, at this time, there were no heat exchanger(s) to work around. The resulting pressure and temperature sensor ports are located approximately 15-inche apart and provide representative temperature and pressure measurements from this riser segment. Riser R3 (as indicated in Figure 2) now has three pressure and temperature sensing ports.

D. Riser R4 Segment. One additional pressure and temperature sensor port has been added to the Riser R4 segment (as indicated in Figure 2). This additional sensor port has been installed approximately 15 inches above the lower flange of this segment, which is about halfway between this flange and the formerly-existing sensor port. Riser R4 now has two pressure and temperature sensing ports.

4.3 Additional Heat Exchangers

During an earlier CFBC test, excess temperatures were detected in the vicinity of the R3/R4 riser flange joint. Some riser insulation components were damaged (aluminum sheeting was melted; Kevlar® outer jacket was charred). No flange gasket damage was detected. Also, 1,800 and 1,900 ºF temperatures were measured inside the riser at the same time. Subsequently, improved insulation application methods have been employed to assure better coverage in flange

areas to reduce the likelihood of a recurrence. However, design review indicates that this area of the riser would benefit from additional heat exchange surface below this area.

A. Riser Transition Joint. Using a similar design to the existing heat exchangers, an additional heat exchanger coolant jacket was constructed over the existing riser transition joint segment. Additional coolant piping, solenoid and proportional valves, flow meters and thermocouples, similar to those used with other existing CFBC system heat exchangers, were installed. This heat exchanger provides an additional 5.6 square feet of heat exchange surface area. With the advent of this heat exchanger installation and another installed on riser R3 segment, much better temperature stability and freedom from extreme temperature excursions has been observed.

B. Riser R3 Segment. Again, using similar design and construction to existing heat exchangers, a heat exchanger coolant jacket was constructed on the Riser R3 segment somewhat below the upper flange joint. This heat exchanger, being 12 -inch in height, adds 4.2 square feet of heat exchange surface area.

4.4 Modification of the Loop Seal Air Supply

A combustion test was terminated after more that 24 hours of continuous operation when ash recirculation could not be maintained. After disassembly, inspection of residual material on the riser side of the lower loop seal above the bubble plate conclusively revealed the presence of an appreciable quantity of bed material. Also, the bubble caps, exclusively on the riser side of the loop seal bubble plate, showed indications of very high temperatures. Furthermore, ash was found to have migrated into the common supply piping used to furnish loop seal control air. It is hypothesized that the downcomer side and the riser side of the loop seal have significantly different control air requirements of pressure and flow. Therefore independently adjustable supplies were provided to sustain and better regulate ash circulation. Finally, an improved control air piping configuration aided in reducing the restriction of control air flow by ash accumulations therein.

Modifications that allow evaluation of the use of two independent control air supplies for the lower loop seal are relatively straight forward. As described in the foregoing, the existing regenerative blower, along with its variable speed drive, was connected exclusively to the riser side of the lower loop seal plenum. Speed control and the resulting display of control air flow are available at the user interface. The loop seal plenum now has a baffle plate welded in place

separating the two supply paths from each other.

For test purposes, a second regenerative blower will have its capacity manually controlled. A rotameter is used to measure air flow. This second blower is temporarily positioned on the third floor of the combustor Tower building near the downcomer viewing ports, allowing an operator to adjust the volume of air flow and observe the results on the ash in the downcomer.

Both control air supply paths, in order to reduce unwanted backward ash migration toward the supply blowers, are piped in such a manner as to create what is we expected to perform like ash traps. The bottom of each plenum port was with a short vertical pipe. Working back toward the supply, a tee and drain valve is installed allowing any accumulated ash present in this first vertical leg that has fallen through the bubble plate to be drained. The side-leg of this tee connects to about 12 inches of horizontal pipe and to an up-turned elbow. Connected to this up-turned elbow is about 24 inches of vertical pipe, another elbow, a short horizontal pipe, a down-turned elbow and finally another vertical run of pipe. What is formed is an up-turned loop (drainable, if required) that leads back to each control air blower. Further, each trap may be blown out with higher pressure compressed air, if needed. At the very least, there are several new "inspection ports" in these traps that may provide additional information if ash migration continues to be a problem.

Standard operating protocol will require each control air blower to be operated at a low stand-by pressure whenever there is any ash in the downcomer or loop seal or whenever primary combustion air is being applied to the bed region of the riser.

5. Experimental Section

5.1 Fuel Characterization

One sub-bituminous coal (Powder River Basin (PRB) coal) and two types of solid waste, (wood pallet (WP) and chicken waste (CW)), were used to evaluate the performance of the 0.6 MW_{th} pilot-scale CFBC. Raw PRB coal was purchased from a coal-fired power plant in Illinois. The CW was collected from a local farm after natural drying. Its moisture content and heating value were 20 % and 9197 Btu/lb, respectively. The WP was purchased from a local wood residue factory. These two solid wastes had a much lower bulk density, were generally moist (6 % for WP and 20 % for CW), and had lower heating values (7752 Btu/lb for WP and 5255 Btu/lb for CW) than PRB coal used. Limestone, used in CFBC system for sulfur capture, had the total

effective constituents (calcium oxides (CaO) and magnesium oxide (MgO)) at over 95% (Ca at 91 % and Mg at 4.3 %). It was purchased local limestone mines from Kentucky. PRB coal was pulverized and sieved. The particle-size distribution of the coal is shown in Figure 8. The particle size distribution of the coal is in reversed bell shape with an average particle size at about 1000μm, which is desired in the 0.6 MW_{th} CFBC system. A narrow particle size of WP (50μm in diameter by 1000μm in length) was selected for this test. The purpose of using larger biomass particles was to satisfy its fluidization conditions and residence time inside the CFBC system. There were two sizes of limestone used in this study. One was averaged at 500μm and the other at 1000μm. The larger size limestone was used as bed material.

Analysis of all fuel samples in this study follows ASTM standard procedures. The detailed description on these ASTM methods is described in a reference[1]. Analytical results of all tested fuels are presented in Table 1. Generally, all tested fuels had a high volatile content of over 30 % on a received basis (34.6 % for PRB coal, 55 % for CW and 77.7 % for WP). The CW had the highest ash content at 15.8 %, then PRB coal at 4.6 % and WP at about 1.1 %. Sulfur content in all fuels was low, at about 0.92 % for CW, followed by 0.32 % for PRB coal and 0.082 % for WP. Chlorine content in all fuels was low, except for CW. For example, chlorine content is about 232 ppm for PRB coal and 262 ppm for WP, respectively. The CW has very high chlorine content (at about 25,147 ppm). Fluorine content was low for PRB coal and CW, but higher for WP (2758 ppm). Only the PRB coal had measurable mercury content at about 0.072 ppm. Mercury in both solid wastes were miniscule, and at about 0.006 ppm. The major metal oxides in the tested fuels are also shown in the Table 8. This study indicates that PRB coal, CW and WP all have a relatively high content of CaO and MgO, which are about 25 % in total ash. All solid wastes have more alkali metal oxides, either sodium oxide (Na_2O) or potassium oxide (K_2O). Among them, both CW and WP have more (K_2O) (21.8 % for CW and 13.6 % for WP), and less Na_2O (6.3 % for CW). However, the total amount of alkali earth metal oxides and alkali metal oxides should be ignored for WP because of its minimal ash content. Chicken waste also has a higher content of phosphorus oxide (P_2O_5) (about 19.6 %).

The major trace metals in the tested fuels are also shown in the Table 8. It indicates that PRB coal, CW and WP all have a relatively low content of three major trace metals (Arsenic (As), Selenium (Se) and lead (Pb)). Arsenic and lead are even below the instrument-detection limit at 1.5 ppm for all three fuels. In decreasing order, Se content for PRB coal, WP and CW is about

1.8 ppm, 8.2 ppm and 6.7 ppm, respectively. Except for CW with a higher content of copper (at 478 ppm), magnesium (at 642 ppm) and zinc (at 528 ppm), all other toxic trace metals (Beryllium(Be) , Cadmium(Cd), Cobalt(Co), Chromium(Cr), antimony(Sb)) are lower and generally below 10 ppm.

Figure 8. Particle Size Distribution of Tested Coal

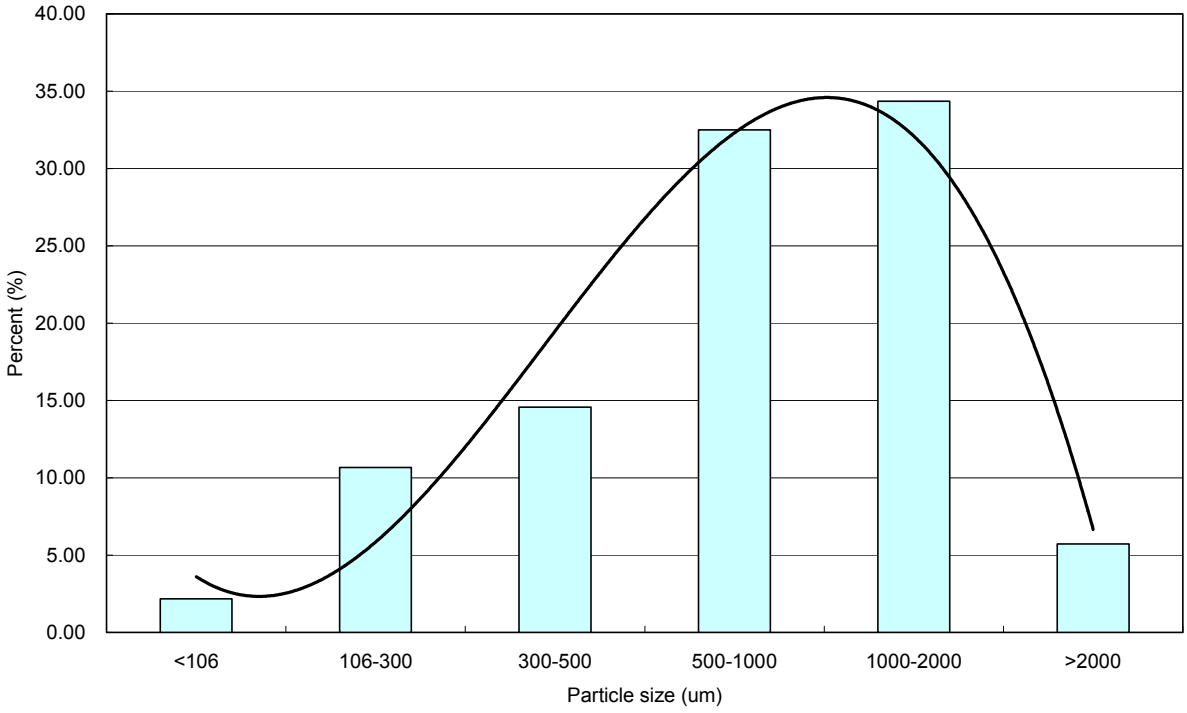

Table 8. Coal and Biomass Analysis

Fuels																				
Proximate&Elemental Analysis	**Moisture**	**Ash**	**Volatile**	**Sulfur**	**Heating Rat**	**Carbon**	**Hydrogen**	**Nitrogen**	**Oxygen**	**Hg**	**Cl**	**F**	**Br**							
	%	%	%	%	**BTU**	%	%	%	%	**ppm**	**ppm**	**ppm**	**ppm**							
CFBC Fuel - PRB Coal	20.76	4.56	34.61	0.32	9197	55.73	6.29	0.56	11.79	0.072	232	61	ND							
CFBC Fule - Wood Pallet	6.06	1.07	76.74	0.08	7752	46.98	6.67	0.06	39.09	0.006	362	2758	ND							
CFBC Fuel - Chicken Waste	20.38	15.82	54.99	0.92	5255	30.72	6.59	2.61	22.97	0.006	25147	ND	ND							
Trace Metal Analysis	**Ag**	**As**	**Ba**	**Be**	**Cd**	**Co**	**Cr**	**Cu**	**Mn**	**Mo**	**Ni**	**Pb**	**Sb**	**Se**	**Tl**	**V**	**Zn**	**B**	**Th**	**U**
	ug/g	**ug/g**	**ug/g**	**ug/g**	**ug/g**	**ug/g**	**ug/g**	**ug/g**	**ug/g**	**ug/g**	**ug/g**	**ug/g**	**ug/g**	**ug/g**	**ug/g**	**ug/g**	**ug/g**	**ug/g**	**ug/g**	**ug/g**
CFBC Fuel - PRB Coal	<1.5	<1.5	237.518	<1.5	<1.5	4.074	3.284	9.376	21.995	<1.5	<1.5	<1.5	<1.5	11.848	<1.5	10.221	3.555	78.231	13.771	9.393
CFBC Fule - Wood Pallet	<1.5	<1.5	37.737	<1.5	<1.5	<1.5	<1.5	1.648	54.198	<1.5	<1.5	<1.5	<1.5	8.167	<1.5	<1.5	8.970	4.807	<1.5	4.912
CFBC Fuel - Chicken Waste	<1.5	<1.5	24.674	<1.5	<1.5	2.155	7.857	479.444	642.578	2.912	9.756	<1.5	<1.5	6.704	<1.5	3.158	528.7435	38.814	4.345	41.481
Minor oxides	SiO_2	Al_2O_3	Fe_2O_3	CaO	MgO	Na_2O	K_2O	P_2O_5	TiO_2	SrO	SO_3	BaO	ZnO	MnO	CuO					
	%	%	%	%	%	%	%	%	%	%	%	%	%	%	%					
CFBC Raw Material PRB Coal	30.53	15.12	3.99	25.71	4.63	1.20	0.37	0.78	1.86	0.35	14.93									
CFBC Raw Material Wood Pallet	7.12	1.54	0.34	40.50	10.34	2.21	31.43	0.76	0.19	0.58	2.27	0.99	0.21	1.47	0.05					
CFBC Raw Material Chicken Waste	7.41	2.60	0.51	18.56	6.88	6.26	21.81	19.59	0.11	0.04	16.23									
Limestone																				
Minor oxides	SiO_2	Al_2O_3	Fe_2O_3	CaO	MgO	Na_2O	K_2O	P_2O_5	TiO_2	SrO	SO_3									
	%	%	%	%	%	%	%	%	%	%	%									
CFBC Raw Material Lime Stone	3.73	0.30	ND	91.31	4.33	ND	0.15	0.04	0.37	ND	0.12									
Trace metals	**Ag**	**As**	**Ba**	**Be**	**Cd**	**Co**	**Cr**	**Cu**	**Mn**	**Mo**	**Ni**	**Pb**	**Sb**	**Se**	**Tl**	**V**	**Zn**	**B**	**Th**	**U**
	ug/g	**ug/g**	**ug/g**	**ug/g**	**ug/g**	**ug/g**	**ug/g**	**ug/g**	**ug/g**	**ug/g**	**ug/g**	**ug/g**	**ug/g**	**ug/g**	**ug/g**	**ug/g**	**ug/g**	**ug/g**	**ug/g**	**ug/g**
CFBC Raw Material Lime Stone	<1.5	9.68	6.39	<1.5	2.27	<1.5	6.16	1.67	62.64	<1.5	8.07	5.549	2.40	9.589	<1.5	11.699	51.66		8.042	59.695
Ash																				
	LOI	**Hg**																		
	%	**ppm**																		
CFBC Fly Ash 7/23/08 (Co-firing WP)	14.16	0.006																		
CFBC Fly Ash 7/30/08 (CO-firing CW)	30.20	0.005																		
CFBC Fly Ash 8/07/08 (Full-load&co-firing)	18.63	0.066																		
Trace Metal Analysis	**Ag**	**As**	**Ba**	**Be**	**Cd**	**Co**	**Cr**	**Cu**	**Mn**	**Mo**	**Ni**	**Pb**	**Sb**	**Se**	**Tl**	**V**	**Zn**	**B**	**Th**	**U**
	ug/g	**ug/g**	**ug/g**	**ug/g**	**ug/g**	**ug/g**	**ug/g**	**ug/g**	**ug/g**	**ug/g**	**ug/g**	**ug/g**	**ug/g**	**ug/g**	**ug/g**	**ug/g**	**ug/g**	**ug/g**	**ug/g**	**ug/g**
CFBC Fly Ash 7/23/08 (Co-firing WP)	3.125	61.259	2147.620	1.972	3.349	30.127	189.016	161.432	888.526	3.494	67.884	15.966	6.402	28.566	<1.5	175.871	116.760	686.933	76.620	166.276
CFBC Fly Ash 7/30/08 (CO-firing CW)	<1.5	<1.5	365.229	<1.5	1.925	12.968	30.803	578.475	713.689	5.321	36.841	7.553	3.559	21.371	<1.5	56.276	519.924	269.303	34.897	75.624
CFBC Fly Ash 8/07/08 (Full-load&co-firing)	<1.5	23.194	185.46	<1.5	3.225	17.4145	51.921	46.624	388.617	<1.5	40.464	13.3555	3.832	22.507	<1.5	60.277	138.028	350.392	54.486	57.531
	LOI																			
	%																			
CFBC Loop seal ash 7.23 - 1 (co-firing WP)	40.57																			
CFBC Loop seal ash 7.30.08 - 1 (CO-firing CW)	44.52																			
CFBC Loop seal ash 7.30.08 - 2 (CO-firing CW)	31.51																			
CFBC Loopseal ash 8.7.08 - 1 (Full-load CO-firing)	45.38																			
CFBC Loopseal ash 8.7.08 - 2 (Full-load CO-firing)	43.09																			
Minor oxides	SiO_2	Al_2O_3	Fe_2O_3	CaO	MgO	Na_2O	K_2O	P_2O_5	TiO_2	SrO	SO_3									
	%	%	%	%	%	%	%	%	%	%	%									
CFBC Loop seal ash 7.23 - 1 (co-firing WP)	16.73	4.68	1.20	64.43	5.27	0.32	0.91	0.87	0.66	0.25	4.59									
CFBC Loop seal ash 7.30.08 - 1 (CO-firing CW)	16.29	4.35	1.00	70.01	5.18	ND	0.28	0.23	0.39	0.25	1.95									
CFBC Loop seal ash 7.30.08 - 2 (CO-firing CW)	21.09	6.02	1.66	59.06	4.40	0.29	0.53	0.28	0.74	0.25	5.57									
CFBC Loopseal ash 8.7.08 - 1 (Full-load CO-firing)	14.54	4.35	1.06	72.38	4.49	ND	0.27	0.25	0.32	0.28	1.98									
CFBC Loopseal ash 8.7.08 - 2 (Full-load CO-firing)	10.05	2.57	0.39	78.87	5.30	ND	0.32	0.18	0.44	0.24	1.61									
CFBC Bottom Ash 7.30 (Co-firing CW)	27.20	5.53	1.22	49.80	4.33	0.28	1.51	0.93	0.55	0.22	8.38									
CFBC Bottom Ash 8.7.08 (Full-load Co-firing)	8.99	1.15	0.90	79.26	7.25	ND	0.33	0.08	0.42	0.18	1.45									

5.2 Procedures for Firing the CFBC System

A. Preparation. Preparation for CFBC operation consists of working through a checklist that insures that electric power is available to all interface cabinets, variable speed drives, etc., that all sensors are functioning normally, that adequate coolant is present and that all actuators such as pumps, solenoid and proportional valves are operating within normal parameters. Preparation also includes the development of a "Test Matrix" to guide the operation of the CFBC system to achieve the established goals for operation and insure that all materials, including fuel types and quantities, and bed/sorbent materials and quantities, are in place for operation.

B. Bed Preheating. Good tests have been achieved by using 175 pounds of crushed limestone with a particle size of 20 to 6 mesh, with minimal dust. HX 1, 2 and 3, covering the dense zone of the riser, are drained of coolant. About 6.8 pounds per minute of primary combustion air is directed through the preheater. Bed temperature can reach 680 ºF within about four hours, which has been sufficient for initiating the firing of PRB coal.

C. Ignition. After fuel kindling has been achieved and a sustained rise in bed temperature is observed, the bed preheater is switched off and the butterfly valve is opened from the user interface. This permits combustion air to flow through the air heater (now de-energized) and directly to the windbox. Fuel feed and primary combustion air flow are increased to bring the bed area and subsequently the entire riser and cyclones to operating temperature.

D. Temperature Management. Typically, a process temperature throughout the riser of 1560 ºF has been desired. As much as 12 hours of fired operation may be required to arrive at this temperature throughout the riser segments. During this stabilization interval, fuel feed and combustion air supplies are optimized with high combustion efficiency as a primary goal. Sufficient primary combustion air flow is required to completely fluidize the bed, but excess air will cool the bed. As the operating temperature is approached, limestone feeding is required to maintain the bed height, but also has a cooling effect. As ash circulation commences to the bed, a cooling effect may also be observed. As lower portions of the bed approach the operating temperature, dense zone heat exchangers are put on-line to help regulate the bed temperature. Secondary combustion air is applied mostly to the lower (R3 and R6) levels of the riser to increase the upper segments of the riser and the cyclones to the desired operating temperature. Long term operation at process temperatures in excess of 1,800 ºF are avoided to measure the reliability of the system components.

E. Heat Exchanger Management. On the "flow screen" of the user interface, all CFBC system heat exchangers are easily monitored and controlled. Coolant flow and discharge temperatures are displayed and coolant flow is adjusted with a virtual slider control for each heat exchanger. Coolant discharge temperatures should not be greater than 240 ºF as damage to the proportional flow control valve damage may occur above this temperature. As the CFBC system reaches stable operations, coolant flow rates through each heat exchanger will have a discernable effect upon the process temperature in the vicinity of that heat exchanger.

F. Circulated Ashflow Management. Each loop seal has control air provided by its own dedicated regenerative blower. These blowers are controlled at the user interface. Ash captured by the cyclones will flow through a loop seal from an area of higher pressure to an area of lower pressure when it is fluidized by the loop seal control air. If the loop seal and stand-pipe (downcomer) have too low a level of ash, unwanted flow from the higher pressure riser to the lower pressure cyclone will occur and ash recirculation will be prevented.

G. Fuel Blending and Fuel Flow Monitoring. As described previously, fuel blending results from the relative rotational rate of each stepper gear motor for each fuel supply bunker. An approximate prediction of blend ratios by volume can be made based upon the ratios of the stepper motor speed setting on the user interface sliders. However, due to different fill percentages for the respective augers, the best measure of flow rate is to observe mass loss from the respective bunkers over a period of time to allow sufficient averaging of data.

H. Air-to-Fuel Management. Theoretical estimates of flow rates for fuels and combustion air flows may serve as a starting point for optimizing air-to-fuel ratios. Added to temperature response data as fuel and air flows are finely adjusted, better air-to-fuel ratio management comes from on-line flue gas analysis for carbon monoxide and oxygen concentration. The IMR 5000 flue gas analyzer provides this data for displays on the user interface "main screen".

I. Bed Material Height Management. Bed material height may be inferred by static pressures measured in the dense zone of the riser. As bed material height increases, windbox pressure rises and inter-port pressures in the dense zone of the riser increase. Primary air flow rate, bed temperature and bed material particle-size distribution all affect these pressures as well. Once stable operation is achieved, maintaining a steady bed-static pressure indicates a reasonably constant bed height in riser.

J. Emergency Recovery. The CFBC system has, thus far, demonstrated a robust and tolerant design and construction and therefore should have little need for recovery from emergency conditions. Structurally, the CFBC system components seem well supported by the Tower framing. Redundant measures have been taken to insure adequate cooling and safe shut-down during normal operation and during unscheduled electric power interruption. The process control computer, the sensor/actuator interfaces, all sensors and all essential actuators are powered by on-line uninterruptible power supplies, which are in turn supported by a stand-by 80 KW generator set. The process control computer has been programmed to provide alarms and to prevent many possible missteps that might lead to troubled operation. The worst outcome of a potential emergency situation should be that fuel flow is terminated and the run comes to a halt. Upon elimination of the condition, normal operation should resume.

K. Routine Shut-down. Upon the completion of an CFBC system test, a working checklist directs the steps to be taken to accomplish a routine shut-down. These steps essentially consist of terminating the feeding of all fuel and bed material. Generally, 30 minutes after fuel feed is terminated, primary air may be reduced to about 8 pounds per minute. Internal and external coolant circulation pumps are unchanged at this time. All CFBC system heat exchangers may be reduced to a slider control position of 40 % of maximum. Induced draft fan operation is unchanged at this time. Secondary combustion air is to be set for a flow of about 1.2 pounds per minute flow at R3 and 0.4 pounds per minute at R6. Loop seal blowers may be shut down at this time. Upon reaching an indicated R1 middle temperature of about 500 ºF, primary combustion air may be reduced to about 4 pounds per minute. The CFBC system should be operated under these conditions for a minimum of 8 hours to insure a gradual and uniform cool down. After this time has elapsed, coolant circulation pumps and the secondary air blower may be shut-down. As long as there is used bed material in the riser, the downcomer or the loop seals, the induced draft fan and forced draft fan should remain in operation and the bed preheater should be programmed to operate at about 240ºF to keep this bed material from becoming hydrated.

5.3 Procedures for Air Pollutant Measurement

5.3.1 Measurement of Combustion Source Flue Gas by Teledyne API.

The concentrations of SO_2, NO_x, CO were measured by Teledyne API M100E, M200E, and M300E, respectively. The M100E is a fluorescence spectroscopy instrument, which measures the intensity of fluorescence that occurs when SO_2 is excited by ultraviolet light. The M200E measures the NO_x concentration by detecting the chemiluminescence, which occurs when nitrogen oxide (NO) reacts with ozone (O_3). A molybdenum oxide is used to convert NO_2 to NO for the chemiluminescence reaction. The Model 300E/EM uses a high energy heated element to generate a beam of broad band Infrared Radiation (IR) light with a known intensity (measured during Instrument calibration). This beam is directed through multi-pass cell filled with sample gas. The sample cell uses mirrors at each end to reflect the IR beam back and forth through the sample gas a number of times. The total length that the reflected light travels is directly related to the intended sensitivity of the instrument. The instrument was calibrated using zero air and a standard gas provided by Airgas Co. (Bowling Green, KY) every day before the measurements started. Data collected during testing period was processed by internal data acquisition systems.

5.3.2 Measurement of Speciated Mercury by Mercury CEM and OHM.

PS Analytical Semi-continuous Emission Monitor was used as mercury semi-continuous emission monitor (CEM) in this test. The (PS) analytical SCEM system consists of six major components, including an inertial sampling probe, heated Teflon sample line, which is normally kept at 150^{o}C, the mercury speciation conversion module for measurement of speciated mercury, the analyzer, and the data collection system. The system also has a mercury-vapor generator. This device supplies a constant stream of mercury vapor at typically 14 liters per minute. These gases go through the valve-switching box and can be directed to the probe to completely check the system bias. This mercury CEM system uses a gold trap to collect the mercury from the flue gas before analysis with an atomic fluorescence detector. Without the aid of a pretreatment system, the atomic fluorescence detector is not protected from the acidic flue gas and is also unable to determine mercury speciation. The pretreatment system splits the incoming flue gas into two streams prior to entering mercury speciation conversion module. One stream passes through a potassium chloride solution, which removes oxidized mercury; thereby allowing only elemental mercury to reach the detector. The other stream passes through a stannous chloride solution, which reduces oxidized mercury to elemental mercury, thus facilitating the measurement of total mercury. Both solutions also serve the dual purpose of removing acidic gases that could damage

the gold detector.

The EPA Ontario Hydro Method, approved by ASTM Method D6784-2, plus the inertial sampling technique, which is to prevent measurement bias from involvement of fly ash during sampling, is used in this test. The OHM data is used to verify data from mercury CEM. The recovery solutions were digested and analyzed using the Hydra Prep mercury solution digestion equipment and the Hydra AA mercury solution analyzer from the Leeman Instrument Company. This mercury analyzer is an automated unit employing a dual beam, cold vapor atomic absorption spectrometer (AAS). This system has a detection limit of 1 part per trillion (ppt) mercury. This method is currently the only available standard method for speciated mercury measurements. Laboratory and field validations have indicated relative standard deviations of 10%, far better than the minimum criteria set by EPA Method 301. The versatile Apex Instruments sampling train was used to conduct sampling. Approximately over one hour of sampling time was required to collect gas samples with a certain volume of flue gas, which is dependent on mercury concentration in the flue gas.

Early indications of a low bias in elemental mercury measurements with high levels of SO_2 in the flue gas were corrected by adding an impinger containing nitric acid/hydrogen peroxide before the acidified permanganate solutions to avoid a possible reduction reaction. Another concern was the possible presence of Hg^{1+} species in the flue gas, which would be captured in potassium chloride impingers and converted to Hg^{2+} in acidified permanganate solutions during subsequent solution recovery. The Hg^{1+} species gives the same results as Hg^{2+} and is therefore counted as oxidized mercury or Hg^{2+}. However, it is generally assumed that all forms of oxidized mercury in the hot flue gas occur as Hg^{2+}. This is a reasonable assumption since Hg_2Cl_2 is not thermodynamically stable in the flue gas and disappear rapidly to produce Hg^0 and Hg^{2+}.

LECO AMA-254 Advanced Mercury Analyzer. Fly ash collected from the OHM standard filter, mechanical hoppers and electric precipitator (ESP) hoppers were analyzed with the LECO AMA-254 mercury analyzer. This direct combustion mercury analyzer was the principal instrument used to develop the newest ASTM standard method of analysis for mercury in coal and combustion residues, D6722. The AMA-254 has a 0.01 ng mercury detection limit, a working range from 0.05 to 600 ng, reproducibility smaller than 1.5 %, and a five-minute analysis time.

5.3.3 Measurement of Speciated Halogens by EPA M26A.

This method is applicable for determining emissions of hydrogen halides (HX) [HCl, HBr, and HF] and halogens (X_2) [Cl_2 and Br_2] from stationary sources. Hydrogen halides and halogens were captured by a 0.1N sulfuric acid and 0.1N hydrogen peroxide solution, respectively. The solution was recovered from the impingers immediately after the sampling, and sent to the analyzer based on ion chromatography. Similar sampling train, as OHM, is applied while conducting EPA M26A. The only difference is in the sampling impinger train that contains different sampling solutions. After sampling, the solution will be analyzed by ion chromatography (IC).

5.3.4 Measurement of Gaseous Trace Metals by EPA M29.

This method is applicable to the determination of trace metal emissions from stationary sources. Measurement of trace metals include Sb, As, Ba, B, Be, Cd, Co, Cr, Cu, Pb, Mn, Ni, P, Se, Ag, Tl, and Zn. The absorption solution (5 %HNO_3/10 %H_2O_2) was recovered from the impingers and then acid digestion followed the standard procedure. The samples were prepared and analyzed using inductively-coupled plasma emission spectroscopy. Similar sampling trains, as OHM, are applied while conducting EPA M29. The only difference is in the sampling impinger train containing different sampling solutions. After sampling, solution will be analyzed by ICP-ES.

5.3.5 Measurement of Condensable Particulate Matter (CPM) by modified EPA OTM 28.

A modified condensable particle matter (CPM) method, as indicated in modified EPA OTM 28, is applied to take CPM samples during tests. APEX particle matter (PM)10&2.5 cyclones are cleaned by detergent, de-ionized water, acetone and dried. Before sampling starts, all used sampling impingers, 100 ml, and 50 ml beakers need to be cleaned using soap, tap water, de-ionized water, acetone and finally methylene chloride (CH_2Cl_2). All these containers are baked at 300 ^oC for 6 hours. The cleaned, dry beakers, FPM filters and CPM filters are desiccated at least 24 hours at room temperature in a desiccator containing anhydrous calcium sulfate, and then are weighed at intervals at least six hours to a constant weight (=< 0.5 mg change from previous weighing) and recorded to the nearest 0.1 mg. The setup of the CPM sampling train is indicated in Figure 9. As soon as possible after the post-test leak check and impingers weighting purge, the impingers train at 20 liters per minute for one hour as seen in Figure 10. After post-test nitrogen purge, FPM and CPM samples together with one field blank will be processed as the processing flow chart shown method.

Figure 9. Sampling Train for Collection of FPM and CPM

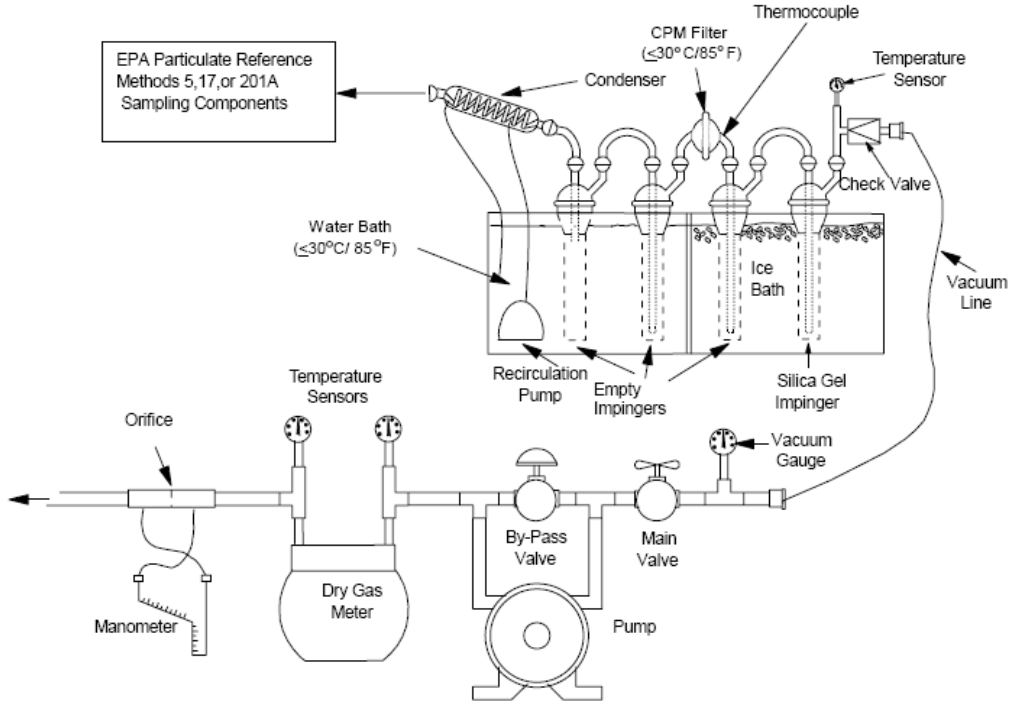

Figure 10. Train Configuration on CPM Post-test Nitrogen Purge

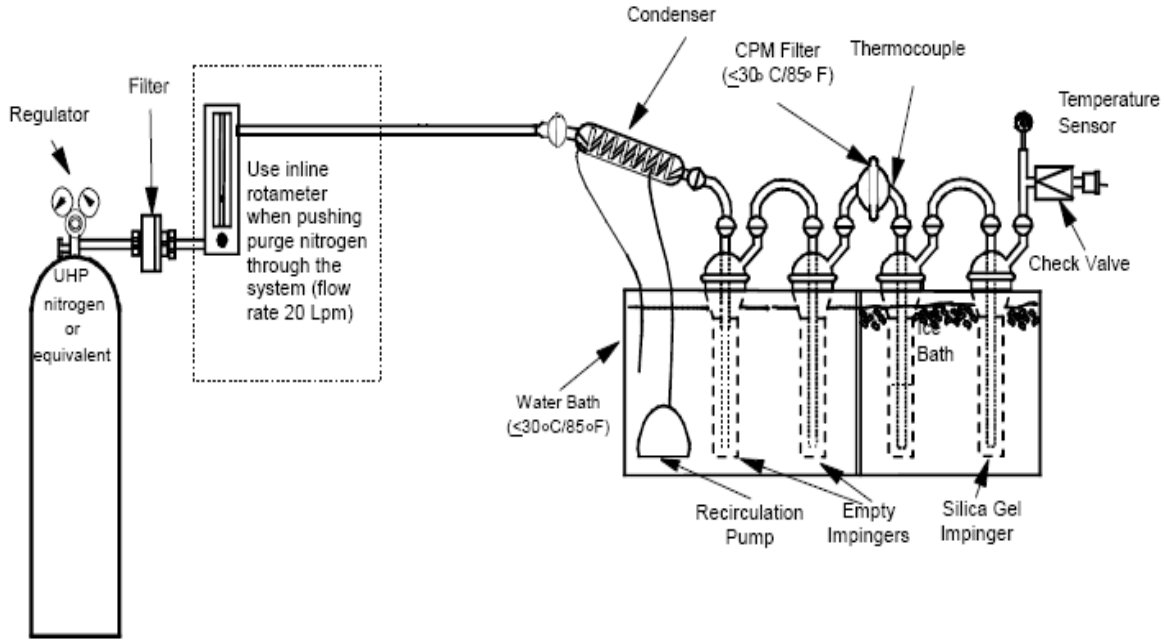

5.3.6 Measurement of Volatile Organic Compounds (VOCs) and Semi-VOCs.

As shown in Figure 11, EPA Method 0010 is used to characterize VOCs and Semi-VOCs,. Sample traps are delivered to Pyrolysis-gas chronograph mass spectroscopy (GCMS) for analysis.

Figure 11. Sampling Train for VOCs and Semi-VOCs

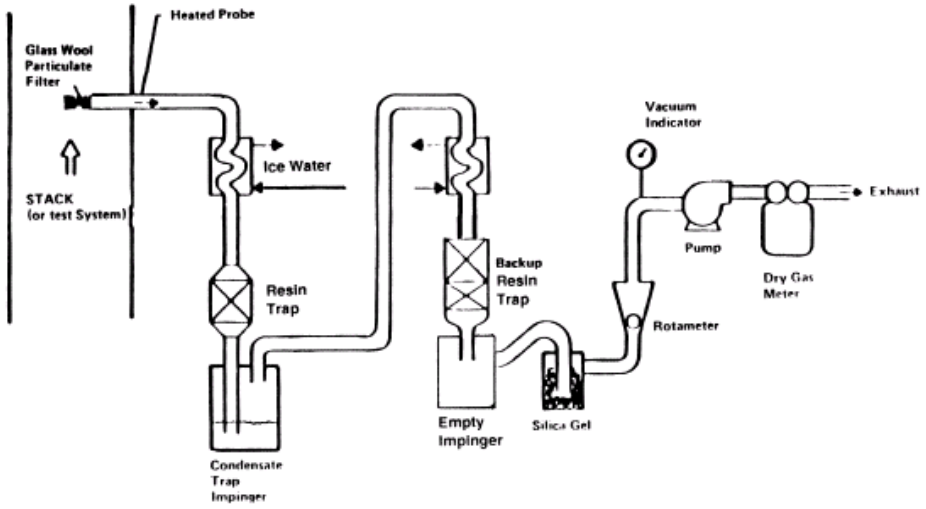

5.3.7 Measurement of Ammonia (NH_3) by EPA OTM27.

This method is used to collect ammonia emissions from the coal-fired boiler at power plants. The impinger system for collecting ammonia consists of 100 mL of 0.1N sulfuric acid (H_2SO_4) in the first and second impingers, an empty third impinger, and 200-300 grams of indicating silica gel in the fourth impinger. All four impingers are weighed for calculate moisture. After sampling, all four impingers are weighed for moisture. An ion chromatograph (IC) equipped with a conductivity detector is used for ammonium ion separation and quantization. A daily calibration curve is prepared using at least six standards that bracket the expected range of sample concentrations before sample solution analysis starts. Calibration standards are prepared in 0.04 N H_2SO_4; the same concentration of acid as in the diluted samples. The setup of IC is as followed:

Instrument:	Dionex Model 2120i or high grade
Separator Column:	Dionex HPIC-CS1
Suppressor Column:	Dionex Cation Micromembrane

Effluent: 0.005 N Hydrochloric Acid

Effluent flow rate: 2.3ml/min

Reagent: 0.1 M Trtrabutylammonium hydroxide

Sample Loop Volume: 100 L

5.3.8 Measurement of SO_2/SO_3 by ASTM Selective Condensation Method.

This method is specially-designed to collect SO_3 in coal-derived flue gas. The principle of this method is to separate SO_3 from SO_2 based on the maximum difference in condensation kinetics of SO_3 and SO_2 at temperature of about 60 to 65 ^oC. CONSOL Energy, Inc. developed this method 15 years ago. It was reported to be accurate in SO_3 collection in the coal-derived flue gas by extensive SO_3 sampling. This method, as shown in Figure 12, is reliable, reproducible and sensitive. Its standard deviation is below 1 ppmv of SO_3 with the relative standard deviation at about 10 %. In this method, the SO_3 sampling probe (initial probe herein) is set up at about 250 ^oC, and thus, eliminates the negative bias from the condensation of SO_3 in the sampling probe. Recent experience of explaining this method indicates that at a temperature of about 60 to 65 ^oC in the condenser and sampling rate of about 3 liters per minute are needed to ensure the completeness of SO_3 condensation. Other experience also indicated that this method would likely have a negative bias due to the setup of its ash filtration system in front of sampling probe, whose temperature is close to the flue gas temperature inside the ductwork. Filtered fly ash will likely collect SO_3 in the gas stream before it enters the SO_3 condenser. In these tests, an inertial probe is always used so that bias brought on by fly ash can be largely eliminated.

Figure 12. Sampling Train for SO_3 Measurement

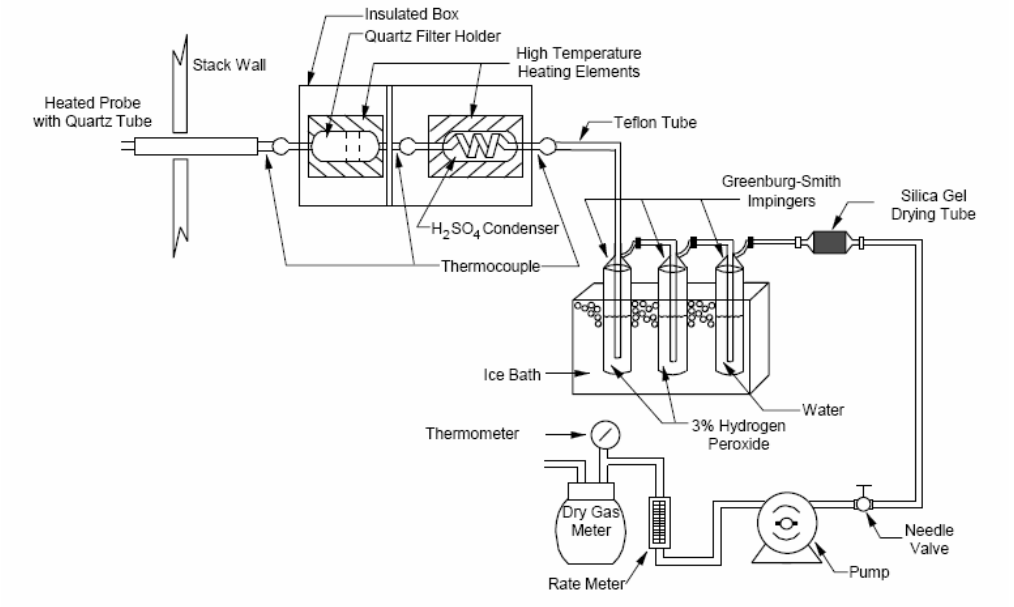

Checking and analyzing all reagent blanks including De-ionized water, acetone and methylene chloride with 100 ml. (Reagent blank should be within 0.001 percent by weight) are required throughout all of EPA standard methods.

5.4 PRB-Fired operation in CFBC System and Switching to Co-firing with Wood Pallet

In the afternoon of July 22, 2008, the firing of the CFBC system started. Overnight firing gradually increased the temperature of the whole system, which was ready for performance evaluation under normal operating conditions. On July 23 2008, the first full evaluation of the 0.6 MW_{th} CFBC system was conducted while firing PRB coal in the morning and co-firing of PRB coal and wood pallets (WP) in the afternoon.

As indicated in Figure 13-1 and Table 9-1, the PRB coal only feed rate was kept nearly constant and averaged about 137 pounds per hour. Therefore, the CFBC system was operated at a thermal input of 320 kW by coal. The thermal output of 206 kW was maintained by heat exchangers (HX), which was over half of the full setting load (600 kW by coal thermal input). As indicated in Figure 13-2 and Table 9-1, the feed rate of the primary air was kept constant and averaged about 9.4 pounds per minute (at standard condition) and a rate of 3.9 pounds per minute on avaerager for the secondary air on average. The ratio of secondary air to total air was about 29.4 %. The air delivery into CFBC system through low loop seal was about 1.74 pounds per minute, a ratio was at 13.1%. Throughout tests, the limestone feeding rate was kept constant. The Ca/S ratio was about 7.3 during the firing of the PRB coal only. The limestone feed was over-supplied for sulfur capture because the limestone also served as initial bed material. The operation seemed very stable throughout testing during the firing of PRB coal only, which was mainly presented by the control of CFBC system temperatures at different locations. As indicated in Figure 13-3 and more detailed in Figure 13-4 which shows the temperature profiles over time at different locations, variations of temperature can be controlled within 100^{o}F. As indicated in Table 9-1 and Figure 13-5, the average temperatures along CFBC system height gradually decreased. Just above the windbox, the temperature was the highest of the whole facility at about 1530^{o}F. In the major parts (from R1 to R8 inside CFBC system riser, the temperature could be controlled above 1300^{o}F. At the secondary cyclone, the temperature dropped to 673^{o}F. The purpose of the higher temperature at the bottom of the riser was to maintain the activity of the limestone for sulfur capture; the lower temperatures at the middle and top of the riser resulted

from testing the functions of HX.

As indicated in Figure 13-1 and Table 9-2, the feed rate of coal was kept slightly lower, about 109 pounds per hour, but WP started to be fed at an average rate of 66 pounds per hour when the CFBC system was switched to operation in the co-firing mode. Therefore, the thermal input by fuels being fed reached 350 kW and thermal output by HX was increased to about 242 kW. Throughout the tests, the limestone feed rate was also kept constant. The feed rate of the primary air was kept constant and averaged at about 13.5 pounds per minute (at standard condition) and 2.7 pounds per minute for the secondary air on average. The ratio of secondary air to total air was decreased to about 16.6 %. The air delivery into the CFBC system through low the loop seal was still at about 1.74 pounds per minute, the ratio of which was decreased to about 10.8 % because of increases of the total air input. The average air to coal ratio (air/coal) was kept at 0.15 lb/lb. The Ca/S ratio was 10.1 during co-firing with the PRB coal and the WP for the same purpose previously mentioned. Similarly, the operation seemed stable after the initial period of feeding WP into the CFBC system during the co-firing of PRB coal. As indicated in Figure 13-3 and more detailed in Figure 13-4, which show the temperature profiles over time at different locations, variations of temperature can be controlled within 100^{o}F. As indicated in Table 9-2 and Figure 13-5, similar temperatures could be found during co-firing compared to that during the firing of PRB coal only, but slightly higher with comparison to two cases at different locations. Just above the windbox, the temperature was increased to about 1580^{o}F at R1. In the majority of parts (from R1 to R8 inside CFBC system riser) temperature could be controlled above 1400^{o}F. Temperature inside the secondary cyclone increased to about 759^{o}F.

Figures 13-6 and 13-7 presented variations of major combustion-source gases (including CO, CO_2 and O_2) and major air pollutants (SO_2 and NO) during the firing of PRB coal only and for the co-firing of PRB coal and WP. There were no major differences on the operational side, which was represented by O_2 and CO_2 concentrations in the flue gas. Under both operational conditions, flue gas O_2 and CO_2 at the flue gas exit were about 1.1 % and 18 %, respectively. Major differences were represented by air pollutant emissions of SO_2, NO and N_2O, as well as CO at the exit. Carbon monoxide was averaged at 358ppm during the firing of PRB coal, which was lower than 584 ppm during the co-firing of PRB coal and WP. It seemed there was no significant correlation between NO and CO concentrations despite a slight decrease of NO from 164ppm under PRB coal firing to 142 ppm under co-firing. However, Figure 13-6 clearly shows

the correspondence between NO and O_2. With increasing O_2, concentrations of NO followed to increase abruptly under both operational conditions. During the same period, the average CFBC system temperatures increased with the increase of O_2 concentration. Therefore, variations of NO should be attributed to generation of thermal NO during temperature increases by adjusting excessive air ratio. The system temperature also has a major impact on effectiveness of sulfur capture by limestone. As indicated in Figure 13-6, under the operational mode of co-firing, the system temperature was maintained at the normal temperature at 1500^{o}F starting from the initial period of WP feeding to the final stable feeding. Sulfur dioxide emissions continuously dropped and finally stabilized. Considering the constant feeding of limestone throughout test, the drop of SO_2 seemed to be attributed to the system temperature. It is generally accepted that the optimal temperature to allow limestone to effectively capture SO_2 is 1550 ^{o}F. Because of the larger particle size (average 1000 um) and the higher density of limestone used in this test, a larger portion of limestone remained at the bottom of the bed as bed material, where generally the highest temperature were at both operational conditions. Sulfur dioxide emissions, measured by emission CEM, were about 3.69 ppm and 10.9 ppm, respectively for both operational conditions. Results were verified by the EPA wet chemical method that SO_2 emissions were about 3.74 ppm and 4.57 ppm, respectively. Due to the lower system operational temperatures and also a lower occurrence of SO_2 in the flue gas, SO_3 emissions were also low at 1.38 ppm. Higher system temperatures also helped to control CO emissions on co-firing, which was represented by the drop of CO concentration when system temperature and O_2 feeding increased (as indicated in Figure 13-7).

Results from mercury CEM indicated that the total vapor phase mercury (Hg(VT)) was about 7.16 ug/NM^3 with over 94 % of Hg(VT) being the elemental mercury (Hg(0)) present during firing of PRB coal only. This result was verified by OHM, which reported similar results of Hg(VT) at 7.69 ug/NM^3 with 98 % of Hg(VT) being Hg(0). After operations began switching from firing of PRB coal only to co-firing of coal with WP, Hg(VT) dropped to 5.22 ug/NM^3 with similar mercury speciation. These CEM results were also verified by OHM, which reported similar Hg(VT) at 5.66 ug/NM^3. Compared to firing PRB coal only, the mercury emissions decreased. This drop is attributed to the decrease of mercury input, represented by the decrease of total mercury input in the fed fuels fed to the system because there is no mercury content in WP. The analysis of collected fly ash during the co-firing period, as shown in Table 8, show the

miniscule amount of mercury captured by fly ash (at about 0.006 ppm) although LOI of collected fly ash was high at about 14.2 %. The lack of mercury capture by fly ash was attributed the very high Hg(0) portion in the flue gas, which was about 95 % Hg(VT). The greater occurrence of Hg(0) in the flue gas was the consequence of very little halogen species in the flue gas in both operational modes, as indicated in Table 9-1 and Table 9-2. Total concentrations of HCl, HF, HBr Cl_2, F_2 and Br_2 were all very low (either below 1ppm or below the instrument detection limit for both operational modes). It's understandable because of the lower content of halogens in the PRB coal. This probably made the transformation of halogens present in the flue gas less effective. However, higher fluorine content was found in the WP, as indicated in Table 8, which did not result in higher content of HF or F_2 in the flue gas. There must be a mechanism that caused the gaseous halogen to be captured by fly ash inside the CFBC system, such as the calcited limestone.

Except mercury, emissions of other major trace metals were lower, as indicated in Table 9-1 and 9-2. When firing PRB coal only, the emissions of all trace metals were below 3.41 ug/NM^3; when co-firing PRB coal and WP, emissions rates of all trace metals were below 3.78 ug/NM^3.

Measurement results of CPM at the flue gas exit are also shown in Table 9-1 for firing PRB coal only and Table 9-2 for co-firing PRB coal with WP. Because of the inertial filter used for CPM sampling, there were no results for the filterable particulate matter (FPM). Results from firing PRB coal only indicated that the total CPM was about 30.13 mg/NM^3 for the first test and decreased to 18.33 mg/NM^3 for the second run. Because the organic CPM was only about 3.41 mg/NM^3 for the first test and 1.83 mg/NM^3 for the second test, more than 90 % of CPM was inorganic CPM. Similarly, for co-firing, the major portion of CPM was also inorganic at about 12.66 mg/NM^3 for the first test and 11.76 mg/NM^3 for the second test. The organic CPM was only about 2.02 mg/NM^3 for the first test and increased to 6.72 mg/NM^3 during the second test. The reason for the increase of organic CPM was likely the increase of unburned hydrocarbon concentrations in the flue gas when co-firing the highly-volatile WP, as indicated in Table 8.

To better understand the species that form CPM, major ions inside inorganic CPM were also analyzed by an IC instrument, including sulfate ion (SO_4^{2-}), nitrate ion (NO_3^{2-}), ammonium ion (NH_4^+), calcium ion (Ca^{2+}), magnesium ion (Mg^{2+}), potassium ion (K^+) and sodium ion (Na^+). When firing PRB coal only, the NH_4^+ ion in the inorganic portion of CPM was highest at about 6.62 and 8.02 mg/NM^3 for two runs. Chlorine (Cl^{-1}) ion in the inorganic portion of CPM was

higher (10.43 mg/NM^3) for the first run. Sulfate (SO_4^{2-}) ion in CPM should only be derived from sulfuric acid mist (SO_3) in the flue gas, as suggested by the Electric Power Research Institute (EPRI) research group. As indicated in Table 9-1 and 9-2, SO_3 concentrations were as low as 1.38 ppmv by better controlling sulfur with limestone feeding, which was equivalent to 1.11 mg/NM^3 SO_4^{2-} ion in CPM. This trend did not change when co-firing. Major organic species, including VOCs and semi-VOCs, in the flue gas were determined by GC-MS. Results, as indicated in Table 9-1 and 9-2, show that the emissions of VOCs and semi-VOCs were both below the detection limit of the instrument during the period of co-firing, except for benzene in the VOC. Benzene was about 21.5 ug/NM3 during test.

Figure 13-1. Variations of Coal Feeding, Limestone Feeding, WP Feeding and Load during Tests Conducted on July 23, 2008

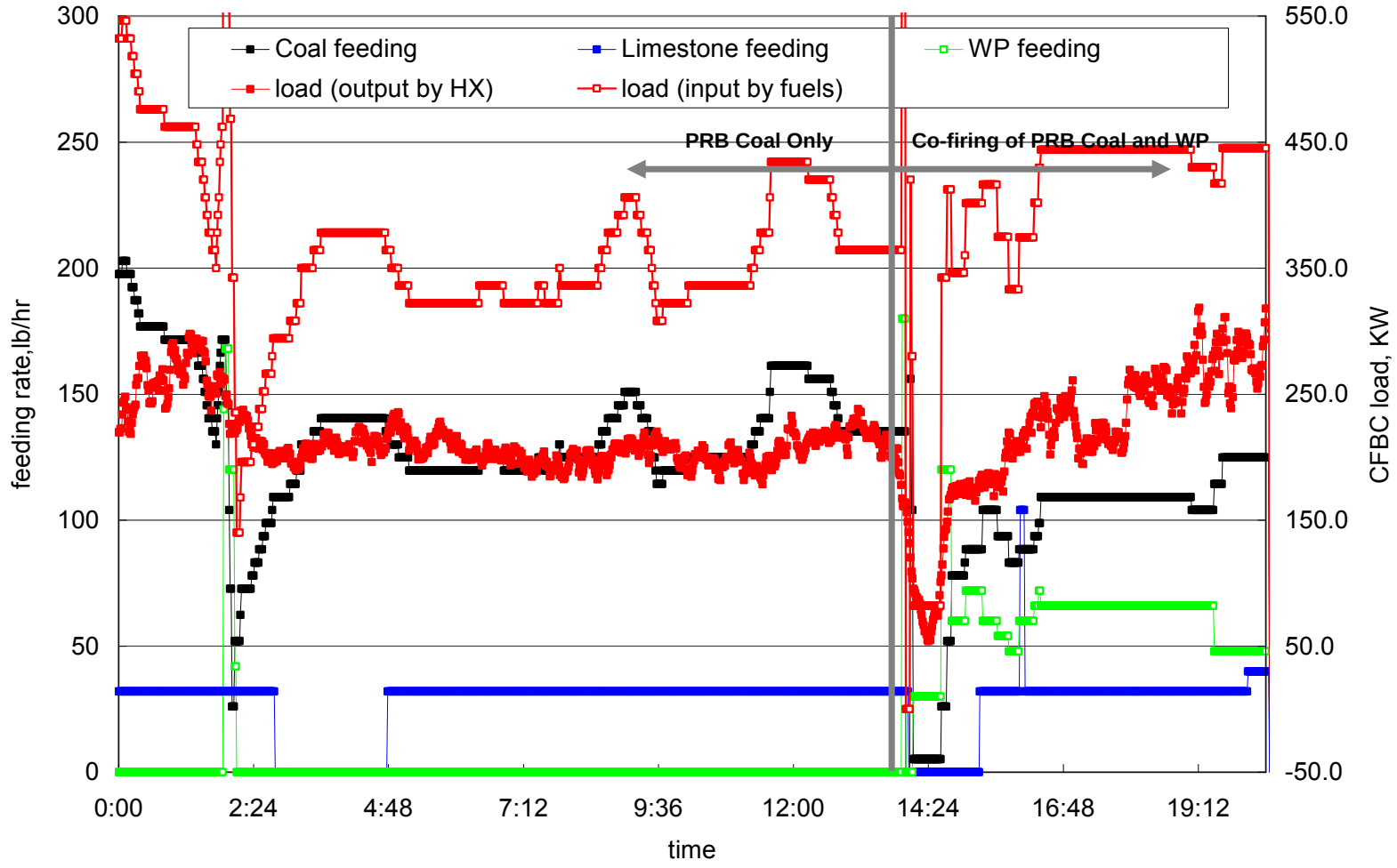

Figure 13-2. Variations of Supplies of the Primary Air, the Secondary Air and the Loop Seal Air during Test Conducted on July 23, 2008

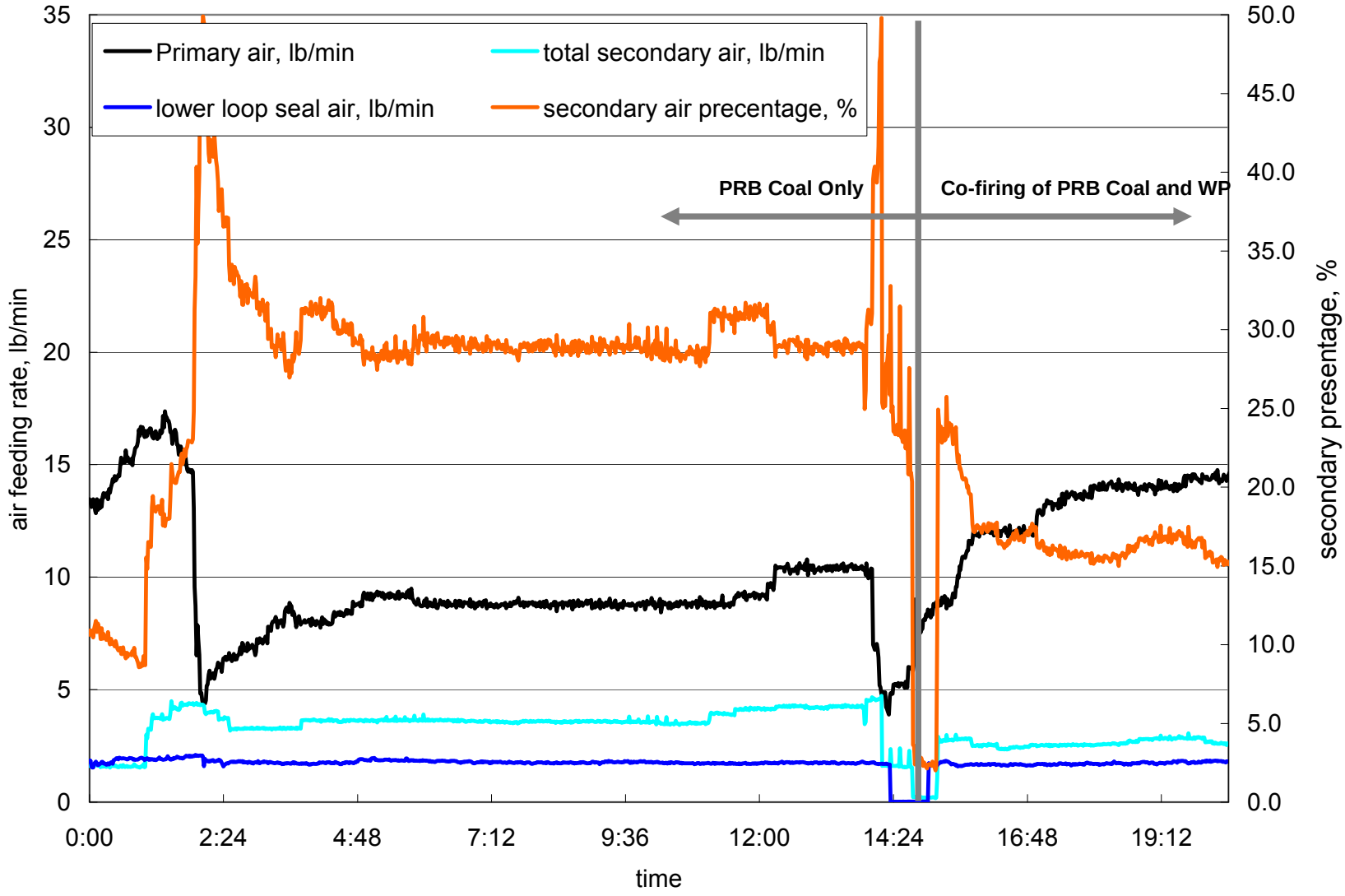

Figure 13-3. Variations of Temperature Profiles over Time in CFBC System Riser during Test Conducted on July 23, 2008

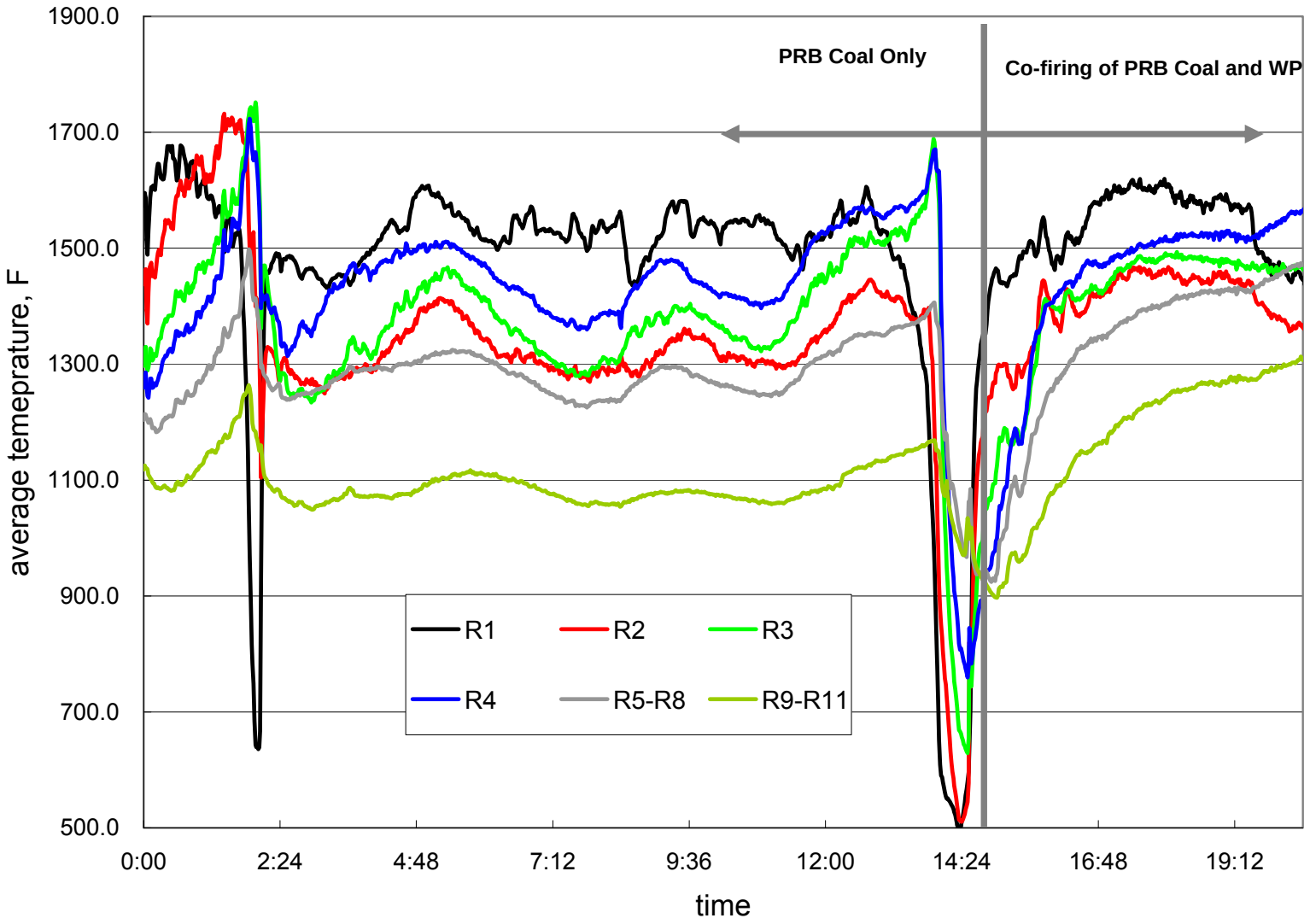

Figure 13-4. Variations of Detailed Temperature Profiles over Time inside CFBC System Riser During Test Conducted on July 23, 2008

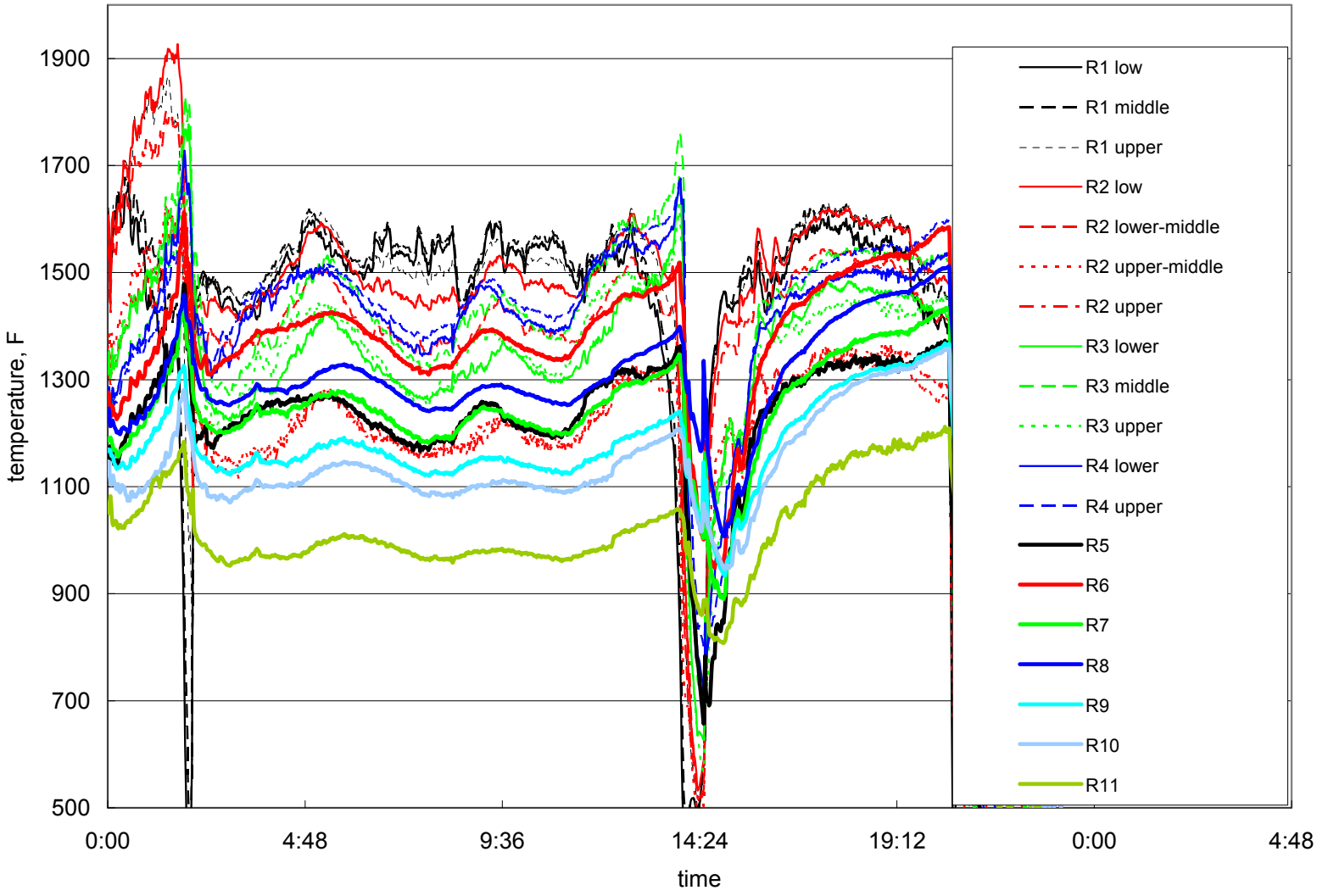

Figure 13-5. Average Temperature Profiles during the Firing of PRB Coal Only and the Co-Firing with WP

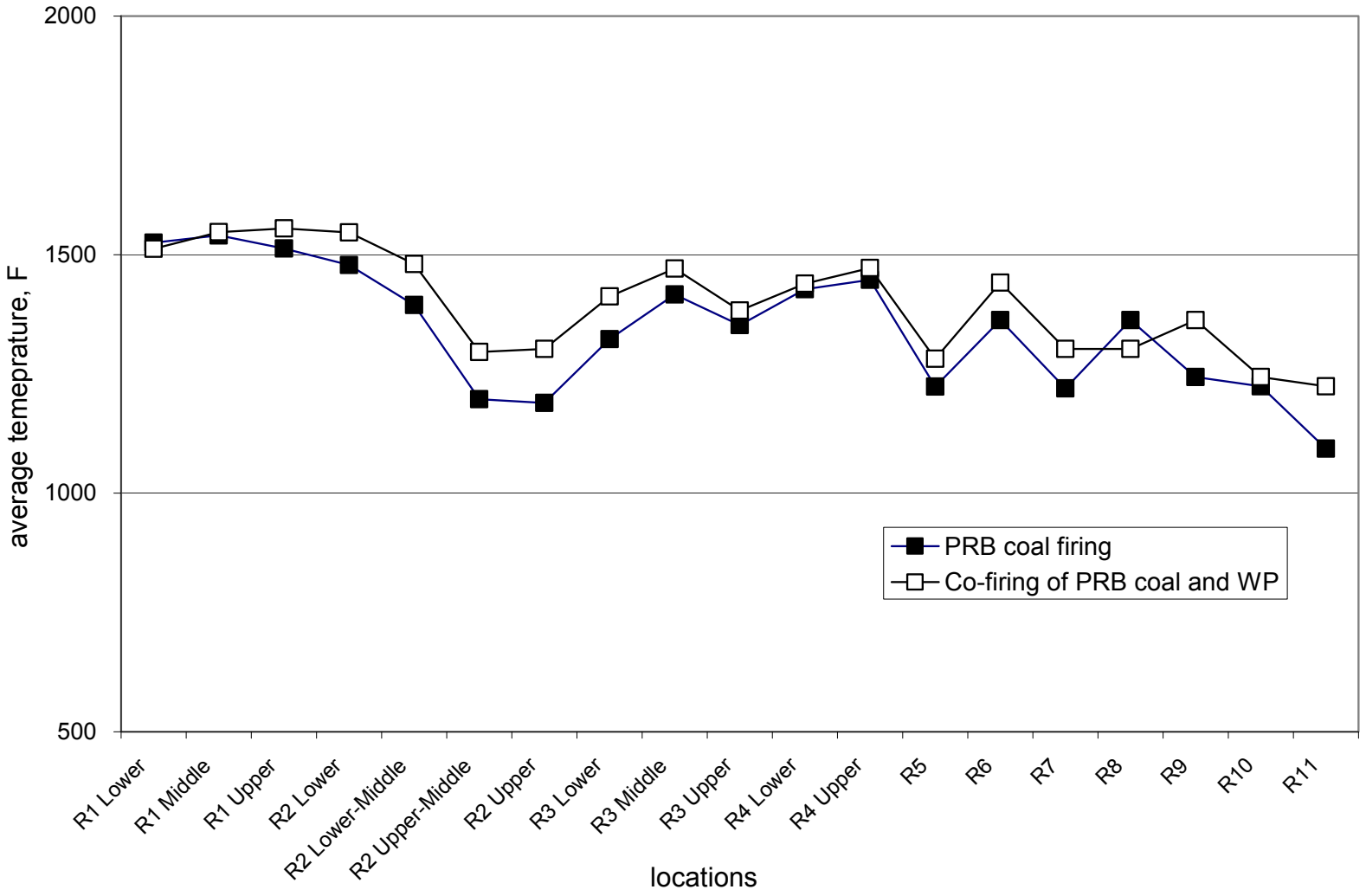

Figure 13-6. Variations of NO, SO_2 and O_2 during the Firing of PRB Coal Only and the Co-Firing with WP

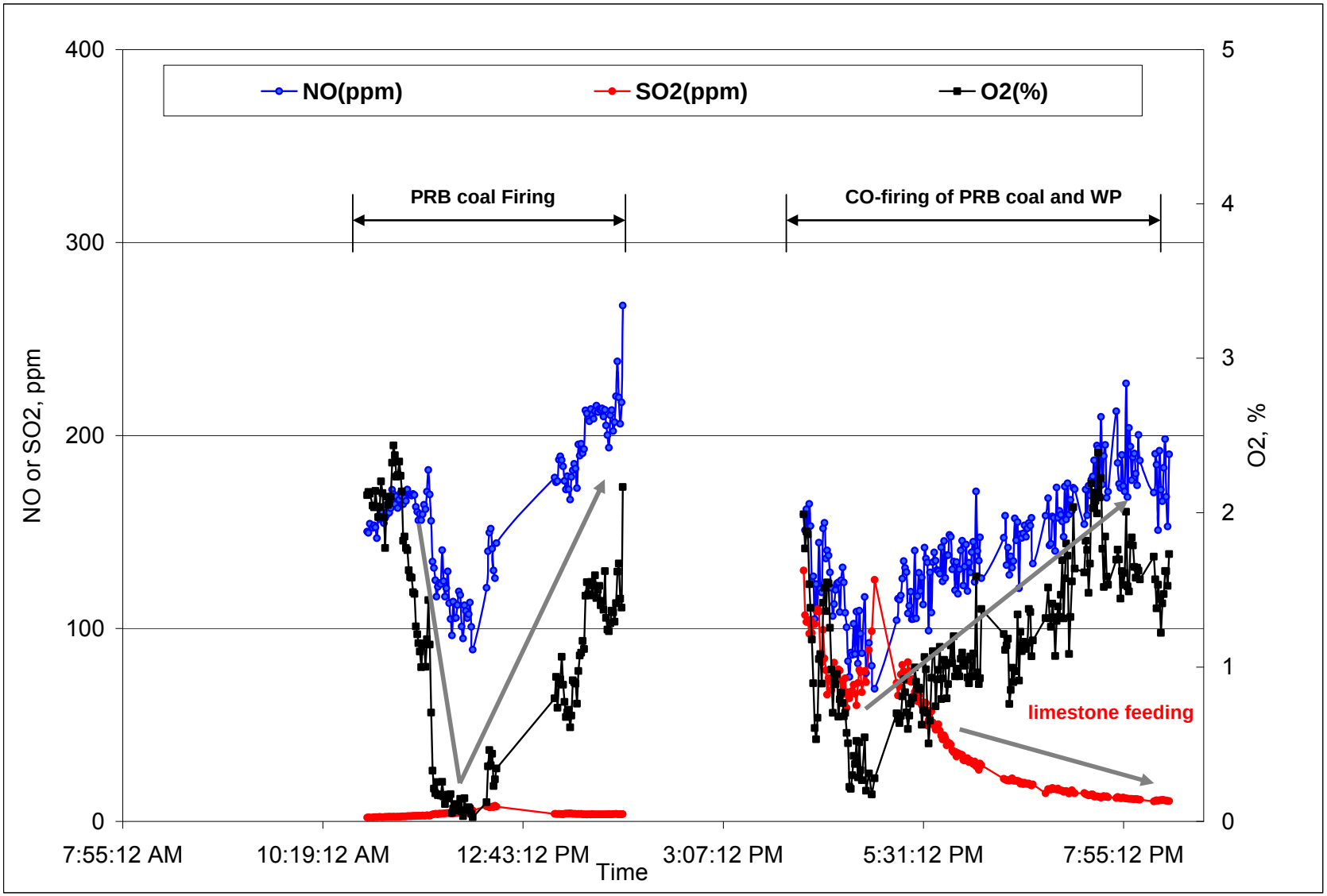

Figure 13-7. Variations of CO, CO_2 and O_2 during the Firing of PRB Coal Only and the Co-Firing with WP

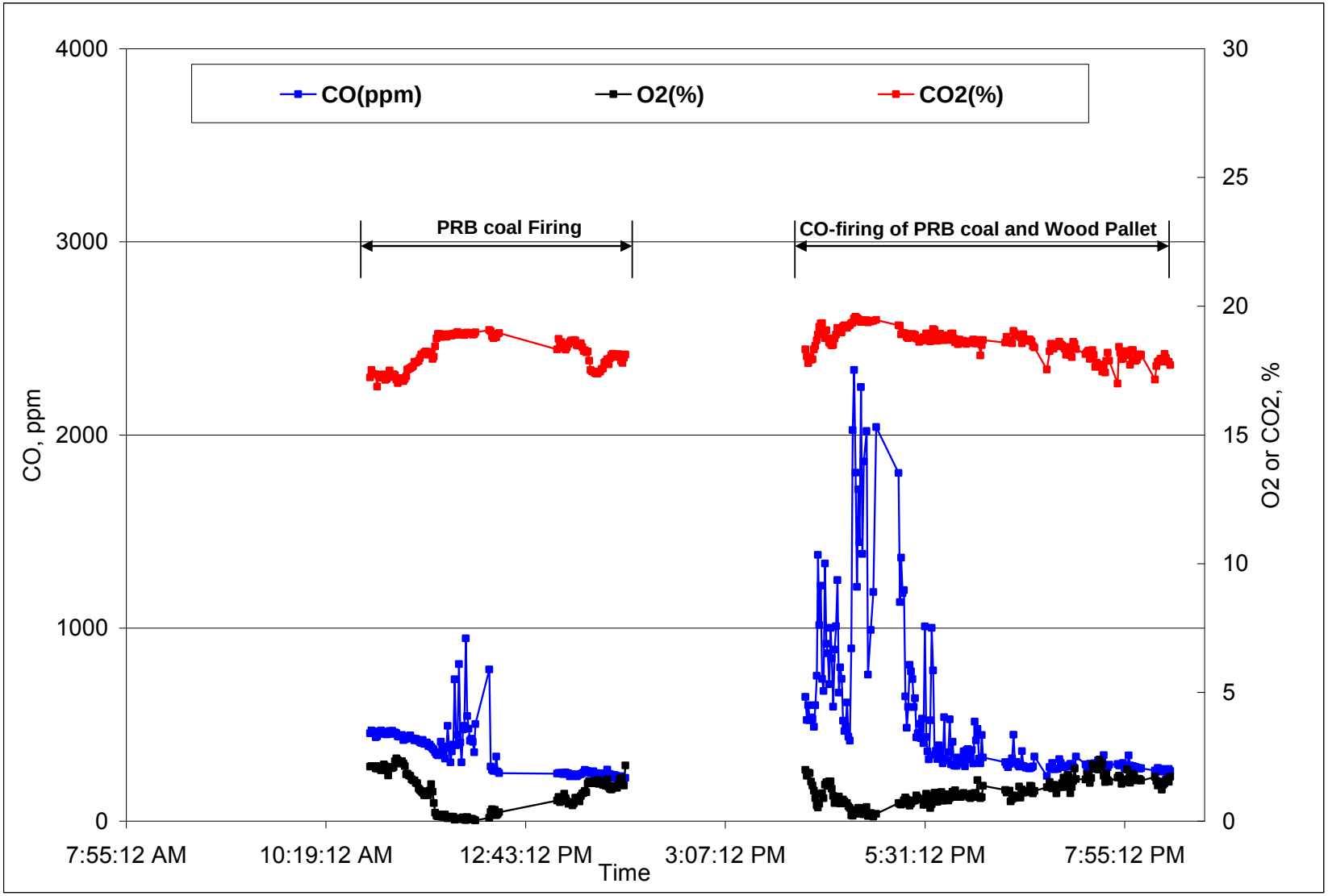

Table 9-1. Operational Parameters and Emission Rates of Air Pollutants during the Firing of PRB Coal Only

CFBC RUN #1-1																			
Mode: PRB coal only	Date: July 23 08																		
A. Operation parameters																			
	Coal feed	Biomass Feed	Limestone feed	Co-firing ratio	Primary air	Secondary air	Loop seal air	Sec air ratio	L-air ratio	Load by coal	Load by HX	Ca/S							
	lb/hr	lb/hr	lb/hr	%	lb/hr	lb/hr	lb/hr	%	%	KW	KW								
	136.8	0	32	0	9.37	3.9	1.74	29.4%	13.1%	320.4	206.6	7.30							
Temeprature Profile																			
Locations	R1	R2	R3	R4	R5	R6	R7	R8	R9	R10	R11	Pri. Cycl. Dis.	Sec. Sysl. Dis.						
°F	1530.3	1353.4	1420.8	1483.5	1255.5	1397.6	1245.6	1296.1	1159.7	1122.2	990.0	770.6	671.9						
B. Gas composition at stack																			
	Temperature																		
1. Permnent gas																			
	O_2, %	N_2, %	CO_2, %	CO, ppm	SO_2, ppm	NO, ppm	N_2O, ppm												
	1.11		18.14	358.55	3.69	164.02													
2. Mercury, corrected to 3% O_2																			
2.1 Methid:OHM	Hg(0)	Hg(2+)	Hg(VT)	Hg(0)/Hg(VT), %															
ug/NM^3	7.57	0.12	7.69	98.4															
2.2 Method:SCEM	Hg(0)	Hg(2+)	Hg(VT)	Hg(0)/Hg(VT), %															
ug/NM^3	6.85	0.31	7.16	95.7															
3. Trace Metals																			
	Ag	As	Ba	Be	Cd	Co	Cr	Cu	Mn	Mo	Ni	Pb	Sb	Se	Tl	V	Zn	Th	U
ug/NM^3	< 3.41	< 3.41	< 3.41	< 3.41	< 3.41	< 3.41	< 3.41	< 3.41	< 3.41	< 3.41	< 3.41	< 3.41	< 3.41	< 3.41	< 3.41	< 3.41	13.34	< 3.41	< 3.41
4. VOCs & Semi-VOCs																			
VOCs																			
Semi-VOCs																			
5. Halogens																			
	HF	HCl	HBr	F_2	Cl_2	Br_2													
	0.018	0.06	UD	0.061	0.58	UD													
6. Others																			
	NH_3	SO_3	SO_2																
	UA	1.38	3.74																
7. PM&CPM																			
	PM	CPM																	
		Inorganic-CPM	Organic-CPM	total															
Sample 1		26.81	3.41	30.22															
Sample 2		16.24	1.83	18.01															
								Inorganic-CPM											
		F	Cl	Br	NO_3	PO_4	SO_4	Li	Na	NH_4	K	Mg	Ca						
Sample 1		0.11	10.43	ND	2.75	ND	1.47	ND	1.10	6.62	0.12	0.05	0.53						
Sample 2		0.12	0.53	ND	3.43	ND	1.12	ND	0.39	8.02	0.07	0.18	1.57						
Note: UA - unavailabe; ND - nondetectable																			

Table 9-2. Operational Parameters and Emission Rates of Air Pollutants during the Co-firing of with WP

CFBC RUN #1-2																			
Mode: co-firing,	Date: July 23 08																		
PRB coal + Wood pallet																			
A. Operation parameters																			
	Coal feed	Biomass Feed	Limestone feed	Co-firing ratio	Primary air	Secondary air	Loop seal air	Sec air ratio	L-air ratio	Load by coal	Load by HX	Ca/S							
	lb/hr	lb/hr	lb/hr	%	lb/min	lb/min	lb/min	%	%	KW	KW								
	108.6	65.8	32	37.7%	9.37	3.9	1.74	29.4%	13.1%	350.6	242.6	10.1							
Temeprature Profile																			
Locations	R1	R2	R3	R4	R5	R6	R7	R8	R9	R10	R11	Pri. Cycl. Dis.	Sec. Sysl. Dis.						
°F	1586.6	1444.0	1468.6	1505.5	1322.3	1495.3	1351.3	1415.8	1287.2	1269.7	1136.1	885.0	759.5						
B.Gas composition at stack																			
	Temperature																		
1. Permnent gas																			
	O_2, %	N_2, %	CO_2, %	CO, ppm	SO_2, ppm	NO, ppm	N_2O, ppm												
	1.15		18.58	584.52	10.9	142.4	304	231											
2. Mercury																			
2.1 Methid:OHM	Hg(0)	Hg(2+)	Hg(VT)	Hg(0)/Hg(VT), %															
ug/NM^3	5.44	0.22	5.66	96.1															
2.2 Method:SCEM	Hg(0)	Hg(2+)	Hg(VT)	Hg(0)/Hg(VT), %															
ug/NM^3	4.8	0.42	5.22	92.0															
3. Trace Metals																			
	Ag	As	Ba	Be	Cd	Co	Cr	Cu	Mn	Mo	Ni	Pb	Sb	Se	Tl	V	Zn	Th	U
ug/NM^3	< 3.78	< 3.78	< 3.78	< 3.78	< 3.78	< 3.78	< 3.78	< 3.78	< 3.78	< 3.78	< 3.78	< 3.78	< 3.78	< 3.78	< 3.78	< 3.78	8.82	< 3.78	< 3.78
4. VOCs & Semi-VOCs																			
VOCs	Benzene	1-Propene, 1,1-dichloro-	Trichloroethylene	Methane, dibromo-	Methane, bromodichloro-	Toluene	1-Propene, 1,3-dichloro-	Ethane, 1,1,2-trichloro-	Propane, 1,3-dichloro-	Tetrachloroethylene	Benzene, chloro-	Ethane, 1,1,1,2-tetrachl	Ethylbenzene	p-Xylene					
ug/NM^3	21.42747	< 0.35	< 0.35	< 0.35	< 0.35	0.60	< 0.35	< 0.35	< 0.35	0.417701754	< 0.35	< 0.35	< 0.35	< 0.35					
	< 0.35	< 0.35	< 0.35	< 0.35	< 0.35	< 0.35	< 0.35	< 0.35	< 0.35	0.350877193	< 0.35	< 0.35	< 0.35	< 0.35					
	styrene	Benzene, bromo-	Benzene, 1-chloro-2-meth	Benzene, 1,3,5-trimethyl	Benzene, 1,2,4-trimethyl	Benzene, 1-methyl-3-prop	Benzene, 4-ethyl-1,2-dim	Propane, 1,2-dibromo-3-c	Benzene, 1,2,4-trichloro	Naphthalene	Benzene, 1,2,3-trichloro	1,3-Butadiene, 1,1,2,3,4	o-Xylene						
	< 0.35	< 0.35	< 0.35	< 0.35	< 0.35	< 0.35	< 0.35	< 0.35	< 0.35	< 0.35	< 0.35	< 0.35	< 0.35						
	< 0.35	< 0.35	< 0.35	< 0.35	< 0.35	< 0.35	< 0.35	< 0.35	< 0.35	< 0.35	< 0.35	< 0.35	< 0.35						
Semi-VOCs	pyridine	1,4-dichlorobenzene	2-methylphenol	3-methylphenol	4-methylphenol	hexachloroethane	nitrobenzene	2,4,5-trichlorophenol	2,4,6-trichlorophenol	2,4-dinitrotoluene	hexachlorobenzene								
ug/NM^3	< 1.064	< 1.064	< 1.064	< 1.064	< 1.064	< 1.064	< 1.064	< 1.064	< 1.064	< 1.064	< 1.064								
	< 1.064	< 1.064	< 1.064	< 1.064	< 1.064	< 1.064	< 1.064	< 1.064	< 1.064	< 1.064	< 1.064								
5. Halogens																			
	HF	HCl	HBr	F_2	Cl_2	Br_2													
	0.012	0.049	UD	0.07	0.45	UD													
6. Others																			
	NH_3	SO_3	SO_2 (M8A)	SO_2 (CEM)															
	UA	1.38	4.57																
7. PM&CPM, mg/NM^3																			
	PM		CPM																
		Inorganic-CPM	Organic-CPM	total															
Sample 1		11.57	2.02	13.59															
Sample 2		10.63	6.72	17.35															
		Inorganic-CPM																	
		F	Cl	Br	NO_3	PO_4	SO_4	Li	Na	NH_4	K	Mg	Ca						
Sample 1		0.09	2.52	ND	0.51	ND	0.30	ND	0.15	7.71	0.04	0.01	0.30						
Sample 2		0.09	0.41	ND	0.70	ND	0.24	ND	0.26	8.55	0.04	0.06	0.09						

5.5 Co-firing of PRB Coal and Switching to Co-firing with Chicken Waste

On the afternoon of July 29 2008, the second firing of the CFBC system continued. As with the previous test, overnight firing was conducted to increase the system temperature close to the normal operating conditions. The following morning, the second full evaluation of the 0.6 MW_{th} CFBC system was conducted starting with firing PRB coal, at an even higher than the test conducted on July 23, 2008. In the afternoon, the system was switched to co-firing PRB coal and chicken waste (CW).

As indicated in Figure 14-1 and Table 10-1, PRB coal feeding was kept nearly constant after an initial temperature ramp. Therefore, the CFBC system was operated close to 60 % of the full setting load (600 kW by coal thermal input) at a thermal input by the coal of 320 kW (the thermal output by the HX at about 263.3 kW). As indicated in Figure 14-2 and Table 10-1, the feed rate of the primary air was kept constant and averaged about 12.37 pounds per minute (at standard condition) and 2.48 pounds per minute for the secondary air. The ratio of secondary air to total air decreased to about 16.7 % compared to that in the first firing on July 23, 2008. The purpose of decreasing the secondary air was the evaluation of its impact on air pollutant emissions. The air delivery into CFBC system through the lower loop seal also decreased to about 1.07 pounds per minute, a ratio of at 7.3 %. Throughout the tests, the limestone feed rate was not kept constant in the initial stage because of frequent jams of limestone screw auger. The operation seemed stable after load tuning when the measurement of air pollutants began. Smaller sizes of limestone were used during this test. The Ca/S ratio was set at about 4.5. Temperatures of the CFBC system at different locations are shown in Figure 14-3. It seemed variations of temperatures could be controlled within 100 ^{o}F. As indicated in Table 10-1 and Figure 14-4, the average temperatures along the CFBC system height gradually decreased as those did in the previous test. Just above the windbox, the temperature was the highest at about 1547 ^{o}F. In the major parts (from R1 to R8 inside CFBC system riser), the temperature could be controlled above 1350 ^{o}F. Only the temperature of R5 in the riser was unusually low (1285 ^{o}F) because of the larger coolant flow rate was used. The temperature of the secondary cyclone at the top of the CFBC system was about 768 ^{o}F.

As indicated in Figure 14-1 and Table 10-2, the coal feed rate was kept slightly lower, about 146.3 lb/hr, but CW started to be fed at an average rate of 32.1 pounds per hour when the CFBC system was switched for operations at a co-firing mode. Therefore, the thermal input by the fuels

feed was about 385 kW and thermal output by HX was increased to about 254 kW. The feed rate of the primary air was also kept constant and averaged at about 12.37 pounds per minute (at standard condition) and 2.87 pounds per minute for the secondary air on average. The ratio of secondary air to the total air was about 18.8 %. The air delivery into the CFBC system through the lower loop seal was still at about 1.08 pounds per minute, a ratio of about 7.1%. Throughout the testing, the limestone feed rate was kept constant. The Ca/S ratio was slightly lower at 3.7 during co-firing of the PRB coal and the CW. Operational conditions during co-firing were maintained really equivalent to those used during the firing of PRB coal only.

The operation was stable, as shown in Figure 14-3 which illustrates temperature variation over time. Temperature variations at different locations can be controlled within 100 ^{o}F, except at location R4 to R8. As indicated in Table 10-1 and Figure 14-4, similar temperatures could be found during co-firing compared to during PRB coal firing only, but was slightly higher compared to two cases at different locations. Just above the windbox, the temperature was maintained at about 1546^{o}F at R1 for the firing of PRB coal only, versus 1537^{o}F for co-firing. In the majority of locations (from R1 to R8 inside CFBC system riser, temperatures were appreciably lower than expected and varied between 1200 ^{o}F and 1400 ^{o}F during co-firing.

Figures 14-5 and 14-6 present variations of CO, CO_2 and O_2, SO_2 and NO during when firing PRB coal only or co-firing PRB coal and CW. There were no major differences in operations, which are represented by O_2 and CO_2 concentrations. Under both operational conditions, O_2 and CO_2 at the flue gas exit varied between 0.68 % and 1.1 % and between 18.9 % and 16.9 %, respectively. Major differences were measured by air pollutant emissions of SO_2, NO, N_2O, as well as CO at the flue gas exit. Carbon monoxide averaged 266 ppm under PRB coal only firing, which was significantly lower than 5663 ppm on average under co-firing with PRB coal and CW. Consequently, NO was very low under co-firing conditions: about 12 ppm. Higher concentrations of reducing agents, such as CO present at concentrations at above 5000 ppm, was likely responsible for the additional drop of NO during co-firing of PRB coal and CW. Nitrogen oxide was about 34 ppm under PRB coal firing only. Similar to tests conducted on July 23, a clear correspondence between NO and O_2 was observed, as indicated in Figure 14-5. Therefore, a better combustion performance inside the CFBC system should be responsible for the lower NO emissions when firing PRB coal only. It is believed that these factors also impacted N_2O emissions, because lower emissions of N_2O were found in both cases during tests conducted on

July 30, 2008. Upon the firing of PRB coal only, the N_2O emission rate was averaged at about 170ppm, and decreased to 110 ppm upon co-firing PRB coal and CW when CO is higher. Despite this, high CO concentrations are not acceptable for the CFBC system. The higher CO emissions could be attributed to lower system temperature caused by a lower secondary air ratio, especially in the upper parts of system. A well maintained bottom temperature at R1 (1537 ^oF) and a smaller size limestone improved the capture efficiency of SO_2 by limestone in both cases although the CW had an increased sulfur content. With these operational conditions, SO_2 emissions were about 3.14 ppm for PRB coal only firing and was even lower at 1.25 ppm during co-firing of PRB coal and CW.

Mercury CEM reported similar mercury emissions when firing only PRB coal in two tests on July 23 and July 30, 2008. The total vapor gas mercury (Hg(VT)) was about 9.03 ug/NM^3 with over 89 % of Hg(VT) being elemental mercury (Hg(0)). After operations were switched to co-fire coal with CW, Hg(VT) dropped slightly to 8.6 ug/NM^3 on average with similar mercury speciation. The CEM results also were verified by OHM, which reported similar Hg(VT) by 8.18 ug/NM^3. A slight drop of mercury emissions are attributed to a decrease of mercury input, as represented by the decrease of total mercury input in the fuels due to minimal mercury content in the CW. The analysis of fly ash collected during the co-firing period, as shown in Table 8, also supported this issue by reporting the miniscule amount of mercury captured by fly ash (about 0.006ppm) although LOI of collected fly ash was as high as about 30.2 %. The ineffectiveness of fly ash to capture mercury was attributed to the higher Hg(0) content in the flue gas, which was more than 90% Hg(VT). The higher occurrence of Hg(0) in the flue gas was the consequence of a very low content of halogen species present in the flue gas in both operational modes, as indicated in Table 10-1 and Table 10-2. The total halogen concentrations in the flue gas were very low (below 1 ppm for both operational modes). Less halogen in the PRB coal may have made transformation of the fuel's halogen in the flue gas less effective. However, the high chlorine content in the CW, as indicated in Table 8, seemed not to be the result of high mercury oxidation. Investigation of a temperature profile inside the riser of the CFBC system revealed that the likelihood of an optimal temperature range for halogen capture not only in limestone, but also a higher content of alkali metal oxides or alkali earth metal oxides in fuels. The occurrence of temperatures lower than 650^oC in the upper part of the fluidized-bed combustor seemed to be responsible for the reduction of gaseous chlorine as well as other halogen species, and

consequently limited mercury emission reductions during co-firing. This study identified the important impacts of temperature profiles and oxides of alkali metal (alkali earth metal) on mercury emissions during co-firing in the circulating fluidized-ed combustor. Results obtained in the 0.6MW_{th} CFBC system matched those from the laboratory-BC facility, as indicated in the Appendix of this report.

Trace metal measurement was only conducted when co-firing PRB coal and CW. As indicated in Table 10-2, emissions of major trace metals were still lower although several major trace metals such as Cu, Mn and Zn in fed CW were higher, It seemed that Cu and Mn were easily bound to the fly ash because of their lower concentration in flue gas (below 4.35 ug/NM^3 which is the detection limit of the instrument). This was not true for Se and Zn, whose concentrations were about 16.69 ug/NM^3 and 22.50 ug/NM^3 in the flue gas, respectively. It was understandable to find a higher occurrence of Zn in the flue gas with its lower vapor pressure. A surprisingly higher amount of Se also occurred in the flue gas. This may have been attributed to operational conditions.

Measurements of CPM at the flue gas exit are also shown in Table 10-1 for firing PRB coal only. Results from firing PRB coal only indicated that the total CPM was extremely low at 2.46 mg/NM^3. The organic portion was only about 0.15 mg/NM^3. Better combustion performance seemed to help control the CPM emissions during when firing only PRB coal only. Characterization of ions in inorganic CPM indicated that the major ion was HNO_3^{-1}, which was about 1.98 mg/NM^3.

The major organic species found during co-firing of PRB coal and CW, including VOCs and semi-VOCs, is reported in Table 10-2. Emissions of the VOCs and semi-VOCs were both below the detection limit of instrument during co-firing, except for unusual higher level of benzene at 12.8mg/NM^3 and styrene at 15.3ug/NM^3in the VOCs, and pysidine at 21.3 ug/NM^3. Co-firing PRB coal with CW should be repeated in a future study to eliminate CO and VOC and semi-VOCs,.

Figure 14-1. Variations of Coal Feeding, Limestone Feeding, WP Feeding and Load during Tests Conducted on July 30, 2008

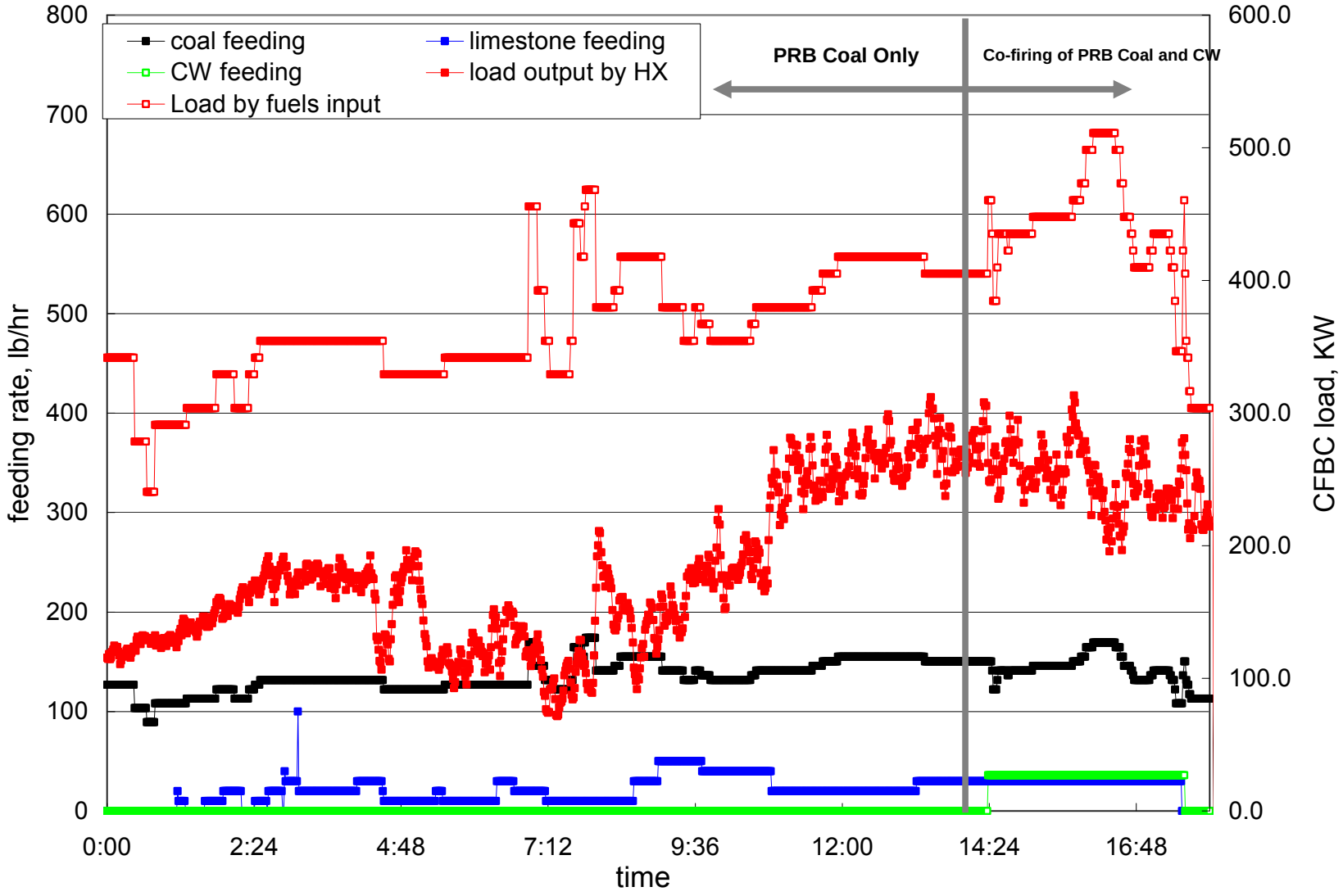

Figure 14-2. Variations of Supplies of the Primary Air, the Secondary Air and the Loop Seal Air during Tests Conducted on July 30, 2008

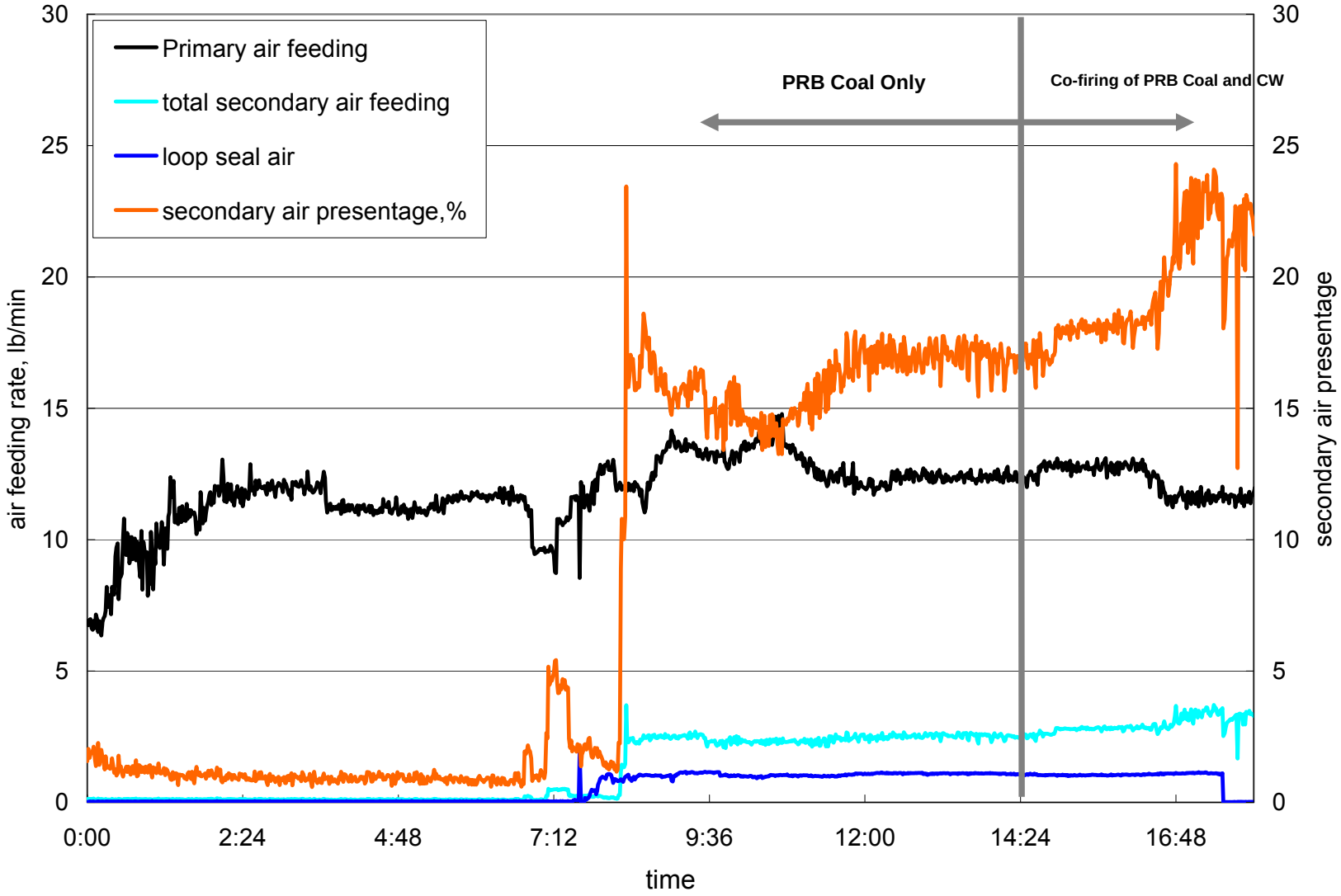

Figure 14-3. Variations of Temperature Profiles over Time in CFBC System Riser during Tests Conducted on July 30, 2008

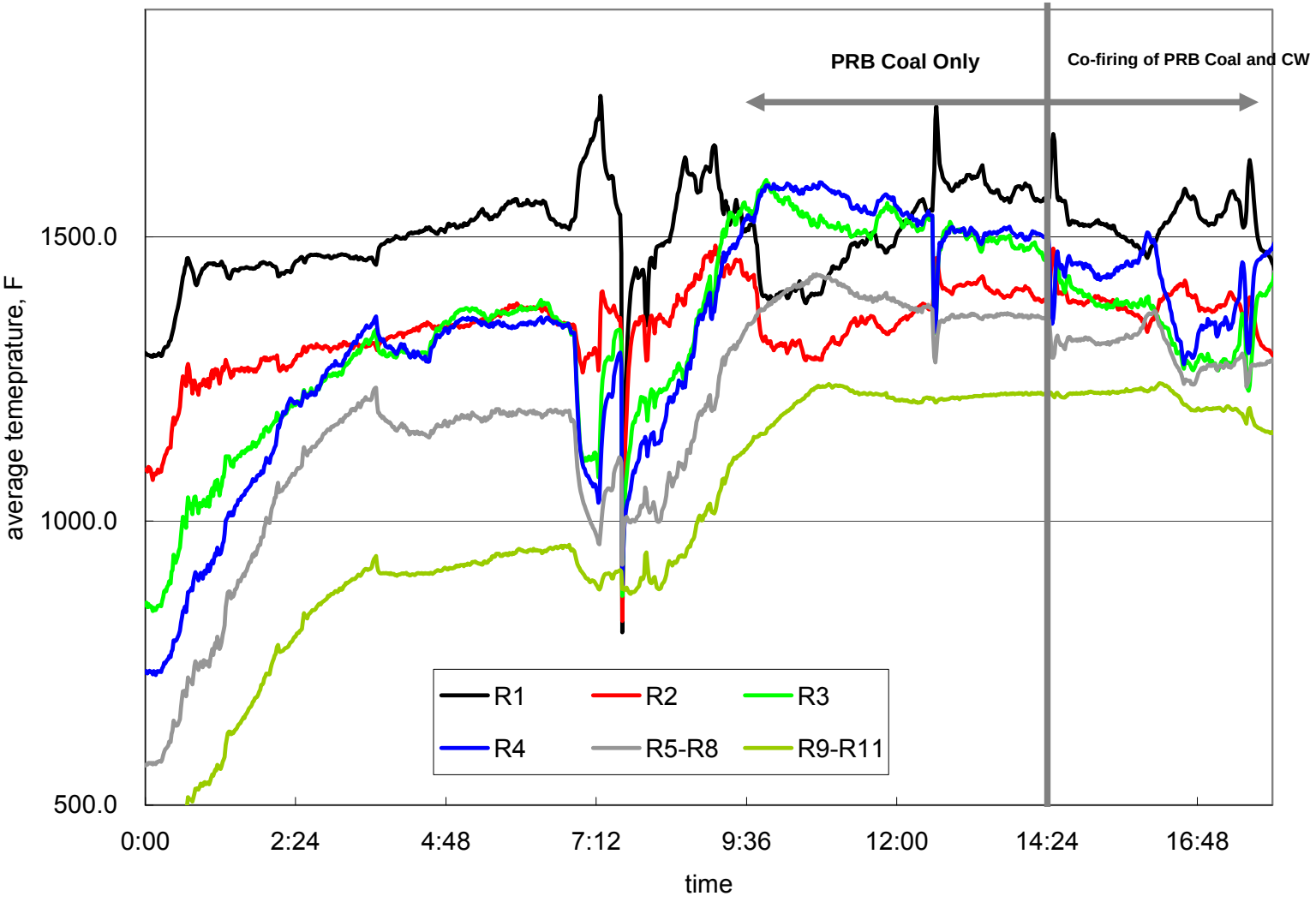

Figure 14-4. Average Temperature Profiles during the Firing of PRB Coal only and the Co-firing of PRB Coal with CW

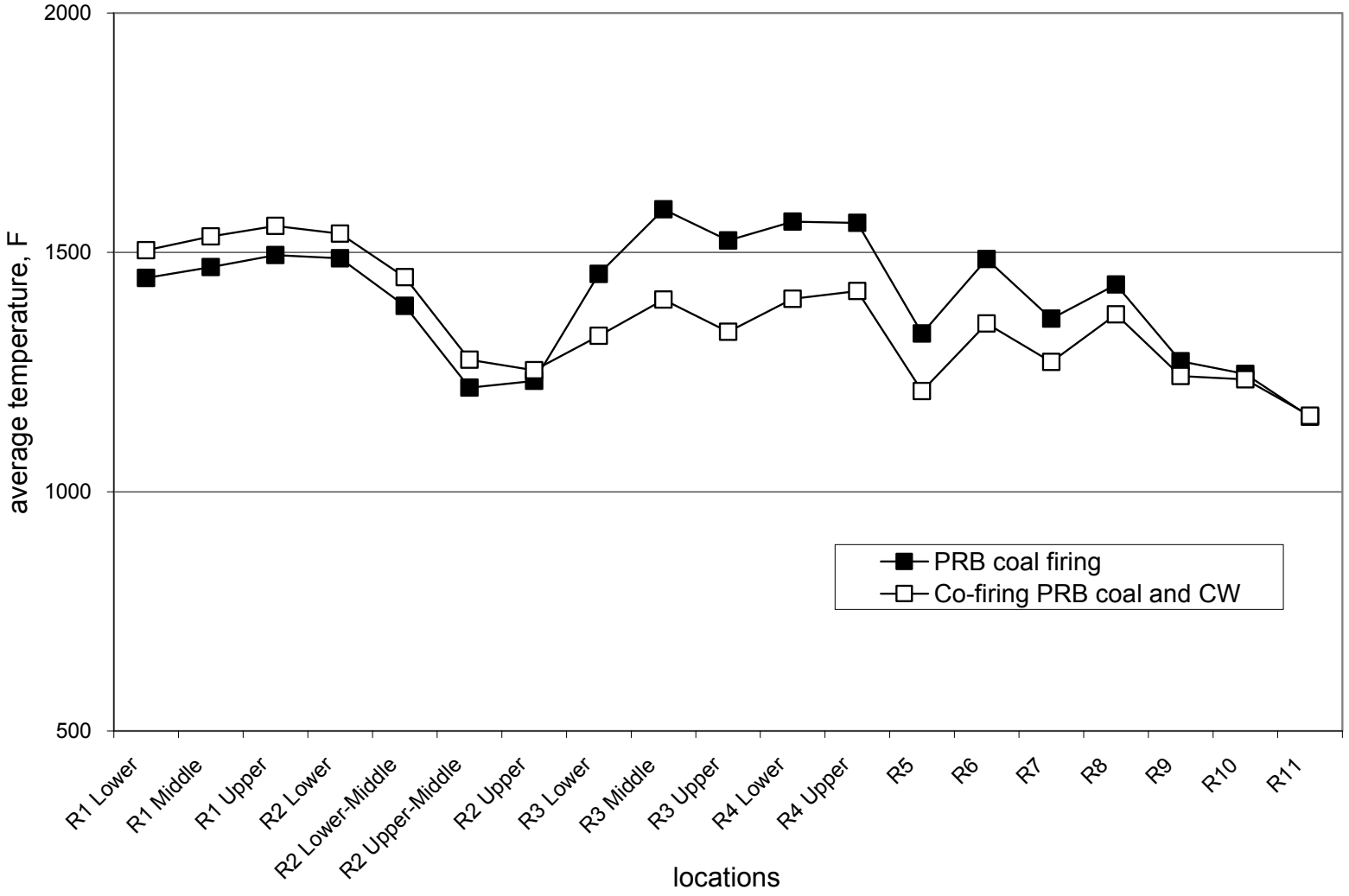

Figure 14-5. Variations of NO, SO_2 and O_2 during the Firing of PRB Coal only and the Co-Firing of PRB Coal with CW

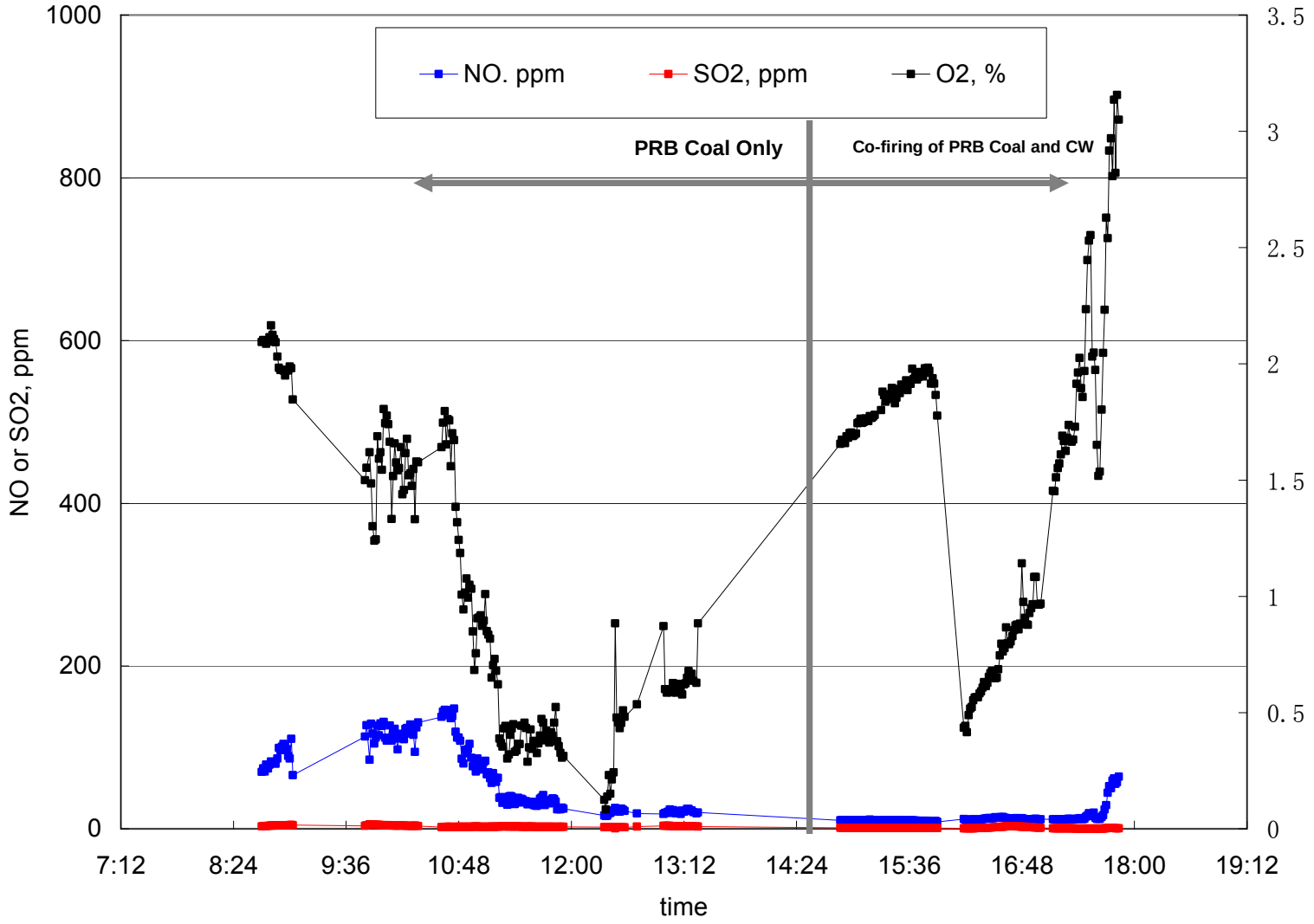

Figure 14-6. Variations of CO, CO_2 and O_2 during the Firing of PRB Coal only and the Co-firing of PRB Coal with CW

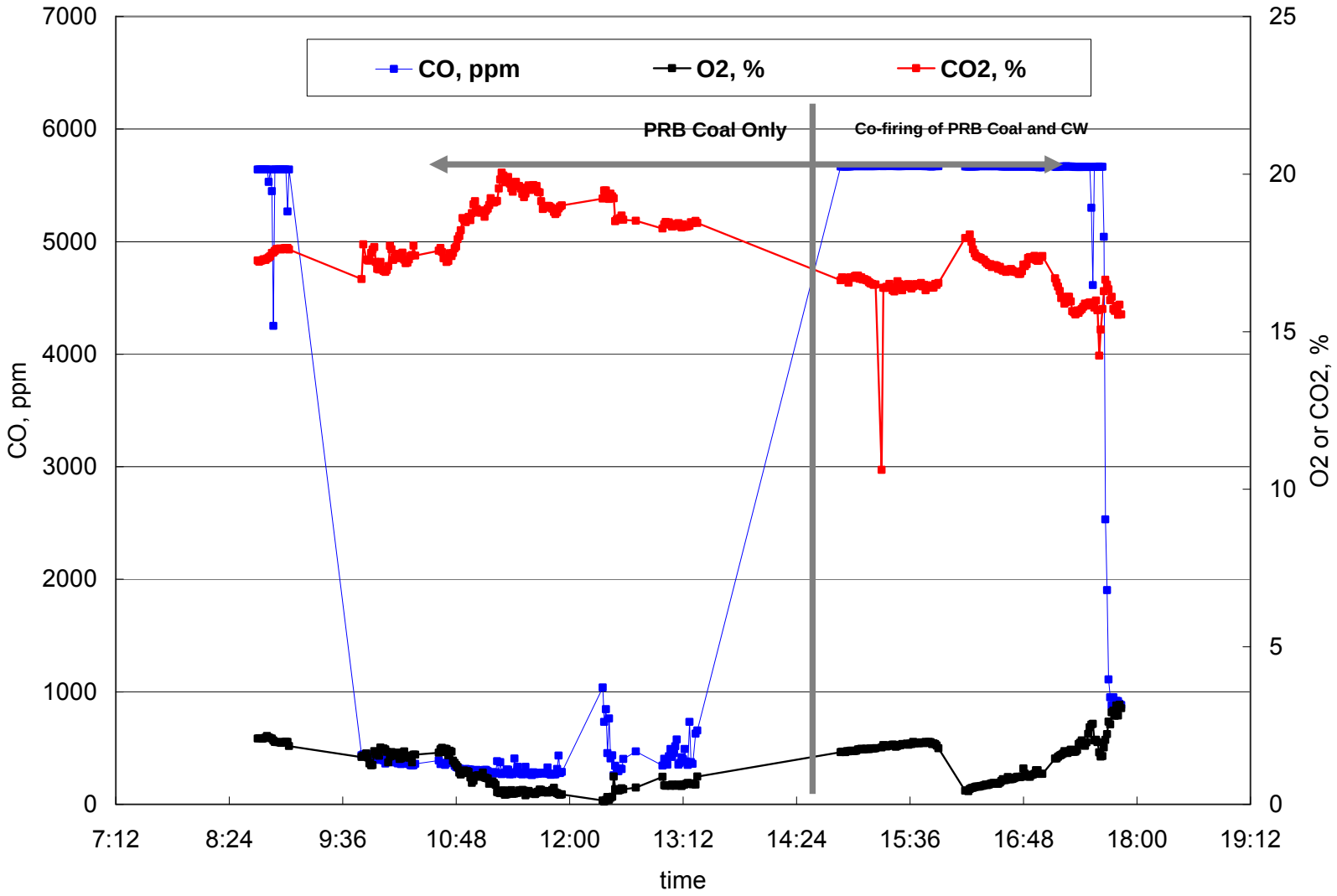

Table 10-1. Operational Parameters and Emission Rates of Air Pollutants during the Firing of PRB Coal Only

CFBC RUN #2-1																			
Mode: co-firing	Date: July 30 08																		
PRB coal-repeated																			
A. Operation parameters																			
	Coal feed	Biomass Feed	Limestone feed	Co-firing ratio	Primary air	Secondary air	Loop seal air	Sec air ratio	L-air ratio	Load by coal	Load by HX	Ca/S							
	lb/hr	lb/hr	lb/hr	%	lb/hr	lb/hr	lb/hr	%	%	KW	KW								
	150.7	0	22.7	0	12.37	2.48	1.08	16.7%	7.3%	353.1	263.3	4.5							
Temeprature Profile																			
Locations	R1	R2	R3	R4	R5	R6	R7	R8	R9	R10	R11	Pri. Cycl. Dis.	Sec. Sysl. Dis.						
°F	1546.6	1378.8	1507.1	1526.3	1284.8	1441.9	1349.3	1422.3	1266.2	1241.3	1153.2	899.1	768.0						
B. Gas composition at stack																			
	Temperature																		
1. Permnent gas																			
	O_2, %	N_2, %	CO_2, %	CO, ppm	SO_2, ppm	NO, ppm	N_2O, ppm												
	0.68		18.9	266	3.13	34	197	153											
2. Mercury																			
2.1 Methid:OHM	Hg(0)	Hg(2+)	Hg(VT)	Hg(0)/Hg(VT)															
ug/NM^3																			
2.2 Method:SCEM	Hg(0)	Hg(2+)	Hg(VT)																
ug/NM^3	8.04	0.99	9.03	89.0%															
3. Trace Metals (UA)																			
	Ag	As	Ba	Be	Cd	Co	Cr	Cu	Mn	Mo	Ni	Pb	Sb	Se	Tl	V	Zn	Th	U
4. VOCs & Semi-VOCs																			
VOCs																			
Semi-VOCs																			
5. Halogens																			
	HF	HCl	HBr	F_2	Cl_2	Br_2													
6. Others																			
	NH_3	SO_3	SO_2																
		0.05	3.84																
		2.28	2.01																
7. PM&CPM, mg/NM^3																			
	PM		CPM																
		Inorganic-CPM	Organic-CPM	total															
		2.31	0.15	2.46															
		Inorganic-CPM																	
		F	Cl	Br	NO_3	PO_4	SO_4	Li	Na	NH_4	K	Mg	Ca	Others					
		0.02	0.56	ND	1.96	ND	1.53	ND	0.13		ND	0.12	1.06						

Table 10-2. Operational Parameters and Emission Rates of Air Pollutants during the Co-Firing of PRB Coal with CW

CFBC RUN #2-2																			
Mode: co-firing	Date: July 30 08																		
PRB coal + CW																			
A. Operation parameters																			
	Coal feed	Biomass Feed	Limestone feed	CO-firing ratio	Primary air	Secondary air	Loop seal air	Sec air ratio	L-air ratio	Load by coal	Load by HX	Ca/S							
	lb/hr	lb/hr	lb/hr	%	lb/hr	lb/hr	lb/hr	%	%	KW	KW								
	146.3	32.1	30	18.0%	12.37	2.87	1.08	18.8%	7.1%	384.9	254.3	3.7							
Temeprature Profile																			
Locations	R1	R2	R3	R4	R5	R6	R7	R8	R9	R10	R11	Pri. Cycl. Dis.	Sec. Sysl. Dis.						
°F	1537.2	1387.3	1365.1	1417.2	1215.9	1359.3	1283.4	1382.4	1251.9	1241.4	1163.0	987.0	837.6						
B. Gas composition at stack																			
Temperature																			
1. Permnent gas																			
	O_2, %	N_2, %	CO_2, %	CO, ppm	SO_2, ppm	NO, ppm	N_2O, ppm												
	1.08		16.9	5663	1.25	12		117	107	117									
2. Mercury																			
2.1 Methid:OHM	Hg(0)	Hg(2+)	Hg(VT)	Hg(0)/Hg(VT)															
Sample 1,ug/NM^3	8.65	0.21	8.86	97.6%															
Sample, 2ug/NM^3	8.4	0.14	8.54	98.4%															
2.2 Method:SCEM	Hg(0)	Hg(2+)	Hg(VT)	Hg(0)/Hg(VT)															
Sample 1, ug/NM^3	8.01	0.14	8.15	98.3%															
Sample 2, ug/NM^3	7.95	0.26	8.21	96.8%															
3. Trace Metals																			
	Ag	As	Ba	Be	Cd	Co	Cr	Cu	Mn	Mo	Ni	Pb	Sb	Se	Tl	V	Zn	Th	U
ug/NM^3	< 4.35	< 4.35	< 4.35	< 4.35	< 4.35	< 4.35	< 4.35	< 4.35	< 4.35	< 4.35	< 4.35	< 4.35	< 4.35	16.69	< 4.35	< 4.35	22.50	<4.35	<4.35
4. VOCs & Semi-VOCs																			
VOCs	Benzene	1-Propene, 1,1-dichloro-	Trichloroethylene	Methane, dibromo-	Methane, bromodichloro-	Toluene	1-Propene, 1,3-dichloro-	Ethane, 1,1,2-trichloro-	Propane, 1,3-dichloro-	Tetrachloroethylene	Benzene, chloro-	Ethane, 1,1,1,2-tetrachl	Ethylbenzene	p-Xylene					
ug/NM^3	12813.1	< 0.85	< 0.85	< 0.85	< 0.85	5.79	< 0.85	< 0.85	< 0.85	< 0.85	6.56	< 0.85	< 0.85	< 0.85					
	styrene	Benzene, bromo-	Benzene, 1-chloro-2-meth	Benzene, 1,3,5-trimethyl	Benzene, 1,2,4-trimethyl	Benzene, 1-methyl-3-prop	Benzene, 4-ethyl-1,2-dim	Propane, 1,2-dibromo-3-c	Benzene, 1,2,4-trichloro	Naphthalene	Benzene, 1,2,3-trichloro	1,3-Butadiene, 1,1,2,3,4	o-Xylene						
	153.511	< 0.85	< 0.85	< 0.85	< 0.85	< 0.85	< 0.85	< 0.85	< 0.85	< 0.85	< 0.85	< 0.85	< 0.85						
Semi-VOCs	pyridine	1,4-dichlorobenzene	2-methylphenol	3-methylphenol	4-methylphenol	hexachloroethane	nitrobenzene	2,4,5-trichlorophenol	2,4,6-trichlorophenol	2,4-dinitrotoluene	hexachlorobenzene								
ug/NM^3	21.235	< 2.941	< 2.941	< 2.941	< 2.941	< 2.941	< 2.941	< 2.941	< 2.941	< 2.941	< 2.941								
5. Halogens																			
	HF	HCl	HBr	F_2	Cl_2	Br_2													
	0.25	0.65	ND	0.07	2.08	ND													
	0.32	0.75	ND	0.08	1.24	ND													

5.6 Operation of the CFBC System Under Full Scale Firing

An evaluation of the 0.6 MW_{th} CFBC system at full-load and tuning was conducted on August 7, 2008. The purpose of this test was to investigate if different parts of the whole CFBC system can properly function under a full-load or over a full-load, as well as during the tuning period. Special focus was on the evaluation of the optimal particle size of the fuel fed materials, the compatibility of feeding materials including fuels and air, the maximum heat exchange capability, and ash recirculation capability of the loop seal. As with previous tests, this third firing of the CFBC system started in the afternoon of August 6, 2008. After an overnight firing, system temperatures were brought up to be ready for full-load evaluation on August 7 2008, Testing would be conducted in the co-firing mode with PRB and WP.

As indicated in Figure 15-1, PRB coal feeding was increased during the initial temperature ramp to full-load. After approximately an hour, the CFBC system was tuned to full-load operation at about 650 kW by feeding only PRB coal (228 pounds per hour). Because of the high primary air feed rate used of at about 21 pounds per minute, the higher temperature zone inside the riser seemed to move upward compared to that of previous tests. The heat exchanger was tuned by decreasing coolant flows at the bottom locations of the riser (R1 to R3), but did not increase temperatures as expected. Increasing the limestone feed rate seemed to partially overcome decreases in the temperature at the bottom zone of the riser (R1 to R2), but not for R3. Following up on this issue, WP was added feed material of the CFBC system with the feed rate of WP averaging about 65 pounds per hour. This measurement seemed to be effective in increasing the temperature at R1 to R3. Simultaneously, temperatures at the upper parts of the riser were kept constant. Therefore, the CFBC system was successfully tuned even over a full-load at 115 % of the full setting load (600 kW by coal thermal input) at thermal input by mixed fuels of 760 kW (the thermal output by heat exchange was about 352 kW). As indicated in Figure 15-2 and Table 11, the feed rate of the primary air was kept constant and averaged about 22.1 pounds per minute (at standard conditions) and 0.53 pounds per minute for the secondary air. The ratio of secondary air to the total air decreased to about 2.3 % compared that used in previous tests. The purpose of decreasing secondary air was to abate higher temperatures at the upper parts of the riser. The air delivery into CFBC system through the lower loop seal was also decreased to about 0.34 pounds per minute, a ratio of 1.5%. Throughout the testing, the limestone feed rate was kept constant at 18 pounds per minute. The Ca/S ratio was controlled at

2.3. A mixture of limestone with two sizes (average of 500 um and 1000 um) at a ratio of 50 % by weight by 50 % was used during this test for sulfur capture optimization. The operation seemed stable after load tuning when measurements of air pollutants started. Temperatures in the CFBC system at different locations are shown in Figure 15-3. Variations of temperatures could be controlled. As indicated in Table 4 and Figure 15-4, the average temperatures at the bottom of the riser were initially about 1300^{o}F, then increased to greater than 1500^{o}F at R4 to R10. The temperature of the secondary cyclone at the top of the CFBC system was about 908 ^{o}F.

After one and a half tests conducted under full-load conditions, the system load dropped to below half of the full-load of 600 kW by decreasing the coal feed rate and simultaneously reducing the feed rate of WP. Soon the load of the CFBC system was increased to 500 kW within one and half hours by increasing the coal feed rate and the WP feed rate. During the whole procedure tuning the load of the CFBC system, feeding systems, HX tuning capability and temperature control seemed to perform well. However, it seemed the optimal size of previously pre-determined 1000 um was not compatible with full load operation. Additionally, the air delivery in the loop seal malfunctioned. It seemed that stopping ash recirculation flow in the downcomer caused the ash height increase. Discharging ash inside the downcomer seemed to solve this issue. A blower was applied to the air supply in the loop seal, which was less effective during this full load test. Two check valves, which were used to prevent ash back flow inside the air-supply line, seemed to lose the capability to stop air delivery into the loop seal. Modifying the air delivery system of the looping seal is scheduled in near future. Two blowers are also planned to replace the one blower that delivers loop seal air into the two sides of the loop seal, individually. Two check valves will be removed in the air delivery line. Additionally, to ensure successful modification, an air delivery line from the compressor will be set up. It will be used to provide enough high pressure of the loop seal air for re circulation ash flow inside the downcomer.

Figures 15-4 and 15-5 present variations of emission concentrations of CO, CO_2 and O_2, SO_2 and NO during the tuning period when co-firing PRB coal and WP. During the full-load operation, the excessive air ratio was lower as O_2 at flue gas exit averaged 0.61%. Emissions of concentrations of SO_2, NO, N_2O and CO were 61 ppm (verified by EPA wet-chemical method at 64.5 ppm), 85 ppm, 145 ppm and 1332 ppm, respectively. Except for slightly higher SO_2 emission concentrations due to the lower Ca/S ratio, all other emissions seemed within

acceptable range compared to those in the full-scale CFBC system firing. Higher CO emissions were expected due to co-firing with the higher-volatile WP, as well as a lower excess air ratio and lower secondary air ratio. Consequently, NO was low due to a lower excess air ratio as well as an available reducing agent such as CO. There was still a clear correspondence between NO and O_2, as indicated in Figure 15-4. Throughout the tuning period of the CFBC firing, CO emissions were well controlled. The preferred temperature profile (higher temperature was achieved) was responsible for abatement of CO emissions. However, NO and N_2O in this full-load test was not optimized, which will be left for further study. Slightly higher SO_2 emissions were attributed to a lower Ca/S ratio, which was 2.4 in this test. The results from this test suggest that the Ca/S ratio should be kept above 3 in future tests. In all, the system tuning at the full-load operation of the CFBC system was successful in that not only have generally acceptable emissions been achieved, but also factors to control emissions have been understood.

Results from mercury CEM indicated that the total vapor-phase mercury (Hg(VT)) concentration was about 9.09 ug/NM^3 with over 86.5% of Hg(VT) being the elemental mercury (Hg(0)) during a period of full-load operation. It was verified by OHM, which reported similar results of Hg(VT) at 8.62 ug/NM^3 with 93.6 % of Hg(VT) being Hg(0). The analysis of the fly ash collected during co-firing, as shown in Table 8, indicated a minimal amount of mercury captured by fly ash (at about 0.006 ppm) although LOI of collected fly ash was as high as about 18.6 %. The ineffective capability of fly ash on mercury capture was attributed to the very high Hg(0) concentration in the flue gas, which was about 90% of Hg(VT). A higher limestone ratio in fly ash.and a preferred temperature profile inside CFBC system for halogen capture by alkali earth metal oxides should be responsible for higher Hg(0).

Except for mercury, emissions of other major trace metals were found to be lower, as indicated in Table 11. During the full-load operation when co-firing PRB coal and WP, emission concentrations of all trace metals were below 6.56 ug/NM^3, except for Cu, Mn, Sb and B. Emissions concentrations of Cu, Mn, Sb and B were about 15.2 ug/NM^3, 17.5 ug/NM^3, 7.7 ug/NM^3 and 731 ug/NM^3, respectively. The trace metals were slightly higher than expected, especially for B. Data will be verified in future testing.

Major organic species, including VOCs and semi-VOCs, in the flue gas were determined by GC-MS. Results during the operational tuning of CFBC system load, as indicated in Table 11, show that the emissions of major VOCs and semi-VOCs were both below the detection limit of

instrument, except for toluene, ethylbenzene and m,p-Xylene in VOC and pyridine, 4-methylphenol, 2-methylphenol. Toluene, ethylbenzene and m,p-Xylene in VOC were about 17.08 ug/NM^3, 27 ug/NM^3 and 75.9 ug/NM^3, respectively. Pyridine, 2-methylphenol and 4-methylphenol were about 162.9 ug/NM^3, 21.9 ug/NM^3 and 4.1 ug/NM^3 during the test. As the load tuning of CFBC system was accomplished, both high VOCs and semi-VOCs dramatically dropped below the detection limit of the GC-MS. Only m,p-Xylene in the VOC and pyridine in the semi-VOCs were slightly high, at 5.97 ug/NM^3 and 139.5 ug/NM^3, respectively. The short period of the run of the CFBC may have meant the system was not fully stabilized. This may be responsible for slightly higher emissions of some VOCs and semi-VOCs. It is expected this issue could eventually be solved during extended operation of the CFBC system.

Figure 15-1. Variations of Coal Feeding, Limestone Feeding, WP Feeding and Load during Tests Conducted on August 7, 2008

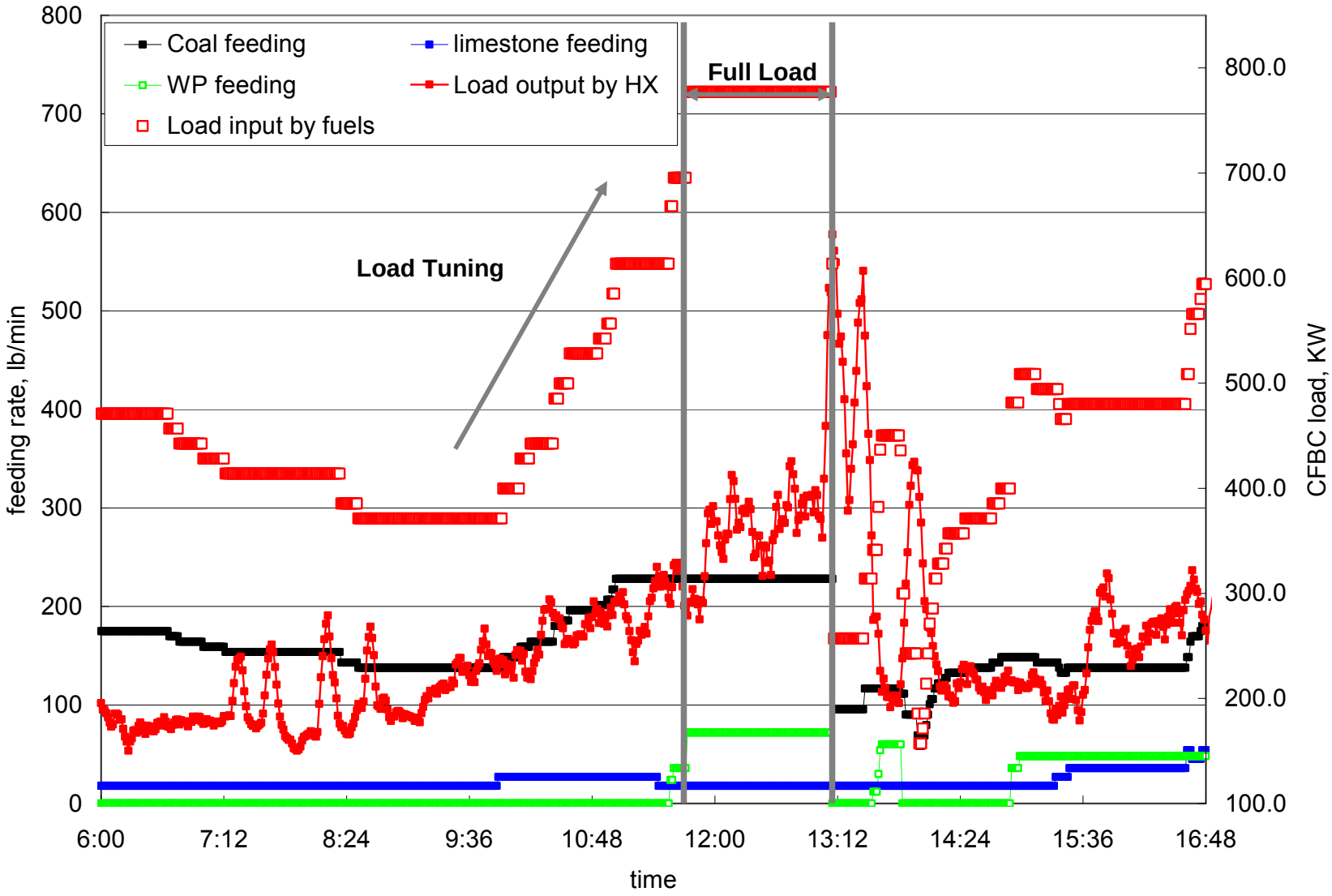

Figure 15-2. Variations of Supplies of the Primary Air, the Secondary Air and the Loop Seal Air during Test Conducted on August 7, 2008

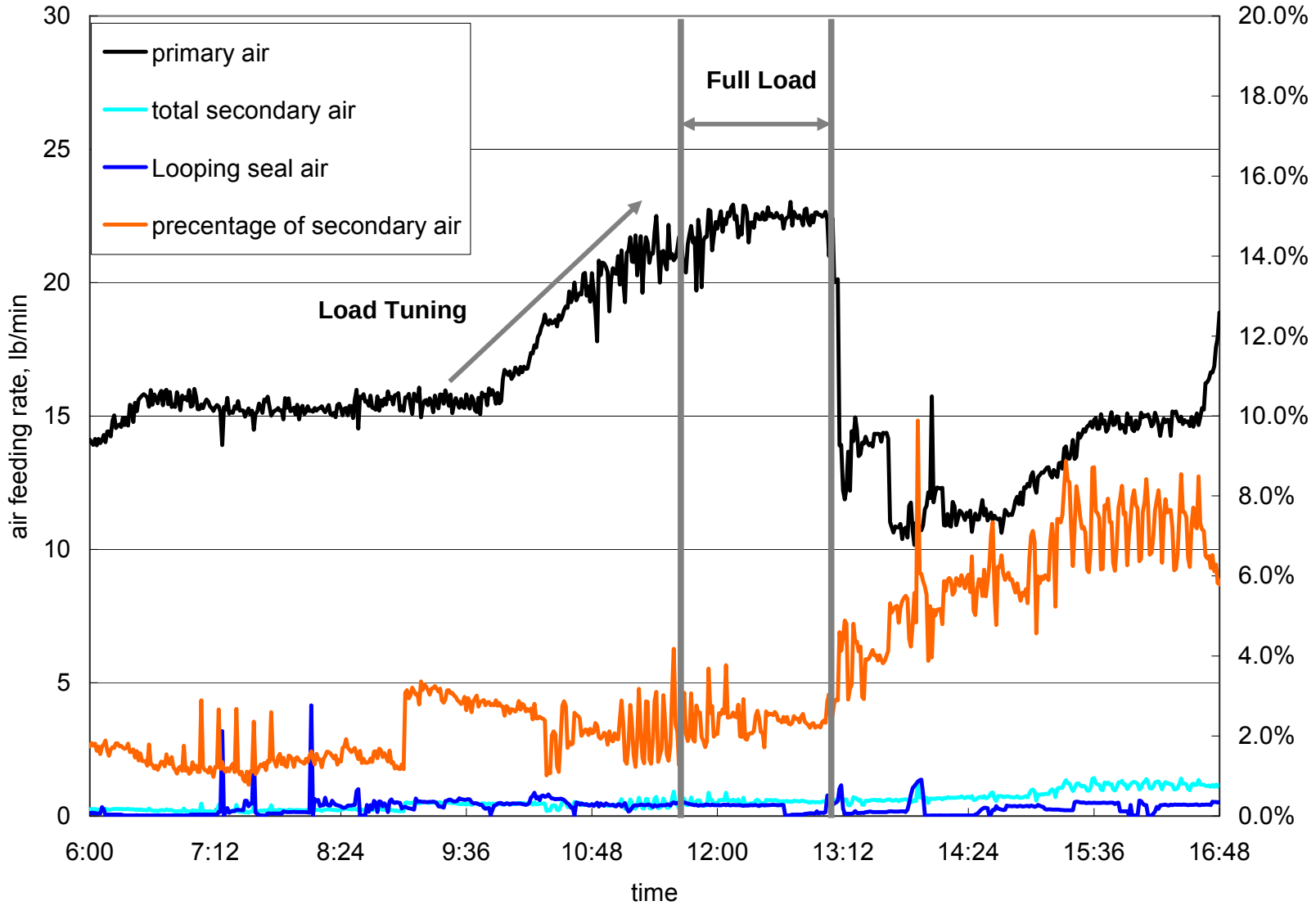

Figure 15-3. Variations of Temperature Profiles over Time in CFBC's Riser during Test Conducted on August 7, 2008

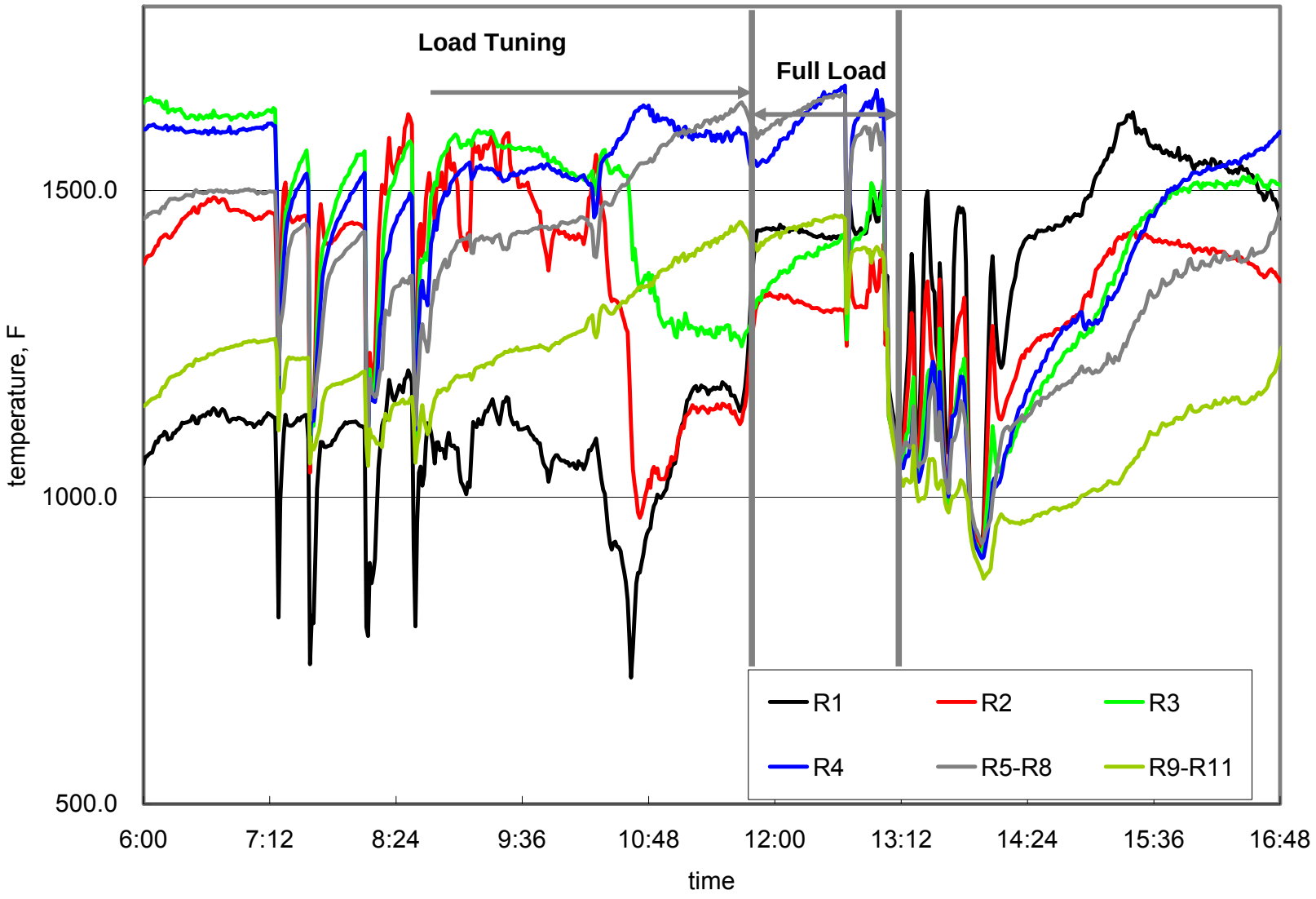

Figure 15-4. Variations of NO, SO_2 and O_2 at the Full-Load Operation and the Load Tuning Period

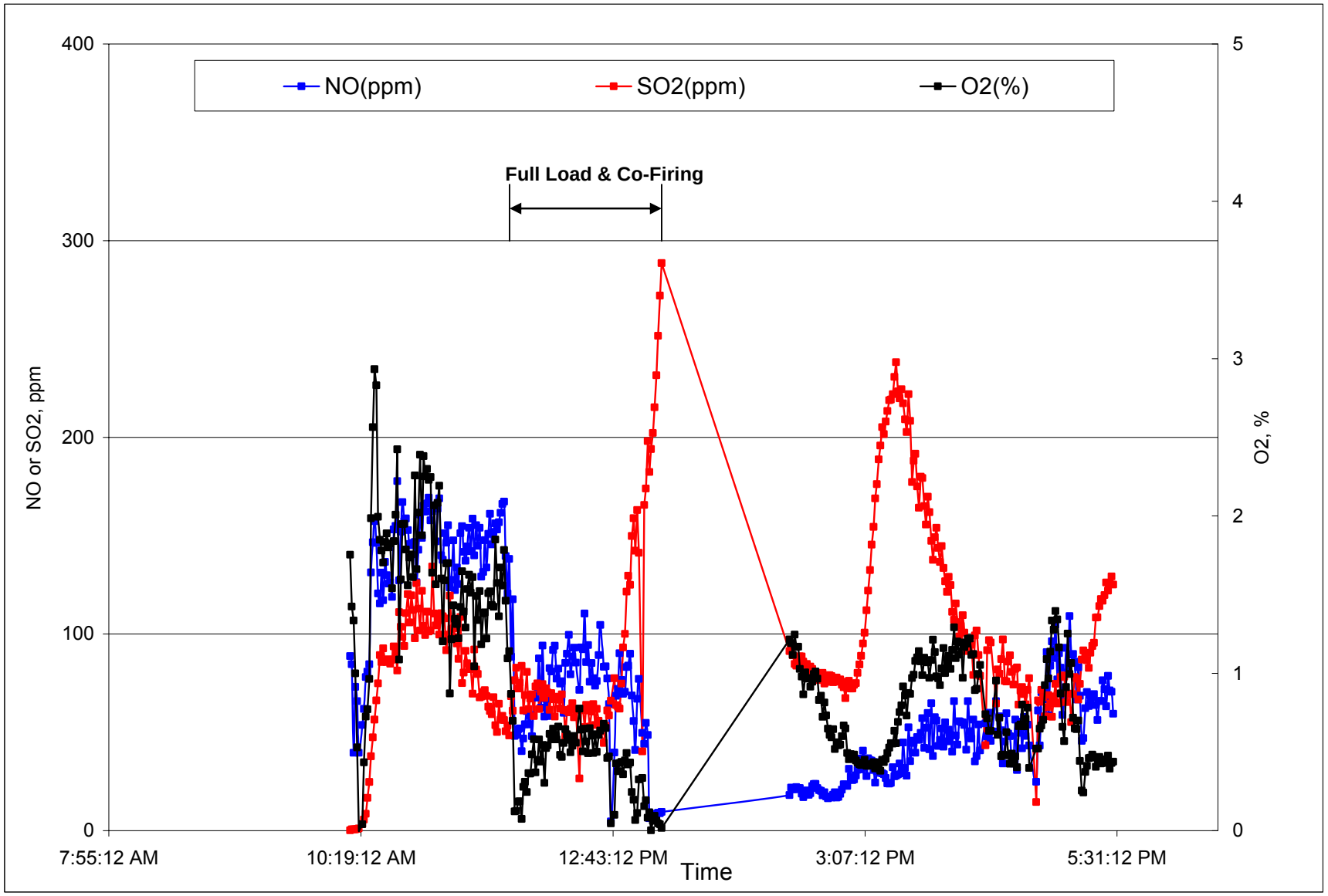

Figure 15-5. Variations of CO, CO_2 and O_2 at the Full-Load Operation and the Load Tuning Period

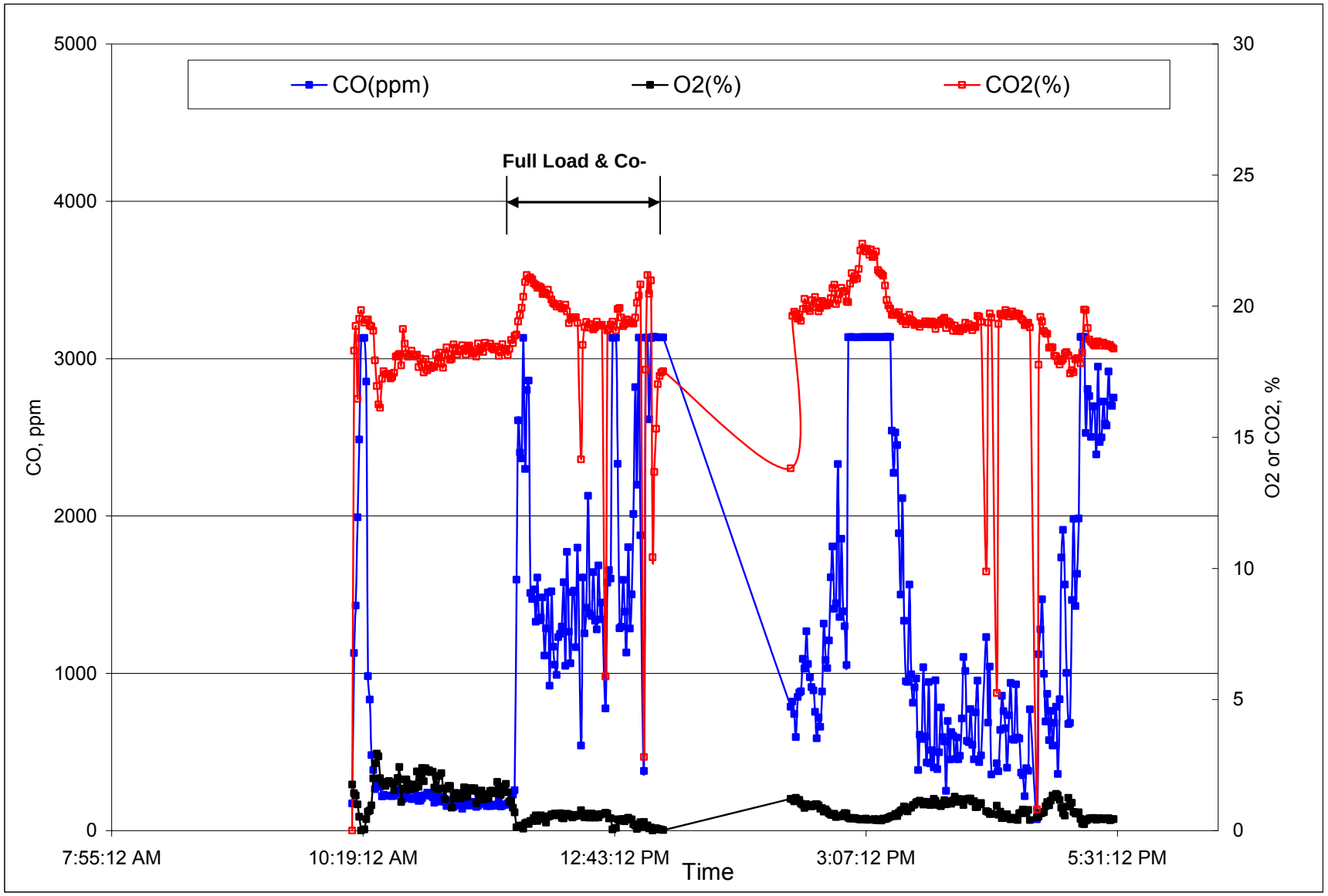

Table 11. Operational Parameters and Emission Concentrations of Air Pollutants during the Co-firing of with WP at the Full-load Operation and the Load Tuning Period.

CFBC RUN #3																			
Mode: co-firing	7-Aug-08																		
Full-load																			
A. Operation parameters																			
	Coal feed	Biomass Feed	Limestone feed	Co-firing ratio	Primary air	Secondary air	Loop seal air	Sec-air ratio	L-seal air ratio	Load by coal	Load by HX	Ca/S							
	lb/hr	lb/hr	lb/hr	%	lb/min	lb/min	lb/min	%	%	KW	KW								
	227.9	64.6	18	22.1%	22.1	0.53	0.34	2.3%	1.5%	760.4	351.5	2.40							
Temeprature Profile																			
Locations	R1	R2	R3	R4	R5	R6	R7	R8	R9	R10	R11	Pri. Cycl. Dis.	Sec. Sysl. Dis.						
°F	1386.6	1288.4	1369.9	1601.6	1499.9	1736.0	1570.5	1653.4	1494.5	1467.3	1320.7	1046.2	907.5						
B. Gas composition at stack																			
	Temperature																		
1. Permnent gas																			
	O_2, %	N_2, %	CO_2, %	CO, ppm	SO_2, ppm	NO, ppm	N_2O, ppm												
	0.61		19.27	1333	61	85	144	151											
2. Mercury																			
2.1 Methid:OHM	Hg(0)	Hg(2+)	Hg(VT)	Hg(0)/Hg(VT)															
ug/NM^3	8.07	0.55	8.62	93.6%															
2.2 Method:SCEM	Hg(0)	Hg(2+)	Hg(VT)	Hg(0)/Hg(VT)															
ug/NM^3	7.86	1.23	9.09	86.5%															
3. Trace Metals																			
	Ag	As	Ba	Be	Cd	Co	Cr	Cu	Mn	Mo	Ni	Pb	Sb	Se	Tl	V	Zn	B	Th
ug/NM^3	< 6.56	< 6.56	7.66	< 6.56	< 6.56	< 6.56	< 6.56	15.317	17.505	< 6.56	< 6.56	< 6.56	7.660	< 6.56	< 6.56	< 6.56	31.729	731.947	< 6.56
4. VOCs & Semi-VOCs, in ug/NM^3																			
VOCs	Benzene	1-Propene, 1,1-dichloro-	Trichloroethylene	Methane, dibromo-	Methane, bromodichloro-	Toluene	1-Propene, 1,3-dichloro-	Ethane, 1,1,2-trichloro-	Propane, 1,3-dichloro-	Tetrachloroethylene	Benzene, chloro-	Ethane, 1,1,1,2-tetrachl	Ethylbenzene	m,p-Xylene					
Sample 1	< 0.67	< 0.67	< 0.67	< 0.67	< 0.67	17.08	< 0.67	< 0.67	< 0.67	< 0.67	< 0.67	< 0.67	27.00	75.87					
Sample 2	< 0.29	< 0.29	< 0.29	< 0.29	< 0.29	< 0.29	< 0.29	< 0.29	< 0.29	< 0.29	< 0.29	< 0.29	< 0.29	5.97					
	styrene	Benzene, bromo-	Benzene, 1-chloro-2-meth	Benzene, 1,3,5-trimethyl	Benzene, 1,2,4-trimethyl	Benzene, 1-methyl-3-prop	Benzene, 4-ethyl-1,2-dim	Propane, 1,2-dibromo-3-c	Benzene, 1,2,4-trichloro	Naphthalene	Benzene, 1,2,3-trichloro	1,3-Butadiene, 1,1,2,3,4	o-Xylene						
	1.08	< 0.67	3.69	681.88	548.16	699.67		0.73	< 0.67	< 0.67	< 0.67	< 0.67	189.27						
	< 0.29	< 0.29	< 0.29	< 0.29	0.41	0.35	< 0.29	< 0.29	< 0.29	< 0.29	< 0.29	< 0.29	< 0.29						
Semi-VOCs	pyridine	1,4-dichlorobenzene	2-methylphenol	3-methylphenol	4-methylphenol	hexachloroethane	nitrobenzene	2,4,5-trichlorophenol	2,4,6-trichlorophenol	2,4-dinitrotoluene	hexachlorobenzene								
Sample 1	162.86	< 1	21.9	< 1	4.06	< 1	< 1	< 1	< 1	< 1	< 1								
Sample 2	139.5	< 1.25	< 1.25	< 1.25	< 12.5	< 1.25	< 1.25	< 1.25	< 1.25	< 1.25	< 1.25								
5. Halogens (UA), ppm																			
	HF	HCl	HBr	F_2	Cl_2	Br_2													
6. Others, ppm																			
	NH_3	SO_3	SO_2																
ppm		0.16	64.5																

6. Conclusion

The renovation of a new space for a 0.6 MW_{th} Circulating Fluidized-Bed Combustor (CFBC) system, which is also a new combustion laboratory, was completed and fully compatible with the designed CFBC system. Half of the space is underground in relationship to this new combustion laboratory and has also been used to set up the laboratory-scale reactor, which generated a large quantity of relevant data to facilitate the operation of the 0.6MW_{th} CFBC system.

Prior to the design of the 0.6 MW_{th} CFBC system, the design calculations, including the mass balances, energy balances, heat transfer, facility strength, and construction dimensions were completed following intensive discussions. Comments received from various experts were also used to improve the design. A detailed design of supporting and hanging structures for the CFBC system was also completed. Discussions with potential contactors regarding the availability of materials and current machining capabilities resulted in the first modification of the original design. The CFBC system coolant production and feed water supply system were strengthened with the addition of a boost pump to assure that coolant can be applied to the cooling system under all operating conditions. Except for the main body of the CFBC facility, the induced draft fan, along with its machine base and power supply, was received and installed. The flue gas duct from the secondary cyclone outlet to the induced draft fan inlet was received and installed, as well as the induced fan flue gas discharge duct. Additionally, a dust control system was installed, which helps maintain a cleaner and safer work environment around the fuel and limestone bunkers during filling operations. Further, all materials for the high temperature insulation of the riser, both cyclones and the downcomer, have been installed. Additional thermal expansion joints were installed, first from the ash supply duct to the lower loop seal; and second from lower loop seal to the riser at R1. The purpose of installing additional thermal expansion joints provides a stable support for the riser and downcomer, as well as safely accommodating the dramatic change in length experienced under high temperature operations. The third modification of the CFBC system started after the initial firing in early 2008. Major modification included an additional heat exchanger and sensor ports as well as sampling ports. During an earlier CFBC system test, excessive temperatures were experienced in the at R3/R4 riser flange joint when system load was brought up. Some riser insulation components were damaged. A design review also indicated that this area of the riser would likely benefit from additional heat exchange surface below this area.

Substantial progress was made on the development and application of software for the effective operation and safe control of the CFB system, as well as for the display and logging of data and operating parameters. Electric power distribution for pumps, blowers, variable speed drives, valves and the bed preheater was completed. Installation of CFBC system temperature, pressure, coolant and air flow sensors, as well as, load cells were completed, along with actuator installation and wiring. Calibration, display and logging of pressure and air flow sensor data was complete.

Powder River Basin (PRB) coal was used for performance evaluation of this CFBC system. Slag from an operating integrated gasification combined cycle (IGCC) facility and a fly ash from a full-scale CFBC utility boiler were used to recirculate fly ash during initial "hot-modeling" tests. For co-firing tests, biomass (wood pallet and chicken waste) was prepared. Wood pallet has a higher fluorine content, and CW has very high chlorine content.

Three full evaluation tests were conducted under different loads and firing of different mixtures of fuels. Finally, an evaluation of the 0.6 MW_{th} CFBC system at its full-load and its tuning were conducted on August 7, 2008. The purpose of this test was to investigate whether different sections of the CFBC system can properly function under full-load or over full-load, as well as during tuning. Special focus was on evaluating the optimal particle size of the feed fuels; the compatibility of feeding materials including fuels and air; the maximum heat exchange capability; and ash recirculation capability by the loop seal. During this period, PRB coal and WP were co-fired.

Evaluation of tests on CFBC system performance indicated that load tuning, fuel switching and the heat transfer by available heat exchangers were successful. Feeding the coal and delivering different air streams inside the CFBC system was constant and smooth. The heat expansion joint worked perfectly to absorb system expansion under high temperatures. Improved setup of the control system and signal collection and transfer system made CFBC system operation less personnel intensive. The current CFBC system could work properly under a low ash recirculation rate with the assistance of two cyclones and two loop seals. Loss on ignition (LOI) in fly ash at the flue gas exit of the CFBC system, which was about 18%, was acceptable under the current initial full-load operation. However, a future modification of the air delivery system into a low loop seal was initiated to reduce the probability of losing ash re-circulation that occurred during full-load operation on the final test. Finally, a lack of enough high pressure air

was found to be responsible for the failure of ash recirculation in the loop seal. A few additional tests will be performed after this report is submitted.

Major air pollutant concentrations (including SO_2, NO, N_2O, CO, mercury (Hg), condensable particulate matters (CPM), sulfuric mist (SO_3), halogens, trace metals) were measured during the three full evaluation tests. Test results indicated that limestone could effectively control SO_2 emissions, but its effectiveness was dependent on the temperature profile of the CFBC system and the particle size distribution of the limestone. Oxygen concentration, available reducing agents, and system temperature profiles had major impacts on both NO and N_2O emission concentrations. Co-firing coal and biomass could increase CO and VOCs and semi-VOC emissions. Good combustion performance inside CFBC system could largely abate emissions of CO, VOCs and semi-VOCs. Trace metals were not a major issue during the test firing. However, mercury was not efficiently controlled. Several major halogens, which impacted mercury oxidation, were probably effectively controlled by limestone and also alkali earth metal oxides in the feed materials Higher portions of the elemental mercury inside the flue gas seemed to have less chance of being adsorbed on the fly ash. On the other hand, lack of availability of common air pollutant control devices (APCD), which have been applied in the industrial CFBC facility, made the unexpected mercury removal efficient.

7. Acknowledgement

Financial support for this project was provided by the U. S. Department of Energy National Energy Technology Laboratory (Cooperative Agreement NO. DE-FC26-03NT41840). Financial support of the Electric Power Research Institute (EPRI) on field testing for development of advanced additives on the mercury oxidation and adsorption, which is also part of this project, is also greatly appreciated.

The contributions of utilities to the success of this project are also recognized. They are:

- Eastern Kentucky Power Cooperative (EKPC)
- We-Energies
- Electric Energy, Inc. (EEI)
- Southern Illinois Power Cooperative (SIPC)
- Illinois Clean Coal Institute (ICCI)

The efforts of the following key members of project task are recognized:

- Fuels Characterization Task – Chien-Wei Chen, Pauline Hack, Jiashun Zhu
- Emissions monitoring – Cheng-Li Wu, Junjie Fan, Tuo Zhou

Engineering and Mechanics Task – Martin Cohron, Roiha Kimmo (VTT), Kevin Duckett
Wendall Myers, Richie Botkin

Finally, the contributions of the project team members and test crews who actually executed the project work are greatly appreciated.

8. Publications

1. Yan, Cao; Chin-Min, Cheng; Chien-Wei, Chen; Mingchong, Liu; Chia-Wei, Wang; Wei-Ping, Pan. “Abatement of Mercury Emissions in the Coal Combustion Process Equipped with a Fabric Filter Baghouse,” *Fuel 87*,3322-3330, 2008.

2. Yan, Cao; Zhengyang, Cao; Jing, Jin; Hongcang, Zhou; Martin, Cohron; Houyin, Zhou; Hongying, Liu; Wei-Ping, Pan. “Synthesis Gas Production with an Adjustable H_2/CO Ratio through the Coal Gasification Process: Effects of Coal Ranks and Methane Addition,” Energy & Fuel, 2008, *22,* 1720–1730.

3. Yan, Cao; Zhengyang, Gao; Jiashun, Zhu; Quanhai, Wang; Yaji, Huang; Chengchung, Chui; Bruce, Bruce; Paul, Paul; Wei-Ping, Pan; " Impact of Halogen Additions on Mercury Oxidation in a Slipstream Selective Catalyst Reduction (SCR), Reactor When Burning Sub-Bituminous Coal," *Environmental Science & Technology*, 2008, 42, 256-261.

4. Hongcang, Zhou; Yan, Cao; Houyin, Zhao; Hongying, Liu; Wei-Ping, Pan. “Investigation of H_2O and CO_2 Reforming and Partial Oxidation of Methane” Catalytic Effects of Coal Char and Coal Ash,” Energy & Fuel,22, 2341-2345, 2008.

5. Yan, Zhang; Hong, Cui; Riko, Ozao; Yan, Cao; Bobby, Chen; Chia-Wei, Wang; Wei-Ping, Pan. “Characterization of Activated carbon Prepared From Chicken Waste and Coal,” *Energy & Fuels*, 2007, 21, 3735-3739.

6. Hong, Cui; Yan, Cao; Wei-Ping, Pan. “Preparation of Activated Carbon for Mercury Capture from Chicken Waste and Coal,” *J. Anal. Appl. Pyrolysis,* 2007, *80(2),* 319-324.

7. Songgeng, Li; Andy, Wu; Shuang, Deng; Wei-Ping, Pan. “Effect of Co-combustion for Chicken Litter and Coal on Emissions in a Laboratory-scale Fluidized Bed Combustor,” *Fuel Processing Technology,* 2007, 89, 7-12.

8. Yan, Cao; Quanhai, Wang; Chien-wei, Chen; Bobby, Chen: Martin, Cohron; Y-chuan, Tseng; Paul, Chu; Wei-Ping, Pan. “Investigation of Mercury Transformation by HBr Addition in a Slipstream Reactor with Real Flue Gas Atmospheres of Bituminous Coal and Powder River Basin (PRB) Coal,” Energy & Fuels, 2007, 21, 2719-2730.

9. Yan Cao, Bobby Chen, Jiang Wu, Hong Cui, John Smith, Chi-Kuan Chen, Paul Chu and Wei-Ping Pan, “Study of Hg Oxidation by Selective Catalytic Reduction Catalyst in a Pilot-scale Slipstream Reactor at a Utility Boiler Burning Bituminous Coal” . Energy & Fuels, 2007, 21, 145-156.

10. Nathan Whitely*, Riko Ozao, Ramon Artiaga, Yan Cao and Wei-Ping Pan, “Multi-utilization of Chicken Litter as Biomass Source – Part I. Combustion,” Energy & Fuels, 2006, 20, 2660-2665 .

11. Nathan Whitely*, Riko Ozao, Yan Cao and Wei-Ping Pan, “Multi-utlization of Chicken Litter as Biomass Source – Part II. Pyrolysis,” Energy & Fuels, 2006, 20, 2666-2671.

13. Yan Cao, Bianca Casenas*, and Wei-Ping Pan, "Investigation of Chemical Looping Combustion by Solid Fuels 2. Redox Reaction Kinectics and Product Characterization with Coal, Biomass and Solid Waste as Solid Fuels and CuO as Oxygen Carrier," Energy & Fuels, 2006, 20, 1845-1854.

14. Yan Cao, Yang Wang, Joho T.Rily, W.-P. Pan, "A novel biomass air gasification process for producing tar-free higher heating value fuel gas,"*Fuel* Processing Technology 87 (2006) 343-353

15. R. Ozao, T. Okabe, T. Arii, Y. Nishimoto, Yan. Cao, N. Whitely, and W.-P. Pan, "Gas and Mecury Adsorption Properties of Woodceramics Made from Chicken Wastes," *Energy & Fuels ,* **2005,** *19,*1729-1734.

16. Yan Cao, Quan-Hai Wang, Jun Li, Jen-Chieh Cheng, Chia-Chun Chan, Marten Cohron, and Wei-Ping Pan. "Enhancement of Mercury Capture by the Simultaneous Addition of Hydrogen Bromide (HBr) and Fly Ashes in a Slipstream Facility" *Environmental Science & Technology ,*submitted.

17. Yan Cao, Hou-Zhao, Quan-hai Wang, Jun Li, Jen-Chieh Cheng, Chia-Chun Chan, Wei-Ping Pan. "Impact of the Addition of Hydrogen Bromide on Lower Temperature Ductwork Corrosion in a Powder River Basin Flue Gas Atmosphere: Slipstream Test Results". Fuel Processing Technology, submitted.

18. Yan Cao, Hongcang Zhou, Junjie Fan, Houyin Zhao, Tupo Zhou, Pauline Hack, Chia-Chun Chan, Wei-Ping Pan. "Mercury Emissions during Co-firing of Sub-bituminous Coal and Biomass (Chicken Waste, Wood, Coffee Residue and Tobacco Stalk) in a Lab-Scale Fluidized Bed Combustor" *Environmental Science & Technology*, submitted.

9. Appendix I

9.1 Tests in a Lab-scale Fluidized Bed

Test Facility. The fluidized bed co-firing combustor has seven major components, as shown in Figure A1. It includes the electrically-heated main body of the fluidized bed combustor; one fuel hopper and one fuel screw feeder; a compressed air-delivery line and its metering flow meter; a flue gas cleanup unit, including a cyclone and a high temperature quartz filter assembly, as well as a wet scrubber. Under the oxygen-firing mode, an oxygen cylinder and flow meter provides oxygen supply and flow control. Simultaneously, a CO_2 cylinder is available to deliver a CO_2 stream for dilution purposes. In this study, results for the oxygen-firing mode were not included. The outside diameter (OD) of the combustor is about 6.4 cm and 1.6 cm thick. The height of the combustor is 110 cm. There is a gas distributor mounted at the bottom of the combustor with a 1 % opening to prevent a maldistribution of gas passing through bed material.

The combustor temperatures are monitored by a platinum-rhodium thermocouple, which is sealed in a stainless steel tube in the combustor. The thermocouple could be moved inside the tube to monitor temperatures along the height of the combustor, as indicated in Figure A1. The bed temperature was 850 - 900 ^oC in the main portion of the combustor at the bottom, but gradually started to decrease to 450 ^oC starting at 2/3 of the distance from the combustor's bottom. The fuel mixtures for co-firing were fed into the combustor through a coal feeder on the top of the combustor. The maximum mixing ratios were 50 %. The fluidized bed combustor was generally operated at a velocity 3-5 times that of U_{mf} (the minimum fluidization velocity). The excessive air ratio was maintained at about 1.2, while the oxygen concentration at the combustor outlet was about 6.0-8.0 %. The flue gas produced with the char residue at the top outlet of the combustor was collected by combining the cyclone and a porous quartz metal filter. The cleaned flue gas was delivered to either gas analyzers (O_2, SO_2, and mercury) or collection impingers to determine the presence and amount of mercury and halogens.

Initially, the fluidized bed combustor was electrically heated to 650^oC. Then the coal was fed into the combustor to increase the temperature. Initial ash produced was left in the combustor as bed material. One hour later the temperatures began to approach 850^oC. Air and coal fed into the combustor were adjusted to stabilize the temperature across the combustor for a few hours. The mercury variation was monitored continuously by the SCEM system. Ontario Hydra Method (OHM) measurements (ASTM 6784-02) were applied to confirm the SCEM sampling results

during test periods. The detailed description of two mercury test methods and QA/QC procedures may be found in the references[1-2]. For every testing condition, at least two tests were conducted. If no abnormal results were found, the average data was accepted.

Materials. One sub-bituminous coal and four types of biomass, (chicken waste (CW), wood pallet (WP), coffee residue (CR) and tobacco stalk (TS)), were studied. Biomass has a much lower bulk density, is generally moist, and has lower heating values and particle densities than coal. Therefore, all raw fuels were first pulverized and sieved. The particle size of the coal sample was 500 to 1000 μm, and those of the biomass were 1000 to 2000μm. The purpose of using slightly larger biomass particles was to satisfy its fluidization conditions and residence time. The selected coal and biomass was pre-mixed before being fed into the combustor. All samples were dried in an oven at 100^{o}C overnight before testing.

Analysis of all fuel samples in this study followed ASTM standard procedures. The detailed description of these ASTM methods was described in a previous study[1]. Analysis results of all tested fuels are presented in Table A1. All tested fuels have a high volatile content. Sub-bituminous coal, CW and CR have comparable volatile content, which varies between 43.3 % and 54.2 % on a dry basis. Much higher volatile content was found in WP and TS, which are both above 75%. CW had the highest ash content at 34.9 %, TS was 11.3 % and sub-bituminous coal was below 10 %. Ash content in WP and CR was generally close to or below 1%. Sulfur content in all fuels was low, at about 1% for CW, followed by 0.54 % for sub-bituminous coal and 0.34 % for TS. Sulfur in CR and WP are even low. Chlorine content in all fuels was below 150ppm, except for CW and TS. CW had very high chlorine content (about 22300ppm). TS had medium chlorine content (about 4500ppm). Only coal had measurable mercury at about 0.12ppm. Mercury in all others was miniscule. The major metal oxides in the tested fuels are also shown in the Table 1. This study indicates that sub-bituminous coal and CW and WP have a relatively high content of CaO and MgO, which are about 25 % in total ash. All biomass has a higher occurrence of alkali metal oxides, such as Na_2O and K_2O. Among them, CR and TS have more K_2O, but no N_2O. However, the total amount of alkali earth metal oxides and alkali metal oxides should be ignored for WP and CR because of their negligible ash contents. One may notice that CW and CR also have a higher content of P_2O_5, which is about 17.5 %.

Impacts of Co-firing on Air Pollutants Emissions. Co-combustion tests of coal with CW have been performed in a laboratory-scale fluidized bed combustor to study the effect of CW

mass fraction and secondary air on the combustion and emission characteristics of the major gaseous pollutants. Major conclusions from the test results can be summarized as follows:

- As CW mass fraction increases, the bed temperature decreases and the temperature in the freeboard region increases. This is attributed to low fixed carbon and high volatile matter contained in CW.
- The introduction of high volatile matter in CW causes CO emissions to be increased.
- SO_2 emissions are lowered by adding CW as a result of fuel-S dilution and CW ash derived natural desulfurization. The ratio of H_2S to SO_2 increases with a decrease of CW mass fraction because high volatile matter released from CW creates a strong reducing atmosphere that suppresses the oxidation of H_2S.
- Introduction of CW at low concentrations causes higher NO emissions because more fuel-N is introduced. However, high levels of CW may reduce NO emissions due to the larger amount of released volatile matter, which suppresses the formation of NO.
- Secondary air introduction contributes to lower pollutant emissions.

Hg Emission during Co-firing. The mercury emission rates and removal efficiencies for the test fuels are summarized in Figure A2 and A3. To accurately estimate the mercury emission rates and removal efficiency during co-firing, a commonly-acceptable unit of mercury emission rates (lb/TBtu) was used. The calculation of mercury emission rates was based on the calculation of F-Factor in Eq (A1) and elemental analysis of fuels, which was introduced in EPA Part 75 - Appendix A - Method 19. The mercury emission rate, during firing of sub-bituminous coal only, was about 6.25 lb/TBtu. When co-firing CW and sub-bituminous coal (weight ratio of CW introduction at 30 %), the mercury emission rate was largely reduced to about 1.27 lb/TBtu on average. Increasing the introduction ratio of CW to 50 % during co-firing with sub-bituminous coal, the mercury emission rate was continuously reduced to 1.02 lb/TBtu. It seemed that mercury emissions were not significantly reduced when continuously increasing CW into the combustor. Regardless of originally occurring alkali metal oxides and alkali earth metal oxides in coal and CW, the additional alkali metal oxides (limestone) at Ca/S ratio of about 2.5 for SO_x capture were fed in the combustor during co-firing of 30 % CW and 70 % sub-bituminous coal. The mercury emissions rate was about 3.48 lb/TBtu, which was much higher than when limestone was introduced into the combustor. Limestone introduction resulted in increased mercury emissions, although it was still lower than burning sub-bituminous coal alone.

Switching co-firing fuels from CW to WP, CR or TS at the same mixing ratio, mercury emissions were similar to co-firing CW and sub-bituminous coal, but with the introduction of limestone. Mercury emission rates of co-firing WP, CR and TS with sub-bituminous coal were about 3.32 lb/TBtu, 2.67 lb/TBtu and 3.21 lb/TBtu, respectively. In all cases, the co-firing reduced mercury emission rates compared to burning sub-bituminous coal alone. Based on the same thermal output in per trillion Btu, mercury emissions for co-firing CW with a greater chlorine content was lowest. Co-firing with different biomass and limestone additions seemed to affect mercury emission rates and mercury removal efficiencies. We achieved a 37.9 % mercury removal efficiency for burning sub-bituminous coal alone. Co-firing with CW at 30 % and 50 % greatly improved mercury removal efficiency at 83.6 % and 84 %, respectively. Limestone introduction reduced mercury removal efficiency to 55.7 % when co-firing CW at a ratio of 30 %. Co-firings of WP, CR and TS with sub-bituminous coal (at ratio of 30 % biomass to 70% coal) had similar mercury removal efficiencies (52.9 %, 62.1 % and 59.1 %, respectively).

Because only a filter was used to remove mercury by deposited fly ash on the filter when co-firing biomass and sub-bituminous coal, reductions of mercury emissions likely suggested an increase of the particle-bound mercury. Co-firing CW with more chlorine indicated more particle-bound mercury was gained, but not always when the introduction of CW to weight ratio was continuously increased from 30 - 50 %. The higher chlorine content in CW may have helped to enhance the mercury capture by fly ash generated. However, this effect was eliminated by the introduction of limestone. Limestone introduction may have decreased the availability of chlorine on mercury oxidation and consequently may have decreased the mercury capture by fly ash. Co-firing biomass with lower chlorine content, such as WP and CR, did not significantly reduce mercury emission rates compared to those during co-firing with CW. Chlorine content in co-firing fuels seemed to be essential on mercury emission rates. However, this was not true for TS. Although it has an appreciable amount of chlorine in it, its mercury emission rate was comparable to those of fuel mixtures with low chlorine content.

F = F-factor (dscf/mmBtu)

$F = 10^6[3.64(\%\ H) + 1.53(\%\ C) + 0.57(\%\ S) + 0.14(\%\ N) - 0.46(\%\ 0)]/GCV$ Eq(A1)

Where % H, % C, % S, % N and O %) = weight percent (dry basis) of each element as obtained from the elemental fuel analysis.

GVC = gross calorific value of fuel (Btu/lb, dry basis).

The mercury speciation at the fluidized bed combustor outlet (after the filter), is shown in Figure A3. Almost 90 % of the total gaseous mercury was elemental mercury after flue gas passed through the filter, when sub-bituminous coal or a combination of sub-bituminous coal and WP, CR and TS was burned. When the co-fired fuel was CW and sub-bituminous coal, the mercury speciation analysis indicated about 50 % of the total gaseous mercury was elemental mercury. Therefore, almost 50 % of the oxidized mercury still in flue gas after fly ash filtration and the oxidized mercury were not fully captured by the fly ash generated when CW was co-fired. With the introduction of limestone, the elemental mercury was 90 % even when co-firing with CW.

It has been reported that the oxidized mercury has more affinity to the surface of fly ash than the elemental mercury[3]. The adsorption of the oxidized mercury on the fly ash occurred instead of the elemental mercury. The elemental mercury needs the additional oxidization step on the fly ash surface prior to its adsorption. However, effectiveness of the oxidized mercury capture by fly ash was also dependent on its contact efficiency with fly ash and residence time. Co-firing CW, inefficient capture (nearly 50 %) of the oxidized mercury by fly ash on the filter may suggest less residence time for its capture by fly ash. This assumption seems reasonable because higher contacting efficiency was generally found for mercury and fly ash on the filter. In those cases of firing fuels with less chlorine content, occurrences of almost 90 % of the elemental mercury may suggest either not much oxidized mercury in flue gas before the filtration step, or little elemental mercury can be oxidized by generated fly ash on the filter after flue gas passes through the fly ash cake on the filter. Therefore, it is difficult to conclude that the mercury adsorption on the fly ash was strongly correlated to the occurrence of the oxidized mercury in the flue gas. In this study, only the temperature of the filter (about 150 ^{o}C) was suitable for mercury adsorption on the fly ash, but not for the fly ash in the cyclone because of a temperature greater than 250 ^{o}C. Mercury oxidation is strongly dependent on chlorine content in the flue gas. This was corroborated during the investigation of chlorine content in flue gas, which is shown in Figure A4. When sub-bituminous coal was burned, HCl and Cl_2 concentrations in the flue gas were 1.42 ppm and 1 ppm, respectively. When it was co-fired with CW at 30 %, HCl and Cl_2 concentrations dramatically increased to 28.2 ppm and 1.85 ppm, respectively. Continuously

increasing the co-firing ratio of CW to 50 %, HCl and Cl_2 concentrations also increased to 36.5 ppm and 1.91 ppm, respectively.

It seemed that the introduction of limestone largely controlled the occurrence of chlorine species in the flue gas, which made occurrences of HCl and Cl_2 drop to 1.81 ppm and 1.01 ppm, respectively. This was similar to burning sub-bituminous coal only. Co-firing WP and CR had similar HCl and Cl_2 profiles, which were 1.23 ppm and 1.25 ppm during co-firing of WP and 1.46 ppm and 106 ppm during the co-firing of CR. Hydrogen chloride (HCl) and Cl_2 were about 7.32 ppm and 2.05 ppm for co-firing TS, which corresponded to its higher chlorine content in feeding TS. The mercury emission rates and mercury speciation strongly correlated to the occurrence of chlorine in the flue gas. Introducing CW greatly increased the occurrence of the total availability of chlorine species in the flue gas, which was supposed to contribute to the oxidation of the elemental mercury. Introduction of limestone in co-firing CW greatly eliminated the occurrence of chlorine in flue gas, which resulted in the reduction of the mercury oxidation. This was very similar to cases when co-firing biomass with low chlorine content, such as WP and CR. Comparably high chlorine content was found in both CW and TS. But the majority of chlorine in these two co-firing fuels did not occur in the gas phase. However, it did in the fly ash, based on the assumption of mass balance closure of chlorine. This could explain why the increasing co-firing ratio of CW and co-firing of high chlorine TS did not significantly increase the partition of particle-bound mercury and further reduction of gaseous mercury emission rates. This also agreed with the previous study that stated the increase of chlorine inputs did not necessarily lead to increased oxidized mercury[4-5].

The presence of less chlorine in the gas phase was better explained by the investigation of greater content of alkali metal oxides (Na_2O and K_2O) and alkali earth metal oxides (CaO and MgO) in tested fuels. The mole ratios of the total CaO, MgO, Na_2O and K_2O to chlorine (ROMC) in tested fuels are shown in Figure A5. This ratio was as high as approximately 250 ^oC for sub-bituminous coal, mainly due to the higher content of CaO and less chlorine in the sub-bituminous coal. The ROMC greatly decreased to approximately eight when co-firing CW with sub-bituminous coal because of very high chlorine content found in the CW. This ratio was again close to that of burning sub-bituminous coal at approximately 190 ^oC during tests with limestone introduction during the co-firing of CW and sub-bituminous coal. When co-firing 30 % WP and CR, The ROMCs were still higher because of less chlorine in these fuels. A

considerable amount of ash occurred and higher content of CaO and K_2O in TS made TS has higher ROMC.

Alkali metal and alkali earth metal oxides can capture Cl in the flue gas more efficiently at a temperature below 650 ^oC[6]. This typical temperature zone was found in the fluidized bed combustor in this study. The major reactions between oxides of alkali metals and alkali earth metals with sulfur in the flue gas occurred at temperatures about 800 ^oC. However, this could not totally consume all oxides of alkali metals and alkali earth metals. Generally, ratios of alkali metal oxides and alkali earth metals to sulfur were higher than three for the tested fuels, which were far more than sufficient for sulfur capture. Considering just partial sulfur was generally captured by these metal oxides, the utilization of available metal oxides for sulfur capture was below 1, as indicated in Figure A6. The remaining metal oxides will be better reactants and also sufficient for Cl capture. Previous studies by both thermodynamics equilibrium calculations[7] and co-firing tests[4,8-9] indicated that their was a smaller occurrence of HCl and Cl_2 in the flue gas, especially when burning low-sulfur coal at temperatures below 800 ^oC. The availability of alkali metal oxides should retain Cl species in the solid phase, which decreases gaseous Cl. Statistical analysis correlating the amount of oxides of alkali metals and alkali earth metals (Ca+Mg+Na+K) and the total gaseous chlorine is shown in Figure A7. This correlation was negative (increasing metal oxides decreased the occurrence of gaseous Cl) and strong with the linear R-square value of 0.98. Similarly, the correlation between gaseous chlorine and mercury emission rates is shown in Figure A7. The linear R-square value was 0.75 for the gaseous chlorine and the mercury emission rate correlation. Therefore, the lower occurrence of Cl in the gas phase, which was attributed to a lower mercury oxidation rate, is a major reason for less mercury capture by fly ash for all fuels except CW. A previous study[10] by ICSET of WKU in a 0.1 MW FBC facility found different trends on mercury speciation and mercury adsorption by fly ash co-firing high chlorine coal with high chlorine PVC. Results indicated that when using high-chlorine coal in an FBC system, the gas-phase mercury, which was around 45 % of the total mercury input, was primarily in the oxidized state (40 % of the total mercury input), while only a small portion (4.5 % of total mercury input) still existed as elemental mercury in the flue gas. Close to 55 % of the total mercury input was found in the solid phase.

In this previous study, higher oxidized gaseous mercury and particle-bound mercury may have contributed to the use of secondary air and lower oxide content of alkali metal and alkali

earth metal in the tested bituminous coal. Generally, higher sulfur content was found in the bituminous coal. Therefore, a lower ROMC ratio should be true when bituminous coal was burned, even though limestone was introduced. Additionally, the secondary air may have produced higher carbon-content fly ash, which is critical for mercury adsorption[11]. Furthermore, the secondary air also increased the temperature in the upper portion of the fluidized bed compared to secondary air injection. It was assumed that higher temperatures at the upper portion of the combustor made captured Cl by limestone inefficient, and thus, more Cl remained in the gas phase to oxidize the elemental mercury. Therefore, both higher content of alkali metal oxides or alkali earth metal oxides in tested biomass, and the occurrence of temperatures lower than 650 ^{o}C in the upper part of the fluidized bed combustor seemed to be responsible for the reduction of gaseous chlorine, and consequently limited mercury emissions reduction during co-firing. This study identified the important impacts of temperature profile and oxides of alkali metals (alkali earth metals) on mercury emissions during co-firing in the fluidized bed combustor.

Figure A1. The Lab-scale Fluidized Bed Coal Combustor

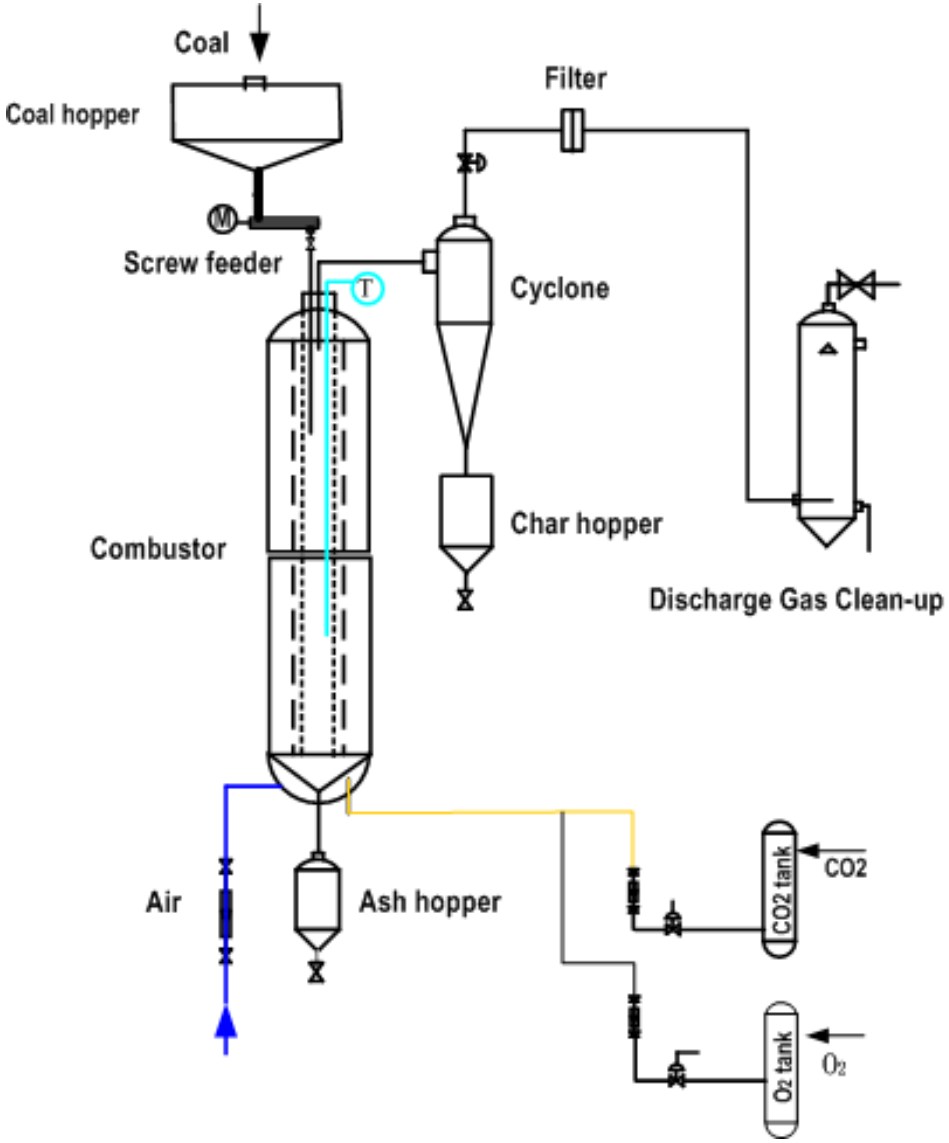

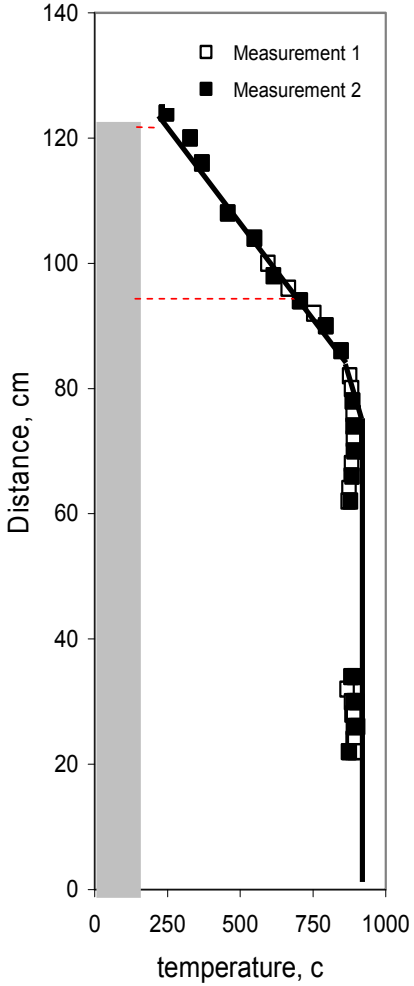

Table A1. Proximate, Ultimate Analysis and Major Oxides of Coal and Biomass Samples (on a dry basis)

		As Deter	Dry Basis											
	ADL	Moisture	Ash	Vol. Mat	Sulfur	Btu	Carbon	Hydrogen	Nitrogen	Oxygen	Chloride	Mercury	Fluoride	Bromide
SampleName		%	%	%	%	BTU/lb	%	%	%	%	ppm	ppm	ppm	ppm
PRB coal		15.01	7.64	43.32	0.54	11818	69.02	4.72	0.80	17.28	82	0.12	54	ND
Chicken waste		9.31	34.91	54.18	1.06	5097	33.32	3.91	4.87	21.91	22340	0.01	51	ND
Wood biomass		6.57	0.56	80.27	0.01	8488	46.65	5.90	ND	46.89	132	< 0.01	15	ND
Coffee residue		6.19	1.08	42.31	0.06	5559	27.86	8.63	0.87	61.49	134	< 0.01	17	ND
Tobacoo stalk		6.31	11.34	74.11	0.34	7079	44.08	5.18	3.77	35.28	4237	0.01	28	ND
	Minor oxides													
SampleName	Na_2O	MgO	Al_2O_3	SiO_2	CaO	K_2O	SO_3	P_2O_5	BaO	SrO	Fe_2O_3	MnO	TiO_2	
	%	%	%	%	%	%	%	%	%	%	%	%	%	
PRB coal	0.40	3.79	13.10	23.69	23.20	0.27	27.84	0.82	0.44	0.34	4.89	0.02	1.19	
Chicken waste	4.77	5.89	3.33	31.95	16.09	12.32	4.88	18.8	0.02	0.02	1.44	0.18	0.32	
Wood biomass	0.16	4.01	9.49	24.3	28.98	20.28	6.7	1.02	0.4	0.12	3.4	0.44	0.69	
Coffee residue	0.08	17.04	0.93	2.14	9.16	49.41	3.12	16.79	0.06	0.06	0.58	0.15	0.49	
Tobacoo stalk	< 0.01	4.2	1.78	17.13	16.86	45.37	6.41	7.2	0.08	0.04	0.73	0.04	0.16	

Figure A2. The Variation of Mercury Emission during Co-firing of Sub-bituminous Coal and Biomass

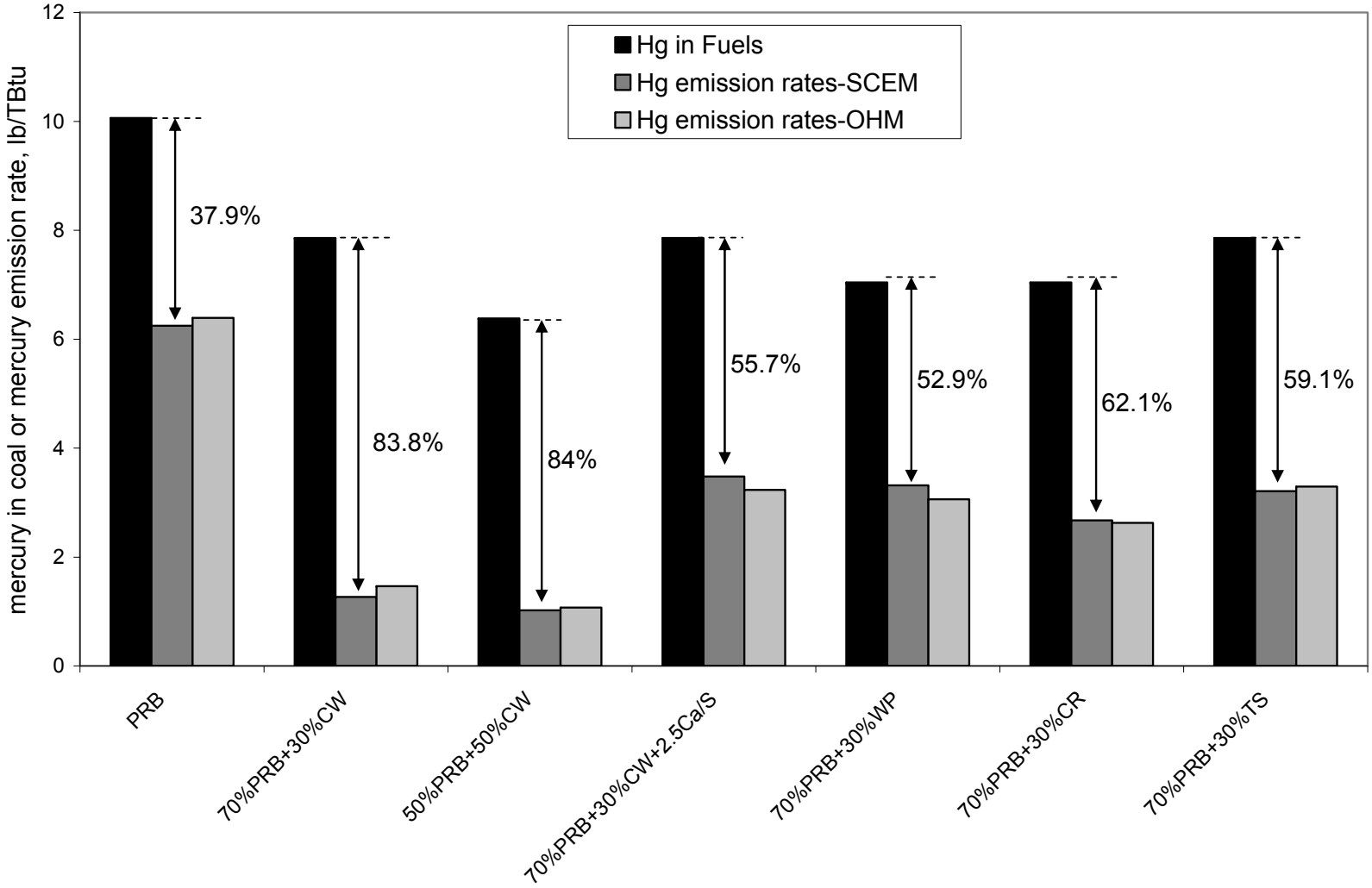

Figure A3. The Mercury Speciation during Co-firing of Sub-bituminous Coal and Biomass

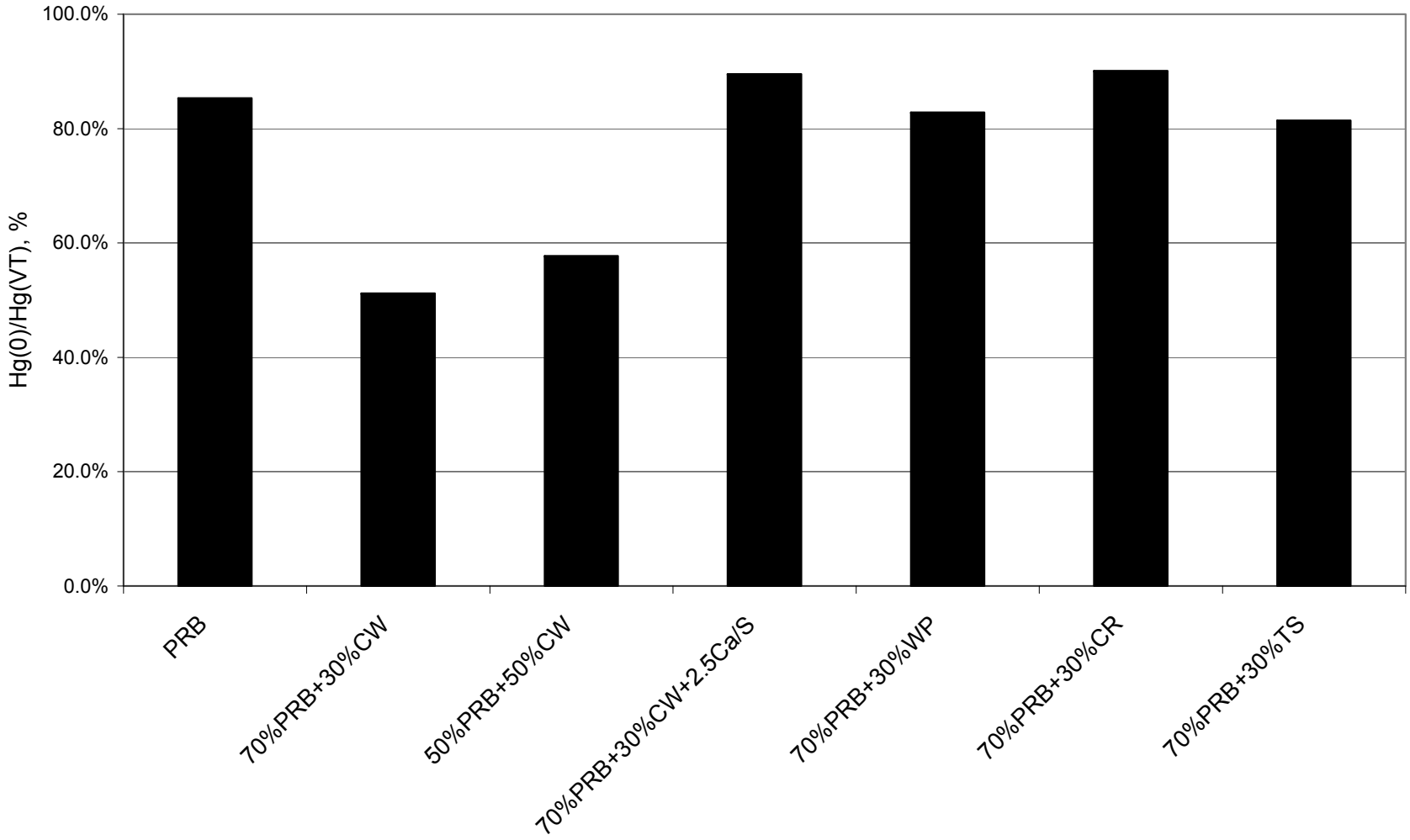

Figure A4. The Gas Phase Chlorine Concentration in the Flue Gas during Co-firing in the Fluidized Bed Combustor

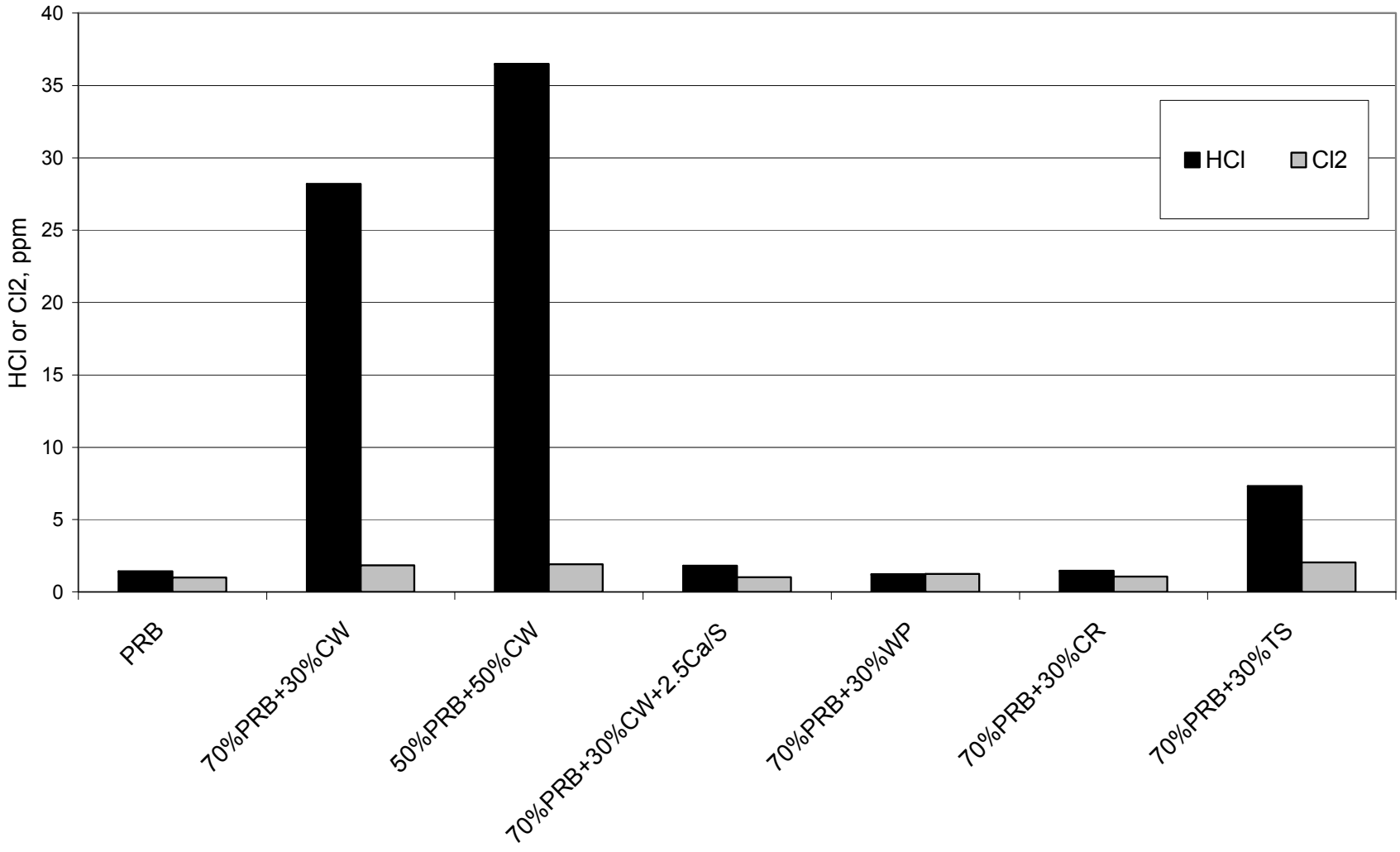

Figure A5. The Ratios of (Ca+Mg+Na+K)/Cl in Tested Fuels during Co-firing in the Fluidized Bed Combustor

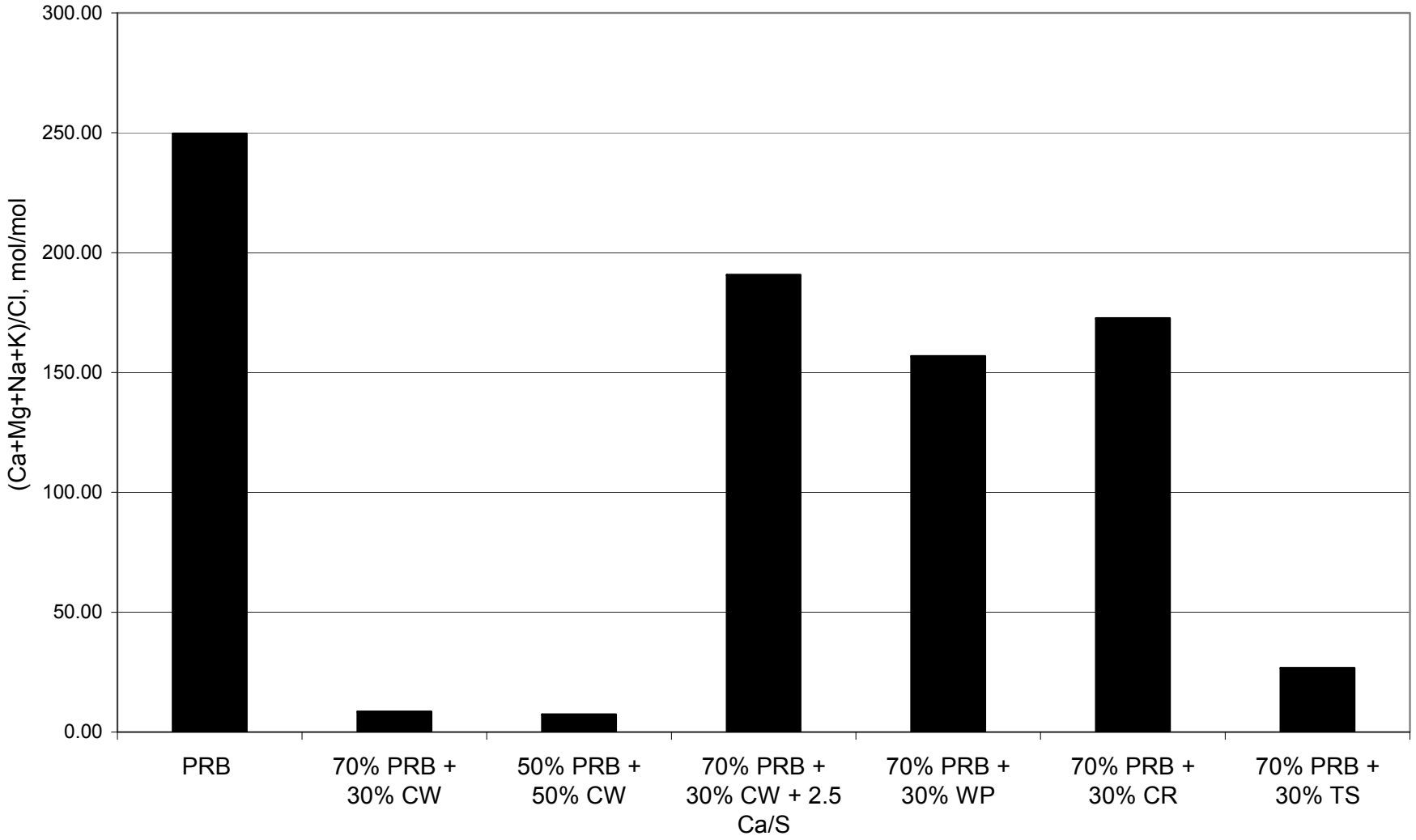

Figure A6. Sulfur Removal Efficiency or (Ca+Mg+Na+K)/S of Mixing Fuels during Co-firing in the Fluidized Bed Combustor

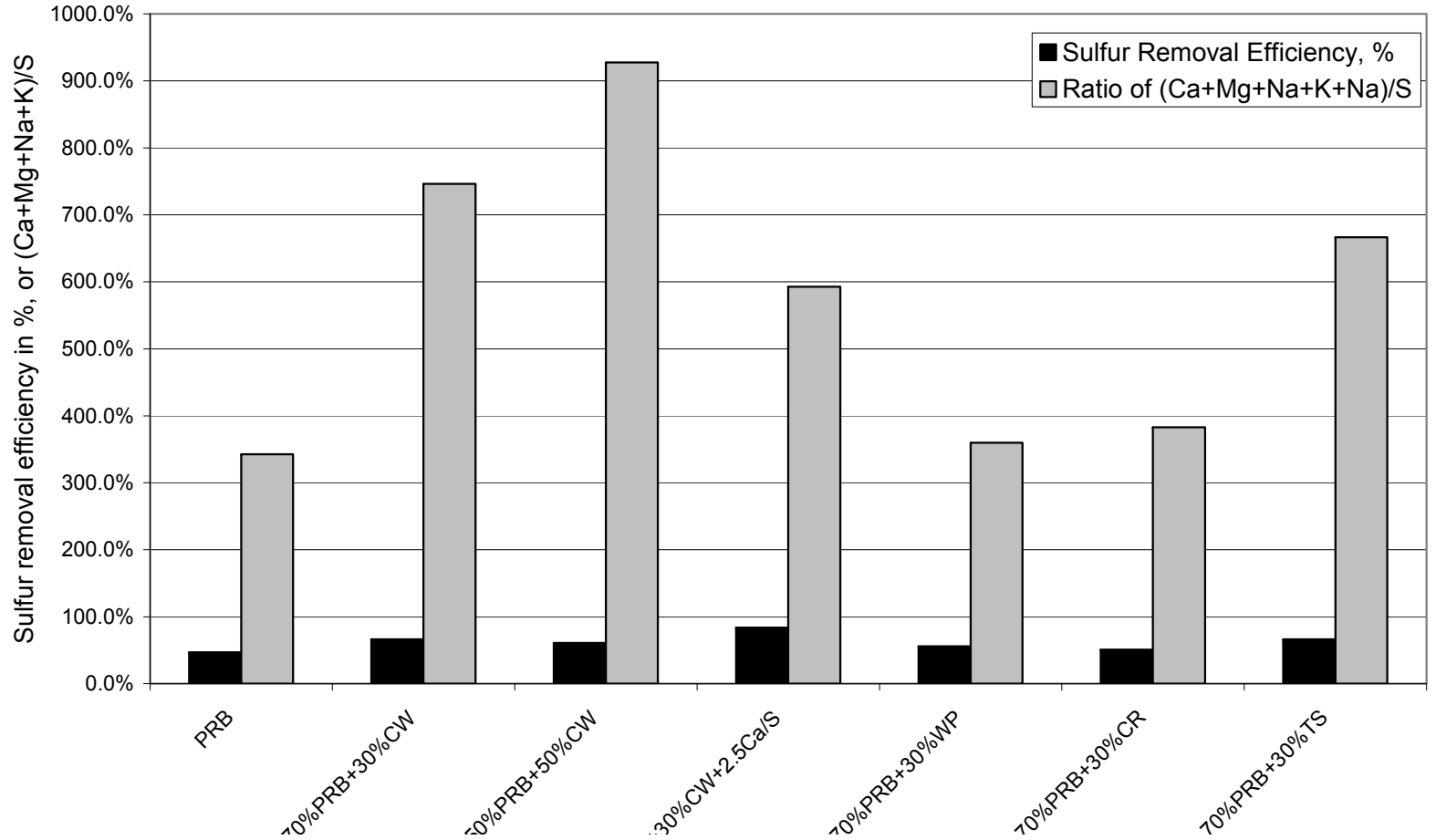

Figure A7. The Correlation of Mercury Emission Rate and Gaseous Cl, the Correlation of Gaseous Cl and (Ca+Mg+Na+K)/Cl

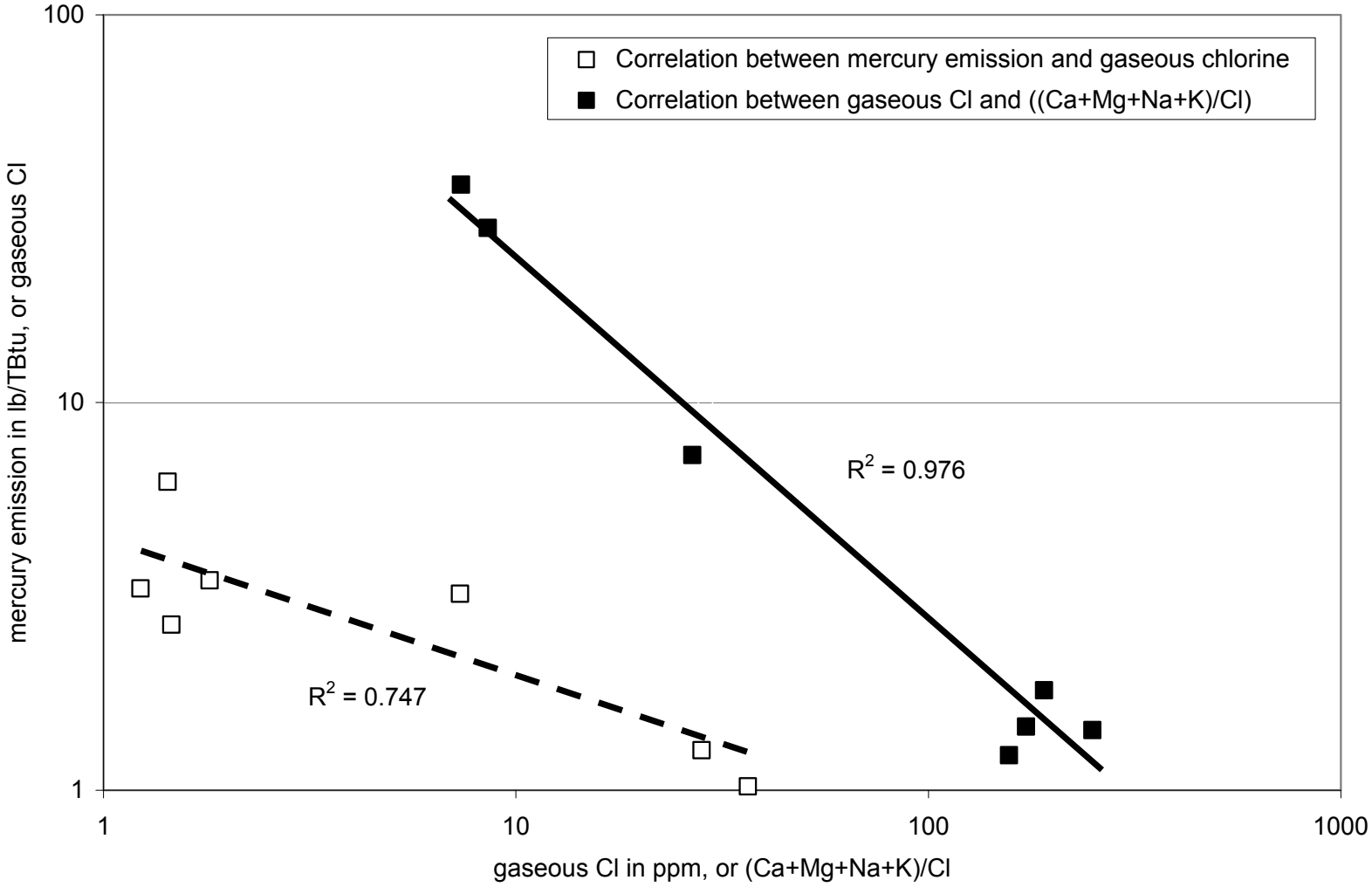

9.2 Tests in an SCR Slipstream Reactor

Test Facility. A pilot-scale slipstream SCR reactor has been designed to simulate the "full-scale" applications of an SCR system, as shown in Figure A8. The site setup picture is shown in Figure A9. The SCR reactor was designed and manufactured in a concentric configuration with inside pass for SCR catalyst loading where the main stream of flue gas passes through, and an outside pass for the bypassed flue gas to pass through. The flue gas, which is extracted from the well-insulated intake pipe before the SCR slipstream reactor, is split into two streams whose ratio is controlled by manual flashboard valves to adjust the slot area of the outside flue gas pass. The bypassed flue gas functions as a “strengthened” heat insulation due to its higher temperature, which minimizes the heat transfer rate by decreasing the temperature difference between the introduced main stream of flue gas and the bypassed flue gas stream. Thus, this slipstream reactor was well insulated so that the temperature drop across the SCR slipstream reactor was below 20 ºC. The section of inside pass is 0.152 by 0.152 square meter (m^2) and square in shape, and the outside pass is a one inch slot around the inside square. The total height of the reactor is 6.6 meter (m). The pilot-scale SCR has a two-layer catalyst to simulate variations in the residence time for gas-solid contact. Each catalyst chamber is 1 meter n height. The specific locations of the sampling ports are in relation to the locations of the catalysts. There are three sampling ports, which are located at inlets and outlets of each SCR catalyst bed. The “inlet” refers to the location before the first catalyst layer, “middle” refers to the location between the first and the second catalyst layers, and the “outlet” is the outlet of the second catalyst layer.

To prevent the fly ash from depositing on the SCR catalysts, an ash-blower using compressed air was designed and installed. The ash-blower control allows each catalyst layer to have the ash purged with high-velocity compressed-air independently. Along with the ash-blower, their ports have also been adapted to allow for pressure differential monitoring using a manometer. The overall ash-blowing cycle time is determined by the length of time it takes for the pressure differential to reach the upper limit. Generally, the first catalyst layer can be set for a blow cycle of five seconds blowing at 30-minute intervals, while the second catalyst layer has a blow cycle of eight seconds blowing at 30 minute intervals. With the aid of cross-catalyst differential pressure monitoring, the ash buildup can be monitored and when the pre-determined upper pressure level is reached, the ash-blowing sequence is activated to blow the ash, thereby bringing

the pressure differential back to normal levels.

To ensure the control and even distribution of spike-gas injection, three static mixers were built and installed at different locations in the SCR slipstream reactor. The first static-mixer is located one duct-diameter below the spiking gas injection ports to ensure homogeneous distribution of spiking gas before reaching the first catalyst layer. The second and third static-mixers have been installed at the bottom of each catalyst layer to ensure homogeneous concentrations of other gases after the flue gas exits each catalyst layer. The precise control of spiking gas addition was achieved through the construction of a multi-port mass-flow controller that has the capability of being set to inject a predetermined amount of gas from one to four attached cylinders. All injection ports for spiking gases are set up below the first sampling port, which leave the "inlet" sampling port unaffected. The injection of NH_3 is separated from other spiking gas lines to ensure operational safety. Considering the actual injection ratio of NH_3 in the commercial SCR facility, the ratio of NH_3 injection is set at NH_3:NO=1 to 1.1. Due to the low-NOx burner used, the NOx level was about 250 ppm during tests.

SCR Catalysts. Commercial monolith (Honeycomb) SCR catalysts were provided by two vendors. Catalyst #1 had an 8.4 mm pitch, and the square cross section had an array of 18 x 18 channels. Catalyst #2 had an approximate 7.5 mm pitch, and the square cross had an array of 20 x 20 channels. Each catalyst section was one meter in length; therefore, the total length of the catalyst was two meters. The SCR catalysts are designed to be operated at a space velocity of 1800 hr^{-1}, which is the actual space velocity used on full-scale coal-fired SCR reactors[18]. These two catalysts were tested in two coal-fired power plants burning eastern bituminous coals and sub-bituminous PRB coal. Two tested honeycomb SCR catalysts were provided by two commercial vendors, which are BASF/CERAM, Inc. and Hitachi, Inc. The pitch sizes and cell numbers are 10 mm and 15 x 16 for Catalyst #3 (BASF/CERAM, Inc.). The main components of SCR catalysts are V_2O_5-WO_3-TiO_2.

Coal and Ash Analysis. Bituminous coal, with medium sulfur and chlorine content, and PRB coal, with low sulfur and chlorine content, were burned during tests with the HBr addition. Coal and ash samples were collected once daily during tests. The proximate analysis, elemental analyses, and mineral metal analysis of the coal samples are shown in Table A2. Analysis of fly ash samples from the ESP hopper, which was the front row, is also shown in Table A2. All data was presented on a dry basis and the testing methods for all these samples can be found in the

reference[1]. The average sulfur, chlorine and mercury content in the tested bituminous coal were about 1.31 %, 1328 ppm and 0.11 ppm, respectively. In comparison, the average sulfur, chlorine and mercury content in the tested PRB coal was about 0.61 %, 170 ppm and 0.08 ppm during tests, respectively. Based on approximate mass balance, 90 % of the sulfur and chlorine content in coal existed in the flue gas during its combustion. CaO, Fe_2O_3 and LOI were about 1.71 %, 17.51 % and 7.13 % for collected fly ash of tested bituminous coal, and 22.95 % and 4.91 % and 0.64 % for collected fly ash of tested PRB. The bromine content in tested coals were under the detection limit.

Selective Catalytic Reduction - NO_x emission Control (the Case of Bituminous coal fired site). The reduction performance of the SCR slipstream reactor was evaluated by monitoring the NO concentration at the inlet and outlet locations of the SCR slipstream reactor. Due to the low-NOx burner installed in the test unit, NO concentrations at the inlet were found to be about 280-300 ppm during the SCR slipstream validation tests. Nitrous Oxide (NO) concentration at the outlet location was almost the same as that at the inlet location with the same O_2 concentration. After the NH_3 addition started with a molar ratio of NO:NH_3 at about 1, the NO concentration decreased gradually, and finally was reduced below 20 ppm, as shown in Figure A10-1 for Catalyst #1 and Figure A10-2 for Catalyst #2. Both catalysts in the SCR slipstream reactor worked properly as expected with above 95 % NO reduction.

Figure A8. The Schematic of the SCR Slipstream Reactor

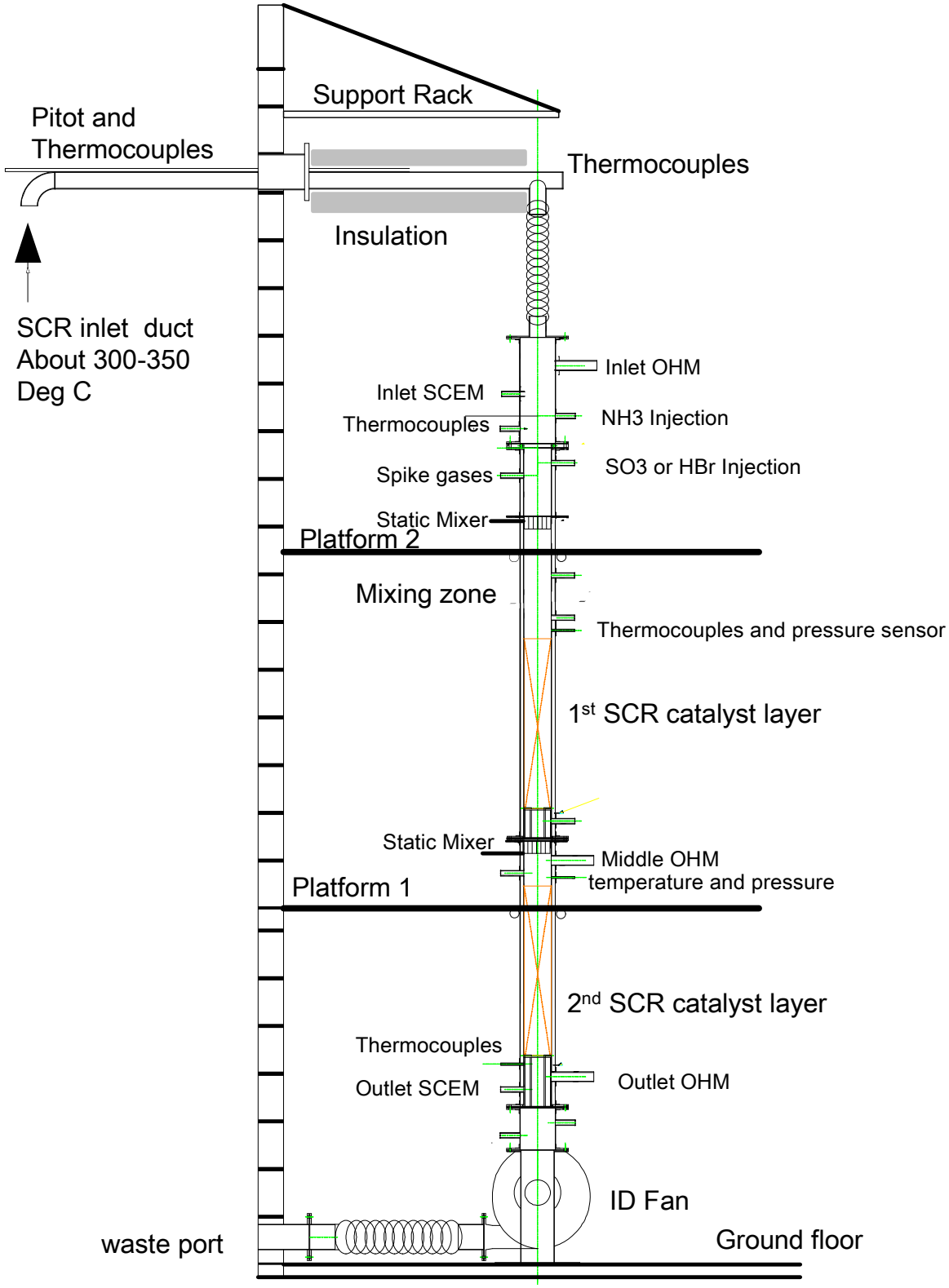

Figure A9. The Actual Setup on Site of the SCR Slipstream Reactor System

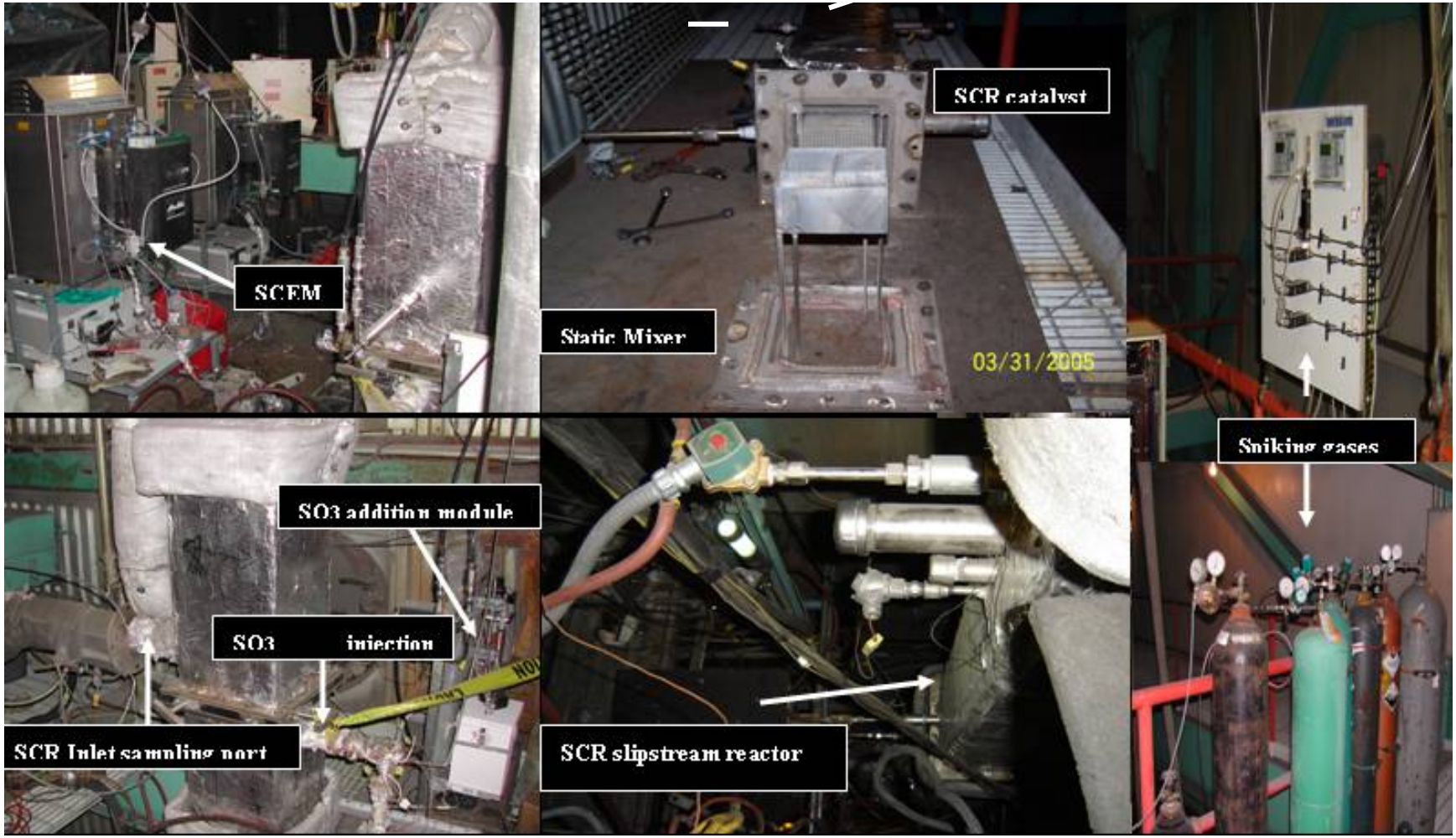

Table A2. The Analysis of Coal And Ash Samples During Tests

Coal analysis

	As Determined					Dry Basis						
	ADL[1]	Moisture	Ash	Vol. Mat	Sulfur	Btu	Carbon	Hydrogen	Nitrogen	Oxygen	Chloride	Flouride	Mercury
SampleName	%	%	%	%	%	BTU/lb	%	%	%	%	ppm	ppm	ppm
Bituminous Coal	3.04	5.41	10.30	37.13	1.31	13423	75.85	4.85	1.79	5.92	1328	ND	0.11
PRB[2] CoalTrial-1	20.75	11.37	6.20	47.07	0.42	12022	70.75	5.00	2.21	15.43	177	42	0.07
PRB[2] Coal Trial-2	18.52	12.15	7.59	45.45	0.81	12173	71.15	4.99	2.32	13.15	164	40	0.09
Average	19.63	11.76	6.89	46.26	0.61	12097	70.95	4.99	2.26	14.29	170	41	0.08

	Na_2O	MgO	Al_2O_3	SiO_2	P_2O_5	SO_3	K_2O	CaO	TiO_2	MnO	Fe_2O_3	BaO	SrO
	%	%	%	%	%	%	%	%	%	%	%	%	%
Bituminous Coal	0.01	0.90	18.14	38.27	0.58	1.94	2.35	1.71	1.14	0.02	17.51	0.15	0.13
PRB[2] Coal	1.02	4.70	14.89	28.63	0.69	11.93	0.39	22.95	1.17	0.02	4.91	0.49	0.30

Ash analysis

	Sulfur	Mercury	Chloride	Bromide	Fluoride	LOI
SampleName	%	ppm	ppm	ppm	ppm	%
Bituminous Coal	0.15	0.35	250	ND	ND	7.13
PRB[2] Coal Trial-1	0.67	0.15	123	ND	95	0.59
PRB[2] Coal Trial-2	0.89	0.18	177	ND	98	0.69
Average	0.78	0.17	150	ND	97	0.64

Note:

ADL[1] - air dry loss

PRB[2] - Powder River Basin coal

Figure A10-1. The NO Reduction Performance of the SCR Slipstream Reactor for Catalyst#1 under Bituminous Coal Flue Gas Atmosphere

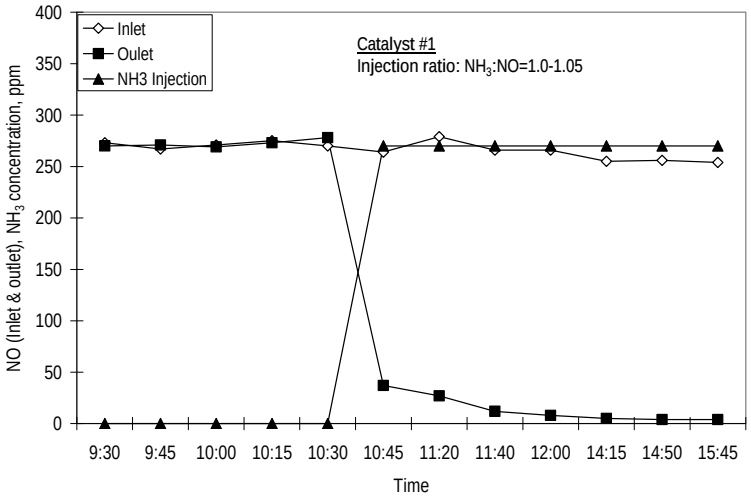

Figure A10-2. The NO Reduction Performance of the SCR Slipstream Reactor for Catalyst#2 under Bituminous Coal Flue Gas Atmosphere

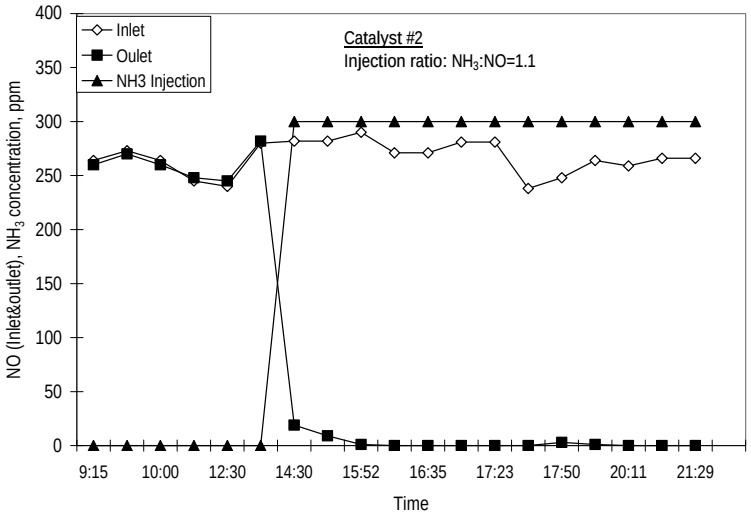

Figure A10-3. NO Reduction by SCR Catalyst#1 and #2 under PRB Coal Flue Gas Atmosphere

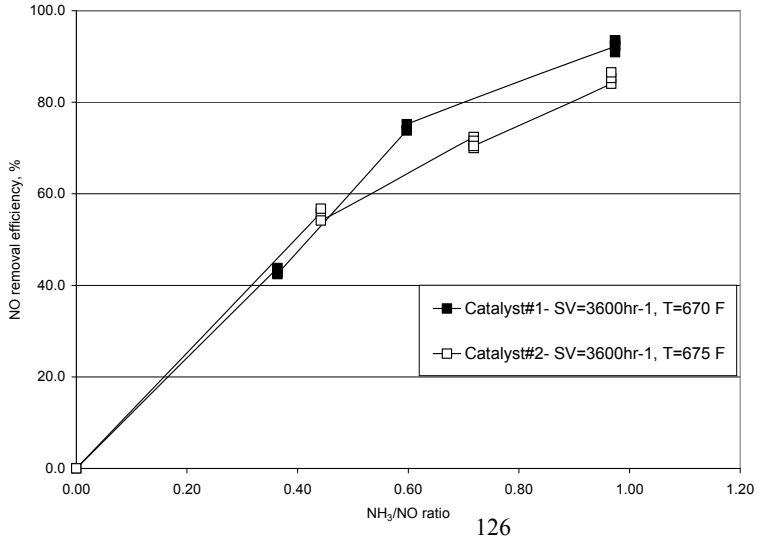

9.3 HBr Injection for Hg Emission Control – Development of New Additives on Effective Mercury Emission Control

Test Facility. The test facility was designed and manufactured to simulate the "full-scale" applications of the ductwork configuration in a coal-fired utility boiler. Its schematic configuration and setup can be found in the Supporting Information of Figure A11. In this study flue gas was introduced into the slipstream reactor from the economizer outlet port of the selected full-scale utility boiler, passing through the slipstream reactor and then back into the utility's ductwork. The addition of HBr or the simultaneous addition of HBr and the selected fly ash in a slipstream reactor (0.152 x 0.152 m) under the real flue gas situation were conducted in a full-scale coal-fired utility boiler burning Powder River Basin (PRB) coal. During tests, the residence time of flue gas inside the reactor was about 1.4 seconds under low temperature operation. The average temperature of a slipstream reactor was controlled at about 155 ^{o}C. Tests were organized into two phases. In Phase 1, only HBr was added to the slipstream; and in Phase 2, there were simultaneous additions of HBr and selected fly ash.

Hydrogen bromide (HBr) gas either from a pressurized cylinder or a diluted HBr acid liquid injector, at a pre-determined concentration using nitrogen as the carrying gas, was injected into the system. The desired spiking concentration of HBr inside the slipstream reactor could be adjusted by the mass flow controller (MFC) or liquid injector. To ensure the controlled and even distribution of the HBr, two static mixers were installed at different locations in this facility. The HBr injection port was located below the Hg sampling port at the inlet, which left this sampling port unaffected. An adsorbent screw feeder was used for adsorbent (fly ashes or the commercial Darco-LH mercury adsorbent) delivery into the slipstream reactor. With the assistance of a pressure balance line located between the adsorbent hopper and the AC injection port, the injection rate was unaffected by pressure fluctuation inside the reactor. The adsorbents underwent the adsorption process by interacting with mercury of the flue gas in this slipstream reactor.

Coal & Ash Analysis. Under low-temperature operation of the slipstream reactor, coal (PRB coal) and ash samples were also collected from coal hoppers and ESP ash hoppers, respectively. Analysis data on coal and ash samples are presented in Table A3. Major constituents in coal and ash samples during two testing phases under low-temperature operation were almost identical. During Phase 1, the average sulfur and mercury content in the tested coal were about 0.63 % with a relative standard variation of 22.6 % and 0.13 ppm with a relative variation of 27.9

%, respectively. The detectable halogen constituents (chlorine and fluorine) in coal samples were lower, averaging 164 ppm and 43 ppm, respectively. There was also no major difference in the LOI and mercury content in collected fly ash during this period time, as shown in Table A3. During Phase 2, the average sulfur and mercury content in the tested coal was about 0.59 % with a relative standard variation of 20 % and 0.12 ppm with a relative variation of 37.9 %, respectively. The detectable halogen constituents (chlorine and fluorine) in coal samples were also lower, averaging 118 ppm and 80 ppm, respectively. As shown in Table A3, the particle-bound mercury (Hg(P)) and LOI of fly ash, which were found in collected ESP fly ash, were about 0.65 ppm and 0.78 % for Phase 1, and 0.61 ppm and 0.58 % for Testing Period 2. There were also no major differences in the LOI and Hg(P) during these two testing periods. Based on analysis of collected coal and ash samples from this full-scale utility boiler, it could be concluded that the tested boiler unit was relatively stable. During Phase 2, additional fly ashes were also collected at the outlet of the slipstream reactor using a standard EPA flue gas sampling probe, in the front of which a finger filter was installed for ash sample collection.

Development of New Mercury Additives.

■ ***Mercury Oxidation during HBr Addition above 300 ^{o}C.*** The effects of HBr additions on Hg(0) oxidation in the empty slipstream reactor and in the SCR slipstream reactor are shown in Figure A12. Whether the SCR catalysts were available or not, HBr showed a very strong impact in increasing Hg(0) oxidation in the PRB coal-derived flue-gas atmosphere. Tests in the empty slipstream reactor indicated the percentage of Hg(0) oxidation increased to 83 % and 85.9 % with additional concentrations of HBr at only 3 ppm and 6 ppm, respectively. With the increase of HBr addition concentration from 3 ppm to 6 ppm, the Hg(0) oxidation curve became flat. This may indicate that no apparent additional Hg(0) oxidation could be achieved by continuous addition of the HBr. During tests with SCR Catalyst #1 at a preferred NH_3 addition ratio (NH_3/NO~1), the percentages of Hg(0) oxidation were approximately 68.2 % and 78.9 % at HBr addition concentrations of 6 ppm and 9 ppm, respectively. With no NH_3 additions, the percentages of Hg(0) oxidation were approximately 57.3 % and 64.4 % at HBr addition concentrations of 3 ppm and 6 ppm, respectively. During tests with SCR Catalyst #2, at a similar NH_3 addition ratio (NH_3/NO~1), the percentages of Hg(0) oxidation were approximately 74.7 % and 83.2 % at HBr addition concentrations of 3 ppm and 9 ppm, respectively. Without the addition of NH_3, the percentages of Hg(0) oxidation were approximately 81 % and 84.2 % at

HBr addition concentrations of 3 ppm and 6 ppm, respectively.

There was a good match between the results from tests in the empty slipstream reactor and SCR slipstream reactor with both Catalyst #1 and Catalyst #2. This indicated the SCR catalyst did not have Hg(0) oxidation and thus was independent of impacts of NH_3 additions. This finding may indicate the promising function of HBr on Hg(0) oxidation. Simultaneously, Hg(0) oxidation was less dependent on the availability of SCR catalysts. This was different from the results found by adding HCl or HF. In this study, The Hg(0) oxidation efficiencies were slightly lower at approximately 6.1 % and 19 % at the baseline level (without addition of HBr) during tests with SCR Catalyst #1 when NH_3 addition was performed. During tests with SCR Catalyst #2, its baseline values increased to 37.2 % and 29.8 % when NH_3 addition was performed. During tests with the empty slipstream reactor, this baseline value was also higher at approximately 29.5 %. Thus, tests with SCR Catalyst #1 showed a little lower Hg(0) oxidation efficiencies by HBr addition, compared to cases in the empty slipstream reactor and SCR slipstream reactor with Catalyst #2.

Figure A13 presents a comparison of impacts of different halogens (HCl, HF, HBr and HI) on Hg(0) oxidation under a PRB coal-derived flue gas atmosphere, which was made using results from the empty slipstream reactor. The maximum Hg(0) oxidation efficiency at approximately 40 % could be achieved by a total HCl concentration at 300 ppm in the flue gas. The increase of Hg(0) oxidation efficiency by HF addition seemed to follow the same trend, and was also comparable to the HCl addition at the same addition concentration. Both SCR catalysts seemed to promote Hg(0) oxidation by HCl and HF at the same addition concentrations. The tests by addition of HCl and HF was consistent with the lower Hg(0) oxidation efficiencies in the full scale utility boilers by burning PRB coal since its chlorine and fluorine contents are lower. As expected, the addition of HCl could further increase Hg(0) oxidation, which can be catalyzed by both of the evaluated SCR catalysts. For comparison, by achieving the same Hg(0) oxidation efficiency at approximately 40 % in the empty slipstream reactor (the baseline Hg(0) oxidation at about 5 %), the addition of HI concentration in the flue gas only needed to be 5 ppm. Moreover, HBr addition concentration at only 3 ppm could achieve the Hg(0) oxidation efficiency as high as about 80 % in the empty slipstream reactor (the baseline Hg(0) oxidation at about 30 %). Both HBr and HI showed much stronger impacts on the Hg(0) oxidation than those by HCl and HF at the same addition concentrations. The catalytic effects by SCR catalysts seemed not to correlate

with Hg(0) oxidation during additions of HBr and HI in the flue gas of PRB coal, at least for both evaluated SCR catalysts in this study.

The sequence, according to their impact strength on Hg(0) oxidation, were HBr, HI and HCl or HF. It seemed to follow their inversed atom sequence in the Periodic Table, except for the order between HBr and HI. The larger the halogen atom is, the greater its impact on Hg(0) oxidation. Two categories could be sorted by considering their interaction with the SCR catalyst and also interaction with NH_3 on the surface of SCR catalysts. SCR catalysts seemed to promote the Hg(0) oxidation through HCl and HF in Category 1, but not through HBr and HI in Category 2. Ammonia (NH_3) seemed to impact the Hg(0) oxidation only by HCl and HF through both SCR catalysts in Category 1.

There were some clues to explain the findings in this study. First, reaction paths for Hg(0) oxidation through halogen molecules (Br_2, I_2, Cl_2 and F_2), as indicated in Eq(A2) to Eq(A5) were generally favored in kinetics more than those through hydrogen halogens, as indicated in Eq(A6) to Eq(A9). This was at least clarified by previous investigation of Hg(0) oxidation mechanisms, which the chlorine or bromine species were involved in Ref[12]. That means kinetics of Hg(0) oxidation should be faster through halogen molecules than those through hydrogen halogens if previous studies on Hg(0) oxidation mechanisms by HCl and HBr could be further extended to those by HF and HI.

$$Hg + F_2 = HgF_2 \qquad \text{Eq(A2)}$$

$$Hg + Cl_2 = HgCl_2 \qquad \text{Eq(A3)}$$

$$Hg + Br_2 = HgBr_2 \qquad \text{Eq(A4)}$$

$$Hg + I_2 = HgI_2 \qquad \text{Eq(A5)}$$

$$Hg + 2HF + \tfrac{1}{2} O_2 = HgF_2 + H_2O \qquad \text{Eq(A6)}$$

$$Hg + 2HCl + \tfrac{1}{2} O_2 = HgCl_2 + H_2O \qquad \text{Eq(A7)}$$

$$Hg + 2HBr + \tfrac{1}{2} O_2 = HgBr_2 + H_2O \qquad \text{Eq(A8)}$$

$$Hg + 2HI + \tfrac{1}{2} O_2 = HgI_2 + H_2O \qquad \text{Eq(A9)}$$

Second, additions of HBr and HI into the elevated temperature conditions would generate almost total conversion of HBr to Br_2, and HI to I_2. The generation of Br_2 could be through the Deacon reaction of Bromine, as indicated in Eq(A10)[12]. By a different reaction routine, I_2 could be generated through decomposition of HI[13-14], as indicated in Eq (A11). However, this was not the case for HCl since the depletion of Cl_2 would occur by the enriched SO_2 in the coal-derived

flue gases[15, 12], as indicated in Eq(A12).

$$2HBr + ½\ O_2 = H_2O + Br_2 \qquad \text{Eq(A10)}$$

$$2HI = H_2 + I_2 \qquad \text{Eq(A11)}$$

$$Cl_2 + SO_2 + H_2O = 2HCl + SO_3 \qquad \text{Eq(A12)}$$

Third, a more complicated mechanism was proposed to occur by addition of HBr and HI in the flue gas, in which interhalogen species (such as BrCl or ICl) were likely to be involved in the elemental mercury oxidation processes. The interhalogen of BrCl may be generated through reaction, as indicated in Eq(A13) or (A14), and depleted through reaction, as indicated in Eq(A15). And the interhalogen of ICl may be generated through reactions, as indicated in Eq(A16) or (A17), and depleted through reaction, as indicated in Eq(A18). Generally the interhalogens are unstable and extremely reactive chemically[16]. The elemental mercury oxidation may occur through reactions by BrCl and ICl[17-18], as indicated in Eq(A19) and (A20), respectively. Thus, outcomes of elemental oxidation may include mutual species of either $HgCl_2$ and $HgBr_2$, or $HgCl_2$ and HgI_2, respectively. Interhalogen species such as ClF also possibly could be generated, but did not seem important due to comparable impact of Cl and F on Hg(0) oxidation kinetics by tests in this study.

$$HBr + HCl + ½\ O_2 = BrCl + H_2O \qquad \text{Eq(A13)}$$

$$Br_2 + HCl = BrCl + HBr \qquad \text{Eq(A14)}$$

$$2BrCl = Br_2 + Cl_2 \qquad \text{Eq(A15)}$$

$$HI + HCl + ½\ O_2 = ICl + H_2O \qquad \text{Eq(A16)}$$

$$I_2 + HCl = ICl + HI \qquad \text{Eq(A17)}$$

$$2ICl = I_2 + Cl_2 \qquad \text{Eq(A18)}$$

$$Hg + 2ICl = HgI_2 + HgCl_2 \qquad \text{Eq(A19)}$$

$$Hg + 2BrCl = HgBr_2 + HgCl_2 \qquad \text{Eq(A20)}$$

Under a temperature of around 300°C, thermodynamics studies indicated there was a limitation on $HgBr_2$ or HI_2 occurrence in the coal-fired flue gas, but not for $HgCl_2$[19]. The oxidized mercury ($HgCl_2$) can proceed to approximately 100 % conversion under the temperature range in this study if kinetics of mercury oxidation by chlorine is quick enough in the slipstream reactor. The enhanced Hg(0) oxidation rate by bromine additions in this study, and likely iodine additions, exceeded the limitation of thermodynamics prediction[19]. It may indicate that the formation of $HgBr_2$ or HgI_2 were not the only new products by the addition of bromine

or iodine. It was possible for the simultaneous formation of $HgBr_2$ and $HgCl_2$ by bromine addition, or HgI_2 and $HgCl_2$ by iodine addition. Bromine or iodine seems to have the capability to attack chlorine species in the flue gas to promote the generation of activated chlorine, which was involved in improving the kinetics of mercury oxidation[16]. This may explain why the total mercury oxidation rate exceeded the thermodynamics limitation on maximum occurrence of $HgBr_2$ and HgI_2. Vosteen, et al. proposed the possible mechanisms on enhanced mercury oxidation by the addition of bromine species based on their extensive studies[12]. Larger generation of free bromine molecules (Br_2), other than free chlorine molecules (Cl_2) by HBr and HCl additions in the flue gas, was his method of distinguishing the different impacts of bromine and chlorine on elemental mercury oxidation kinetics. The bromine Deacon reaction is favored to produce comparatively more free Br_2, as shown in Eq(10), while the reversed chlorine Deacon reaction is favored by depletion of SO_2 in the flue gas. However, the bromine addition in the flue gas was conducted by co-firing bromine species and coal in Vosteen's tests (higher temperatures than in the current study) and the oxidized mercury included both $HgBr_2$ and $HgCl_2$ in their tests. These two instances may have discovered that, firstly bromine species had enough residence time (in several seconds) to produce Br_2; and secondly, Br_2 could not convert all mercury to $HgBr_2$ and left some of the Hg(0) to be reacted with active Cl to produce $HgCl_2$, even in this longer residence time than the current study. Chlorine species seemed to be involved in its competition with bromine species in the Hg(0) oxidation process. This evidence could support our findings by thermodynamics prediction that there existed a limitation of mercury oxidation by bromine species. Considering our test conditions showed that the residence time of flue gas in an empty slipstream reactor was just one second (too short for total conversion of HBr to Br_2) there must be other mechanisms regarding mercury oxidation with both bromine and chlorine species in the flue gas. To figure out the conflict, thermodynamic prediction and test results, the occurrence of the intermediate species of BrCl and ICl was proposed in this study, which brought in the competition of chlorine on mercury oxidation under enhanced kinetics.

Thus, by a combination of findings in this study and previous studies, one may reasonably conclude that different impacts of halogens on Hg(0) oxidation should result from different kinetics between the Hg(0) and halogens in the kinetics-controlled Hg(0) oxidation process. Comparably, HCl was not effective in oxidizing Hg(0) due to its ineffective conversion to their molecule (Cl_2) under coal-fired flue gas atmosphere. Thus, Eq(A7) may be the main reaction

routine for Hg(0) oxidation through HCl. The addition of HF most likely follows the same mechanisms, as indicated in Eq (A6), if the presumption of ineffective conversion of HF to F_2 in the flue gas could be valid. With HBr or HI additions in the flue gas, Hg(0) oxidation occured through two routes, which were dependent on temperature ranges. Under higher temperatures (generally higher than 650 ^oC[14]), HBr and HI was converted to Br_2 and I_2. These elements made Hg(0) oxidation proceed very quickly through reactions Eq(A8) and Eq(A9), respectively. Thus, $HgBr_2$ and HgI_2 were the main types of oxidized mercury in the flue gas. In a lower temperature range (around 300 ^oC), HBr and HI interacted with HCl. The HCl was available in the coal-fired flue gas, to generate interhalogens such as BrCl and ICl[20]. The interhalogens, BrCl and ICl also caused Hg(0) oxidation to proceed faster through reactions Eq(A19) and Eq(A20). Thus, both $HgBr_2$ and $HgCl_2$, or HgI_2 and $HgCl_2$, are occurrences of oxidized mercury in the flue gas. All reactions listed in this study were presented as global reactions. Detailed mechanism studies should be addressed in further studies.

■ ***Mercury Oxidation and Adsorption on Fly Ash during HBr Addition at 155 ^oC.*** Unlike the case when HBr addition was pursued under higher temperature ranges (above 300^{o}C), Hg(VT) (the total vapor phase mercury) at the outlet of the slipstream reactor was decreased during HBr addition under a lower temperature range (about 155^{o}C). It seemed the occurrence of the transformation of Hg(VT) to Hg(P), which meant the adsorption of speciated mercury on the originally-occurring PRB-derived fly ash in the flue gas. Under testing conditions of the slipstream reactor (temperature of 155^{o}C and the residence time of 1.4 seconds), the overall mercury removal efficiency (as defined in the Eq-1) was increased by increasing the HBr concentrations in the flue gas. As indicated in Figure A14, HBr addition concentrations at 1.1 ppm, 1.8ppm, 2.65ppm and 3.5ppm in the flue gas increased the overall mercury removal efficiency inside the slipstream reactor to about 30, 40, 47 and 50 %, respectively. The mercury removal efficiency inside the slipstream reactor was only 5% on average, when HBr addition is not available. Therefore, 45 % of net mercury removal efficiency could be expected under HBr addition into the slipstream reactor at about 3.5ppm. The addition of HBr significantly increased the mercury capture capability of PRB-derived fly ash. It seemed the curve of the overall mercury removal efficiency correlated to the HBr addition concentrations, becoming flat as the HBr injection rate increased. This was likely attributed to the interactions among the HBr, fly ash and mercury. Shorter residence time of HBr within the slipstream reactor and less developed pore

structure of PRB-derived fly ash, may have made the adsorption of HBr on the fly ash close to saturation, and thus fly ash was less effective under the increasing HBr injection rates. If this was a real case, the adsorped HBr or bromine species on the fly ash would be responsible for the enhanced mercury capture capability of PRB-derived fly ash.

The overall mercury removal efficiency (%) = $[Hg(VT)_{inlet} - Hg(VT)_{outlet}]/Hg(VT)_{inlet}$ Eq(A21).

The total mercury oxidation efficiency (%) = $[Hg(VT)_{inlet} - Hg(0)_{outlet}]/Hg(VT)_{inlet}$ Eq(A22)

Because of the decrease of the total gaseous mercury at the outlet of the slipstream reactor during low temperature operation when HBr was injected, we used the total gaseous mercury at the inlet of the slipstream reactor as a base to calculate the mercury oxidation efficiency, as indicated in Eq(A22). The total mercury oxidation efficiency was presented by a ratio between the difference of the total vapor phase mercury at the inlet of the slipstream reactor and elemental mercury at the outlet of the slipstream reactor $[Hg(VT)_{inlet} - Hg(0)_{outlet}]$, and the total gaseous mercury concentration at the inlet of the slipstream reactor ($Hg(VT)_{inlet}$). It presented the absolute mercury oxidation efficiency, which included two mercury oxidation processes occurring inside the boiler prior to inducing flue gas inside the slipstream reactor. Figure A15 shows the effectiveness of the elemental mercury oxidation efficiency during HBr injection under low temperature operation. Similar to the higher temperature range (above 300^{o}C), HBr addition into the slipstream reactor under the lower temperature range (155^{o}C) and the shorter residence time (1.4 second) could also result in significant mercury oxidation. The HBr solution addition and HBr gas injection functioned identically on mercury oxidation. However, the effectiveness of the HBr solution addition on mercury oxidation was dependent on if it was pre-vaporized prior to its injection. As indicated in Figure A15, total mercury oxidation efficiencies were about 30, 55, 70, and 90%, at HBr addition concentrations in the flue gas of 0ppm, 0.9ppm, 1.8ppm, 3.5ppm. OHM data matched with SCEM data and confirmed the effectiveness of HBr injection on mercury oxidation under the lower temperature operation conditions. By deduction of the total mercury oxidation efficiency under HBr addition from that without HBr addition (HBr addition concentration= 0 ppm), the net mercury oxidation, which was probably caused by the HBr addition, could be calculated. This net mercury oxidation efficiency was about 25, 40 and 60% under HBr addition concentrations of 0.9ppm, 1.8ppm and 3.5ppm, respectively.

■ ***Mercury Adsorption during Simultaneous Addition of HBr and Selected Fly Ashes at 155 ^{o}C.*** Test results of simultaneous injection of HBr and fly ash from different utility boilers are shown in Figure A16. The average mercury removal efficiency by original PRB-coal-derived fly ash was only 3% in Phase 2. With addition of HBr at 4ppm, the total mercury removal efficiency increased to about 44.4 %. Commercial brominated activated carbon product, such as Darco LH, was effective on mercury capture. With availability of HBr addition at 4ppm, addition of Darco LH adsorbent could increase the total mercury removal efficiency to 76%. The reason might be that the pre-oxidized mercury can be easily captured by fly ash. Because of concerns of the increase of LOI content in generated fly ash when activated-carbon-based adsorbent was injected, a group of selected fly ash samples from different utility boilers was tested with simultaneous addition of HBr at 4ppm. It was found that the minimum amount of injected fly ash could result in additional gain of mercury removal efficiency for bituminous-derived or lignite-derived fly ashes, but not always for the addition of PRB-derived fly ash. For example, with the simultaneous addition of HBr at 4ppm and PRB-derived fly ash at 10 lb/MMacf, there was no distinct increase of mercury removal efficiency. For bituminous-derived fly ash #1, addition at 10 lb/MMacf could increase mercury removal efficiency to 60.8 %. Increasing the addition rate of bituminous-derived fly ash #1 to 30 lb/MMacf, increased the mercury removal efficiency to 72.5 %. Switching the addition of bituminous-derived fly ash to bituminous-derived fly ash #2, increased the mercury removal efficiency to about 76 %. The addition of another fly ash from the utility boiler burning bituminous coal did not achieve higher mercury removal efficiency. This fly ash was actually a bed slag, which was from a circulating fluidized bed combustor. The lower BET and LOI content in this CFBC slag was likely responsible for its lower mercury capture capability. For comparison, Bituminous-derived fly ash #1 and #2 both present good mercury capture efficiency with their minimum addition. The difference in their developed pore structure can possibly explain it. It's interesting to find lignite-derived fly ash had a better performance on mercury capture than bituminous-derived fly ash. With additional lignite-derived fly ash at 10 lb/MMacf and HBr at 4ppm, mercury removal efficiency was kept at about 65 %. Increasing the addition of lignite-derived fly ash to about 30 lb/MMacf, also increased mercury removal efficiency to over 80%. Based on the assumption of mass balance of fly ash, the original occurrence of PRB-derived fly ash in the fly ash should be about 220 lb/MMacf. Therefore, the

maximum addition of different fly ashes at 30 lb/MMacf would not dramatically change the fly ash properties of generated PRB fly ash.

The addition of fly ash without availability of HBr addition did not significantly contribute to the increase of mercury removal efficiency. For example, the mercury removal efficiency was about 14.5 % with the addition of CFBC slag at 30 lb/MMacf compared to 3 % without the addition of CFBC slag at similar addition rates, which did not significantly increase mercury removal. This was also far less than the mercury removal efficiency at 58 % with both addition of HBr and CFBC slag. It was likely that the addition of HBr made fly ash enhance its mercury capture capability based on enhanced mercury capture capability using brominated activated carbons. If this is the case, the bromine content in the fly ash should be increased after HBr addition in this study. Further study by characterizing halogen content in fly ash indicated, as shown in Figure A17, that there was increasing bromine content in the fly ash. The same figure shows that there was significant correlation between particle-bound mercury (Hg(P)) and bromine content in fly ashes. The correlative factor (R^2) was about 0.767, which could present a valid correlation between bromine content in the fly ash and Hg(P). But it was not the case for the correlations of Hg(P) and fluorine and chlorine. This may indicate that injected HBr into ash-laden flue gas could create fly ash that is bonded with some bromine, which means this brominated fly ash has mercury capture capability under a lower temperature range. Oxidized mercury can be more easily captured by fly ash than the elemental mercury under the lower temperature range. The HBr addition was confirmed to enhance mercury oxidization under both higher temperature and lower temperature ranges. Therefore, there was a likelihood that more occurrence of the oxidized mercury under HBr addition in the flue gas could also contribute to the enhancement of mercury capture by fly ash.

This study confirmed that under lower temperature ranges (around 155^{o}C) and shorter residence time (about 1.4 second), HBr addition can not only enhance the mercury oxidization, but also promote the transformation of mercury from gas phase to the available fly ash in the flue gas. The doped HBr on the fly ash should be responsible for the additional mercury capture on the fly ash. Under a minimum addition of HBr, additions of minimal amounts of bituminous-derived or lignite-derived fly ashes can further improve mercury capture efficiency by injected fly ash. Therefore, fly ash can be a cheap source of mercury adsorbent with minimum impact on fly ash properties for re-utilization. Longer ductworks can achieve the longer contact

time of HBr, fly ash and mercury in the full-scale utility boiler, by which even higher mercury capture efficiency by fly ash can be expected. This combination technology could maximize Hg capture efficiency with minimized injection rates of both HBr and Hg adsorbents which likely control the total costs of Hg capture using cheaper untreated fly ash. This synergetic simultaneous injection of both HBr and activated carbon may be an optimal technology and strategy for Hg capture in PRB-fired utility boilers with a goal of 90% Hg control efficiency with better economic prospects.

■ ***Corrosion Investigation.*** Several carbon steels and stainless steels, which are generally used in coal-fired utility boilers, were subjected to static corrosion tests under a Powder River Basin (PRB) coal flue gas atmosphere with the addition of hydrogen bromide (HBr) at 4ppm. This investigation of corrosion likelihood was conducted using prepared sample coupons, which were installed inside a slipstream reactor. The slipstream facility was controlled at two temperature conditions of about 307^{o}C for 720 hours or 155^{o}C for 300 hours. Scanning electron microscopy (SEM) with energy-dispersive X-ray (EDS) analysis was used to determine the corrosion performance mechanisms of sample coupons. Results indicated that all tested sample coupons were corrosion resistant under the protection of the original occurrence of the oxide layer outside of tested materials. There were two ash layers outside of the naturally occurring iron oxide layer, including loosely deposited fly ash on the outside and the intensively-packed ash deposit layer, mainly CaO and $CaSO_4$, on the inside. There was a clear interface between the inside ash-deposit layer and the iron oxide layer outside of the tested materials. There was no distinct evidence of enrichment of halogens (including fluorine, chlorine and bromine) inside both the inside ash deposit layer and the iron oxide layer. This inside ash deposit layer protected the metal material from corrosion. The quick quenching rate of the flue gas was responsible for shorter contact time and the subsequent reaction between halogens and calcium-rich ash.

Figure A18 shows the backscatter electron images (BEIs) and EDS analysis of corrosion coupon samples obtained from 720 hour tests under 307^{o}C (HT) and 300 hour tests under 155^{o}C (LT). The mark ‘I’ indicates the coupon sample was the original, which was not exposed under the test environment. The mark ‘II’ indicates the coupon sample was the test sample, which was exposed under the test environment. Coupon samples of A242 and SS310 were only tested under 155^{o}C and 307^{o}C, respectively. A full spectrum of occurring elements were included in EDS analysis, but only major elements found on cross-sections of coupon samples were included in

Figure A18. Other elements, which were in almost no content, are not presented here.

For coupon sample A36 carbon steel material, the original iron oxide layer was still available on the sample surface after exposure under the testing environment. This originally occurring oxide layer may have remained in its original, undamaged status after its exposure in the test environment. Since loosely-deposited fly ash was cleared before SEM-EDS analysis, there was no ash layer found outside of the iron oxide layer even under a higher magnified scale by the SEM. This was also the case for the sample coupon of A242 under investigation by SEM. A line scan of EDS revealed commonalities for both of these carbon steel samples. There was a sharp increase of both oxygen and iron elements outside of carbon steel materials, which were followed by a sharp decrease of oxygen content and a simultaneously sharp increase of iron. These phenomena were not changed when temperatures of sample coupons were switched from 155^{o}C to 307^{o}C. The highest temperature in this study (307^{o}C) was still below the critical point when significant corrosion occurred. For two sample coupons of stainless steels (SS 310 and 316L), oxygen content showed a sharp peak at the thin layer outside the pure steel material together with an increased content of iron. This layer originally occurred before the sample coupon was exposed to the testing environment compared to two sample coupons before and after exposure under the testing environment. This phenomenon was also not dependent on test temperatures of sample coupons within this study.

Figure A11. The Schematic Configuration of the Slipstream Reactor

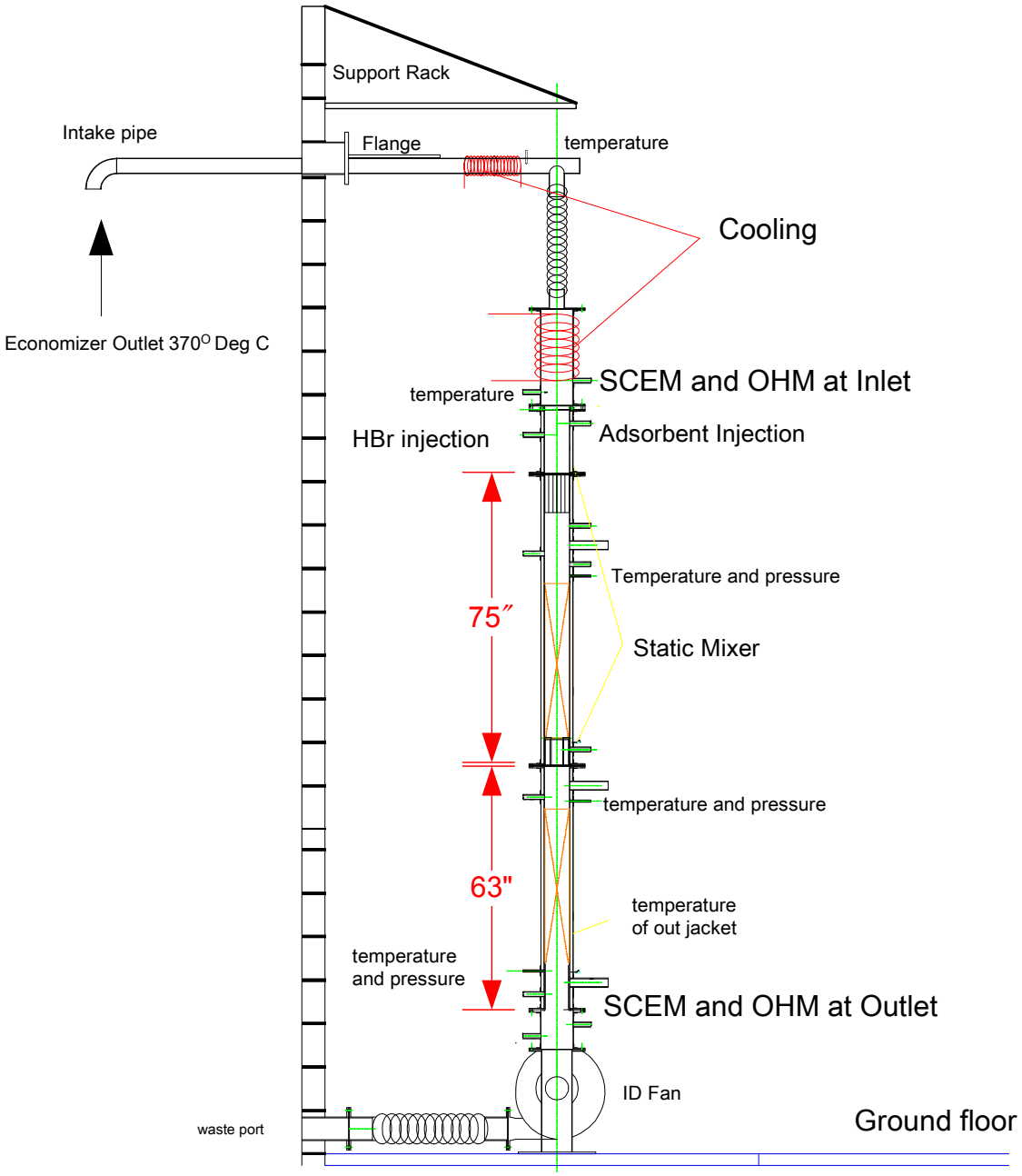

Table A3. Characterization of Coals and Collected Ash at the Outlet of Testing Slipstream Reactor

Phase 1		"As Deter"	Dry Basis											
Coal Samples	ADL	Moisture	Ash	Vol. Mat	Sulfur	Btu	Carbon	Hydrogen	Nitrogen	Oxygen	Chloride	Mercury	Fluoride	Bromide
		%	%	%	%	BTU/lb	%	%	%	%	ppm	ppm	ppm	ppm
Coal - Day 1	11.67	17.10	8.66	41.16	0.73	12342	73.43	4.67	1.02	11.48	165	0.14	43	ND
Coal - Day 3	19.14	11.89	9.74	42.88	0.61	11441	69.05	4.76	0.86	14.98	176	0.14	48	ND
Coal - Day 5	26.67	6.32	7.63	43.67	0.62	11939	70.45	4.87	0.93	15.51	143	0.16	58	ND
Coal - Day 7	26.64	6.50	7.10	43.40	0.59	11970	70.33	4.86	0.95	16.17	187	0.10	37	ND
Coal - Day 9	24.11	8.22	7.21	43.84	0.61	11962	70.55	4.86	0.92	15.84	161	0.12	49	ND
Coal - Day 11	18.58	13.59	7.52	43.72	0.61	11918	70.80	4.87	0.90	15.30	152	0.12	21	ND
Average	**21.13**	**10.60**	**7.98**	**43.11**	**0.63**	**11929**	**70.77**	**4.81**	**0.93**	**14.88**	**164**	**0.13**	**43**	**ND**
Relative variation					**22.6%**		**6.2%**				**21.3%**	**27.9%**	**86.7%**	
Phase 2 Coal Samples														
Coal - Day 1	17.06	13.43	7.65	43.82	0.58	11833	75.24	4.46	1.28	10.79	108	0.10	77	ND
Coal - Day 2	15.98	17.21	7.77	44.13	0.57	11820	76.17	4.54	1.14	9.81	117	0.11	81	ND
Coal - Day 3	15.68	17.17	7.06	44.29	0.55	11927	77.44	4.60	1.09	9.27	106	0.09	76	ND
Coal - Day 4	24.48	13.04	8.61	44.07	0.60	11681	76.41	4.55	1.06	8.76	115	0.14	88	ND
Coal - Day 5	13.99	21.79	9.41	43.78	0.69	11557	75.72	4.49	1.11	8.58	140	0.12	80	ND
Coal - Day 6	12.54	20.98	7.25	45.15	0.57	11872	77.77	4.58	1.11	8.73	123	0.13	80	ND
Average	**16.62**	**17.27**	**7.96**	**44.21**	**0.59**	**11782**	**76.46**	**4.54**	**1.13**	**9.32**	**118**	**0.12**	**80**	**ND**
Relative variation					**20.0%**		**3.3%**				**26.7%**	**37.9%**	**13.5%**	

Injected Fly Ashes	LOI	SSA (BET)	Na_2O	MgO	Al_2O_3	SiO_2	CaO	K_2O	SO_3	P_2O_5	BaO	SrO	Fe_2O_3	MnO	TiO_2
	%	M^2/g	%	%	%	%	%	%	%	%	%	%	%	%	%
Bituminous #1	4.57	4.41	<0.01	1.20	25.79	49.75	3.35	2.54	2.39	0.33	0.15	0.13	12.54	0.02	1.81
Bituminous #2	3.49	3.62	0.15	0.95	18.63	43.49	8.88	2.53	1.82	0.12	<0.01	0.03	22.21	<0.01	1.19
Bituminous #3	35.2	0.42	<0.01	0.66	6.00	23.26	40.14	0.60	24.99	0.09	<0.01	0.05	3.81	<0.01	0.39
SB (PRB)	0.75	5.42	1.12	4.65	18.76	38.39	25.20	0.63	1.96	0.97	0.67	0.42	5.49	0.02	1.72
Lignite	0.46	0.7	0.27	3.15	18.76	58.12	12.41	0.81	0.44	0.17	0.26	0.22	3.82	0.05	1.51
Darco-LH AC		305													

Note: ADL- air dry loss; ND - not detected

Note: LOI: Loss of Ignition; SSA: Specific Surace Area

Figure A12. Effect of HBr Addition on Hg(0) Oxidation

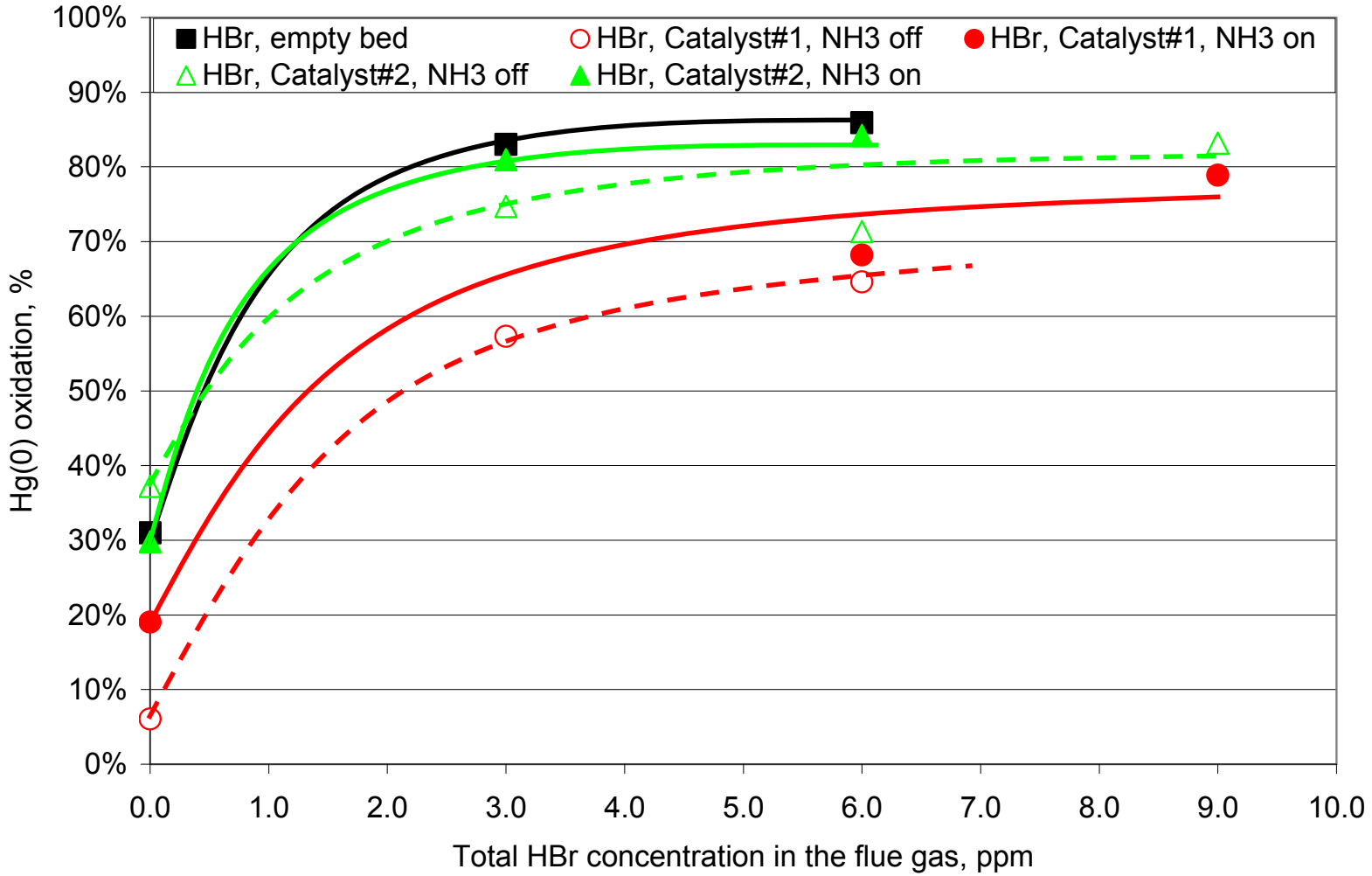

Figure A13. Comparison of Effects of Additives on Hg(0) Oxidation in the Empty Bed

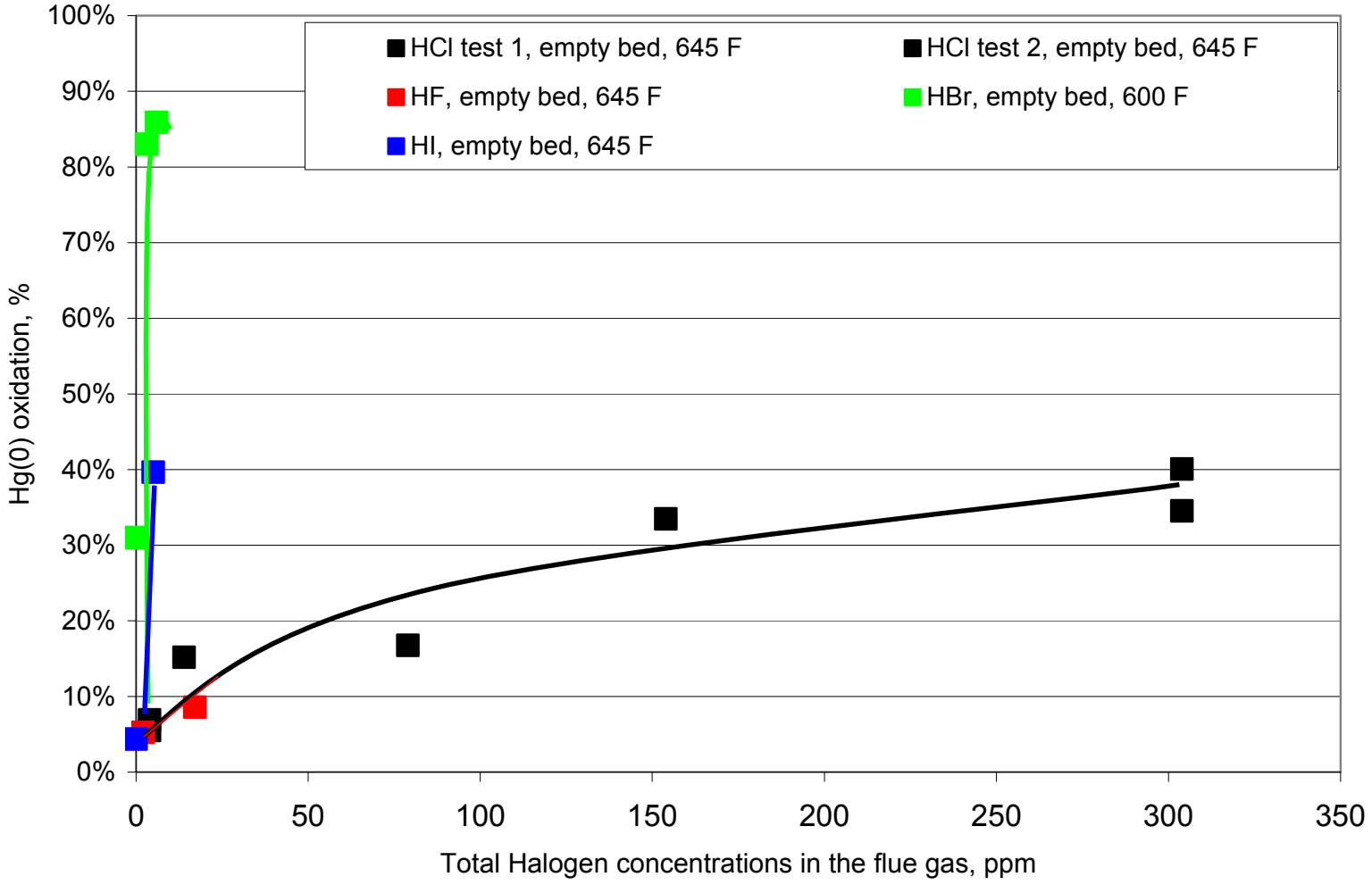

Figure A14. Correlation of HBr Injection Concentrations and Mercury Removal Efficiency in the Slipstream Reactor

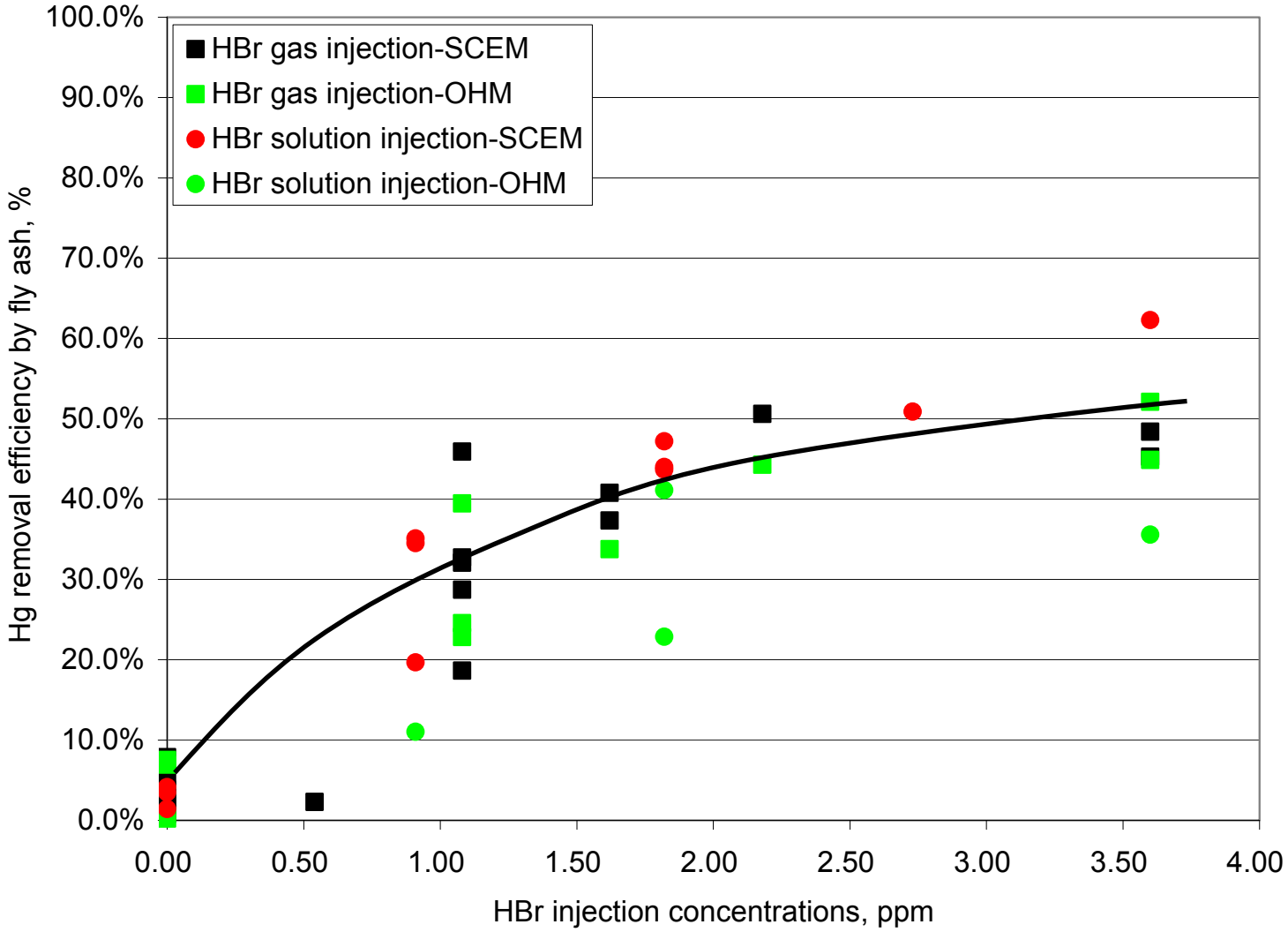

Figure A15. Correlation of HBr Injection Concentrations and Mercury Oxidation Efficiency in the Slipstream Reactor

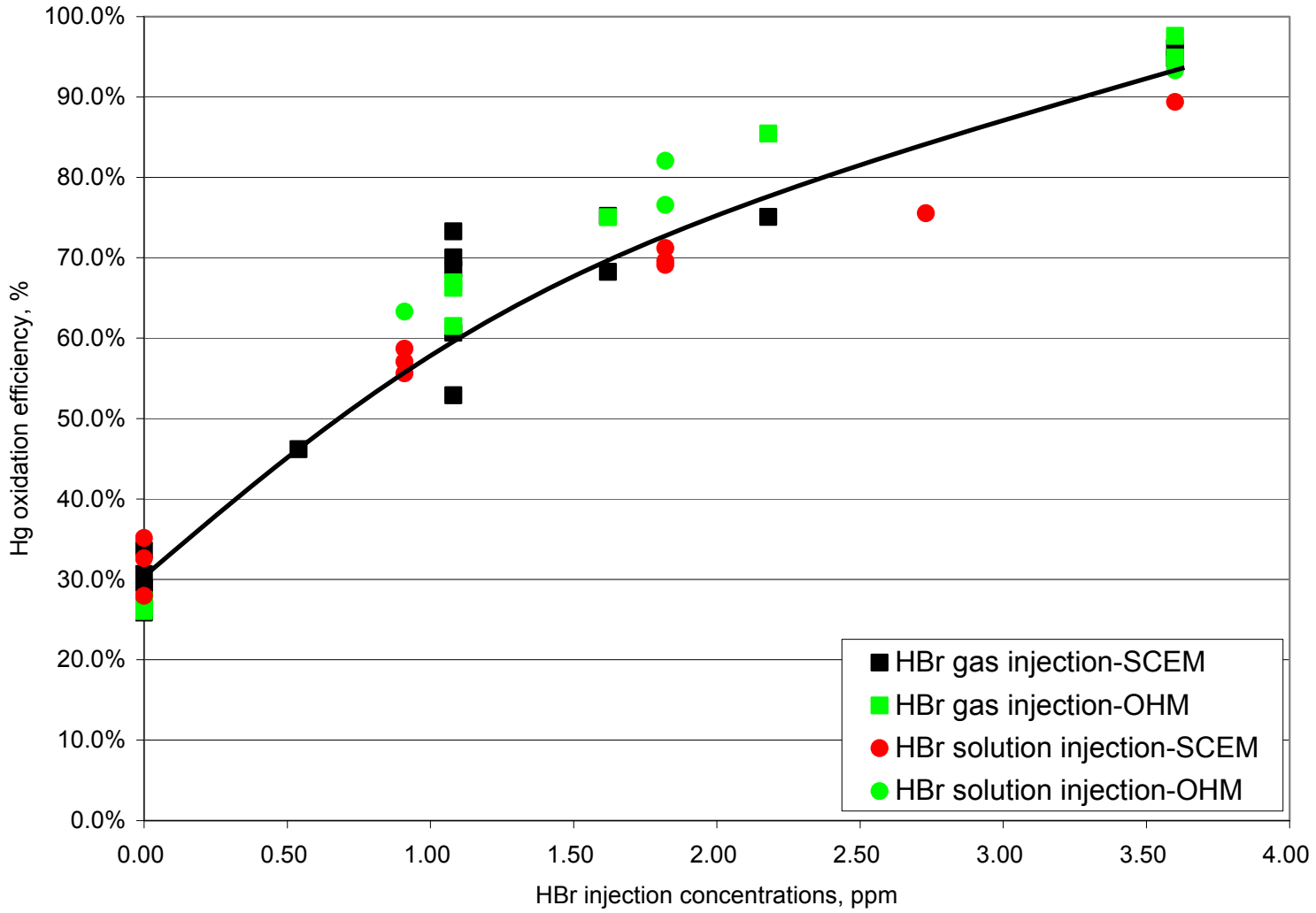

Figure A16. The Mercury Removal Efficiencies by Simultaneous Additions of HBr (at 4 ppm) and Selected Fly Ashes

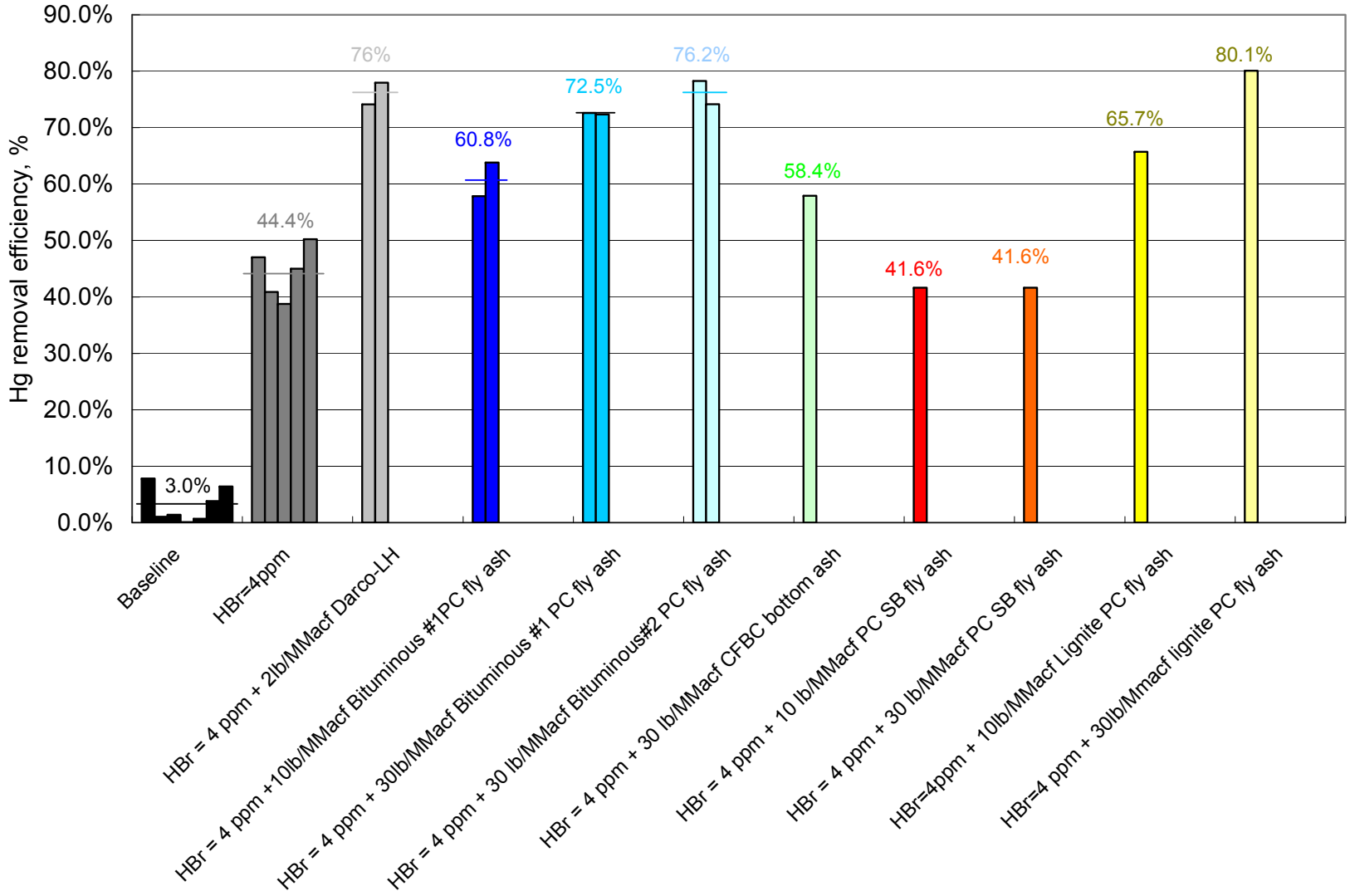

Figure A17. The Correlation of Particle-bound Mercury and Fluorine, Chlorine and Bromine Contents on Fly Ashes

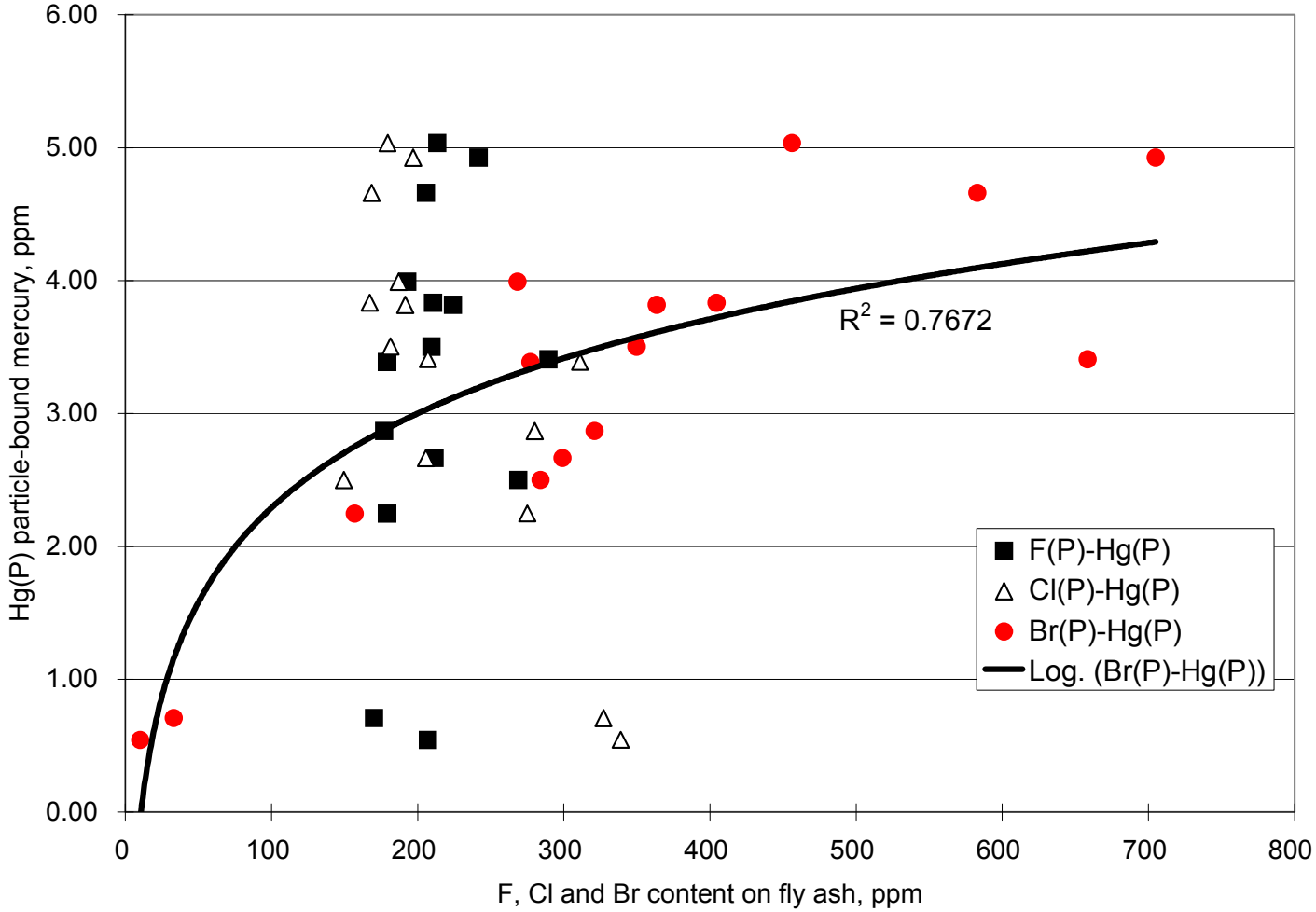

Figure A18. Comparison of Cross-section BEI Images and EDS Analysis of Alloys (A36, A242, 310, SS316L) Before and After Exposure Under Testing Atmospheres (LT: 150 ^{o}C, HT: 350 ^{o}C; I: Original coupon sample, II: coupon sample after exposure under test environment)

Coupon sample of carbon steel (A36 and A242)

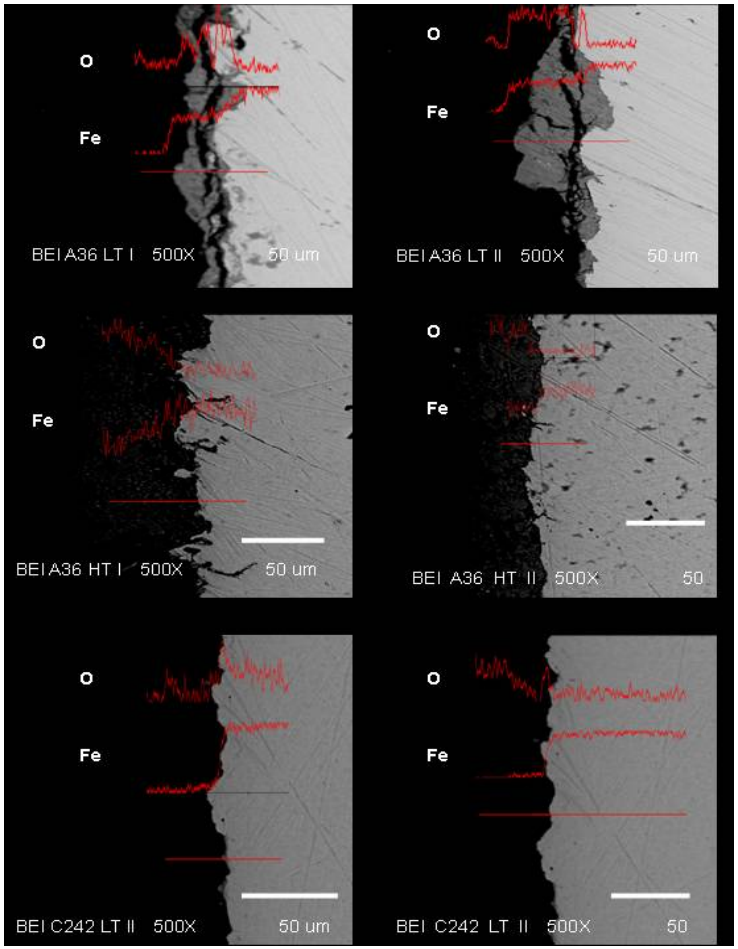

Coupon sample of carbon steel (SS310 and 316L)

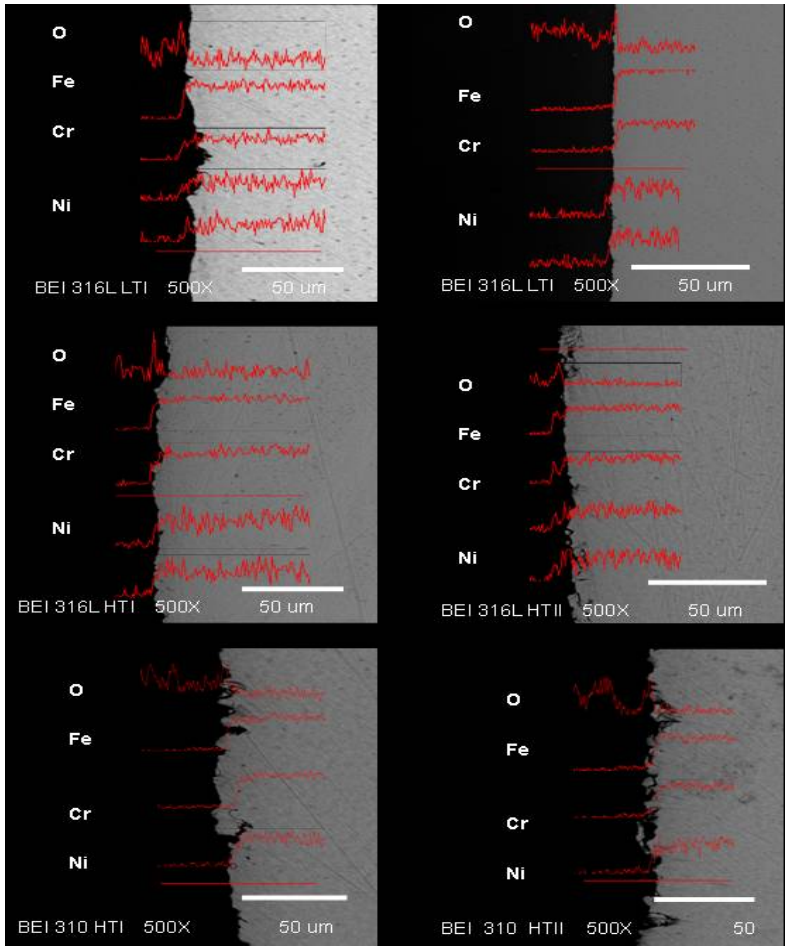

9.4 Chemical Looping Combustion

Theoretical Analysis and Selection of Oxygen Carriers.

■ ***Kinetics.*** The metal oxides with its reduced metal oxides or metals, which are used as oxygen carriers in the CLC must have sufficient reaction activity in reduction and oxidation and enough strength to limit particle breakage and attrition. A number of metals have been discussed in the literature[21,22-38], such as Fe, Ni, Co, Cu, Mn, and Cd, as well as some metal composites. The investigation of the oxidation and reduction kinetics of selected metal oxides have been intensively carried out in either a TGA, a lab-scale fixed bed or a fluidized bed using gaseous fuels such as H_2, CO or CH_4. The kinetics of reactions varied widely depending upon the type of metal oxide, particle size (70 μm-2 mm), reduction gas (H_2, CO and CH_4) and temperature (600-1000^{o}C). Generally, Cu, Ni and Co and their oxides showed higher oxidation and reduction reaction activity and greater durability after repeated oxidation and reduction cycles than Fe. It was also found that an impregnated type of oxygen carrier could increase the reactivity, attrition-resistance and durability, even with their particle size being as large as about 2 mm in diameter. Almost full conversion of reactants could be achieved in minutes for the impregnated type of oxygen carriers. The candidates for the inert support materials could be SiO_2, Al_2O_3, yttria-stabilized zirconium (YSZ), TiO_2 and MgO. However, different combinations of active materials of oxygen carriers with inert support materials showed different crushing strength and sintering temperature.[33-34] During the experiments with CH_4, carbon deposition may have occurred, which could cause a dramatic loss of reactivity. However, a high concentration of water vapor available in the reducer could help to eliminate carbon deposition.[28,33,35] Based on an oxygen transfer capability, energy balance analysis and thermodynamics analysis, copper (Cu) seems to be the better choice as an oxygen carrier for the CLC system of solid fuels. The CuO-Cu series will be used as oxygen carriers for developing CCLPCM.

■ ***Physical properties of Oxygen Carriers.*** For a reactor in which solid particles are flowing, moving and re-circulating, the possibility of the particle agglomeration should be avoided. For metal-based oxygen carriers, the melting points of the selected metals, reduced metal oxides and metal oxides are important parameters in evaluating their agglomeration tendencies. The melting of oxygen carriers may also have resulted in the loss of reactivity. The melting points of oxygen

carrier candidates are shown in Table A4[39]. The majority of metals and their metal oxides have very high melting points, which are always higher than 1200 ^{o}C, except those with melting points around 1050 ^{o}C, which are within the operational temperature range of CLC processing such as Cu, CuO, and $Mn_2O_{3,}$ which are highlighted in light gray. Some metals and their metal oxides have very low melting points such as PbO, CdO and Co_3O_4, which are highlighted with dark gray and must be removed from the candidate list to be oxygen carriers in the CLC process. Operating temperatures of the CLC process are also dependent on the acceptable reactivity of oxygen carriers. Previous studies indicated that Cu-based oxygen carriers had reactivity of 100 % reduction within minutes at lower temperatures (600-900 ^{o}C)[37-40] in the fixed bed or fluidized bed testing facilities. When copper oxide was doped on substrate, it indicated that most of its oxygen is active for reaction with methane, and the highest efficiency could be achieved with reduction rates up to 100 %/min and oxidation rates up to 25 %/min.[28,33,35]

■ ***Oxygen Transfer Capability of Oxygen Carriers.*** The utilization efficiency of an oxygen carrier depends on its oxygen transfer capability, which is listed in Table A4 as the mol of metal per mol of oxygen transfer (N). On the other hand, the re-circulation of the oxygen carrier required energy consumption, which is proportional to the pressure drop across the reactor[38]. In a fast fluidization bed oxidizer, the pressure drop is proportional to the terminal velocity Ut[41]; and in a bubble fluidization or moving bed reducer, the pressure drop is proportional to the minimum velocity U_{mf}[41]. As indicated in Eq(A23) and Eq(24), ρ_p which is the particle density of oxygen carriers, is the most important parameter affecting the Ut (factor value at 0.5) and U_{mf} (factor value at 1). These two parameters can be multiplied by N relative to the same parameters of the CuO-Cu system, which are $(Nx\rho_p)/ (Nx\rho_p)_{Cu\text{-}CuO}$ or $(Nx\rho_p)/(Nx\rho_p^{0.5})_{Cu\text{-}CuO}$, to evaluate the relative energy consumption by using different oxygen carriers.

$$Ut = [4d_p(\rho_{p-}\rho_g)g /(3\rho_g C_D)]^{1/2} \qquad \text{Eq(A23)}$$

$$U_{mf} = [d_p^{2}(\rho_{p-}\rho_g)g(\varepsilon_{mf}^{3}\Phi_s^{2})]/ [(150\mu)(1-\varepsilon_{mf})] \qquad \text{Eq(A24)}$$

As shown in Table 1, N values and $(Nx\rho_p)/(Nx\rho_p)_{Cu\text{-}CuO}$ or $(Nx\rho_p)/(Nx\rho_p^{0.5})_{Cu\text{-}CuO}$ values follow the same trend so we can focus on the N value to evaluate energy consumption. The best candidates for oxygen carriers should be those with a smaller N values. The minimum value of N

is 0.67 for reactions (9) and (15) and the next is 0.75 for reactions (5) and (11) and (17) for Co-based, some of Mn-based and some of Fe-based oxygen carriers. N values of other reactions are close to 1 for Cu-, Ni-, and some of Co-based and some of Fe-based oxygen carriers. By similarly evaluating the parameters of $(N x \rho_p)/(N x \rho_p)_{Cu\text{-}CuO}$ and $(N x \rho_p)/(N x \rho_p^{0.5})_{Cu\text{-}CuO}$, the same conclusion can be made. Any candidates without a gray mark have passed the selection criteria. They include Ni-based (NiO-Ni), Co-based (CoO-Co), Mn-based (Mn_3O_4-Mn, MnO-Mn) and Fe-based (Fe_2O_3-Fe, Fe_3O_4-Fe, FeO-Fe) to be oxygen carrier candidates. Copper-based oxygen carriers are also included in this list due to their perfect reactivity even at lower temperatures.

■ ***Energy Balance Analysis.*** The oxygen carrier reduction process by solid fuel is far more complicated compared to that by gaseous fuels. The process is governed by the prevailing chemical thermodynamics and kinetics. If the indirect path (gasification of solid fuels followed by reduction of metal oxides by gaseous gasification products) is dominant, the properties of pyrolysis and gasification of solid fuels should be considered. All reactions related to the pyrolysis and gasification of fossil fuel are endothermic, as illustrated by Eq (A25), (A26) and (A27). All enthalpy data are based on 1 atm and 25 ^{o}C.[39] In conventional gasification technologies, self-combustion of solid fuel is needed to provide the heat request of the endothermic pyrolysis and gasification processes. This is called the auto-thermal process. In the proposed CLC system, the gasification process for solid fuel occurs simultaneously with a reduction process for the oxygen carrier in the reducer where no oxygen exists. There are two ways to supply heat for the solid fuel gasification process. One is the reduction of the oxygen carrier indirectly by solid fuels or their product gases. .The other method is to use a heat-transfer material with a high-heat capacity to transfer heat from the oxidizer to the reducer. Obviously, the previous one is the better choice to prevent additional energy consumption by recycling the heat-transfer material.

$$C_nH_mO_p \rightarrow aCO_2 + bH_2O + cCH_4 + dCO + eH_2 + f(C_2\text{-}C_5),\ 20.9\ kJ/mol \quad Eq(A25)$$

$$C + H_2O \rightarrow CO + H_2,\ 118.3\ kJ/mol \quad Eq(A26)$$

$$C + CO_2 \rightarrow 2CO,\ 160.5\ kJ/mol \quad Eq(A27)$$

Until now, just a few metal oxides that have been examined as oxygen carriers for the CLC process show exothermic properties when reacted with carbon or syngas. The possible reactions related to oxygen carrier candidates and carbon in the reducer, are shown in Table A5. There are

two steps (oxidizing and reducing) in the process of chemical looping for solid fuel combustion. Thus, the enthalpy of solid fuel combustion in the chemical looping process is equal to the sum of the enthalpies of the two steps. For the different oxygen carriers shown, there is a different distribution of enthalpies in two steps, and even the endothermic and exothermic reactions may be changed. Copper-based and CoO-Co oxygen carriers are the only three choices whose reduction is exothermic due to the smaller enthalpy of the oxidation compared to the direct combustion of solid fuel. The Mn_3O_4-MnO oxygen carrier should be removed from the suggested candidate list due to the reason (N=6) previously mentioned. Despite endothermic properties in the reducer, oxygen carriers such as NiO-Ni, CoO-Co, Co_3O_4-Co, Mn_3O_4-MnO and Fe_2O_3-Fe_3O_4 have smaller reaction enthalpies so they can be included as candidates for oxygen carriers if heat-transfer materials will be used for heat transfer in the reducer. Due to the reason previous mentioned (melting points and N values), Co_3O_4-Co, Mn_3O_4-MnO and $Fe_2O_{33}O_4$ can be removed from the suggested candidate list.

■ ***Thermodynamics Analysis.*** Chemical reaction thermodynamics are important for the control of CO_2 purity. From the standard Gibbs free energy changes, the equilibrium constants can be calculated for the various reactions of metal oxide reduction and solid fuel gasification for a wide range of operating temperatures. The phase diagram for the reduction reactions using the reducing agents CO and H_2 produced from the solid fuel gasification process at atmospheric pressure are shown in Figures A19-1 and A19-2, respectively.

Figure A19-1 shows the equilibrium gas ratio of P_{CO2}/P_{CO} as a function of temperature for the reduction of various metal oxides. It shows that the ratio varies from approximately 10^5 for the reduction of CuO to Cu, Cu_2O to Cu, Mn_3O_4 to MnO and Fe_2O_3 to Fe_3O_4, to values on the order of 10^{-5} or less for the reduction of MnO to its elemental state of Mn. Information related to the Boudouard reaction, as illustrated in Equation (5), is also presented in Figure A19-1. For the reduction of a metal oxide with CO in the absence of solid carbon, the oxides of copper and nickel will be reduced to the elemental form at gas ratios between 10^5 and 10^2. Therefore, the completeness of the reaction could be achieved and a highly concentrated CO_2 stream will be obtained in the proposed CLC system. On the other hand, the reduction of MnO requires a CO_2-free environment, which is practically impossible for the CLC of solid fuel to achieve.

Because carbon is also present in the reaction mixture in the proposed reducer, the reduction of metal oxide and carbon gasification to CO occurs simultaneously. As shown in Figure A20, above the simultaneous equilibrium temperature where two curves for the reduction of metal oxides and the Boudouard reaction intersect, Fe_3O_4 will be converted to FeO above 650 ^{o}C and then to Fe above 700 ^{o}C under a low P_{CO2}/P_{CO} ratio of ~10. In contrast, the curves for CuO, Cu_2O, NiO and Fe_2O_3 do not intersect with the carbon curve even at the interested temperature range (600-1200 ^{o}C). The simultaneous reactions are not limited by thermodynamics; they are determined entirely by kinetics. In this case the gas constituents produced will have an intermediate impact on the value of the P_{CO2}/P_{CO} ratio. Generally, the reduction reaction of metal oxide is faster than the solid fuel gasification in the CLC process. Hydrogenis another product from the solid fuel gasification process using H_2O as the gasification agent. Figure A19-2 is the thermodynamics diagram for the P_{H2O}/P_{H2} equilibrium system, similar to the P_{CO2}/P_{CO} system presented in Figure A19-1. The reduction of metal oxides with H_2 is less exothermic than its corresponding reaction with CO. Moreover, equilibrium of the water-gas reaction will occur and shift to the right at lower temperatures. This shows that H_2 at high temperatures is a better reducing agent than CO for oxygen carriers. Solid fuel pyrolysis and gasification may produce some CH_4 in the reducing stream. Thermodynamics shows that CH_4 could be a better reducing agent than either CO or H_2 at high temperatures. The tendency of CH_4 decomposition to result in oxygen carrier deactivation by carbon deposit may be largely eliminated under higher partial pressure of H_2O and CO_2 in the reducer.

The main constituent of solid fuels is carbon. The possibility of directly reducing metal oxides with carbon can also be calculated using thermodynamic theory[39]. All these reduction reactions with carbon are heterogeneous reactions with only one gaseous species included. Based on thermodynamics theory, if the gas (CO_2) is ideal, the equilibrium constant expressions for these reactions can not include the solid phase due to the fact that pure solid phases are nearly equal to unity for moderate pressures. Thus, a phase diagram relating the partial pressure of CO_2 and temperature can be constructed as shown in Figure A20. In this figure the equilibrium line for each oxygen carrier divides the 2-D area of temperature and CO_2 partial pressure (P_{CO2}) into

two zones in the temperature range of interest. Metal oxides, reduced metal oxides or metals, carbon and CO_2 are present simultaneously only at the equilibrium line correlating the reaction temperature and CO_2 partial pressure. Above this equilibrium line, metal oxides and carbon can have a stable existence. Under this equilibrium line, metal or reduced metal oxides can have a stable existence. The temperature and CO_2 partial pressure are the parameters that control reaction extent and have a higher equilibrium at about 10, but it still needs to be rejected as an oxygen carrier due to a high N value, which was mentioned previously.. Figure A20 indicates that CO_2 partial pressure (P_{CO2}) of Cu-based, Ni-based and Co-based oxygen carriers can reach above 10^3 so that 99.999 % purity of the CO_2 stream can be assured in view of the reduction of a metal oxide directly by carbon in the temperature range of interest. Above 1000 ^oC, Fe-based oxygen carriers can only assure the P_{CO2} to be above 10 with a CO_2 stream purity of 90 %. Generally, Mn-based oxygen carriers lack practicality due to a very low P_{CO2}, at about 10^{-7} for MnO-Mn and 10^{-3} Mn_3O_4-MnO reaction systems [17]

Table A4. Physical Properties and Oxygen Transfer Capability of Oxygen Carriers

NO.	Reduction reaction	Melting point of the reduced metal form, ^{o}C	Melting point of the oxidized metal form, ^{o}C	Specific density of the reduced metal form ρ_R, kg/m^3	Specific density of the oxidized metal form ρ_O, kg/m^3	mol of metal per mol of oxygen transfer N, mol/mol	$(N x \rho_R)_M/(N x \rho_R)_{Cu}$ in reducer	$(N x \rho_O^{0.5})_M/(N x \rho_O^{0.5})_{CuO}$ in oxidizer
1	**$2CuO + C = 2Cu + CO_2$**	1083	1026	8920	6450	1	1.0	1.0
2	**$2Cu_2O + C = 4Cu + CO_2$**	1083	1235	8920	6000	2	2.0	1.9
3	**$2NiO + C = 2Ni + CO_2$**	1452	1452	8900	7450	1	1.0	1.1
4	**$2Co_3O_4 + C = 6CoO + CO_2$**	1480	895	8900	6070	3	3.0	2.9
5	**$1/2Co_3O_4 + C = 3/2Co + CO_2$**	1480	895	8900	6070	0.75	0.7	0.7
6	**$2CoO + C = 2Co + CO_2$**	1480	1800	8900	5680	1	1.0	0.9
7	**$6Mn_2O_3 + C = 4Mn_3O_4 + CO_2$**	1564	1080	4856	4810	6	3.3	5.2
8	**$2Mn_2O_3 + C = 4MnO + CO_2$**	1650	1080	5180	4810	2	1.2	1.7
9	**$2/3Mn_2O_3 + C = 4/3Mn + CO_2$**	1260	1080	7200	4810	0.67	0.5	0.6
10	**$2Mn_3O_4 + C = 6MnO + CO_2$**	1650	1564	5180	4856	3	1.7	2.6
11	**$1/2Mn_3O_4 + C = 3/2Mn + CO_2$**	1260	1564	7200	4856	0.75	0.6	0.7
12	**$2MnO + C = 2Mn + CO_2$**	1260	1650	7200	5180	1	0.8	0.9
13	**$6Fe_2O_3 + C = 4Fe_3O_4 + CO_2$**	1538	1560	5200	5120	6	3.5	5.3
14	**$2Fe_2O_3 + C = 4FeO + CO_2$**	1420	1560	5700	5120	2	1.3	1.8
15	**$2/3Fe_2O_3 + C = 4/3Fe + CO_2$**	1275	1560	7030	5120	0.67	0.5	0.6
16	**$2Fe_3O_4 + C = 6FeO + CO_2$**	1420	1538	5700	5200	3	1.9	2.7
17	**$1/2Fe_3O_4 + C = 3/2Fe + CO_2$**	1275	1538	7030	5200	0.75	0.6	0.7
18	**$2FeO + C = 2Fe + CO_2$**	1275	1420	7030	5700	1	0.8	0.9
19	**$2PbO + C = 2Pb + CO_2$**	327.5	886	11340	8000	1	1.3	1.1
20	**$2CdO + C = 2Cd + CO_2$**	320.9	900	8650	8150	1	1.0	1.1

Table A5. Enthalpies of Reduction Reaction by Carbon at 1000°C and 1 atm (calculations based on data from reference).

$C + O_2 \rightarrow CO_2$, -392.75 KJ/mol	
Endothermic	***Exothermic***
$2\ NiO + C \rightarrow 2\ Ni + CO_2$, 75.21kJ/mol	$2\ CuO + C \rightarrow 2Cu + CO_2$, -96.51 kJ/mol
$2\ CoO + C \rightarrow 2\ Co + CO_2$, 73.92 kJ/mol	$2\ Cu_2O + C \rightarrow 4\ Cu + CO_2$, -61.04 kJ/mol
$1/2\ Co_3O_4 + C \rightarrow 3/2\ Co + CO_2$, 53.9 kJ/mol	$6Co_3O_4 + C = 6CoO + CO_2$, -8.63 kJ/mol
$2/3\ Mn_2O_3 + C = 4/3\ Mn + CO_2$, 239.61 kJ/mol	$6Mn_2O_3 + C = 4Mn_3O_4 + CO_2$, -216.63 kJ/mol
$6\ Mn_3O_4 + C = 4\ MnO + CO_2$, 54.21 kJ/mol	$2Mn_2O_3 + C = 4MnO + CO_2$, -36.07 kJ/mol
$1/2\ Mn_3O_4 + C \rightarrow 3/2\ Mn + CO_2$, 296.65 kJ/mol	
$2\ MnO + C \rightarrow 2\ Mn + CO_2$, 378.98 kJ/mol	
$6\ Fe_2O_3 + C \rightarrow 4\ Fe_3O_4 + CO_2$, 83.56 kJ/mol	
$2\ Fe_2O_3 + C \rightarrow 4\ FeO + CO_2$, 158.40 kJ/mol	
$2/3\ Fe_2O_3 + C \rightarrow 4/3\ Fe + CO_2$, 146.37 kJ/mol	
$2\ Fe_3O_4 + C = 6\ FeO + CO_2$, 195.78 kJ/mol	
$1/2\ Fe_3O_4 + C = 3/2\ Fe + CO_2$, 151.27 kJ/mol	
$2FeO + C = 2\ Fe + CO_2$, 136.44 kJ/mol	

Figure A19-1. Variation of the Thermodynamic Equilibrium Factor for Me_xO_y-CO as a Function of Temperature (calculations based on data from reference).

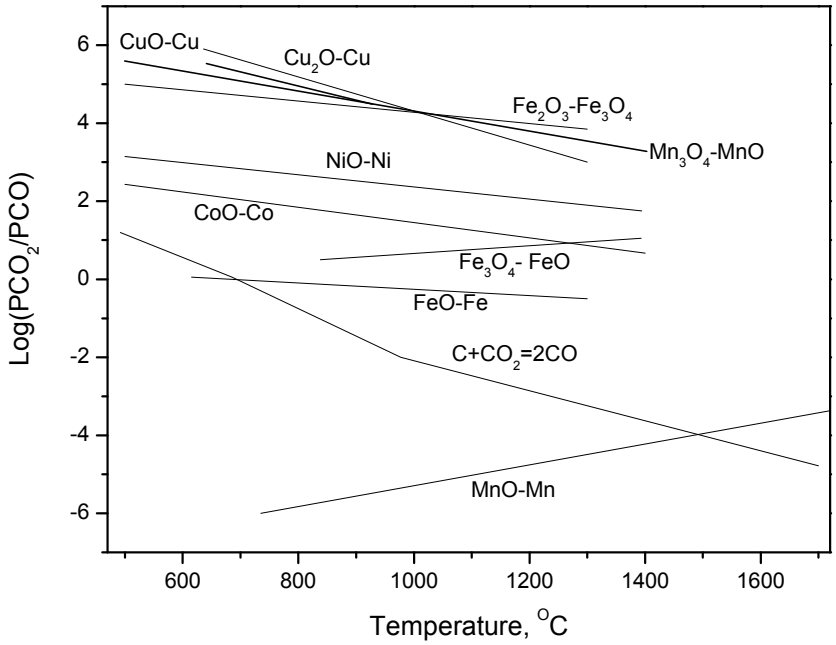

Figure A19-2. Variation of the Thermodynamic Equilibrium Factor for Me_xO_y-H_2 as a Function of Temperature

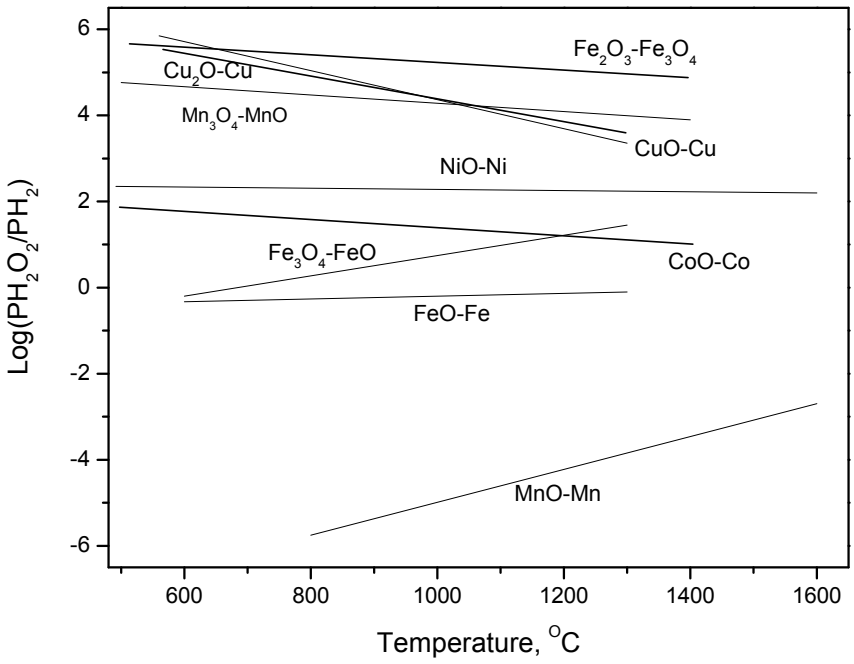

Figure A20. Variation of the Thermodynamic Equilibrium Factor for Me_xO_y-C as a Function of Temperature

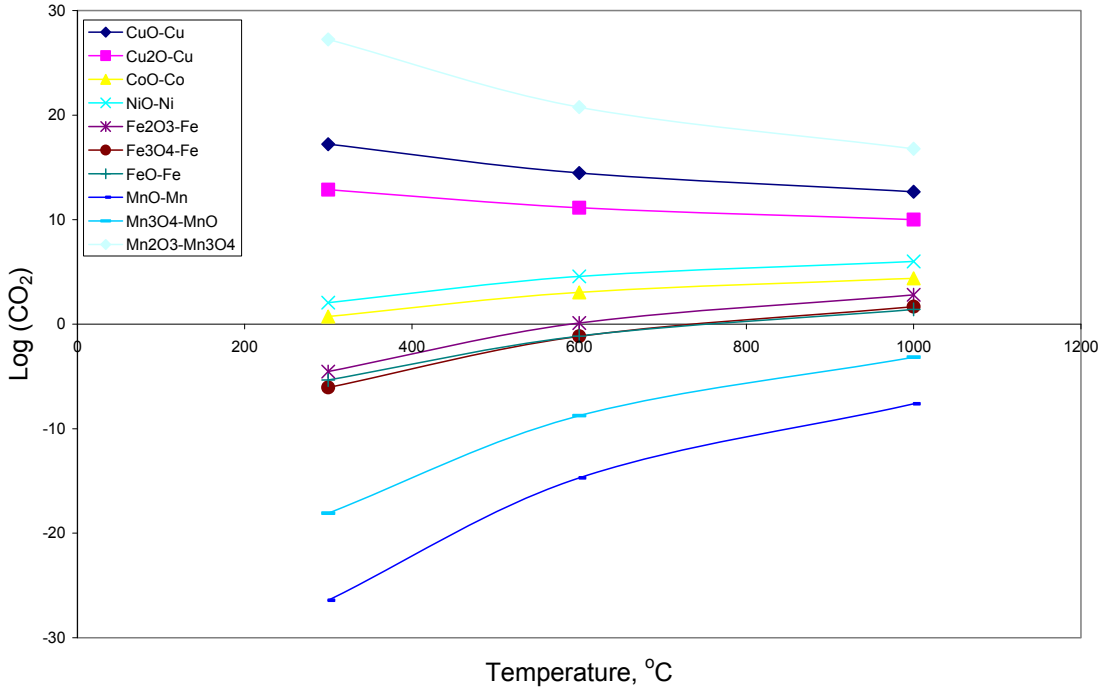

9.5 Statistics Analysis of CFBC Mercury Emission Rate

Methods. Mercury emissions data were collected from data bases of the EPA's mercury ICR program and WKU ICSET mercury field testing. The EPA ICR data are from sampling activities, which were obtained based on ASTM D6784 Ontario Hydro Method (OHM). Besides ASTM OHM used, ICSET data were also from sampling activities by the semi-continuous Mercury Monitor (SCEM) and EPA Appendix K method. The EPA ICR data were collected upstream of the last air pollutant control device and the stack. The ICSET data were collected from sampling activities, which have been extended to varied APCD locations and boiler operation conditions. Thus, it could provide additional information about the dependence of mercury transformation at different locations and mercury emission rates on the boiler performance. Boilers equipped with Fabric Filter (FF) were selected in this study because FF was predicted to be more efficient for mercury emission control than ESP. In the collected ICR data, there were 18 PC units, one cyclone unit, nine CFBC units, three stoker-fired units and 2 IGCC units. Coals burned in these units included bituminous, sub-bituminous, lignite and their blends. All ash characterization data were from the ICSET database. The mercury emission rate, which is commonly expressed as lb/TBtu, was not used in this study. It does not include information on mercury input levels so that it is not accurate herein. In this study, the new mercury emission rate ($\mu g/NM^3/(ug/g \cdot Btu/lb)$) is defined as mercury emissions in the stack (Hg_{stack}, $\mu g/NM^3$), per the mercury content (Hg_{coal}, $\mu g/g$) and also per heating value of the ($BTu_{coal,}$ Btu/lb), see Eq (A28). This factor can be used to evaluate the mercury emission rates, which are dependent upon the mercury content of the coal (Hg_{coal}) and coal heating value (Btu_{coal}). We found loss of information in ICR data (for example, a complete analysis of coal) to calculate F-Factor for every case and thus to correlate BTU and flue gas volume to make its unit have a simple look.

$$mercury\quad emission\quad rate\quad = Hg_{stack} / [(Hg_{coal})(Btu_{coal})] \qquad \text{Eq (A28)}$$

The collected data were subjected to the stepwise regression to build up a statistics model of significant analysis of factors affecting mercury emission rates. Stepwise regression can remove and add variables into the regression model to identify a useful subset of the factors. The basic principle in this stepwise regression is to calculate an F-statistic and p-value for each variable in the model. If the p-value for any variable is greater than *Alpha to remove* (0.15), then the variable with the largest p-value is removed from the model. If no variable can be removed, the procedure attempts to add a variable, and the next step begins. After trial and error calculations, the

regression model will supply the most significant factors that fit the prediction. The selection or definition of the data's subset is also dependent upon understanding mercury transformation in the coal-fired combustion process. In this study, SPSS statistics software was used to fulfill the stepwise regression analysis. We can keep variables in the model regardless of their p-values. Because analysis procedures require that factor variables, and their corresponding response variables should have an equal amount in data size, we compiled the data bank into two groups (mercury emission rate and fly ash). The factor prediction on the mercury emission rate has 81 sets of data (54 sets from PC units and 27 sets from CFBC). Nine sets of data from stoker-fired units and six sets from IGCC data were excluded in the statistical analysis because little data was available and some of the required information was not collected during tests in the EPA ICR program for those units that were IGCC and stoker-fired. The fly ash characterization has 38 data sets (30 from PC units and 8 from CFBC units).

Statistical Analysis. The mercury emission rates in boilers with different configurations and different coals are presented in Figure A21. The mercury emission rates of stoker-fired units are generally low, approximately $1.0x10^{-3}$ ($\mu g/NM^3/(\mu g/g \cdot Btu/lb)$). The PC boilers burning bituminous coals are also low, approximately $9.0x10^{-4}$($\mu g/NM^3/(\mu g/g \cdot Btu/lb)$). The mercury emission rates increase in PC boilers when the coal is switched from bituminous coal to a blend of bituminous coal and petroleum coke or sub-bituminous coal. PC boilers burning sub-bituminous coal show an even higher mercury emission rate than those burning bituminous coal. This increasing trend reaches its peak when lignite coal is burned in the PC boilers, approximately $2.0x10^{-2}$ ($\mu g/NM^3/(\mu g/g \cdot Btu/lb)$). By burning bituminous coal the cyclone-fired boiler showed a very high mercury emission rate, approximately $4.0x10^{-2}$ ($\mu g/NM^3/(\mu g/g \cdot Btu/lb)$) among all coal-fired combustion processes. However, there is only one such unit in the present study. The reason may be due to the higher combustion temperature and more ash discharge from the cyclone boiler. These conditions likely result in the lower reactivity and lower concentration of fly ash available from mercury capture than from PC boilers. Circulating Fluidized Bed boilers burning bituminous and sub-bituminous coals show very low mercury emission rates. Mercury emissions could be efficiently controlled in an CFB boiler by burning sub-bituminous coal or blending it with bituminous coal. Compared to PC boilers burning lignite, a CFB boiler shows lower mercury emission rates of about $1.0x10^{-2}$ ($\mu g/NM^3/(ug/g \cdot Btu/lb)$). When bituminous and sub-bituminous coals are burned in a CFB, the mercury emissions rate is

not as low. The coal gasification-based IGCC process appears to have a higher mercury emission rate, around $6.0x10^{-3}$ ($\mu g/NM^3/(\mu g/g \cdot Btu/lb)$), than those coal-combustion based boilers burning bituminous coal. From analysis, mercury emission rates appear to be strongly related to the type or rank of coal burned, and type of boilers used.

Shown in the Figure A21, similarly there is an apparent correlated trend of Hg_{ash}/Hg_{coal} and mercury emission rates. This may indicate that mercury adsorption by generated fly ash in boilers is a major measure to control mercury emissions in coal-fired boiler equipped with FF. Mercury in coal is initially present in the gas phase at high temperatures during the coal combustion process. Mercury adsorption by fly ash occurs when the flue gas temperature is decreased downstream of the boiler. In this process, rank-related coal properties (such as the chlorine, sulfur, moisture and ash content), may influence mercury adsorption on the fly ash. An apparent decreasing trend of chlorine content in coals is found when the rank of coals decreases. This is followed by an increasing trend in mercury emission rates. This may imply that chlorine content in the coal could be the possible factor affecting mercury emission rates. However, there is no significant correlation between mercury emission rates and mercury speciation in the stack ($Hg(0)/Hg(VT)_{stack}$, the ratio of the elemental mercury and the total gaseous mercury), at least by available data shown in Figure A21. The possible explanation for this could be that the great change of mercury speciation by the interaction between gaseous mercury and fly ash occurs after flue gas passes through the FF. The loss on ignition (LOI) content of the fly ash, which is relative to boiler type and coal rank, seemed to be correlated with the mercury emission rate based on limited data available, as shown in Figure A21.

To more accurately predict the factors affecting mercury emission rates, three trials by a stepwise regression analysis based on two available data banks were conducted. All three trials investigated the trends in mercury emission rate by different boiler types burning different coals. In the first trial, all affecting factors were chosen and included boiler type, coal properties, such as coal rank, moisture (M_{coal}), ash content (A_{coal}), sulfur content (S_{coal}), chlorine content (Cl_{coal}), Hg content (Hg_{coal}) and heating value (Btu_{coal}). Four factors were chosen by the built-up regression model based on their importance. The four factors explained 75.4 % of the variation in mercury emission rates, as shown in Table A6. Among them, the most significant effects on mercury emission rates are coal rank and boiler type with higher confidence limits (very low statistical P-value). The other factors, which are based on the decreasing sequence of significance,

were S_{coal} and M_{coal}. According to the affecting trends, four factors can be categorized as a group of positive factors, which include coal rank, S_{coal} and M_{coal}; and a group of negative factors, which include only boiler type. Increases in the levels of coal rank (Level 1: bituminous, Level 2: sub-bituminous, Level 3: lignite), as well as S_{coal} and M_{coal} leads to increases in the level of mercury emission rates. An increase in the boiler-type level (Level 1: PC and Level 2: CFBC) leads to a decrease in the level of the mercury emission rate. Based on the definition of levels of coal rank and boiler type, it was found that burning low rank coal or blending it with higher-rank coals in the conventional PC unit result in relatively higher mercury emission rates. Increased levels of S_{coal} and M_{coal} also result in higher mercury emission rates.

In order to increase the accuracy of prediction by the regression model, one more factor, mercury speciation in the flue gas ($Hg(0)/Hg(VT)_{stack}$), was included in the model build-up in the second trial. All factors were now able to explain 81.7 % of the variation in the mercury emission rate, as seen in Table A7. This is a slight improvement over results achieved in the first trial. The most significant factors affecting mercury emission rates were still coal rank and boiler type. Other factors, which were found to be less significant, were Btu_{coal}, S_{coal} and M_{coal}. The same trends of factors repeatedly appear in both trials. For the new factor, $Hg(0)/Hg(VT)_{stack}$, it appeared that an increase in the $Hg(0)/Hg(VT)_{stack}$ level led to an increase in mercury emission rates. It is unusual that the critical factor for mercury speciation, Cl_{coal}, was not a significant factor in the regression model. Nevertheless, S_{coal} was found to be a factor in the regression model. It may be implied that Cl_{coal}, which was found to be a critical factor affecting mercury speciation, did not have a direct effect on mercury adsorption on the fly ash. S_{coal} may have some direct effect on mercury adsorption on the fly ash[43-44]. An alternative possibility is that coal rank, which was positively correlated with Cl_{coal}, may replace the function of Cl_{coal} in the regression model. The third trial by the stepwise regression procedure was conducted to pursue the most significant factors affecting the mercury emission rates. Results indicated the regression model chose two factors, boiler type and coal rank, as the most significant factors on the variation of mercury emission rates. Those two factors explained 71.6 % of the variation in mercury emission rates within the confidence limits. The CFB burning higher rank coal achieved the best mercury removal efficiency among all other boilers burning the same rank of coal.

Table A6. Stepwise Statistical Analysis on Factors of Mercury Emission Rates

Code	Factor	Linear Coefficient	P-Value	Adjusted-R^2	Code	Factor	Linear Coefficient	P-Value	Adjusted-R^2
1	Coal Rank	0.005	<0.001		1	Coal Rank	0.0044	<0.001	
2	Boiler Type	-0.00733	<0.001		2	Boiler Type	-0.00864	<0.001	
3	S_{coal}	0.00101	0.021		3	$Hg(0)/Hg(VT)_{stack}$	0.0056	<0.001	
4	M_{coal}	0.00016	0.063		4	BTU_{coal}	<-0.00001	0.001	
				75.4%	5	S_{coal}	0.0080	0.034	
					6	M_{coal}	0.00013	0.083	
									81.7%

Code	Factor	Linear Coefficient	P-Value	Adjusted-R^2
1	Coal Rank	0.00738	<0.001	
2	Boiler Type	-0.00571	<0.001	
				71.6%

Note:			level vaue			level value
	Coal Rank:	Bituminous coal	1	Boiler:	PC	1
		Sub-bituminous coal	2		CFBC	2
		Lignite	3			

Table A7. Stepwise Statistical Analysis on Factors of Fly Ash Properties

Code	Factor	Linear Coefficient	P-Value	Adjusted-R^2
		BET		
1	Boiler Type	9.51	<0.001	
2	Coal Rank	-1.39	<0.001	
				82.2%
		Pore volume		
1	Boiler Type	0.0168	<0.001	
2	Coal Rank	-0.0085	<0.001	
				75.2%
		Pore size		
1	Boiler Type	4.6	<0.001	
2	Coal Rank	5	<0.001	
				57.9%

		level value			level value
Coal Rank:	Bituminous coal	1	Boiler Type	PC	1
	Sub-bituminous coal	2		CFBC	2
	Lignite	3			

Figure A21. The Dependence of Mercury Emission Rates on Boiler Types with FF and Coal Ranks
(B-Bituminous coal; P: Petcoke; SB-Sub-Bituminous coal; A: Anthracite coal; L: Lignite)

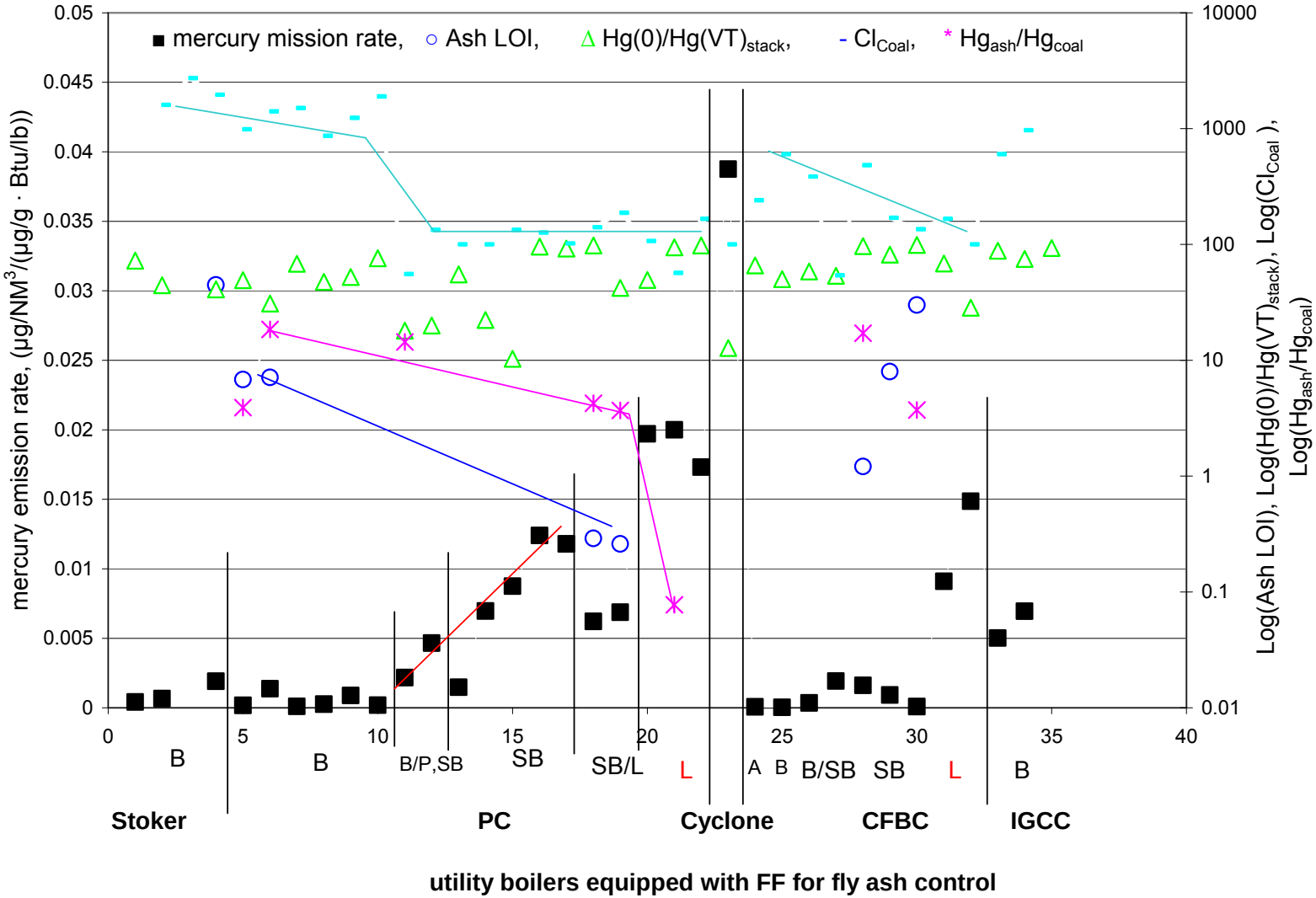

Figure A22. The Factors on Fly Ash Properties

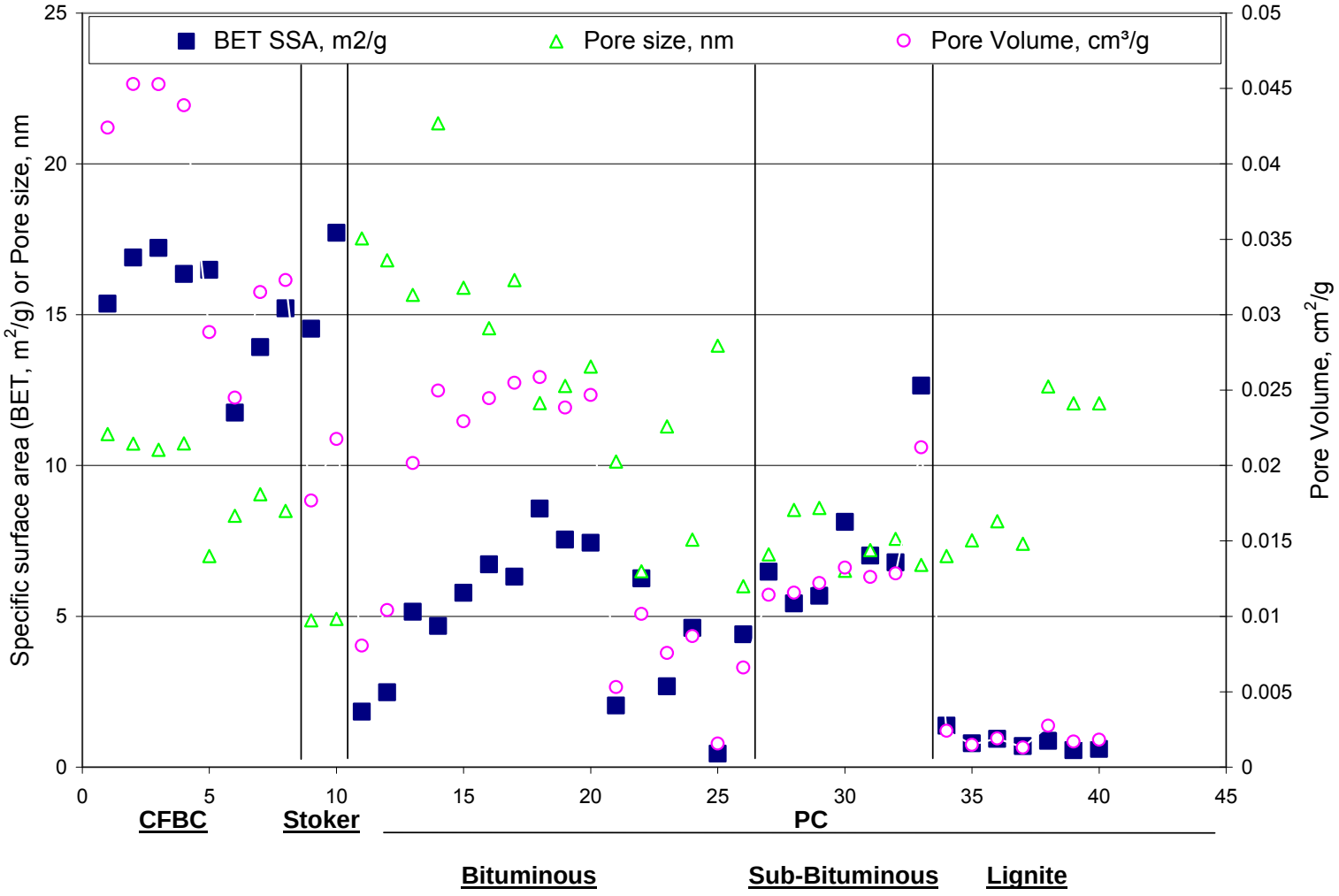

10. References

1. Cao Y.; Duan, Y. F.; Kellie, K; Li, L. C.; Xu, W. B.; Riley, J. T.; Pan, W. P. Impact of coal chlorine on mercury speciation and emission from a 100-MW utility boiler with cold-side electrostatic precipitators and low-NO*x* Burners. *Energy & Fuels* **2005,** *19,* 842-854.

2. Kellie, S.; Cao, Y.; Duan, Y.D.; Li, L. C.; Chu, P.; Mehta, A.; Carty, R.; Riley, J. T.; and Pan. W.P. Factors affecting mercury speciation in a 100-MW coal-fired boiler with low-NO*x* burners. *Energy & Fuels* **2005**, *19,* 800-806.

3. Pavlish JH, Scondreal E A, Mann MD, Olson ES, Galbreath KC, Laudal DL, Benson SA. Status review of mercury control options for coal-fired power plant. Fuel Processing Technology **2003**; *82*: 89-165.

4. Hilber, Th.; Thorwarth, H.; Stack-Lara, V.; Schneider, M.; Maier, J.; Scheffknecht. Fate of mercury and chlorine during SRF co-combustion. *Fuel* **2007,** 86, 1935-1946.

5. Zhang, Y.; Miller, S. J. Impact of supplemental firing of tire-derived fuel (TDF) on mercury species and mercury capture with the advanced hybrid filter in a western subbituminous coal flue gas. *Energy&Fuel* **2006**, 20, 1039-1043.

6. Sable, S. P.; Jong, W. D.; Meij, R.; Spliethoff, H. Effect of secondary fuels and combustor temperature on mercury speciation in pulversized fuel CO-combustion: Part 1. *Energy & Fuel* **2007**, 21, 1883-1890.

7. Gupta, R. P. Coal research in Newcastle—past, present and future. *Fuel* **2005,** 84(10), 1176-1188.

8. Olsson, J. G.; Jaglid, U.; Pettersson, J. B. C.; Hald, P. Alkali metal emission during pyrolysis of biomass. *Energy & Fuels* **1997**, 11(4), 779-784.

9. Jenkins, B. M.; Baxter, L. L.; Miles Jr., T. R.; Miles, T. R. Combustion properties of biomass. *Fuel Process. Technol.*, **1998**, *54(1-3)*, *17-46.*

10. Liu, K. L.; Gao, Y.; Riley, J. T.; Pan, W. P.; Mehta, A. K.; Ho, K. K.; Smith, S. R. An investigation of mercury emission from FBC system fired with high-chlorine coals. *Energy&Fuel* 2001, 15(5), 1173-1180.

11. Sable, S. P.; Jong, W. D.; Meij, R.; Spliethoff, H. Effect of air-staging on mercury speciation in pulversized fuel co-combustion: Part 2. *Energy & Fuel* **2007**, 21, 1891-1894.

12. Vosteen, B. W.; Kanefke, R.; Koser,H. Bromine-enhanced mercury abatement from combustion flue gases - recent industrial applications and laboratory research. VGB Power Tech, *International Journal for Electricity and heat Generation*, **2006**, *86(3)*, 70-75.
13. Sakuri, M.; Nakajima, H.; Onuki, K.; Ikenoya, K.; Shimizu, S. Prelinary process analysis for the closed cycle operation of the iodine-sulfur thermochemical hydrogen production process. *International Journal of Hydrogen Energy*, **1999**, *24*, 603-612.
14. Giaconia, A.; Caputo, G.; Ceroli, A.; Diamanti, M.; Barbarossa, V.; Taruini, P.; Sau, S. Experimental study of two phase separation in the bunsen section of the sulfur-iodine thermochemical cycle. *International Journal of Hydrogen Energy* **2007**, *32*, 531-536.
15. Cao, Y.; Chen, B.; Wu, J.; Cui, H.; Li, S. G.; Herren, S. M.; Smith, J.; Chu, P.; and Pan, W. P. Study of mercury oxidation by selective catalytic reduction catalyst in a pilot-scale slipstream reactor at a utility boiler burning bituminous coal. *Energy & Fuels*, **2007**, *21*, 145-156.
16. Nebergell, W. H.; Schmidt, F. C.; Jr. Holtzclaw, H. F. In *College Chemistry with Qualitative Analysis.* 5th Edition, D.C. Heath and Company, 1976.
17. Calvert, J. G.; Lindberg, S. E. The potential Influence of iodine-containing compounds on the chemistry of the troposphere in the polar spring. II. mercury depletion. *Atmosphere Environment,* **2004**, *38*, 5105-5116.
18. Geoffrey D. S. Senior, C. L.; O'Palko, A. Analysis of Bromine-Mercury Reactions in Flue Gas. In *University Coal Research / Historically Black Colleges and Universities & Other Minority Institutions Contractors Review Meeting*, U.S. Department of Energy, 2007.
19. Cao, Y; Wang, Q. H.; Chen, W. C.; Chen, B.; Cohron, M.; Chiu, C. C.; Tseng, Y. C.; Chu, P.; Pan W. P. Investigation of mercury transformation by HBr addition in a slipstream facility with real flue gas atmospheres of bituminous coal and Powder River Basin (PRB) Coal. *Energy & Fuels*, **2007**, *21*, 2719-2730.
20. Geoffrey D. S. Senior, C. L.; O'Palko, A. Analysis of Bromine-Mercury Reactions in Flue Gas. In *University Coal Research / Historically Black Colleges and Universities & Other Minority Institutions Contractors Review Meeting*, U.S. Department of Energy, 2007.
21. Ishida, M.; Jin, H. A Novel Combustor Based on Chemical Looping Reactions and its Reaction Kinetics. *J. Chem. Eng. Japan* **1994**, *27*, 296.
22. Ishida, M.; Jin, H. "Novel Chemical-looping Combustor without NO_x Formation," *Industrial and Engineering Chemistry Research*, **1996,** *35*, 2469–2472.
23. Ishida, M.; Jin, H.; Okamoto, T. "A Fundamental Study of a New Kind of Medium Material for Chemical-looping Combustion," *Energy & Fuels*, **1996,** *10*, 958–963.
24 Ishida, M.; Jin, H.; Okamoto, T. "Kinetic Behaviour of Solid Particle in Chemical-looping Combustion: Suppressing Carbon Deposition in Reduction," *Energy & Fuels*, **1998,** *12*, 223–229.

25. Ishida, M.; Yamamoto, M.; Ohba, T. "Experimental Results of Chemical-looping Combustion with NiO/$NiAl_2O_4$ Particle Circulation at 1200C," *Energy Conversion and Management,* **2002,** *43*, 1469.

26. Jin, H.; Ishida, M. "Reactivity Study on Natural-gas-fueled Chemical-looping Combustion by a Fixed Bed," *Ind. Eng. Chem. Res*., **2002,** *41*, 4004-4007.

27. Jin, H.; Okamoto, T.; Ishida, M. "Development of a Novel Chemical-looping Combustion: Synthesis of a Looping Material with a Double Metal Oxide of CoO–NiO," *Energy & Fuels*, **1998,** *12*, 272–1277.

28. Jin, H.; Okamoto, T.; Ishida, M. "Development of a Novel Chemical-looping Combustion: Synthesis of a Solid Looping Material of NiO-$NiAl_2O_4$," *Industrial and Engineering Chemistry Research*, **1999,** *38*, 126–132.

29. Cho, P.; Mattisson, T.; Lyngfelt, A. Comparison of iron-, nickel-, copper- and manganese-based oxygen carriers for chemical looping combustion. *Fuel* **2004**, *83*, 1215-1225.

30. Mattisson, T.; Johansson, M.; Lyngfelt, A. Multi-cycle reduction and oxidation of different types of iron oxide particles Application to chemical-looping combustion. *Energy Fuels* **2004**, *18*, 628-637.

31. Johansson, M.; Mattisson, T.; Lyngfelt, A. Investigation of Fe_2O_3 with $MgAl_2O_4$ for chemical-looping combustion. *Ind. Eng.Chem. Res*. **2004**, *43*, 6978-6987.

32. Mattisson, T.; Ja¨rdna¨s, A.; Lyngfelt, A. Reactivity of some metal oxides supported on alumina with alternating methane and oxygens Application for chemical-looping combustion. *Energy Fuels* **2003**, *17*, 643-651.

33. Adanez, J.; de Diego, L. F.; Garcia-Labiano, F.; Gayan, P.; Abad, A. Selection of Oxygen Carriers for Chemical-Looping Combustion. *Energy Fuels* **2004**, *18*, 371-377.

34. de Diego, L. F.; Garcia-Labiano, F.; Adanez, J.; Gayan, P.; Abad, A.; Corbella, B. M.; Palacios, J. M. Development of Cu-based Oxygen Carriers for Chemical-Looping Combustion. *Fuel* **2004**, *83*, 1749-1757.

35. Cho, P.; Mattisson, T.; Lyngfelt, A. Carbon Formation on Nickel and Iron Oxide-Containing Oxygen Carriers for Chemical- Looping Combustion. *Ind. Eng. Chem. Res.* **2005**, *44*, 668-676.

36. Mattisson, T.; Lyngfelt, A.; Cho, P. The use of iron oxide as an oxygen carrier for chemical-looping combustion of methane with inherent separation of CO_2. *Fuel* **2001**, *80*, 1953-1962.

37. Mattisson, T.; Jarders, A.; Lyngfelt, A. "Reactivity of some Metal Oxide Support on Alumina with Alternating Methane and Oxygen-application for Chemical-looping Combustion," *Energy & Fuels*, **2003,** *17*, 643-651.

38. Lyngfelt, A.; Leckner, B.; Mattisson, T. A fluidized-bed combustion process with inherent CO2 separation; application of chemical-looping combustion. *Chem. Eng. Sci.* **2001**, *56*, 3101-

3113.

39. Perry, R. H.; Green, D. W. Perry's Chemical Engineers' Handbook, seventh edition, **1997**, The McGraw-Hill Companies, Inc.

40. Zafar, Q.; Mattisson, T.; Gevert, B. R. Integrated Hydrogen and Power Production with CO_2 Capture Using Chemical-Looping Reforming Redox Reactivity of Particles of CuO, Mn_2O_3, NiO, and Fe_2O_3 Using SiO_2 as a Support. Ind. Eng. Chem. Res., **2005,** 44(10).

41. Kunii, D.; Levenspiel, O. Fluidization Engineering. Second edition, **1990**, Butterworth-Heineman series in Chemical Engineering, ISBN: 0-409-90233-0.

42. Cao, Y.; Pan, W. P. Chemical Reversal Cycle of Solid Oxygen Carrier for Producing Pure Oxygen or Oxygen Rich Gas Stream. Prepr. Pap.-Am. Chem. Soc., Div. Fuel Chem. **2005**, 51, 415-416.

43. Behra P, Bonnissel-Gissinger P, Alnot M, Revel R, Ehrhardt J. XPS and XAS study of the sorption of Hg0 onto Pyrite. Langmui. 2001; 17: 3970-3979.

44.Rio S, Delebarre A. Removal of mercury in aqueous solution by fluidized bed plant fly ash. Fuel. 2003; 82: 153-159.

11. Acronyms and Abbreviations

- **APCD:** Air Pollutant Control Devices
- **BEI:** Backscatter Electron Images
- **CEM:** Continuous Emission Monitoring
- **CFBC:** Circulating Fluidized Bed Combustor
- **CPM:** Condensable particulate Matter
- **CR:** Coffee Residue
- **CW:** Chicken Waste
- **DOE:** U.S. Department of Energy
- **EDS:** Energy-dispersive X-Ray
- **EEI:** Electric Energy, Inc.
- **EKPC:** Eastern Kentucky Power Cooperative
- **EPA:** Environmental Protection Agency
- **EPRI:** Electric power Research institute
- **FBC:** Fluidized Bed Combustor
- **FF:** Fabric Filter
- **FPM:** Filterable Particulate Matter
- **GVC:** Gross Calorific Value
- **HID:** Human Interface Device
- **HP:** Horse Power
- **HX:** Heat Exchanger
- **I/O:** Input / Output
- **IC:** Ion Chromatograph
- **ICCI:** Illinois Clean Coal Institute
- **ICSET:** Institute for Combustion Science &Environmental Technology
- **IGCC:** Integrated Gasification combined Cycle
- **LOI:** Loss of Ignition
- **MSW:** Municipal Solid Waste
- **NETL:** National Energy Technology Laboratory
- **OHM:** Ontario Hydro Method
- **PPM:** Parts Per Million
- **PPT:** Parts Per Trillion
- **PRB:** Powder River Basin
- **PVC:`** Polyvinyl Chloride
- **QA/QC** Quality Assurance / Quality Control
- **RDF:** Refuse-derived Fuel

- **ROMC:** Region of Minimum Choice
- **SCR:** Selective Catalytic Reduction
- **SEM:** Scanning Electron Microscopy
- **SIPC:** Southern Illinois Power Cooperative
- **TS:** Tobacco Stalk
- **VOC:** Volatile Organic Compound
- **WKU:** Western Kentucky University
- **WP:** Wood Pellets